Infra-Red Studies of Peptide Nitrosation

Thesis

INFRA-RED STUDIES OF PEPTIDE NITROSATION

A Thesis submitted by

Margaret Russell, BSc, MSc

in partial fulfilment of the requirements for the
degree of Doctor of Philosophy

at the Open University

Date of submission: 12 June 1992
Date of award: 7 August 1992

April 1992

Department of Chemistry
The Open University

Acknowledgements

I would like to thank Professor BC Challis, Dr JN Iley and Dr RC Mitchell for all the guidance and encouragement they have given me during their supervision of this project.

I also wish to thank Messrs J Gibbs, G Jeffs, A Leslie and P Patel for help with equipment on innumerable occasions.

Finally, I would like to thank the Science and Engineering Research Council and SmithKline Beecham for financial support.

Abstract

The synthesis, chemical properties and biological properties of both diazopeptides and N-nitrosopeptides are reviewed. The feasibility of assaying these compounds and studying their formation by Fourier transform infra-red spectroscopy (FTIR) is analysed.

The development of experimental procedures to facilitate kinetic studies of the nitrosation of peptides by FTIR is described. Methods to overcome the principal problems of solvent absorption and the continuous decomposition of the nitrous acid reagent are outlined and tested for the nitrosation of 2-pyrrolidinone as a model substrate.

The infra-red carbonyl bands of N-(N'-acetylglycyl)glycine are unambiguously assigned, via the synthesis and investigation of ^{13}C labelled compounds.

Investigation of the nitrosation of N-(N'-acetylglycyl)glycine by nitrous acid in deuterium chloride is reported. This includes the measurement of reaction rates by FTIR and the identification of products by a combination of FTIR and mass spectroscopy. The kinetic results show that these reactions follow similar mechanisms to those found previously for amide nitrosation. The effect of peptide structure on reactivity towards N-nitrosation is also reported. It is shown that the most important factor influencing reactivity is the accessibility of the peptide N-atom to nitrosation.

The development is described of an FTIR method to measure the formation of diazopeptides. Kinetic studies are reported for the formation of N-(2-diazoacetyl)glycine by the reaction of N-glycylglycine with 2-ethoxyethyl nitrite in aqueous buffers at pH 7.5-11 and 25°C. The results are discussed in terms of possible mechanisms of diazopeptide formation. The effect of structure on diazopeptide reactivity towards diazotisation is also briefly examined and reported.

Abbreviations

^{13}C-AcGlyGly	N-(N'-1-^{13}C-acetylglycyl)glycine
^{13}C-AcGlyGlyOBz	N-(N'-1-^{13}C-acetylglycyl)glycine benzyl ester
Ac(NO)Gly(NO)GlyOBz	N-(N'-acetyl-N'-nitrosoglycyl)-N-nitroso glycine benzyl ester
Ac(NO)GlyGly	N-(N'-acetyl-N'-nitrosoglycyl)glycine
Ac(NO)GlyGlyOBz	N-(N'-acetyl-N'-nitrosoglycyl)glycine benzyl ester
AcAlaAla	N-(N'-acetyl-L-alanyl)alanine
AcAlaAlaOBz	N-(N'-acetyl-L-alanyl)alanine benzyl ester
AcAlaGly	N-(N'-acetyl-L-alanyl)glycine
AcAlaGlyOBz	N-(N'-acetyl-L-alanyl)glycine benzyl ester
AcGlyAla	N-(N'-acetylglycyl)-L-alanine
AcGlyAlaOBz	N-(N'-acetylglycyl)-L-alanine benzyl ester
AcGlyGly	N-(N'-acetylglycyl)glycine
AcGlyGlyOBz	N-(N'-acetylglycyl)glycine benzyl ester
AcGlyVal	N-(N'-acetylglycyl)-L-valine
AcGlyValOBz	N-(N'-acetylglycyl)-L-valine benzyl ester
AcProGly	N-(N'-acetyl-L-prolyl)glycine
AcProGlyOBz	N-(N'-acetyl-L-prolyl)glycine benzyl ester
AcValGly	N-(N'-acetyl-L-valyl)glycine
AcValGlyGly	N-((N"-acetyl-L-valyl)-N'-glycyl)glycine
AcValGlyGlyOBz	N-((N"-acetyl-L-valyl)-N'-glycyl)glycine benzyl ester
AcValGlyOBz	N-(N'-acetyl-L-valyl)glycine benzyl ester
AlaOBz	L-alanine benzyl ester
GlyGly	N-glycylglycine
GlyGlyOBz	N-glycylglycine benzyl ester
GlyLeu	N-glycylleucine
GlyOBz	glycine benzyl ester
GlySar	N-glycylsarcosine
LeuGly	N-leucylglycine
ValOBz	L-valine benzyl ester

Contents

Chapter 1

Introduction and Historical Review

1.1 Introduction

Peptides are present in the diet and, like amides, may be attacked by nitrosating agents (NOX). All peptides can undergo nitrosation in two possible ways (Scheme 1.1): either at the terminal primary amino group to produce a diazo derivative (1) which then deaminates, or at a peptide NH to give an N-nitroso product (2). Both diazopeptides and N-nitrosopeptides are of concern because of their carcinogenic activity. Both could, in principle, be formed in the body by nitrosating agents which enter in the diet (eg NO_2^-) or by inhalation (eg NO_2 gas).

Scheme 1.1

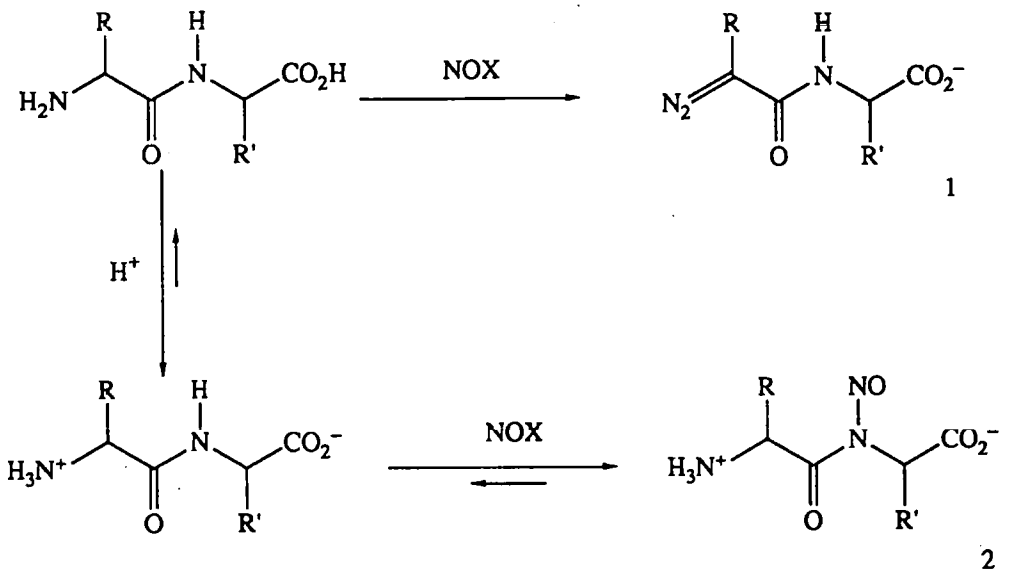

In addition certain amino acid residues may undergo nitrosation at the side chain[1]: cysteine at sulphur, arginine and tyrosine in the aromatic ring, lysine, glutamine and asparagine at nitrogen, together with proline and tryptophan.

1.2 Diazopeptides

1.2.1 Synthesis

Diazoglycylpeptides were first prepared, as ethyl esters, amides or hydrazides, by Curtius *et al*, using nitrite in aqueous acetic acid at 0°C[2 3 4 5]. Diazopeptides are labile in acid solution so that a two phase system, which allows the product to be extracted into an organic solvent such as dichloromethane, has proved more satisfactory[6].

In aqueous nitrous acid, various nitrosating agents such as N_2O_3, NOCl or NOSCN, may be present. By comparison with amino acids[7], the neutral peptides would react with these nitrosating agents in a rate-limiting step. The resulting N-nitrosoammonium ion intermediate rapidly loses H_3O^+ to give the diazopeptide, which immediately decomposes under the reaction conditions (Scheme 1.2).

Scheme 1.2

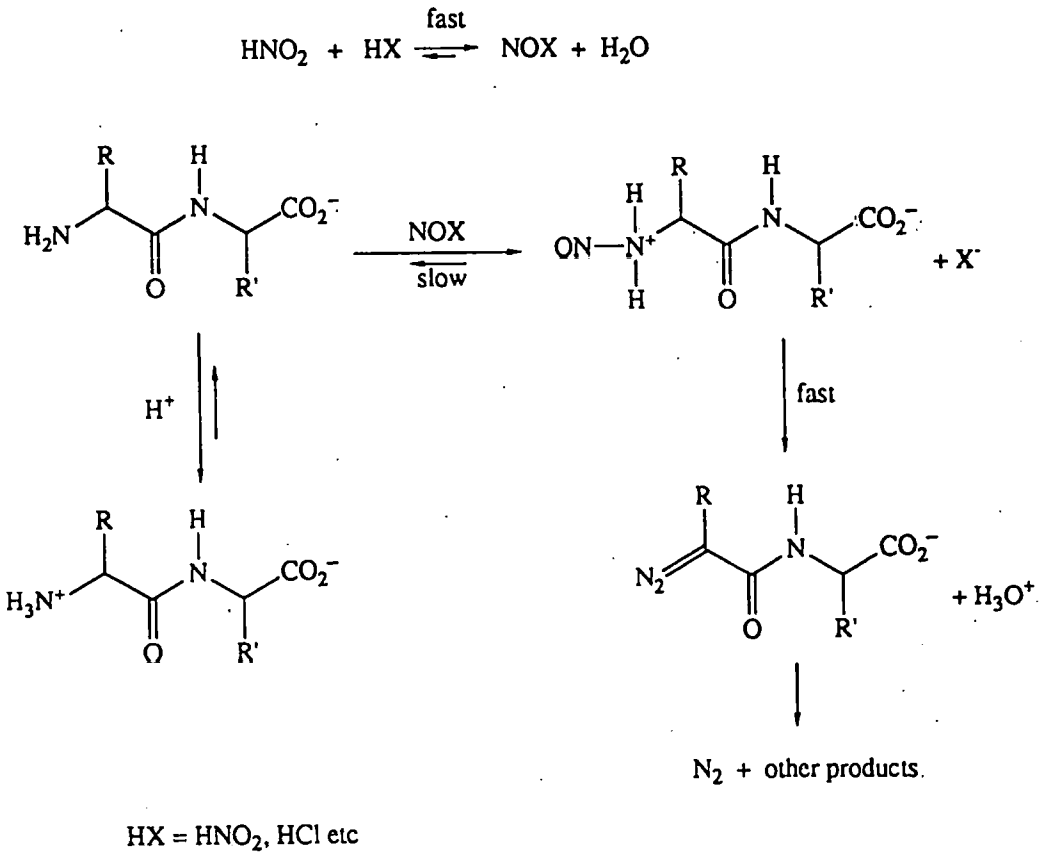

Kurosky and Hofmann[8] found the reaction of isoleucine methyl ester with nitrous acid at 4°C and pH 4 to have a linear dependence on the square of HNO_2 concentration, indicating that N_2O_3 was the reacting species. Challis et al[9] found that, for N-glycylglycine in dilute HCl at 37°C with nitrite < 1mM, the nitrosation was first order in peptide, nitrite and chloride ion. Thus, NOCl is likely to be the predominant nitrosating agent in normal gastric conditions where pH is 1-4 and nitrite concentration 1-10μm[10]. Under the same conditions, the nitrosation of N-acetylglycylglycine to give the N-nitroso compound was 20 times slower than that of N-glycylglycine to give the diazopeptide. Thus diazo derivatives are the most likely

products of the gastric nitrosation of peptides, but in acid conditions, these would readily decompose by loss of nitrogen ($t_{1/2}$<1s at normal gastric pH) and would be unlikely to cause genetic damage. Kinetic studies at pH 7.5 show that the stability of diazopeptides is decreased by electron donating substituents adjacent to the diazo group, which stabilise the carbonium ion generated by the expulsion of N_2[11].

In order to prepare a wider range of diazopeptides, including those with a free carboxylic acid terminus, aprotic nitrosation by N_2O_4 has been developed. Gaseous NO_2 reacts rapidly with peptides in aqueous buffers at pH > 6, to give diazopeptides, with similar yields from different peptide substrates[11]. For 0.1M N-glycylglycine and 200ppm NO_2 at 25°C, about 3.8% of the NO_2 forms N-(2-diazoacetyl)glycine at pH 6.8, and this rises to a maximum of 11.5% at pH 9.6, following the titration curve for the terminal primary amino group of the peptide. The reaction probably involves nitrosation of the peptide anion by an NO_2 dimer, followed by rapid loss of H_3O^+ (Scheme 1.3).

Scheme 1.3

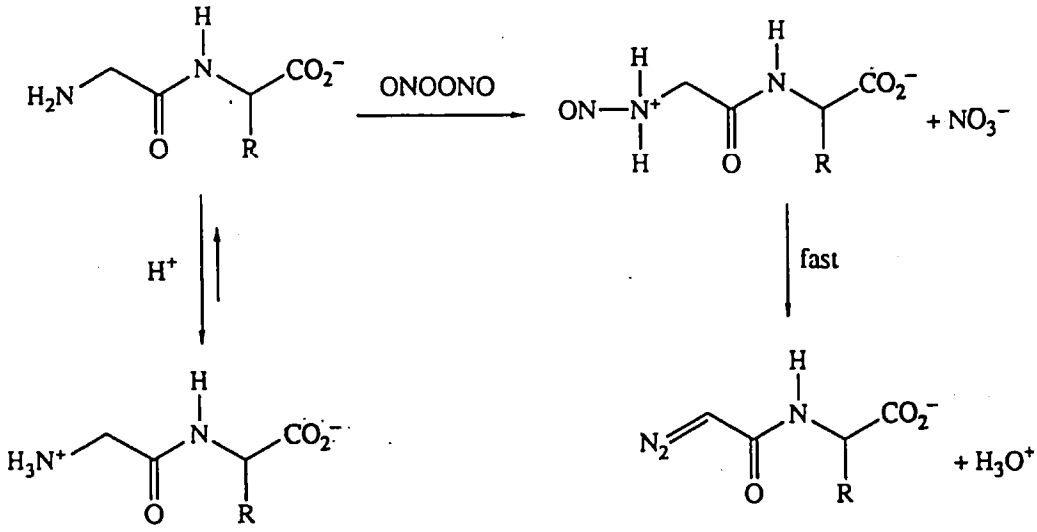

Diazopeptides are also produced in comparable yields from the reaction of NO_2 gas with peptides added to serum and whole blood[11]. It was found in animal studies that ca 60% of inhaled NO_2 gas is retained and that $^{13}NO_2$ can be detected in the lungs 20 minutes after exposure[12]. Diazopeptides may therefore be a factor in cancers associated with smoking and urban environments.

1.2.2 Chemical properties

Diazopeptides are alkylating agents as shown by the reaction of N-(2-diazoacetyl)glycine derivatives with γ-(4-nitrobenzyl)pyridine[13]. Nitrosation of peptides such as L-phenylalanyl-L-alanine was found by Pollock to produce N-nitrosodialkanoic acids[14]. This was confirmed using lower reactant concentrations[15] and also with gastric juice and nitrite[16]. The formation of N-nitrosodialkanoic acids is explained by an intramolecular Wolff rearrangement of the diazopeptide (Scheme 1.4).

Scheme 1.4

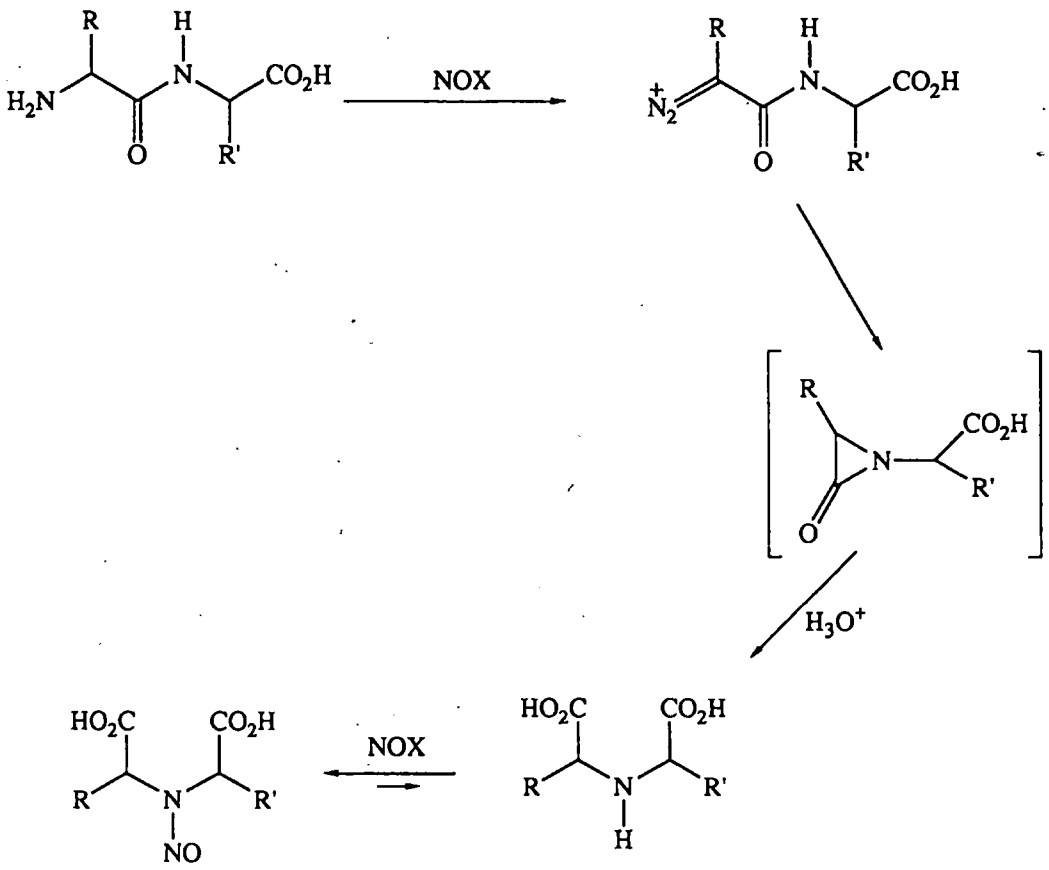

N-Nitroso dialkanoic acids are probably, like N-nitroso-α-aminoacids, non-carcinogenic.

Under alkaline conditions, diazopeptides cyclise to triazoles[17].

1.2.3 Biological properties

Baldini and Brambilla in 1966 tested six N-(2-diazoacetyl)glycine derivatives for antineoplastic activity in mice bearing Sarcoma 180 (solid and ascitic forms), Ehrlich carcinoma (solid and ascitic forms) and Harding-

Passey melanoma, and in rats bearing Galliera sarcoma[18]. They found that four N-(2-diazoacetyl)glycine derivatives, including the Curtius compounds, inhibited this range of tumours to varying degrees whilst two N-(N'-(2-diazoacetyl)glycyl)glycine derivatives were inactive. Giraldi and Nisi[19] in 1976 obtained similar results for the Ehrlich carcinoma as did Sava et al[20] in 1979 for leukaemia and melanoma in mice. A study[21] of mice bearing Lewis lung carcinoma, however, using the same compounds found that none caused marked inhibition of primary tumour growth but that N-(2-diazoacetyl)glycine amide and N-(N'-(2-diazoacetyl)glycyl) glycine amide caused different degrees of inhibition of lung metastasis formation. These diazopeptides are thus selective in their effects.

The carcinogenic activity of N-(2-diazoacetyl)glycine amide was established by Brambilla et al[22], who found that short treatments with relatively high doses of this compound induced pulmonary tumours and lymphatic leukaemia in both newborn and adult Swiss mice. In the Ames Test for mutagenesis[23], N-(2-diazoacetyl)glycine amide, N-(2-diazoacetyl)glycine ethyl ester and N-(2-diazoacetyl)glycine hydrazide were found to be very effective mutagens for strain TA1535 of *Salmonella typhimurium*, which is sensitive to base-pair substitution, but not for three other strains which are frameshift mutants. The results strongly suggest that these diazopeptides are able to alkylate bacterial DNA, the accepted mode of action for base pair substitution mutagens. Additional evidence to support this conclusion is provided by the fact that the mutagenic activity of these compounds is more pronounced in strains of *Salmonella typhimurium* which have a defect in the excision repair system[24].

N-(2-diazoacetyl)glycine amide, N-(2-diazoacetyl)glycine ethyl ester and N-(2-diazoacetyl)glycine hydrazide also show mutagenic activity towards Chinese hamster cells, in which all three induce 6-thioguanine resistant variants at non-cytotoxic concentrations[25]. N-(2-diazoacetyl)glycine amide shows dose dependent DNA damage in mouse cells *in vitro*[26]. This damage is slow to repair and can occur after incubation at 4°C in EDTA solution and so does not appear to require metabolic activation. A similar study using a range of diazopeptides found varying degrees of dose dependent unscheduled DNA synthesis for all the N-2-diazoacetyl derivatives tested[27]. Comparison of the unscheduled DNA synthesis produced by diazopeptides with their ability to alkylate γ-(4-nitrobenzyl)pyridine, showed a qualitative relationship[28].

N-(2-Diazoacetyl)glycine amide and three other diazoglycine derivatives show immunodepressive activity in mice for both the primary immune response to sheep erythrocytes and the allograft reaction[29]. The exponential dose-response curve obtained for N-(2-diazoacetyl)glycine amide suggests that its action is like that of an alkylating agent.

N-(2-Diazoacetyl)glycine derivatives show antibacterial activity[30]. Interestingly, N-(2-diazoacetyl)glycine ethyl ester, which is the most effective of the group in inhibiting bacterial growth, has no effect on tumour or immunocompetent cells. A similar group of N-(2-diazoacetyl)glycine derivatives show cytotoxic activity to human KB cells *in vitro*, which seems to be related to liposolubility[31]. 2-Diazoacetyl derivatives have been found to inhibit irreversibly or to denature several proteases[32 33 34].

Whilst there is not yet any direct evidence that the biological effects of diazopeptides are caused by their alkylation of DNA, this seems the most likely explanation.

1.3 N-Nitroso peptides

1.3.1 Synthesis

N-Nitrosopeptides were unknown until 1984, but are like N-nitrosamides in structure. The nitrosation of side-chains of α-acyl amino acid derivatives was observed by Bonnett and Nicolaidou[35 36]. Chow *et al* prepared N-acetyl-N-nitroso amino acids in solution [37 38] and Garcia[39] obtained either mono- or poly- N-nitroso derivatives of N-protected peptide esters, the product depending on steric effects. The first authentic N-nitrosopeptides were synthesised and characterised in 1984 by Challis *et al*[40 41]. The N-(N'-acetyl-L-prolyl)-N-nitroso derivatives of glycine, alanine and phenylalanine were prepared by NO_2 nitrosation of the corresponding benzyl esters, followed by catalytic hydrogenolysis.

A study[41] of the formation of N-nitrosopeptides by aqueous nitrite was carried out at 25°C in concentrated perchloric acid, where diazotisation of the terminal primary amino groups is minimised by extensive protonation. It found that the formation of N-nitrosopeptide followed Equation 1.1 and that k_2 values increased with acidity to reach a maximum in about 8M $HClO_4$.

$$\text{Rate} = k_2[\text{peptide}][HNO_2] \qquad \text{Equation 1.1}$$

This is consistent with a rate-limiting reaction of NO^+ with the conjugate acid of the peptide (Scheme 1.5).

Scheme 1.5

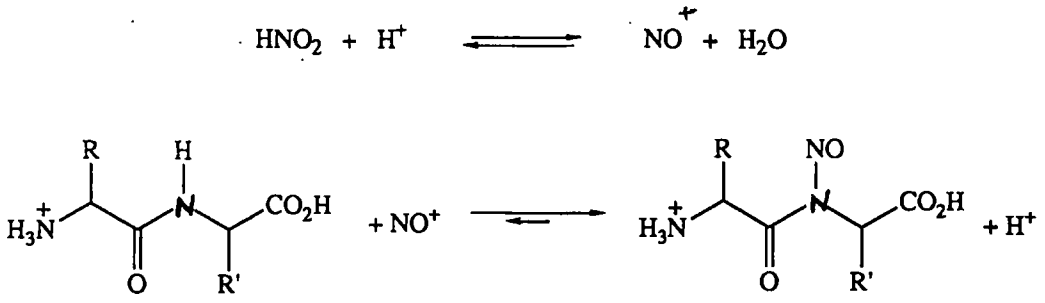

A second investigation of the nitrosation of N-acetylglycylglycine in aqueous buffers at pH 0-4 and 37°C found that these reactions also followed Equation 1.1[9]. The reactions were strongly catalysed by acid, but not by Cl^- or SCN^-. The diazotisation of N-glycylglycine was found to be about 20-fold faster than the nitrosation of N-(N'-acetylglycyl)glycine at pH 1 and 37°C, indicating that diazotisation will be the principal reaction of small peptides under gastric conditions.

1.3.2 Chemical properties

N-nitrosopeptides are relatively stable from pH 1-8 at 25°C. Below pH 1 (Scheme 1.6), decomposition proceeds via concurrent denitrosation to give the parent peptide (1) and hydrolytic deamination to give a diazotic acid (2) or, for longer chain peptides, a diazopeptide[42].

Of the two reactions, denitrosation is more highly acid catalysed and predominates at high acidity. Above pH 1, only deamination, catalysed by OH^-, thiols and amines, is important. The formation of the diazotic acid as a metastable intermediate is confirmed by the alkylation (by $CHRCO_2H$) of 4-(4-nitrobenzyl)pyridine and benzenethiol. Thus, N-nitrosopeptides could be stable enough to survive in the gastric tract and vascular system and to act as 'carriers' of diazotic acids or diazopeptides to remote parts of the body.

The mechanism of denitrosation and deamination (Scheme 1.7) of N-nitrosopeptides was studied by Challis et al[42]. The deamination reaction involves rate-limiting attack by H_2O on the O-conjugate acid formed in a rapid pre-equilibrium. For denitrosation, H^+ transfer to the peptide nitrogen atom is taken to be rate-limiting because of substantial normal solvent deuterium isotope effects. The N-conjugate acid thus formed breaks

down rapidly into products. The kinetics and mechanism for the decomposition of N-nitrosopeptides are thus very similar to those for N-nitrosamides[43].

Scheme 1.6

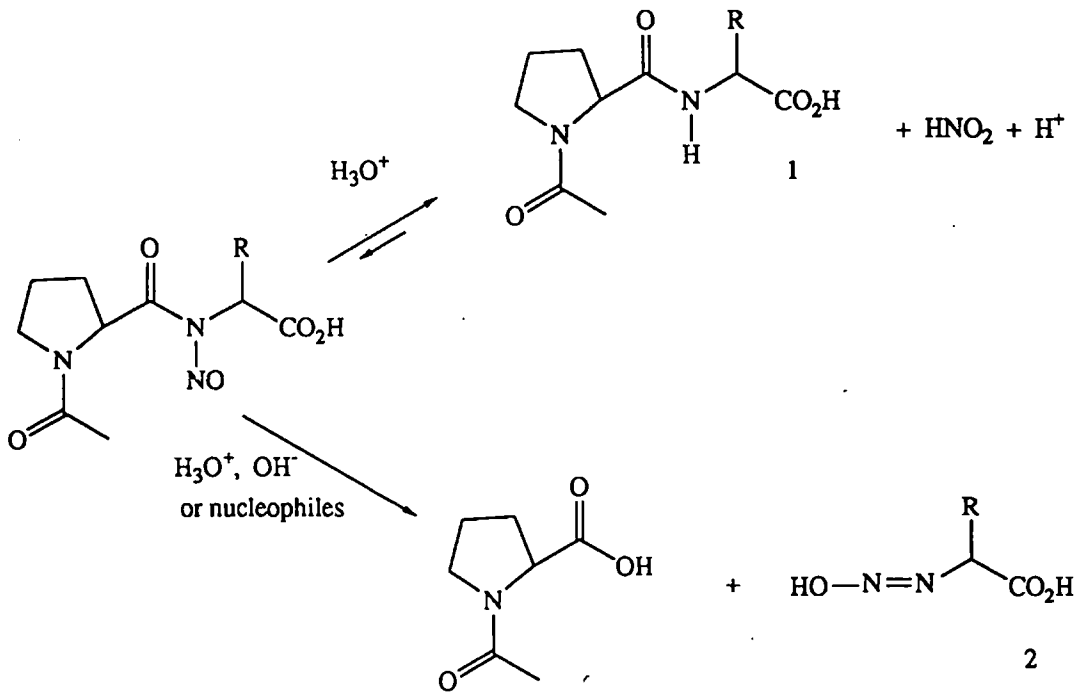

1.3.3 Biological Properties

Since N-nitrosopeptides decompose via diazopeptide intermediates[40], they might be expected to show similar biological properties. Both N-(N'-acetyl-L-prolyl)-N-nitrosoglycine and N-(N'-acetylvalyl)-N-nitrosoglycine are direct acting mutagens in vitro[44], giving a dose-related positive response in base-pair substitution in strain TA100 of *Salmonella typhimurium*. This occurs both with and without S9 activation. No dose-related effects were observed for N-(N'-acetyl-L-prolyl)-N-nitrosoglycine in the frame shift mutation-detecting strains.

The same two N-nitrosopeptides gave dose-related responses to genetic damage in Chinese hamster ovary cells[45], on all three indices of chromasome aberrations, sister chromatid exchange and the induction of 6-thioguanine resistant variants.

N-(N'-Acetyl-L-prolyl)-N-nitrosoglycine has an LD_{50} of 90-575mg/kg in rodents and is genotoxic *in vivo*[46]. The dominant lethal assay for mice showed an increase in late foetal deaths only and is attributed to genetic damage to the sperm. The micronucleus test gave a positive response.

Scheme 1.7

Mechanisms for concurrent denitrosation and deamination of N-nitrosopeptides in aqueous acid

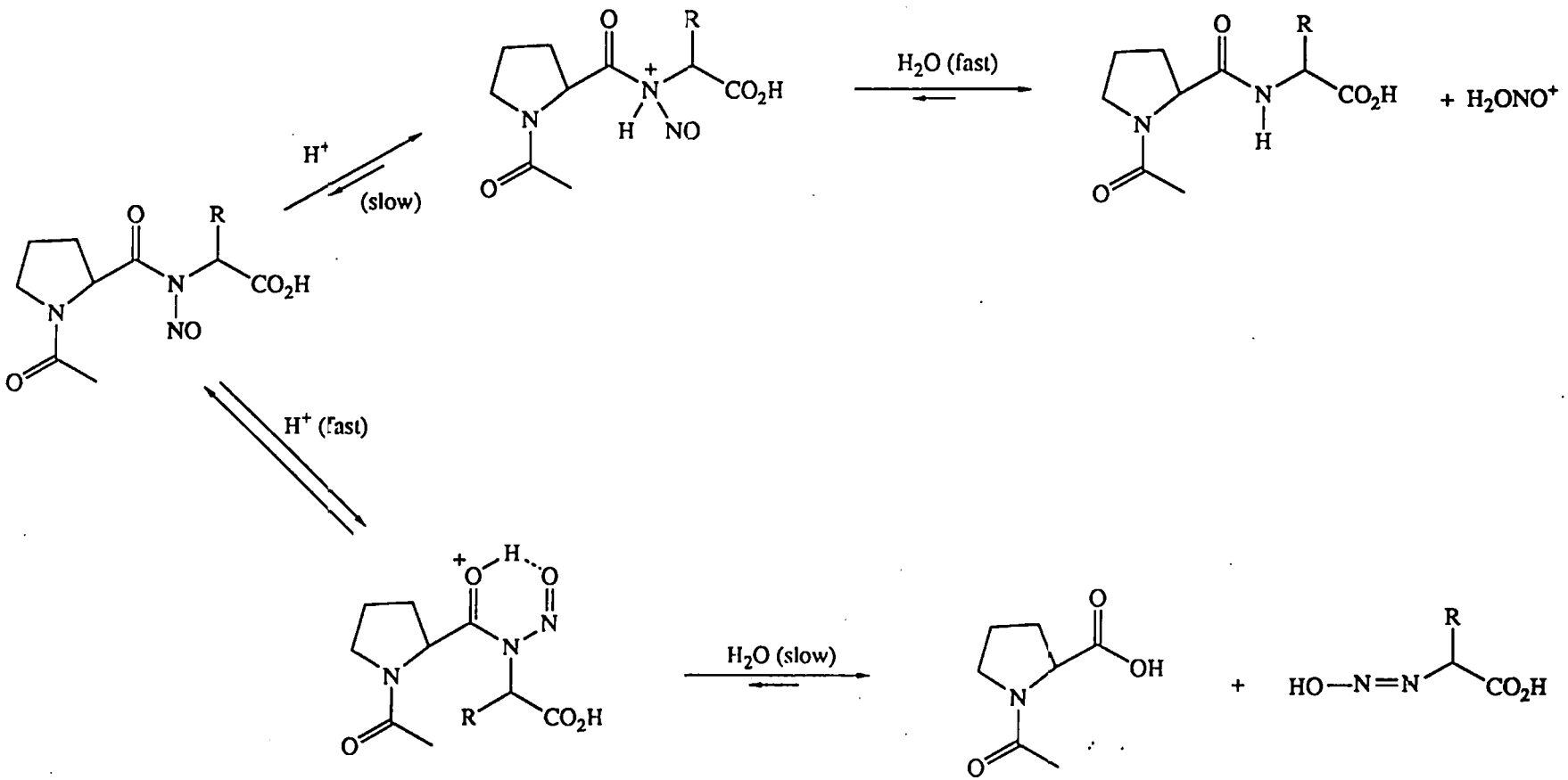

However, in the rat bone marrow metaphase analysis, no significant differences were seen between the incidences of chromosomal aberrations in the control and treated groups[46].

N-(N'-Acetyl-L-prolyl)-N-nitrosoglycine has been examined for mutagenicity in the mouse host-mediated assay using Salmonella typhimurium strain TA100[47]. This gave a dose related increase in revertants after oral or intraperitoneal administration, which disappeared after 30-40 minutes, suggesting that the mutagenic product of N-(N-acetyl-L-prolyl)-N-nitrosoglycine is short-lived *in vivo*.

1.4 Fourier transform infra-red (FTIR) spectroscopy

1.4.1 The use of FTIR to study peptide nitrosation

The biological effects of diazopeptides and N-nitrosopeptides are of sufficient concern for the compounds to merit further study. While attention has been given to the reactivity of diazopeptides, little is known about their rates of formation. The rates of formation and decomposition of N-nitrosopeptides have been studied, but the methods used have not allowed the identification of the site of nitrosation in the peptide chain.

Infra-red spectroscopy is a possible way to investigate the formation of diazopeptides because the diazo band near 2100cm^{-1} can be monitored. This band is well suited to the purpose, being intense and isolated. The requirement would be, after subtraction of the solvent, to obtain a high signal to noise (S/N) ratio in order to measure the low concentrations of diazo products.

The production of N-nitrosopeptides can be monitored using the intense carbonyl bands because conversion of a peptide NH to NNO causes the frequency of the adjacent CO vibration to increase by *ca* 100cm^{-1}. Thus, the nitrosation reaction can be followed either by the decrease in intensity of the peptide carbonyl band, or by the increase in intensity of the N-nitroso peptide carbonyl band. In this case, both a high S/N ratio and high resolution would be required because the several carbonyl bands of the peptide will occur in the same region of the spectrum. Provided that these carbonyl bands can be resolved, it should be possible to determine at which peptide residue nitrosation occurs.

For both types of compound, kinetic studies will require fast scanning and good instrument stability over hours or days.

Figure 1.1

The Michelson interferometer and interferograms of single frequency sources[50]

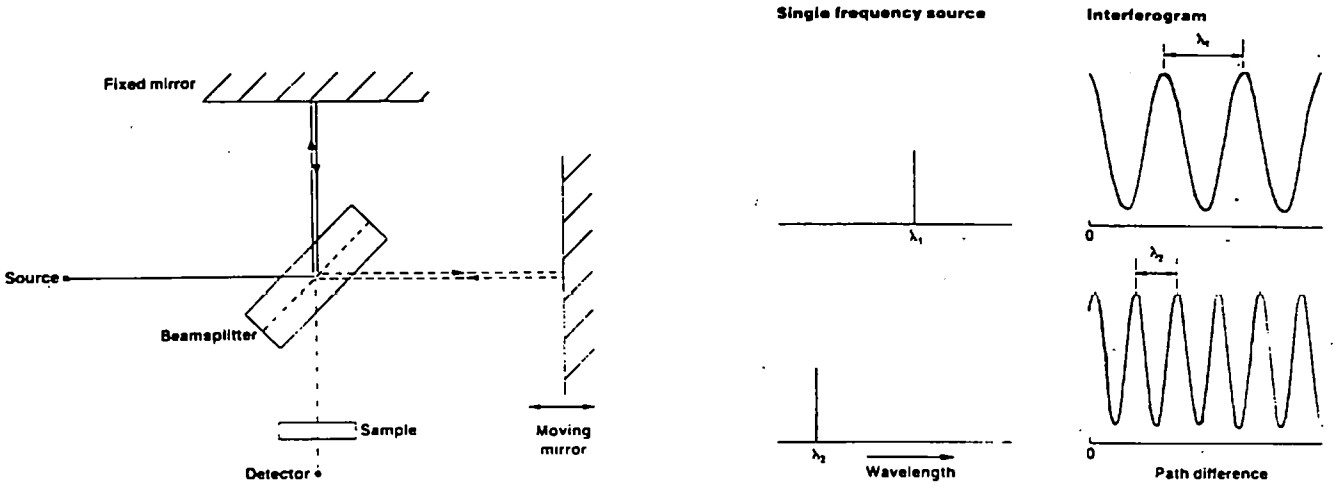

Figure 1.2

Use of laser signal to sample the IR interferogram[50]

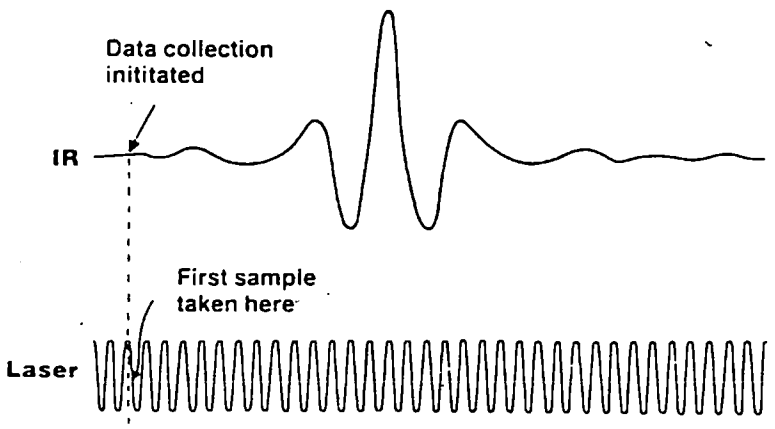

1.4.2 Principles of FTIR [48 49 50]

The FTIR spectrometer incorporates a Michelson interferometer in which the IR beam is divided at a beamsplitter (Figure 1.1): 50% strikes a moving mirror and the other 50% a fixed mirror before the beams recombine and proceed through the sample to the detector. As the mirror's position, and hence the path difference between the two parts of the beam varies, an interference pattern is obtained. The highest intensity of this interferogram is at its centre, which corresponds to the mid-point of the mirror's path. Here, there is zero path difference between the two halves of the beam so that all its component frequencies are in phase. On either side of the mid-point, the intensity falls off rapidly as various frequencies in turn interfere destructively. Thus, the interferogram is the sum of the interference patterns of all the component frequencies in the IR beam.

A reference laser beam follows the same two optical paths as the IR beam. The interference pattern of the single frequency of the laser beam is a sine wave which is measured by a separate detector. The maxima of this sinusoidal signal, which are separated by the laser wavelength, are used to trigger the sampling of the IR interferogram at equal steps in path difference (Figure 1.2). The interferogram, representing the IR beam energy as a function of path difference, may then be converted into a conventional spectrum, showing the beam energy as a function of frequency, by the mathematical procedure of the Fourier transform.

There are several advantages of the FTIR instrument over conventional, dispersive instruments. The interferometer measures all the IR frequencies simultaneously instead of successively, which allows many spectra to be obtained in the time that would previously have been needed for one. This is the Fellget or multiplex advantage. Because slits are not required, the energy throughput in the FTIR instrument can be higher for the same resolution than in the dispersive instrument. This is the Jaquinot or throughput advantage. These two effects allow the FTIR instrument to obtain the same S/N ratio as the dispersive instrument in a much shorter time.

As in a conventional spectrometer, signal to noise ratio, measurement time and resolution are related by the following 'trading rules':

1. $S/N \propto \sqrt{(\text{measurement time})}$ or $S/N \propto \sqrt{(\text{number of scans})}$

2. $S/N \propto (\text{resolution in } cm^{-1})$ with constant throughput

In some circumstances, it may be possible to open the Jaquinot stop to optimise the energy throughput, in which case

$$S/N \propto (\text{resolution in } cm^{-1})^2.$$

The time taken for a scan depends on the mirror velocity which in turn is determined by the detector in use. Of the two common detectors, the deuterated triglycine sulphate (TGS) detector is a pyroelectric device which operates at room temperature and is suitable for most normal applications, but requires a slow scan speed for maximum efficiency. The mercury cadmium telluride (MCT) detector is a photoconductive device which requires liquid nitrogen temperature. It can operate at faster scan speeds than the TGS detector, having a much better response at high modulation frequencies, and is about 10 times more sensitive. It becomes partly saturated, however, and produces distorted spectra at high beam energies.
The frequency scale of the FTIR spectrometer is provided by a laser. It is accurately known and has better long-term stability than the calibration of dispersive instruments.
An infinitely long sine wave contributing to the interferogram would produce, after the Fourier transform, an infinitely narrow line in the spectrum. In reality, the sine waves contributing to the interferogram are finite, decreasing in amplitude as the path difference increases, and produce spectral lines of finite width. The interferogram should be measured out to a path difference where the contribution from the narrowest line has been reduced to a negligible value. If this condition is not met, the resulting spectral line will be broadened and have sidelobes (Figure 1.3). These sidelobes can be reduced by a process called apodisation which involves multiplying the interferogram by a function which itself goes to zero at the maximum path difference. Apodisation causes further line broadening but reduces the noise in the final spectrum.

1.4.3 Summary

FTIR was judged to be a suitable method for investigating the formation of diazopeptides and N-nitrosopeptides for the following reasons. High sensitivity (ie S/N ratio) is achievable by averaging many scans, which can be run in a relatively short time with stable referencing to a fixed laser frequency. The detector and other scan conditions can be optimised for the purpose required. Modern developments in software allow solvents, air

Figure 1.3
The effect of apodisation[50]

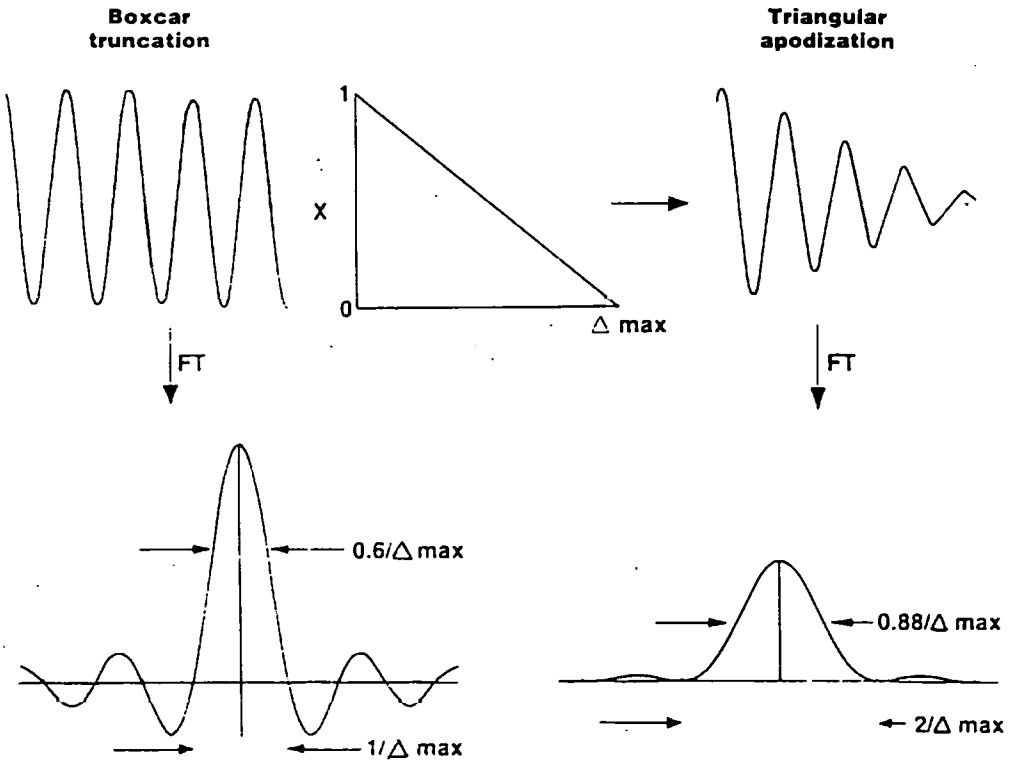

backgrounds and other interfering spectra to be subtracted accurately and easily. Diazopeptides and N-nitrosopeptides have intense IR bands which are suitable for monitoring the reactions. Hence, the present study.

Chapter 2

Results and Discussion 1

Method Development and Nitrosation of Amides

2.1 Introduction
2.2 The relevance of IR spectroscopy
2.3 The solvent
2.4 Temperature choice and control
2.5 Choice of cell, instrument and scan conditions
2.6 Preventing the decomposition of HNO_2
2.7 Quenching the reaction
2.8 Procedure for filling the IR cell
2.9 An internal standard
2.10 Evaluation of the kinetic procedure
2.11 Relation between FTIR absorbance and concentration
2.12 Trial nitrosations of 2-pyrrolidinone
2.13 Site of peptide nitrosation
2.14 Assignments of the carbonyl bands in N-(N'-acetylglycyl)glycine
2.15 The spectrum of N-(N'-acetyl-N'-nitrosoglycyl)glycine
2.16 Choice of concentrations for the kinetics of the nitrosation of N-(N'-acetylglycyl)glycine

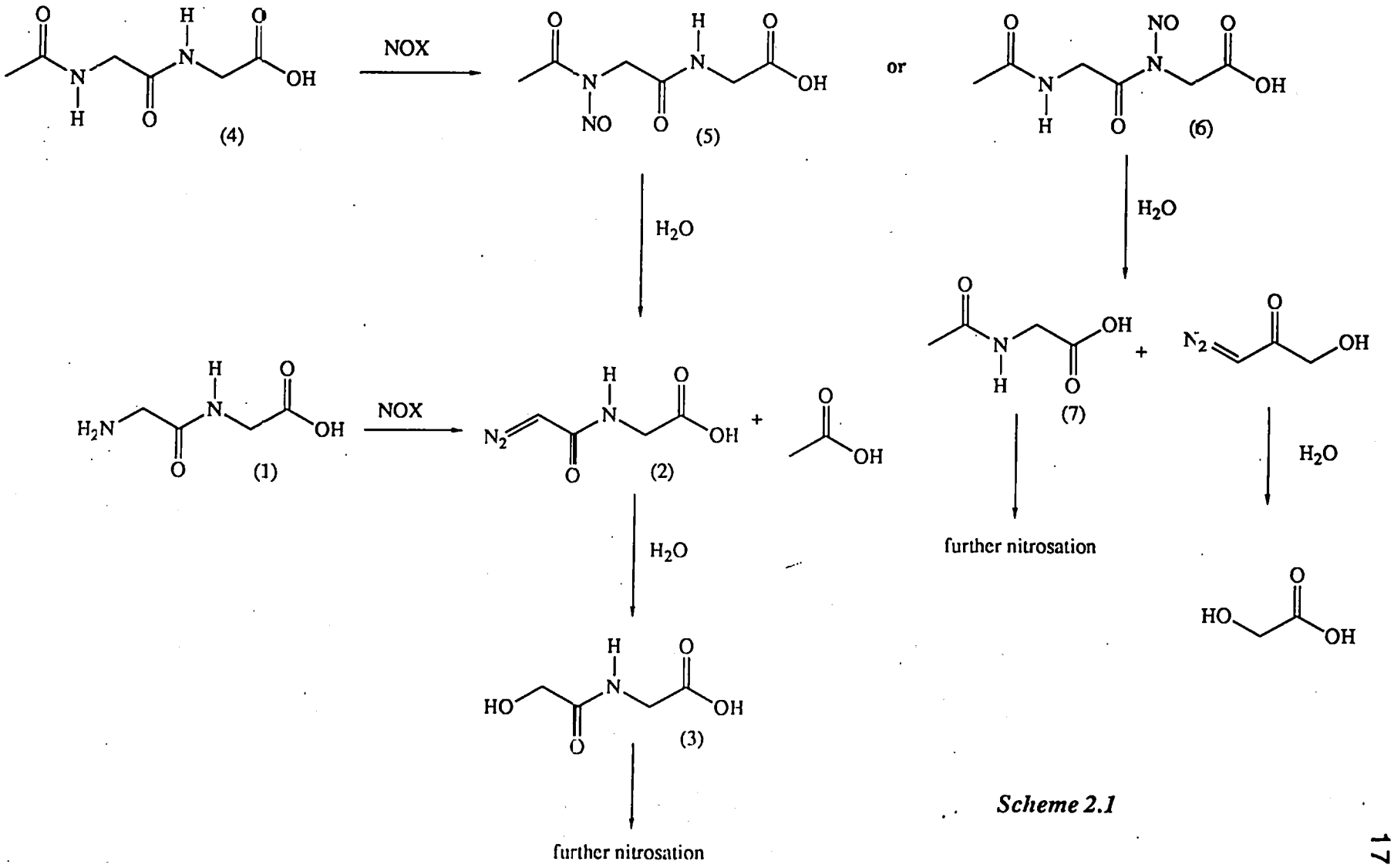
NOX
(4)
(5)
or
(6)
H_2O
NOX
(1)
(2)
(7)
H_2O
H_2O
further nitrosation
(3)
H_2O
further nitrosation

Scheme 2.1

2.1 Introduction

In principle, N-nitrosation can occur at any N-H group in the peptide moiety, so there are several possible sites for reaction. For a simple dipeptide such as N-glycylglycine (1), nitrosation in dilute acid (< 2M) preferentially proceeds at the terminal primary amino groups to give initially the diazopeptide (2), which is rapidly hydrolysed to N-(2-hydroxyacetyl)glycine (3) or, in the presence of chloride ion, N-(2-chloroacetyl)glycine (Scheme 2.1). This reaction can be circumvented, however, by using N-(2-acetylglycyl)glycine (4) where the N-terminal of the peptide is deactivated by the N-acetyl group. Nitrosation must then proceed at either one of the two peptide (amide) N-atoms. The resultant N-nitrosopeptides (5 and 6) may hydrolyse under the reaction conditions via the respective diazo intermediates to the corresponding products (3 and 7). Under appropriate conditions (eg excess HNO_2) the products (3) and (7) may undergo further nitrosation and hydrolytic decomposition[51].

While peptide nitrosation is now well-known, no information is available about the relative reactivities of N-atoms in the peptide chain, and therefore the preferred reaction site. Such information may be important, however, because site of nitrosation could affect the carcinogenic activity of the N-nitroso product.

A purpose of the present study was to examine the utility of IR spectroscopy for studying peptide nitrosation and revealing the preferred reaction site.

2.2 The relevance of IR spectroscopy

IR spectroscopy is a possible way to investigate peptide nitrosations because the C=O bands are intense and easily identified. On nitrosation of the N-H group adjacent to C=O in a peptide link, the electron withdrawing effect of N-N=O increases the frequency of the C=O moiety by about $100cm^{-1}$[52]. Hence nitrosation can be followed by both the loss of peptide (amide) and the appearance of N-nitrosopeptide bands. In due course, the N-nitrosopeptide band will itself disappear due to further reaction.

The introduction of Fourier transform (FT) methods into IR spectroscopy has facilitated the acquisition of IR spectra of relatively dilute solutions in IR absorbing media, including aqueous solutions. Thus, FTIR procedures seemed suitable for studying peptide nitrosation reactions, provided that the measurements could be carried out quantitatively. Much of the early work on the project (reported briefly below) therefore involved a critical

Figure 2.1

Solvent spectra at 25°C

(a) H_2O (50μm)

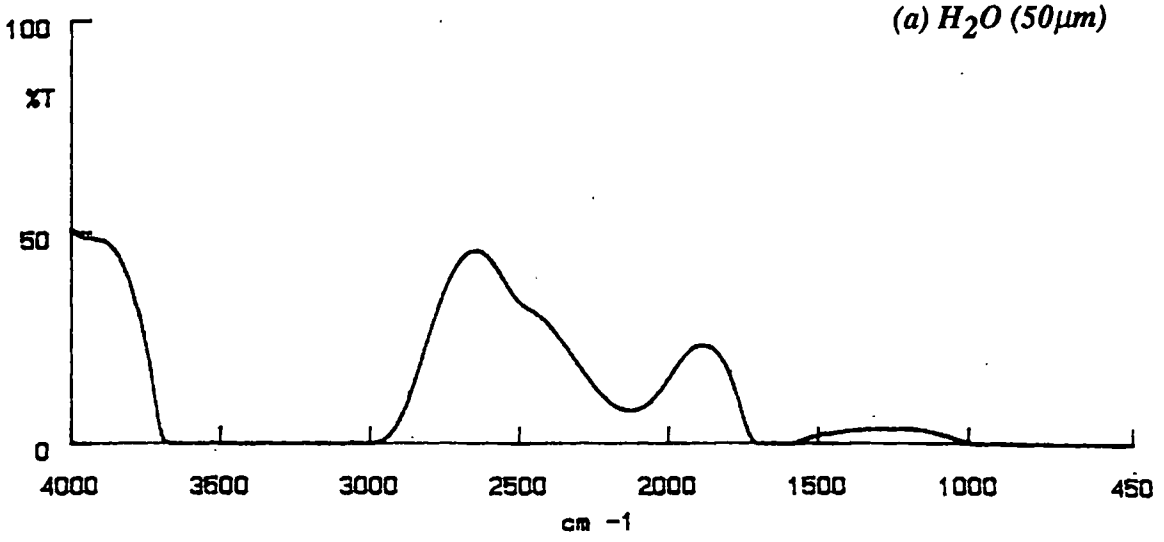

(b) D_2O (50μm)

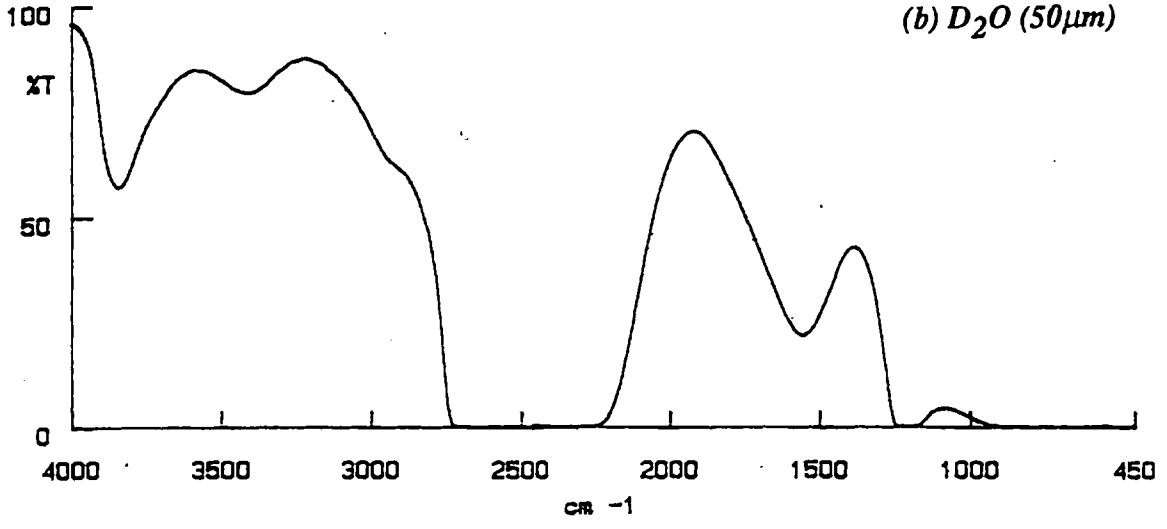

(c)1.0M DCl (50μm)

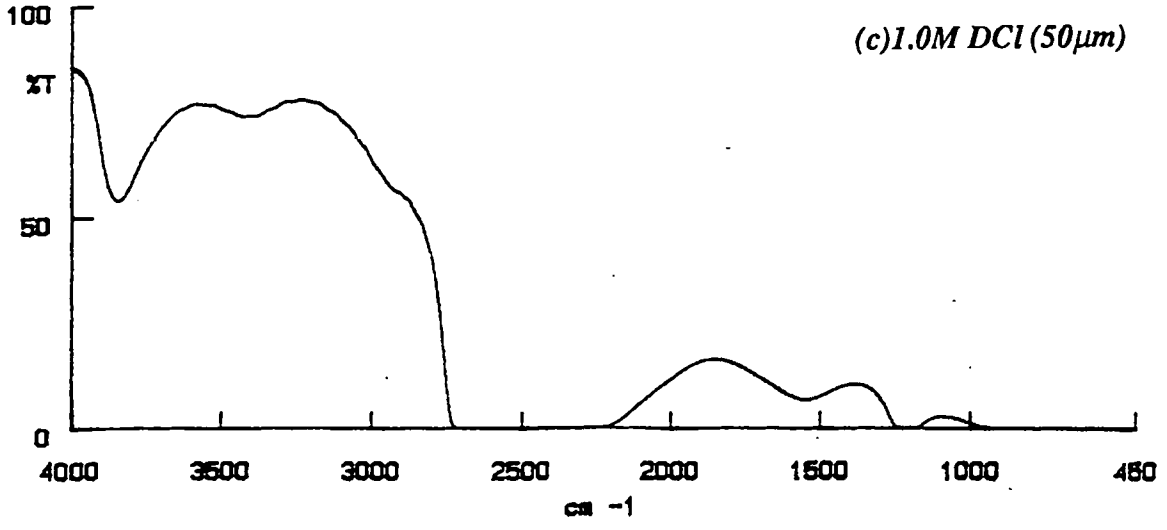

Figure 2.2

FTIR spectra of D_2O at different temperatures (50μm)

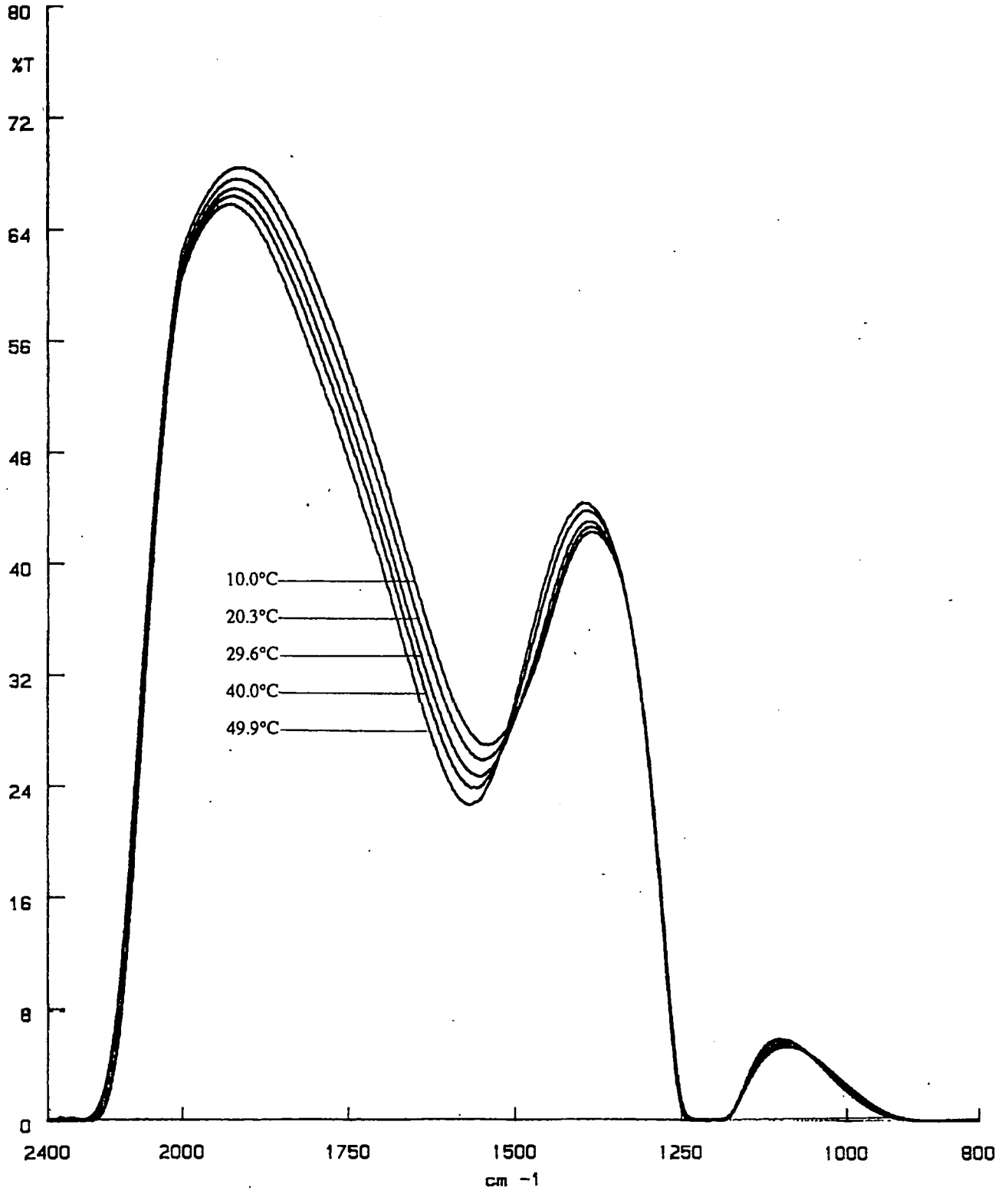

evaluation of the design and utility of FTIR spectroscopy to assay peptide moieties in aqueous media. The Perkin-Elmer 1710 instrument was used.

2.3 The solvent

Peptide nitrosation reactions in biological systems take place in what are best regarded as aqueous media. Carbonyl absorptions of peptides and N-nitrosoderivatives are observed in the region 1400-1800cm^{-1}. The spectrum of water (Figure 2.1a), however, shows a region of zero transmittance between 1500 and 1700cm^{-1}, at 50μm pathlength. A shorter pathlength increased transmittance but decreased sensitivity to the peptide solutes. The D_2O spectrum (Figure 2.1b) is shifted to lower frequencies which means that the required region is clear. Even in 1M DCl (Figure 2.1c), the minimum transmittance at 1400-1800cm^{-1} and 50μm pathlength is 5%, which is acceptable. D_2O was therefore used as the solvent for the peptide nitrosations. Clearly, this means that all hydrogen atoms in peptide N-H and O-H bonds will exchange with the solvent.

2.4 Temperature choice and control

Preliminary experiments showed that the infra-red absorption spectrum of the D_2O solvent was temperature dependent. Results in Figure 2.2 for D_2O in a 50μm pathlength cell show that both the position and intensity of the D_2O absorption bands vary with temperature. Thus, both the absorption maximum at ca 1550cm^{-1} and the absorption minimum at ca 1330cm^{-1} shift to lower frequencies and decrease over the temperature range 10°C - 50°C. Since the changes in peptide substrate absorptions are smaller than those of the D_2O solvent, it is necessary to control the IR cell temperature to obtain reliable quantitative data. In the present investigation, the cell was maintained at 25°C ± 0.2°C. Inspection of Figure 2.3 shows that, at each of the C=O frequencies of N-(N'-acetylglycyl)glycine, AcGlyGly, (Figure 2.6), the change in D_2O solvent absorption is less than 5.0 x 10^{-4}A for ± 0.2°C, which is unlikely to perturb the acquisition of reliable quantitative data. The cell temperature of 25°C is arbitrary because the reaction solutions are quenched before quantitative assay (see below). It was originally chosen, however, in the hope that the peptide nitrosation reactions could be carried out in the infra-red cell itself.

Figure 2.3
Absorbance of D_2O against temperature at the carbonyl band frequencies of AcGlyGly

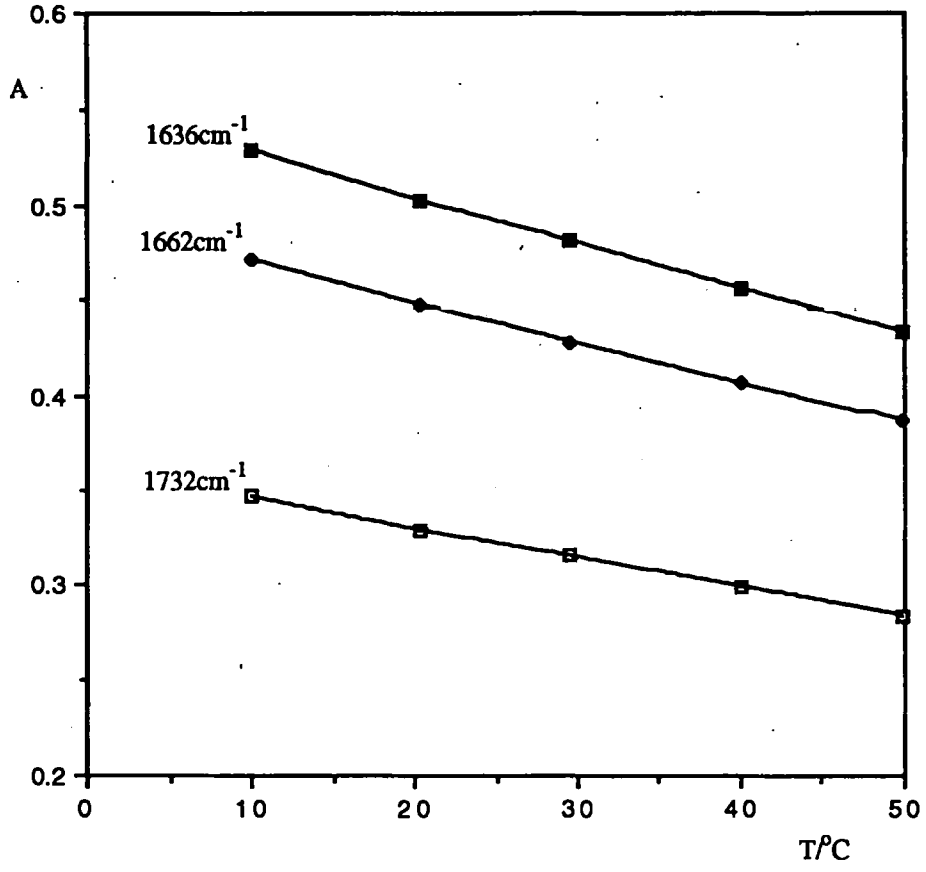

Figure 2.4a

Background (air in spectrometer sample chamber)

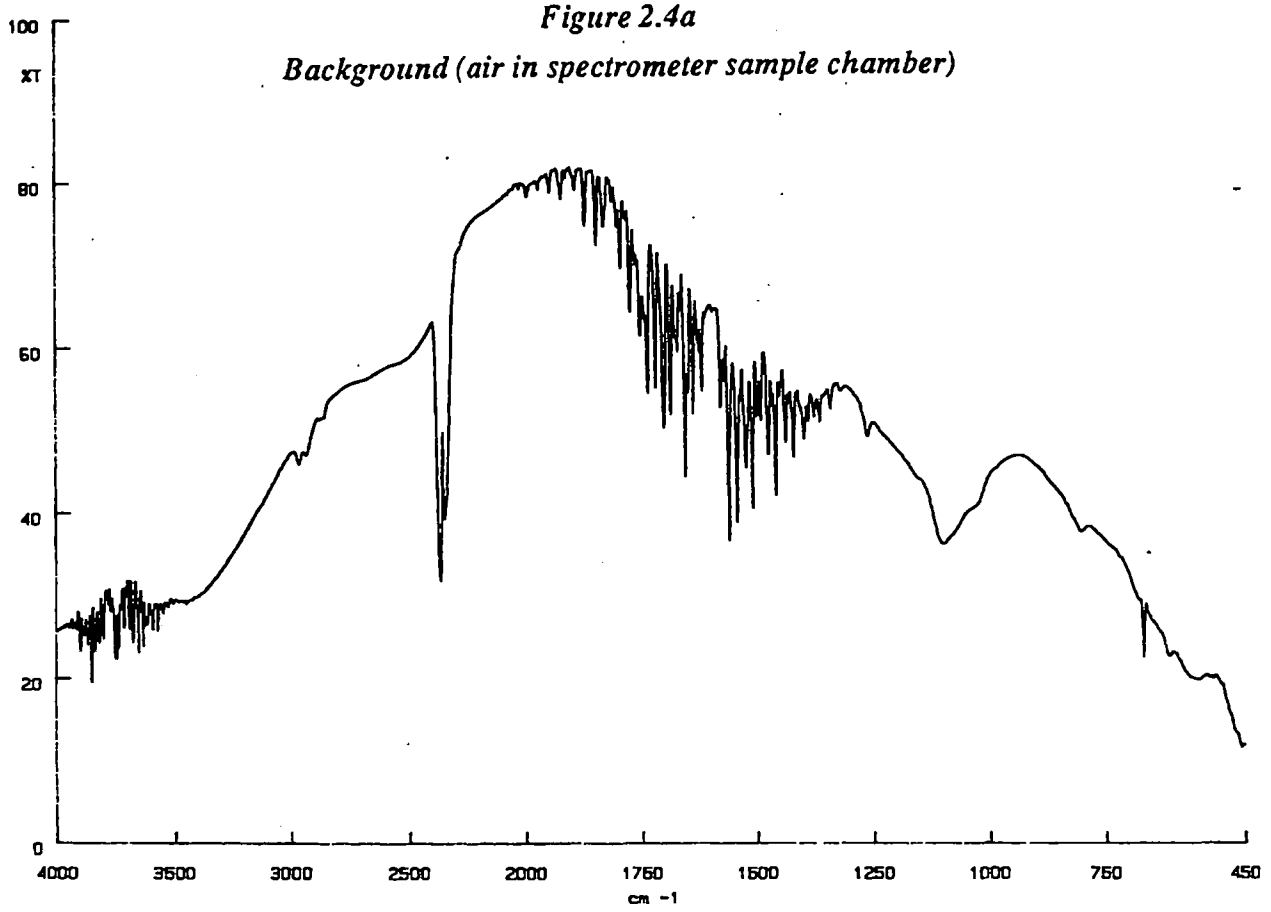

Figure 2.4b

Background after 15min purge

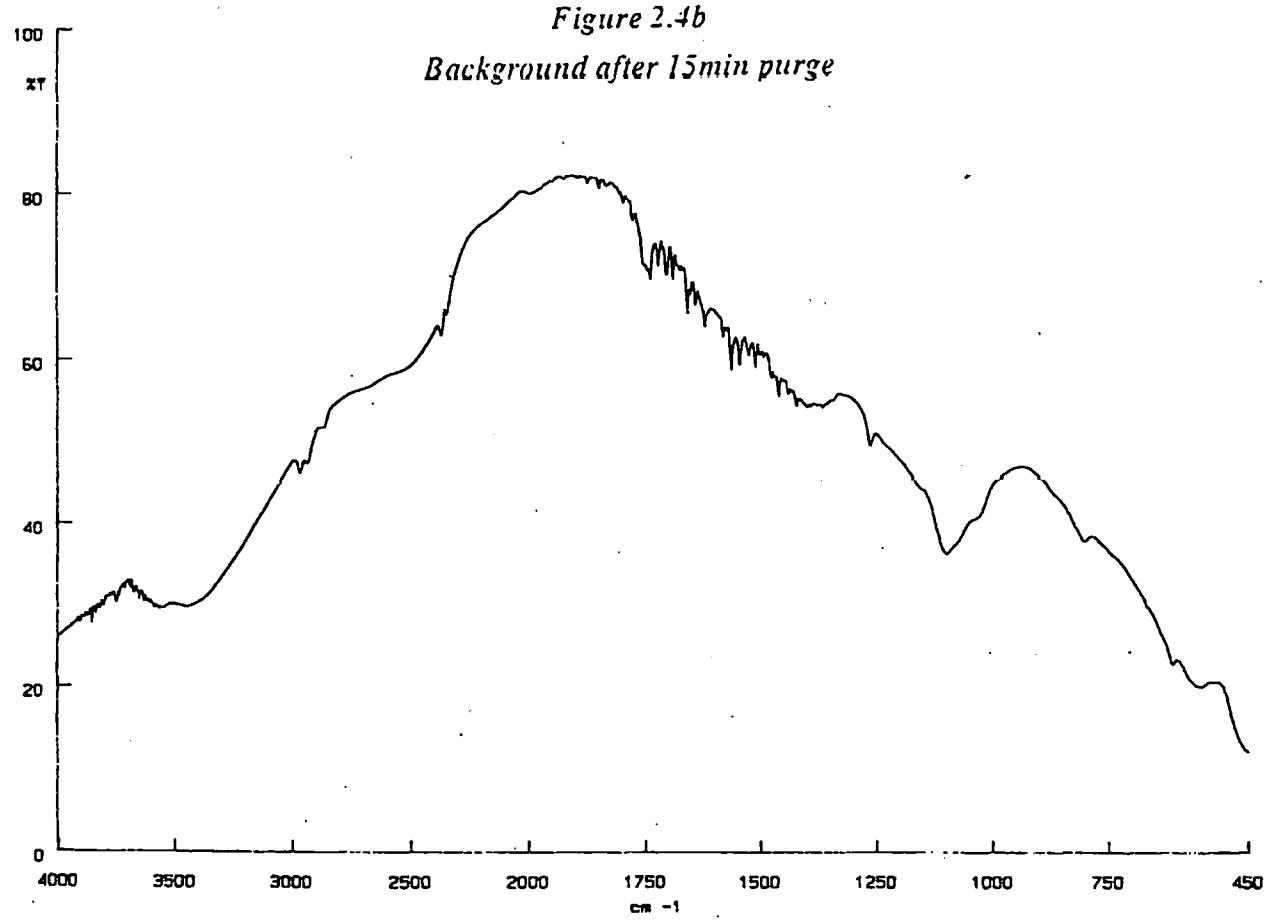

2.5 Choice of cell, instrument and scan conditions

To observe small changes in the peptide carbonyl absorbances, it is necessary to eliminate the water vapour bands which occur in the same region of the spectrum (Figure 2.4). For this reason, the infra-red instrument was purged continuously with dry nitrogen and a sample shuttle was employed. The sample shuttle continuously moves the infra-red cell into and out of the beam. This allows continuous interleaving of background spectra with sample spectra, rather than obtaining a background spectrum only at the beginning and end of each quantitative measurement. The only suitable detector using the sample shuttle is then the deuterated triglycine sulphate (TGS) detector.

Initially, it was hoped to carry out the peptide nitrosation reactions directly in a Circle cell. This proved unsuitable, however, because the zinc selenide crystal quickly became opaque on contact with the reaction solution, presumably because it was oxidised by the HNO_2. It was therefore decided to use conventional infra-red solution cells, fitted with windows resistant to aqueous (D_2O) solutions. Experiments with AgCl windows showed that the peptide substrate interacted with the window material. A sticky film collected on the surface and the cell required dismantling and cleaning before every experiment. The formation of Ag-amine complexes is well-documented[53]. This left calcium fluoride as the only suitable cell window material, being both transparent in the region of interest and reasonably resistant to attack by aqueous solutions of nitrous acid and peptide. In practice, it was found that calcium fluoride solution cells could be used for up to 20 reactions without significant deterioration of spectrum quality.

In other preliminary experiments using N-(N'-acetylglycyl)glycine as a typical substrate, it became apparent that, under a wide range of instrument conditions, the overlapping peptide (amide) bands at 1663 and 1636cm^{-1} in the zero order spectrum (Figure 2.5) were too broad to be resolved. This problem was overcome by using the second derivative spectrum as shown in Figure 2.6. Within the constraints imposed by the use of conventional calcium fluoride solution cells, sample shuttle operation using the TGS detector and second order spectra, a wide range of instrument and reaction conditions was examined to optimise the acquisition of quantitative data. This involved combinations of the following variable parameters:

Figure 2.5

AcGlyGly in 1.0M DCl at 25°C, zero order

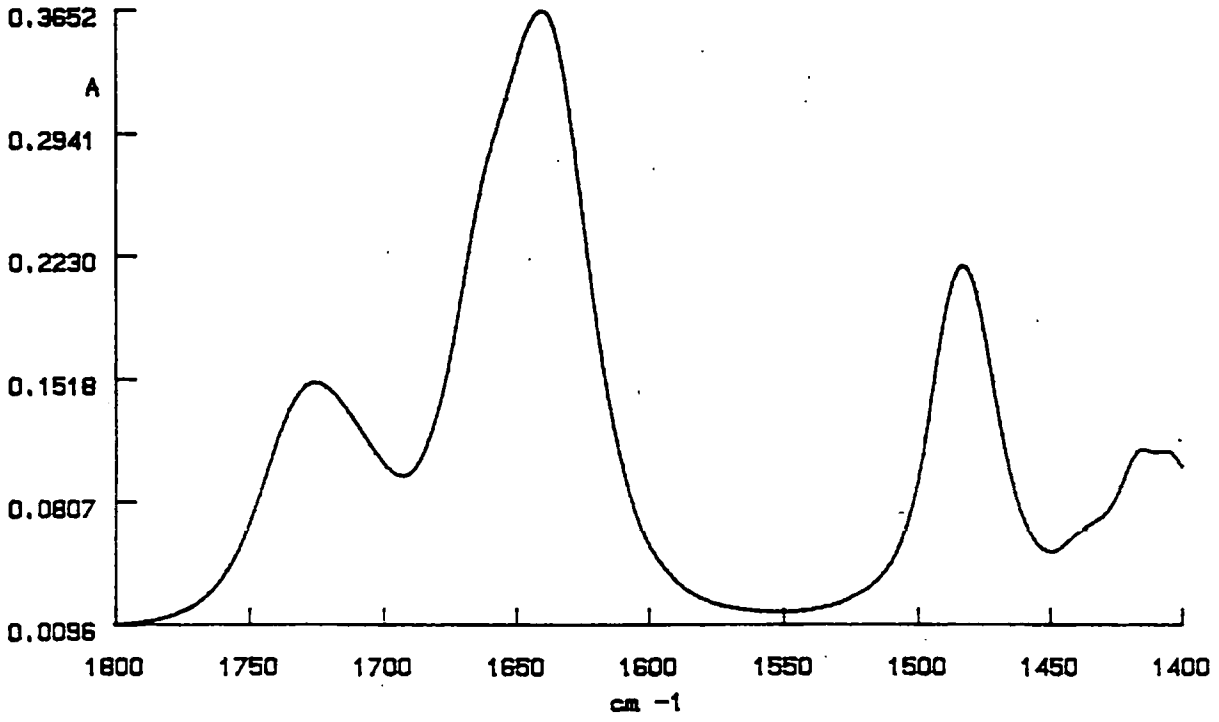

Figure 2.6

AcGlyGly in 1.0M DCl at 25°C, 2nd derivative

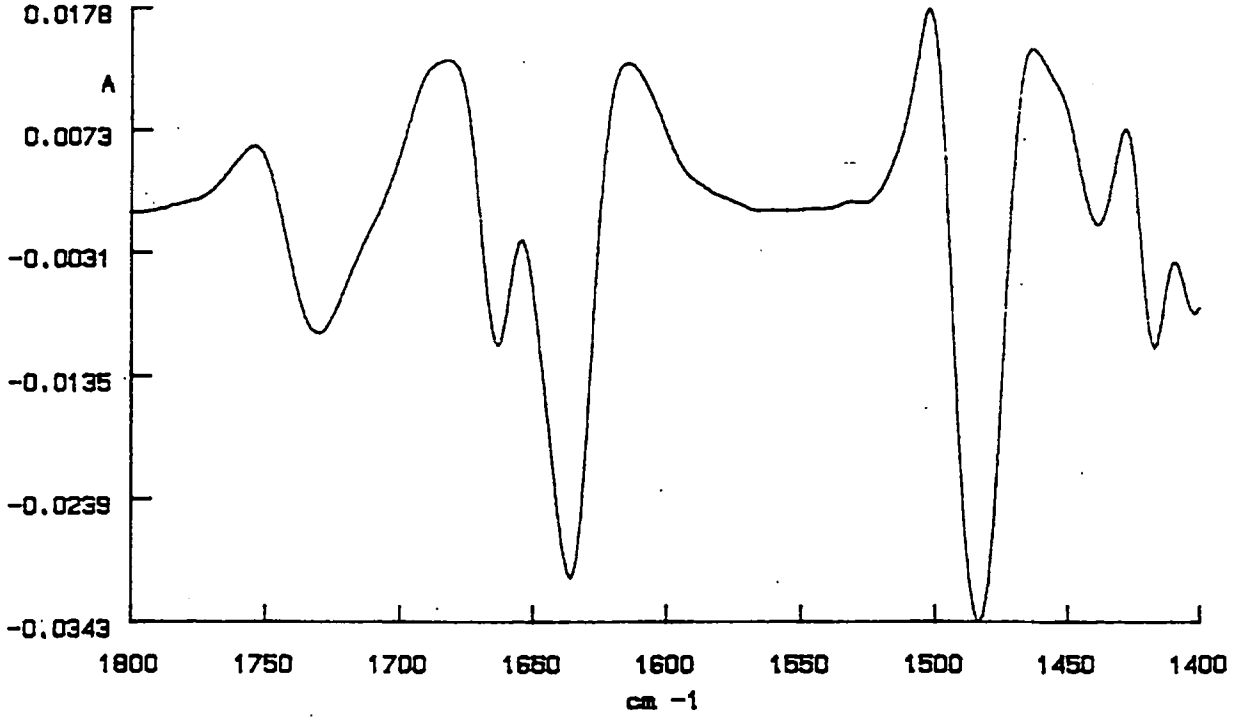

Concentration of AcGlyGly	0.03, 0.01, 0.005M in D_2O.
Number of scans	8, 16, 32, 48, 64, 80, 96, interleaved
Cell pathlength	50, 100μm
Resolution	2, 4, 8cm^{-1}

For each set of conditions, the noise level in the region 1500 - 1600cm^{-1} was compared with the strongest carbonyl absorption of N-(N'-acetylglycyl)glycine at 1636cm^{-1}. The following conditions were found to give the best signal to noise ratio and these were therefore used for the kinetic studies.

Detector	TGS
Number of scans	48 or 64 interleaved
Pathlength	50μm
Resolution	4cm^{-1}

The experiments also showed that the lowest peptide concentration suitable for reliable quantitative work is of the order of 0.01M.

2.6 Preventing the decomposition of HNO_2

In acid media at 25°C, HNO_2 is unstable and decomposes to form a mixture of nitric oxide (NO) and nitrogen dioxide (NO_2) (Scheme 2.2).

Scheme 2.2

$$2HNO_2 \rightleftharpoons N_2O_3 \rightleftharpoons NO + NO_2$$

Bayliss and Watts[54] found that the rate of decomposition depended on $[HNO_2]^2$ and the acidity, reaching a maximum in about 50% by mass H_2SO_4. Further, the decomposition rate increased when the gaseous NO and NO_2 products were purged from the reaction solution. It follows that in the course of a peptide nitrosation at 25°C, the decomposition of HNO_2 could perturb the acquisition of reliable kinetic data. In preliminary experiments, it was found that loss of nitrite on mixing the reacting solutions could be minimised by precooling the solutions to 0°C, but some effervescence still occurred. Independent experiments showed that the nitrite loss in aqueous acid was prevented by carrying out the reaction in vials filled to the brim and closed with a PTFE coated septum and screw ring in such a way as to be airtight, without air trapped inside.

Measurements were carried out as in Section 5.3.4 and results in Table 2.1 show that the concentration of nitrite (0.4M $NaNO_2$) in HCl (1.0M) at 25°C remains constant over about 8h in sealed vials containing no air. By comparison, the same concentration of nitrite in reaction tubes at 25°C with an air space above the solution showed a loss of 85% over 5h, even in glass vials sealed in a flame. Consequently, peptide nitrosation reactions were carried out in screw sealed vials filled to the brim.

Table 2.1

Loss of nitrite from reaction vials at 25°C

Screw-top/air		*Flame-sealed/air*		*Screw-top/no air*	
t/min	A(541nm)	t/min	A(541nm)	t/min	A(541nm)
0	0.310	0	0.249	0	0.325
101	0.135	58	0.155	60	0.324
160	0.093	152	0.081	240	0.325
250	0.057	279	0.034	510	0.331
				1380	0.310

2.7 Quenching the reaction

At the outset, it was envisaged that if possible, the peptide nitrosations would be carried out and monitored continuously in the infra-red cell. This procedure was quickly abandoned, however, because concurrent decomposition of the HNO_2 affected the kinetic integrity and produced gas bubbles which perturbed the acquisition of reliable spectra. This led to the use of sealed vials, containing aliquots of the reaction solution, each of which was analysed by FTIR at timed intervals. This procedure also was unsatisfactory because effervescence occurred as soon as the vials were opened for sampling. The bubbles generated in the IR cell led to erroneous absorbance measurements or even prevented the spectrum from being seen at all. To prevent this, an aliquot was therefore transferred from the reaction vial to a flask containing sulphamic acid (1.4M in D_2O) to remove unreacted HNO_2. The transfer was made quickly so that the drop of solution displaced from the pipette tube by the nascent gas did not grow big enough to fall from the tip. The sulphamic acid destroyed excess nitrite (Scheme 2.3) and the gaseous products of the reaction escaped within 10 min, to allow the IR spectrum to be run reliably in the normal way.

Scheme 2.3

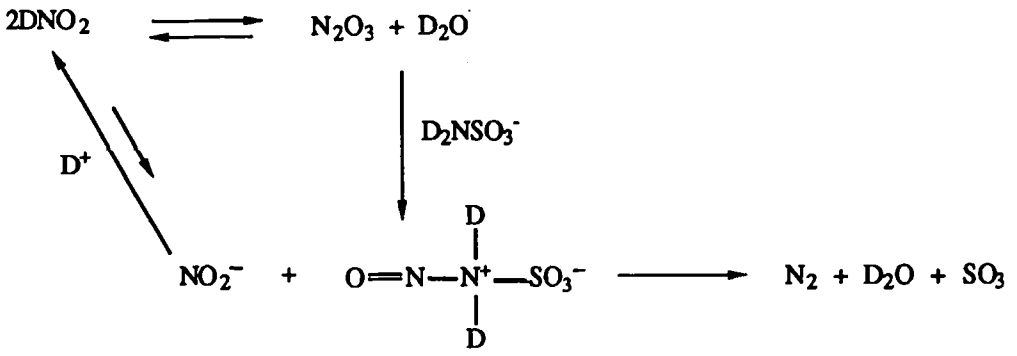

Independent experiments established that the use of sulphamic acid did not interfere with the results. Thus, the sulphamic acid IR spectrum (Figure 2.7) has no bands between 1400 and 1800cm^{-1}. The only interference with the peptide IR spectrum is the increased intensity of the HOD bands caused by exchange of the sulphamic acid protons with D_2O. This can be dealt with by the normal subtraction procedure (Section 5.3.1).

Figure 2.7
Sulphamic acid in 1.0M DCl at 25°C, 2nd derivative

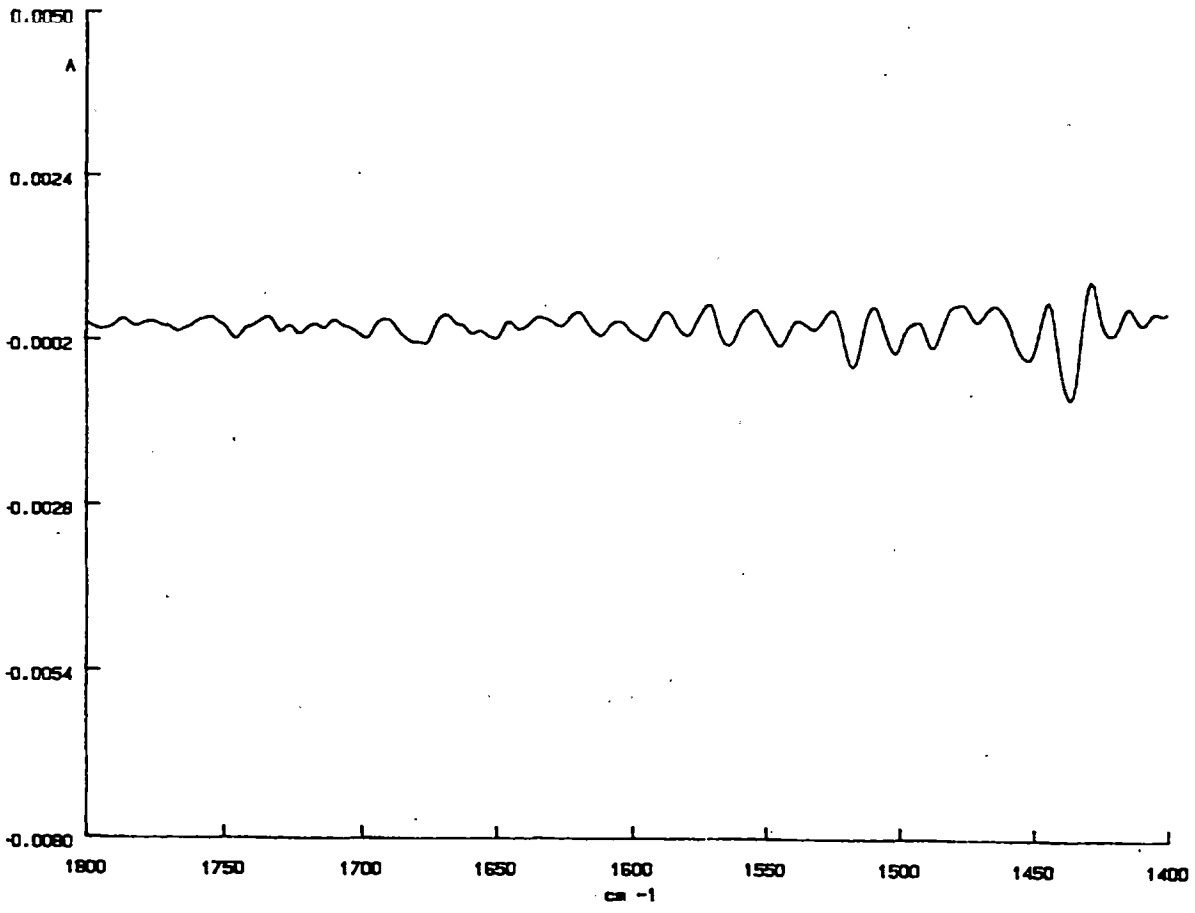

To check whether sulphamic acid reacts with the N-nitrosopeptide product, a saturated solution of N-acetyl-N-nitrosoglycylglycine benzyl ester in water was placed in a 1cm cell in a UV-visible spectrophotometer. The absorbance at 410nm, due to the N-nitrosopeptide ester, when measured at timed intervals after adding a few crystals of sulphamic acid, remains constant for 2h at 25°C (Table 2.2), showing that negligible reaction occurs in the time (15-30min) between quenching the reaction solution with sulphamic acid and running the FTIR spectrum.

Table 2.2

Absorbance of Ac(NO)GlyGly in the presence of H_2NSO_3H at 25°C

t/min	A(410nm)
0	0.225
15	0.230
35	0.220
43	0.215
82	0.210
119	0.205

2.8 Procedure for filling the IR cell

When fitted with a 50μm spacer, the IR solution cell had a volume of $1.6x10^{-2}cm^3$, with ports top and bottom to allow the solution to flow through. It could be filled by removing the cell from the instrument, introducing the solution from a syringe at the lower port and allowing the excess to flow out at the top. Alternatively, the cell could be filled with entry and exit tubes (PTFE, 0.6mm bore, length 50cm, volume $0.14cm^3$) and filled by syringe from outside the instrument without removing the cell from its holder. Independent checks using a solution of N-n-butyl acetamide (0.1M in M DCl) were carried out to see whether either method was preferable.

The instrument settings were those in Section 2.5. Four consecutive spectra taken without removing the cell from the instrument gave absorbance differences of ±4% on the $1615cm^{-1}$ band. When the cell was removed and replaced between readings, four consecutive spectra gave absorbance differences of ±6% on the same band. External filling was therefore chosen for the reaction spectra. It also had the advantage of

Figure 2.8

2-pyrrolidinone at 25°C, 2nd derivative

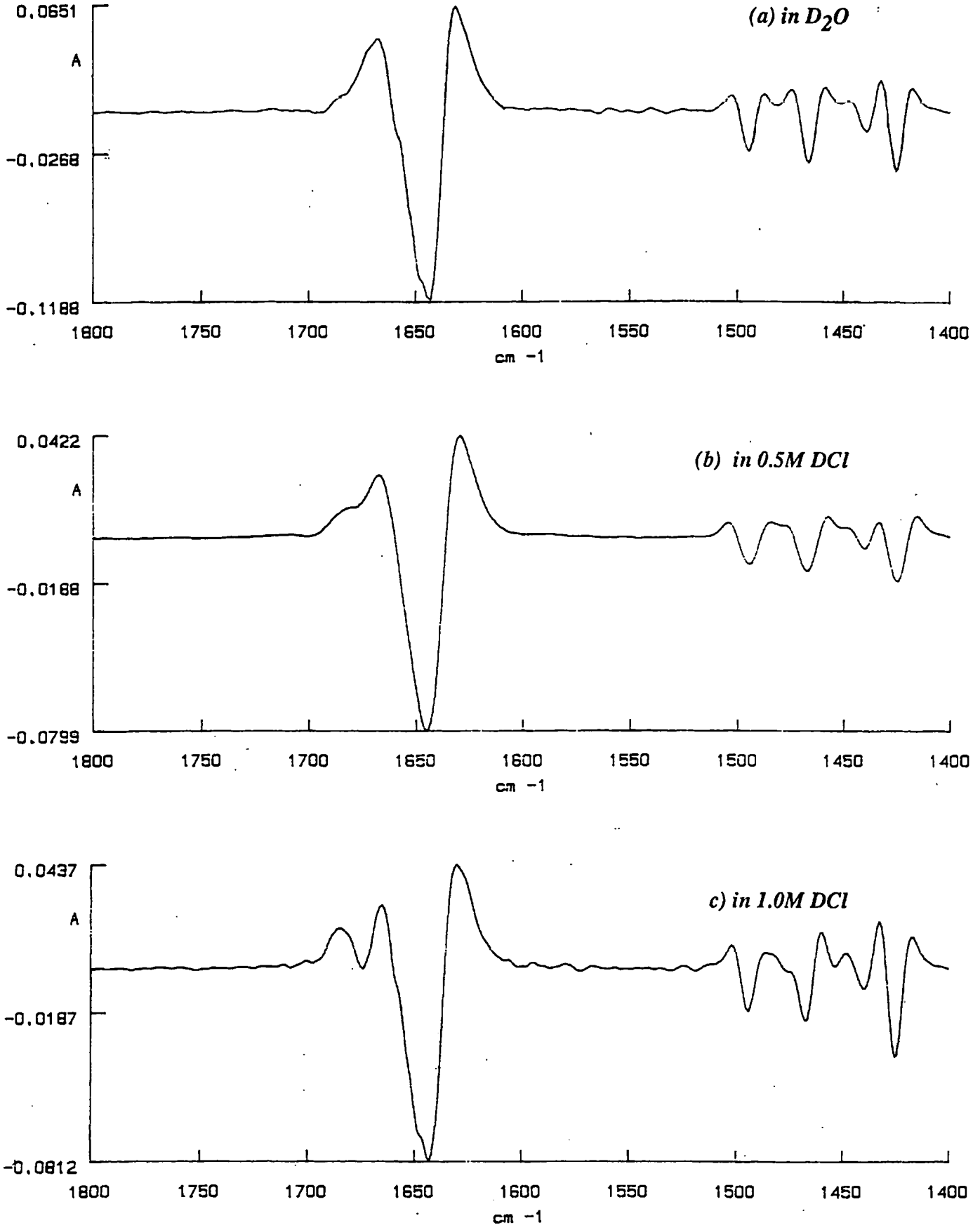

Figure 2.9

N-methyl acetamide at 25°C, 2nd derivative

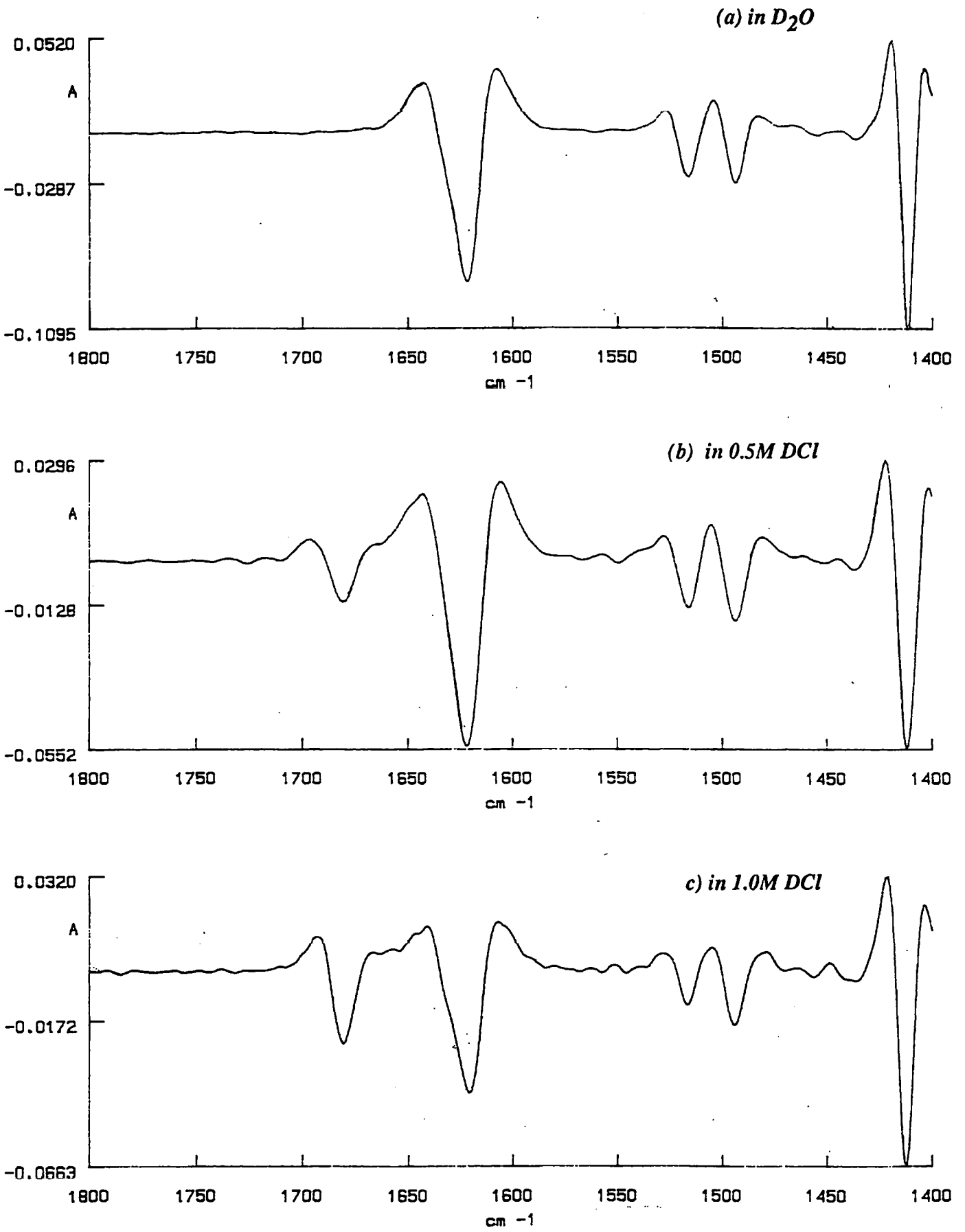

Figure 2.10

N-n-butyl acetamide at 25°C, 2nd derivative

(a) in D_2O

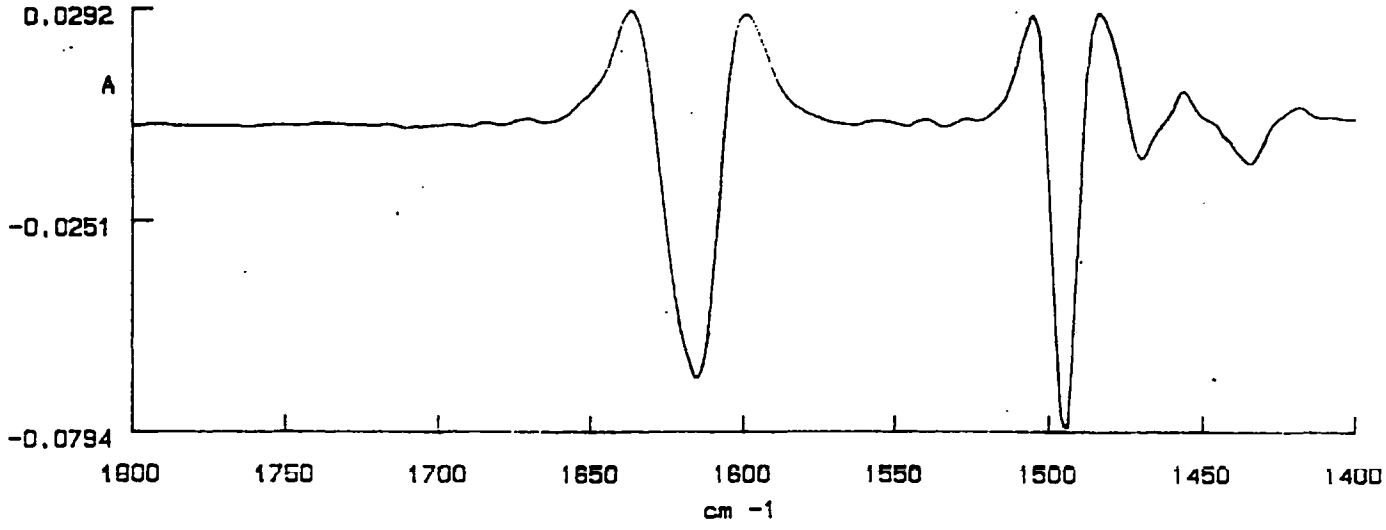

(b) in 0.5M DCl

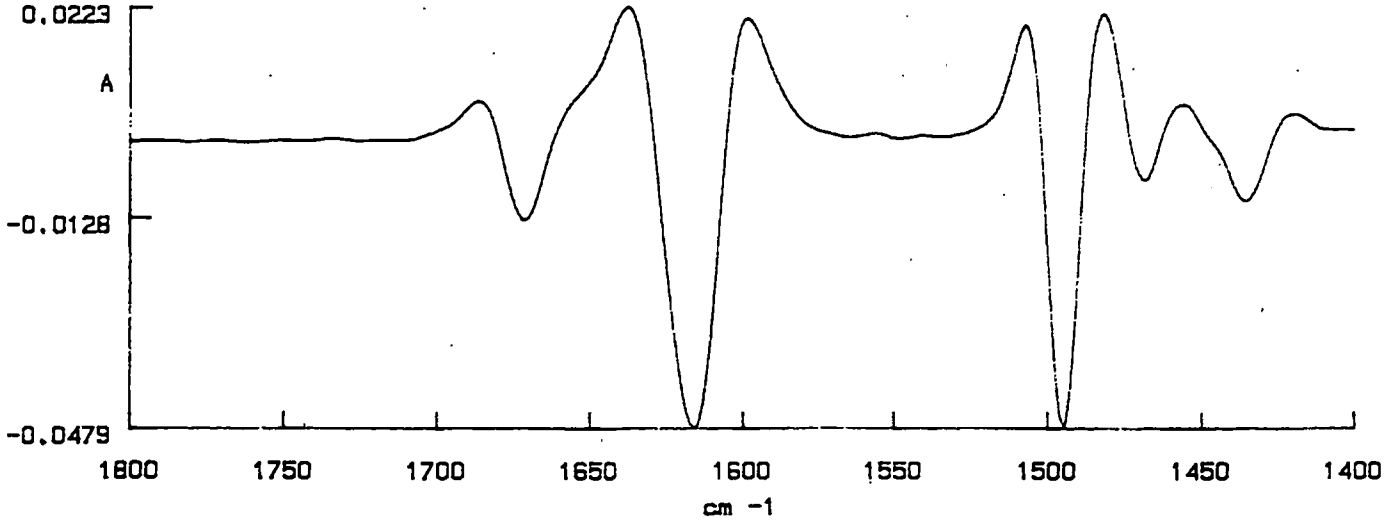

c) in 1.0M DCl

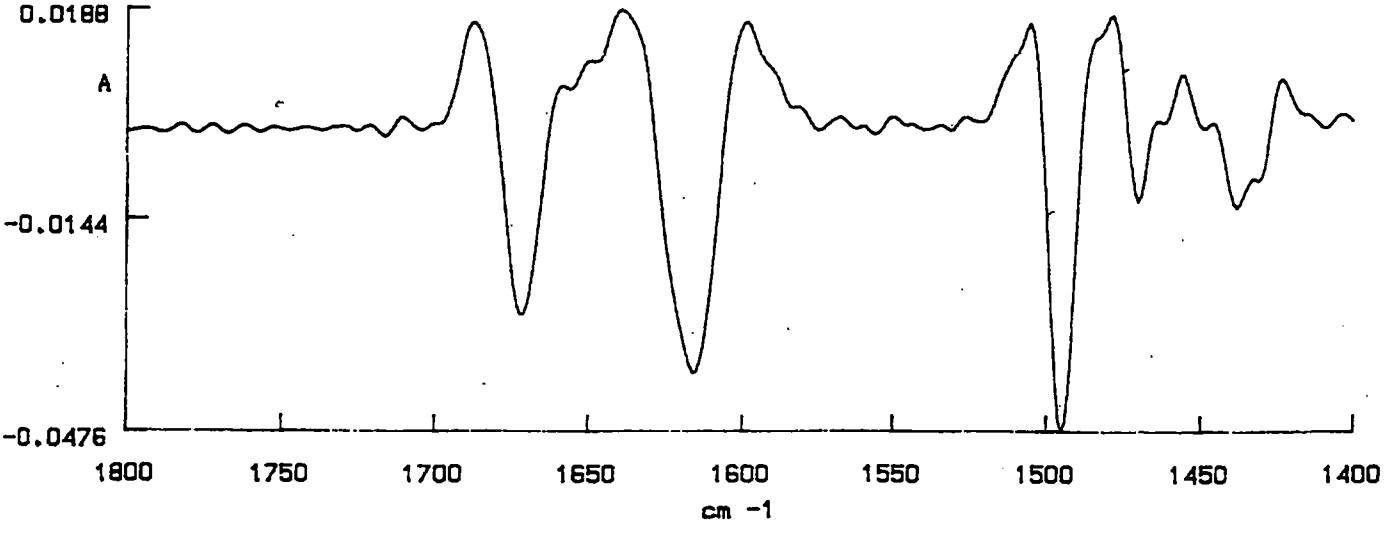

allowing several spectra to be run in quick succession without breaking the nitrogen gas purge.

2.9 An internal standard

The scope for normalising each spectrum from the kinetic experiments by reference to a suitable internal standard was examined in preliminary experiments. A suitable compound for an internal standard needed to be soluble in D_2O, to have intense absorption bands away from those of the peptide and to be stable for one or two days in nitrous acid. Both acetonitrile and poly(acrylonitrile) have a C≡N absorption near 2200cm^{-1} which seemed suitable for use as a standard. In practice, both were under the solvent absorption. There are few regions of the N-nitrosopeptide and N-nitrosamide spectra which are free from absorbance by either D_2O, HOD or solute. Propargyl alcohol (2-propyn-1-ol) gave a C≡C absorption at 2121cm^{-1} which was apparent in D_2O media, but the absorbance is only 1/20 of the absorbance of the strongest peptide carbonyl band at the same molar concentration. No suitable internal standard was therefore found.

2.10 Evaluation of the kinetic procedure

The optimum procedure for following the kinetics of peptide nitrosation were evaluated in trial experiments using secondary amides as the substrates. Both the initial infra-red spectra and the spectral changes on nitrosation are simpler than those with peptides, and problems can be more readily identified and resolved.

In the FTIR spectra of secondary amides, the amide I bands for D_2O solutions of 2-pyrrolidinone, N-methyl acetamide and N-n-butyl acetamide occur at 1644, 1622 and 1615cm^{-1} respectively (Figures 2.8 - 2.10). These bands are due mainly to C=O stretch vibrations, with contributions from C-N stretch and N-D bend[55]. The cis form is determined by the ring structure in 2-pyrrolidinone while the trans form has been found to predominate in the N-alkyl amides[56]. The higher frequency band which appears for all three amides in DCl and which increases in intensity with acid concentration must therefore be due to protonation rather than to cis/trans isomerism. While the appearance of the higher frequency carbonyl band could be attributed to N-protonation, the weight of evidence is that amides protonate on oxygen[57].

Figure 2.11

Relation between FTIR absorbance and concentration for 2-pyrrolidinone in D_2O at 25℃

a) Zero order

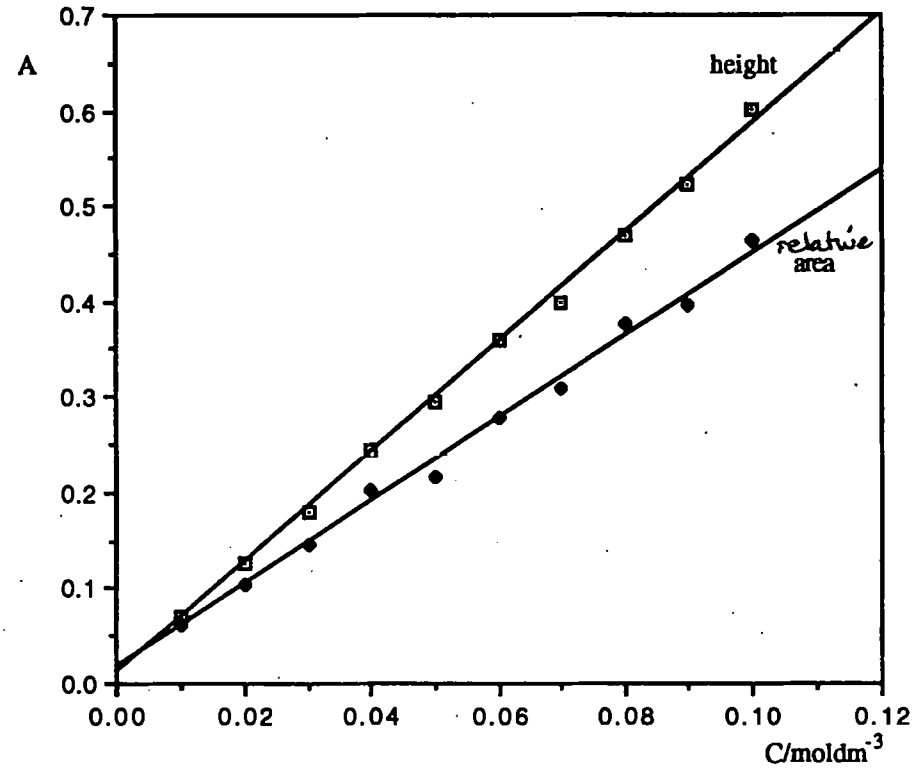

b) 2nd derivative

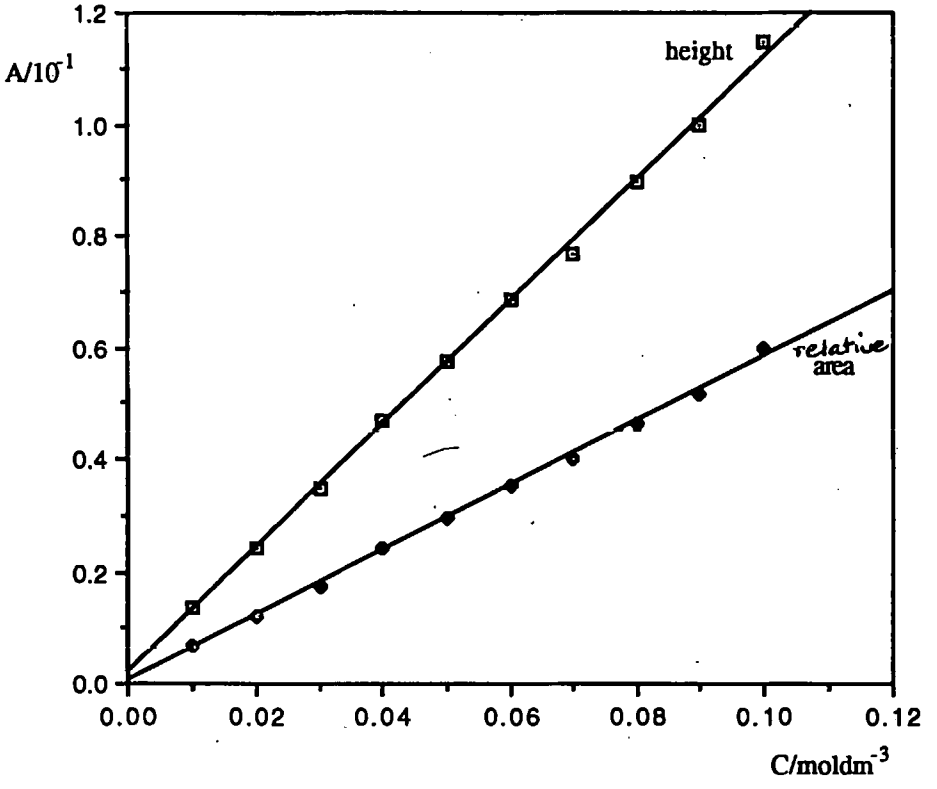

2.11 Relation between FTIR absorbance and concentration

Solutions of 2-pyrrolidone were made up in D_2O at different concentrations between 0.01M and 0.50M by series dilution. FTIR spectra were recorded and the absorbance at 1644cm^{-1} measured. Peak heights were measured with a ruler and areas by paper weighing. The results are summarised in Table 2.3.

Table 2.3

Relationship between FTIR absorbance at 1644cm^{-1} and concentration for 2-pyrrolidinone

	Peak heights		*Peak areas*	
C/moldm^{-3}	*A(zero order)*	*A(2nd deriv)*	*A(zero order)*	*A(2nd deriv)*
0.01	0.0714	0.0134	0.0632	0.0067
0.02	0.1264	0.0239	0.1031	0.0119
0.03	0.1808	0.0347	0.1454	0.0174
0.04	0.2458	0.0469	0.2019	0.0239
0.05	0.2959	0.0573	0.2174	0.0292
0.06	0.3604	0.0686	0.2782	0.0350
0.07	0.4002	0.0766	0.3086	0.0398
0.08	0.4708	0.0895	0.3761	0.0465
0.09	0.5219	0.0996	0.3959	0.0518
0.10	0.6010	0.1147	0.4636	0.0596

The results are plotted in Figure 2.11, where a good linear relationship between absorbance and concentration for both zero order and second derivative spectra from 0.01M to 0.10M is apparent. There was no advantage in using peak areas rather than heights, so the latter were chosen as easier to measure. The result for second derivatives is in accordance with a mathematical treatment which indicates that the peak intensity of the second derivative is proportional to the original, zero order peak intensity and inversely proportional to the square of the half band width[58]. It is therefore permissible to assume that second derivative absorbance is proportional to concentration provided that the half band width remains the same.

Figure 2.12a

Second derivative FTIR spectra with respect to time for reaction of 0.03M 2-pyrrolidinone, 0.1M $NaNO_2$ and 0.5M DCl at 25°C

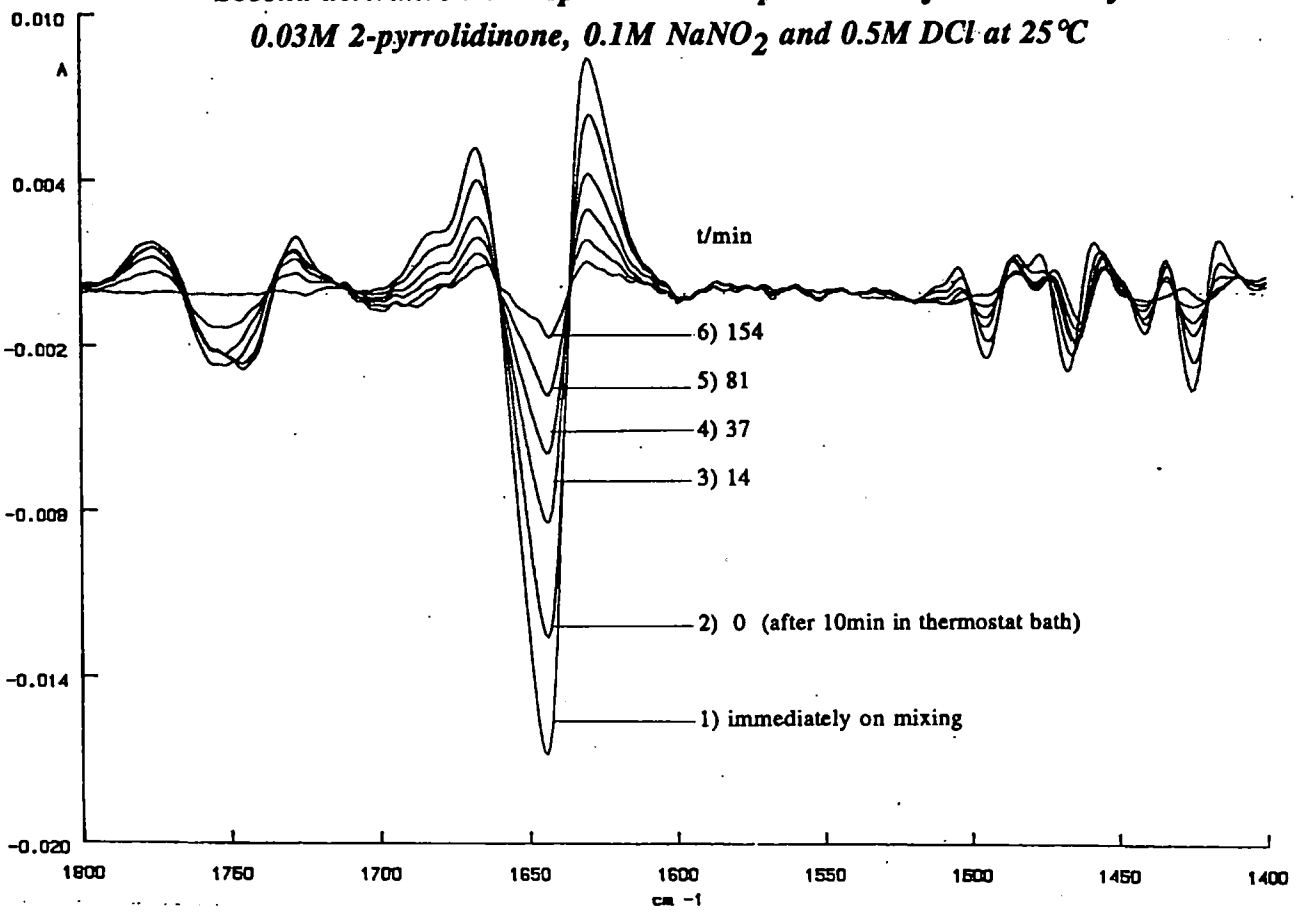

Figure 2.12b

Fourth derivative FTIR spectra with respect to time for reaction of 0.03M 2-pyrrolidinone, 0.1M $NaNO_2$ and 0.5M DCl at 25°C

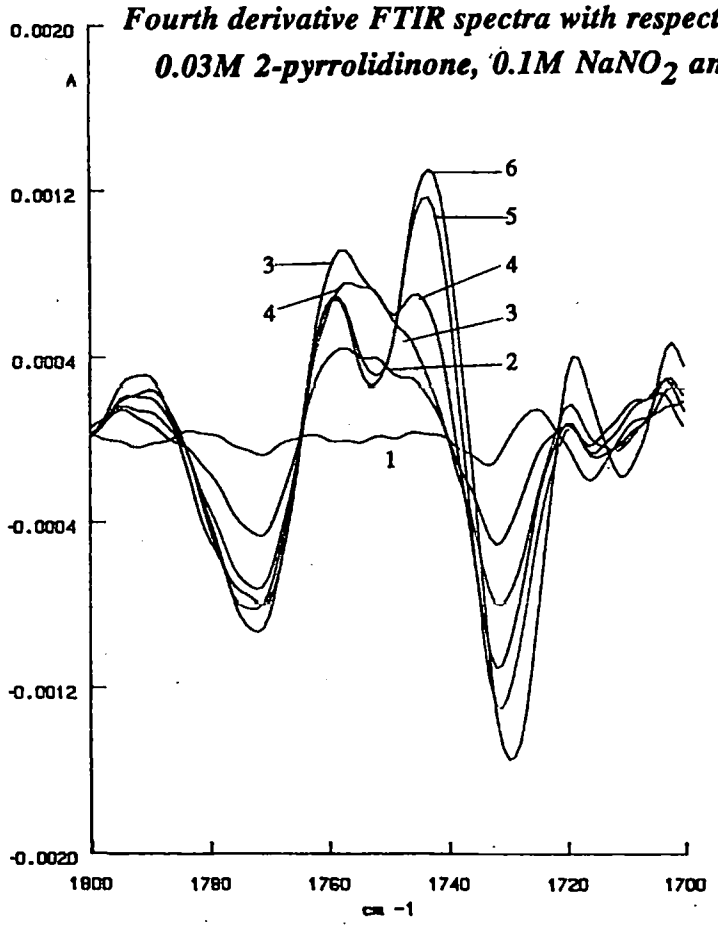

Figure 2.13

Variation of UV absorbance with time for the reaction of 0.03M 2-pyrrolidinone, 0.1M $NaNO_2$ and 0.5M DCl at 25℃

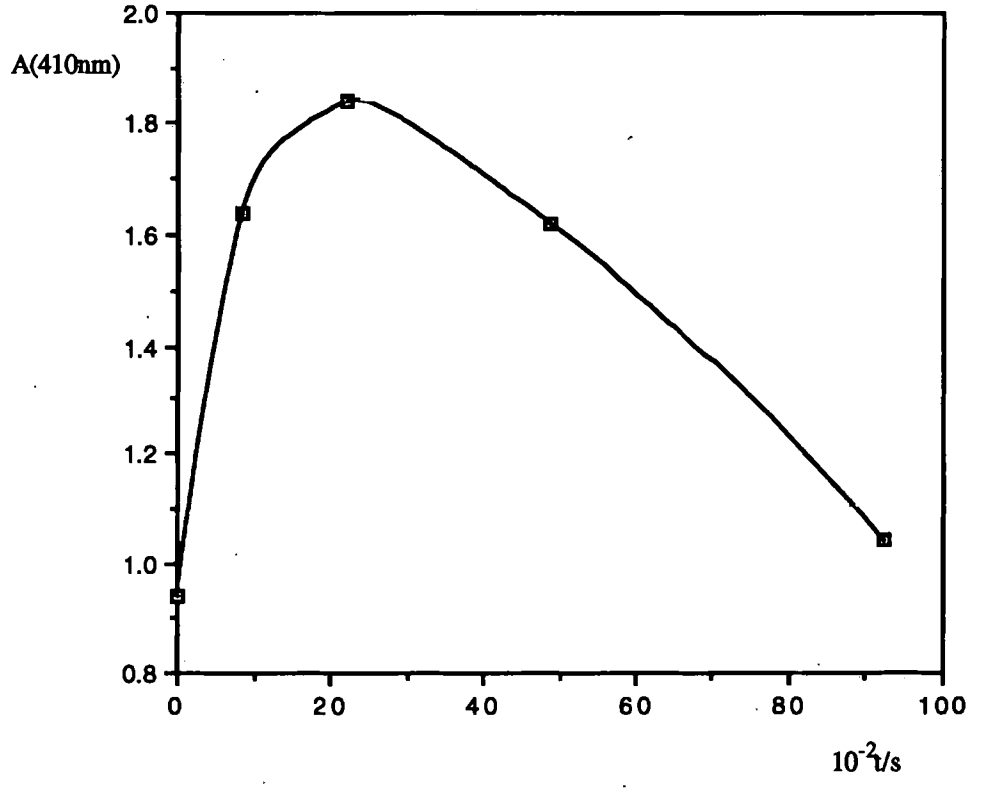

Figure 2.14

Variation of FTIR absorbance with time for the reaction of 0.03M 2-pyrrolidinone, 0.1M $NaNO_2$ and 0.5M DCl at 25℃

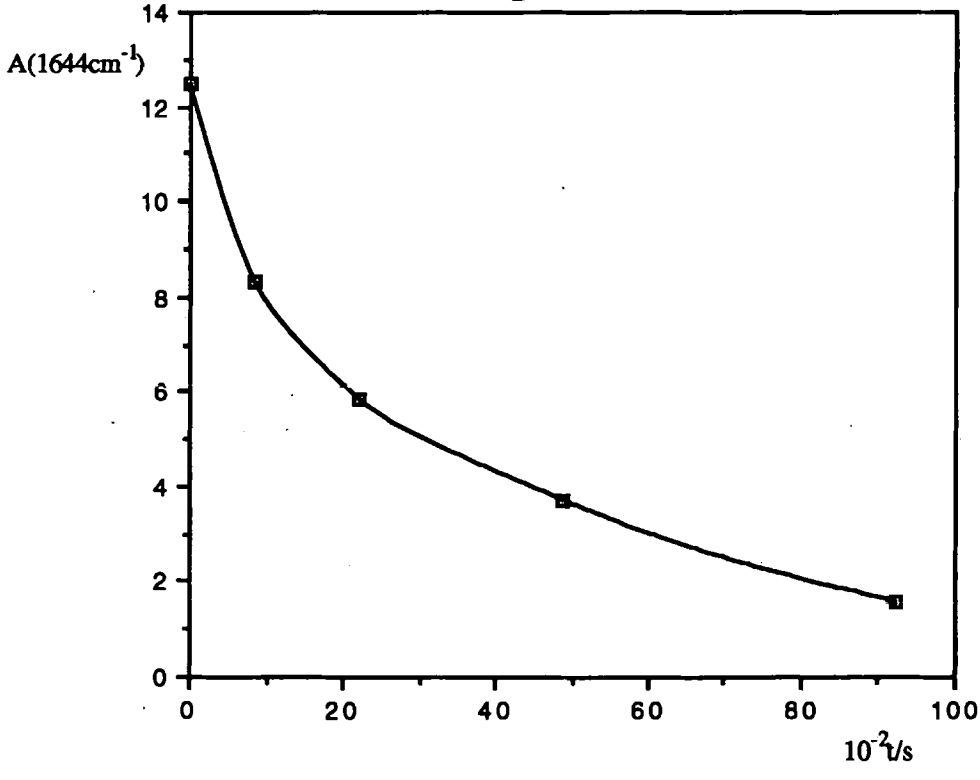

2.12 Trial nitrosations of 2-pyrrolidinone by FTIR

Preliminary experiments using UV spectrophotometry to monitor the formation of the N-nitrosamide showed that 2-pyrrolidinone (0.03M) in conjunction with $NaNO_2$ (0.1M) and DCl (0.5M) would be most suitable to follow quantitatively by FTIR. During the reaction, the loss of starting material was measured by the intensity of the amide I, 1644cm^{-1}, band. The second derivative spectra obtained are shown in Figure 2.12a.

The amide I band intensity decreases continuously, as expected, while a new band due to the N-nitrosamide appears at 1750cm^{-1}. The N-nitrosamide product band, however, is broad and appears to move to lower frequencies as the reaction progresses. Fourth derivative spectra of this region (Figure 2.12b) show that the N-nitrosamide band at 1754cm^{-1} is first formed, which then decreases in intensity while another band at 1743cm^{-1} increases. The changes in the 1754cm^{-1} IR band are exactly paralleled by the increase and decrease of the UV absorbance at 410nm, characteristic of N-nitrosamides (Figure 2.13). These changes can be explained by initial formation of the N-nitrosamide product, which then decomposes by deamination to the 4-hydroxybutyric acid (X) as shown in Scheme 2.4.

Scheme 2.4

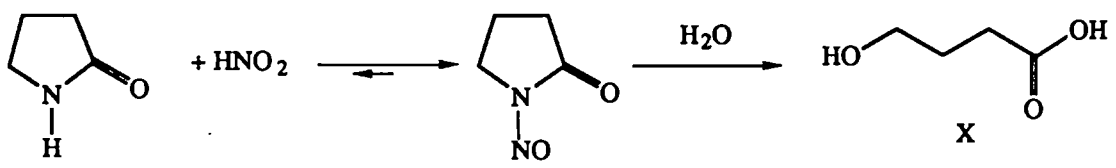

This explanation was confirmed by monitoring the hydrolysis of authentic N-nitroso-2-pyrrolidinone by FTIR. These results are shown in Figure 2.15 where the decrease in the 1754cm^{-1} band is accompanied by an increase in the 1743cm^{-1} band as well as of the 1644cm^{-1} band, which is due to pyrrolidinone. A plot of amide I absorbance against time for the nitrosation of 2-pyrrolidone is shown in Figure 2.14.

2.13 Site of peptide nitrosation

As mentioned previously, the nitrosation of peptides is complicated by the presence of more than one reactive site and a key aim of the present study was to identify the site of nitrosation. This information can be obtained from the FTIR spectra, provided that the amide carbonyl bands are

Figure 2.15

Second derivative FTIR spectra with respect to time for hydrolysis of N-nitroso-2-pyrrolidinone in 1.0M DCl at 25℃

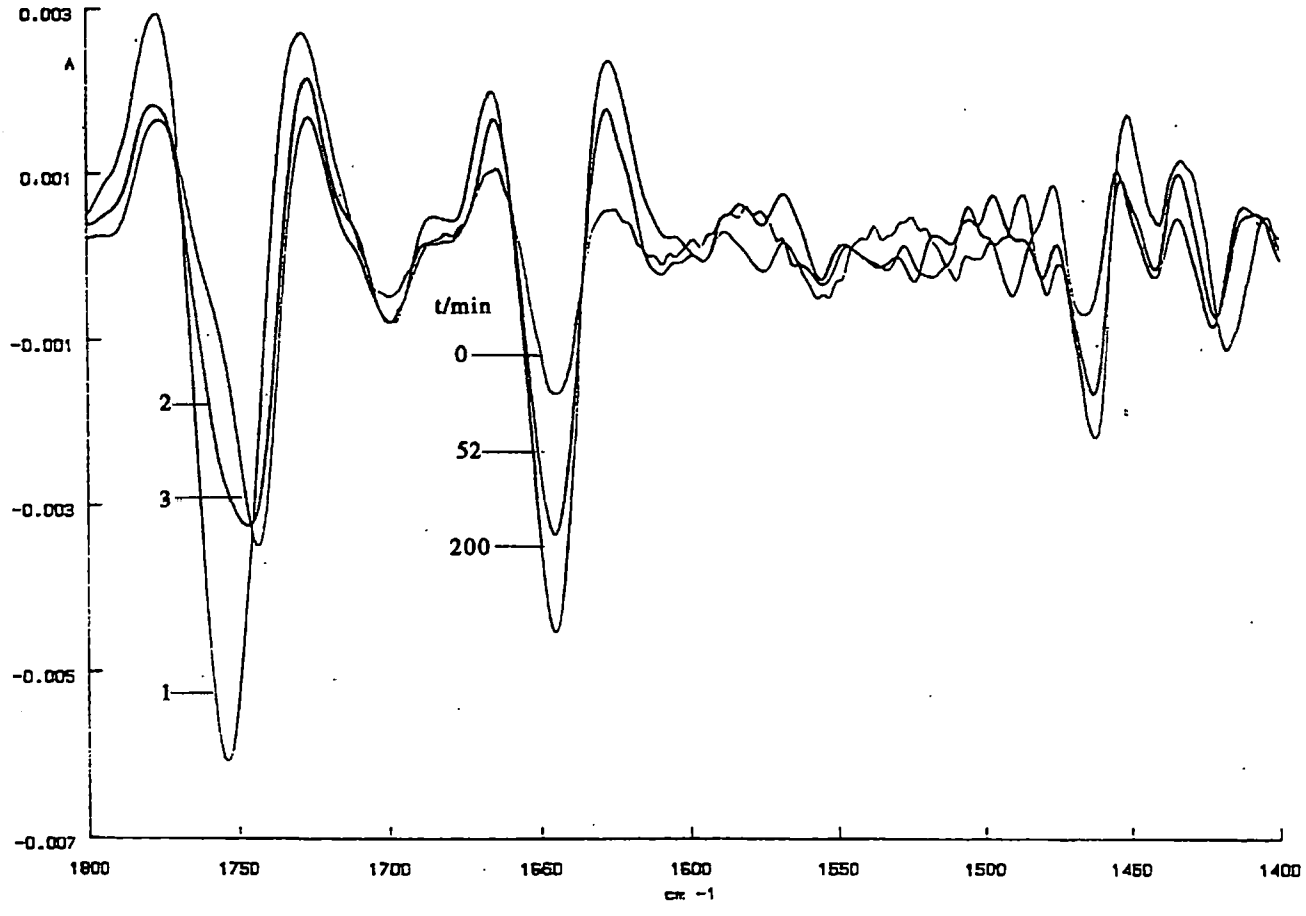

assigned to specific groups in the peptide. The IR assignments were therefore made for the simplest dipeptide (N-(N'-acetylglycyl)glycine) used in the present study. It was anticipated that this information would also enable the assignment of the amide carbonyl bands for more complicated peptides.

2.14 Assignment of the carbonyl bands in N-(N'-acetylglycyl)glycine

The zero order spectrum (Figure 2.5) of N-(N'-acetylglycyl)glycine, AcGlyGly, shows two carbonyl bands, at 1731 and 1641cm^{-1} respectively and the latter has a shoulder on the high frequency side. All three bands, for the three carbonyl groups, are resolved in the second derivative spectrum of AcGlyGly (Figure 2.6), giving frequencies of 1731, 1662 and 1636cm^{-1}. Good resolution is essential to observe changes in the band

Figure 2.16a

GlyGly in 1.0M DCl at 25°C, 2nd derivative

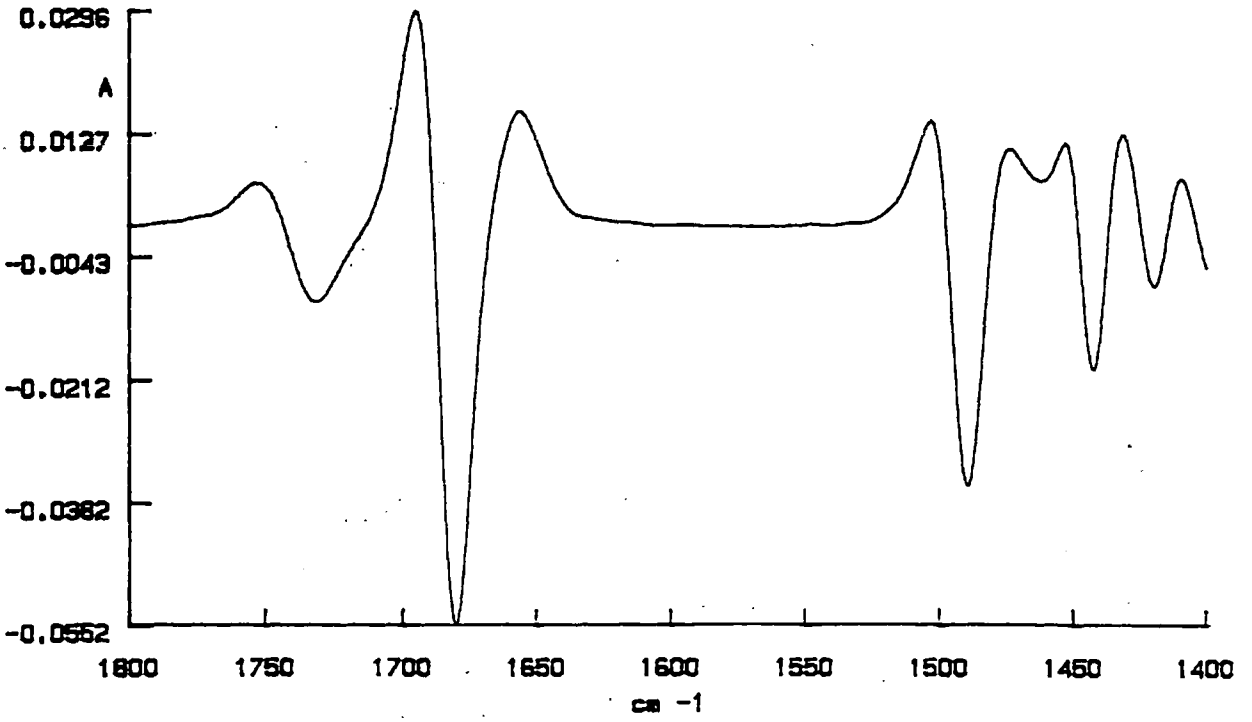

Figure 2.16b

GlyGly in D_2O at 25°C, 2nd derivative

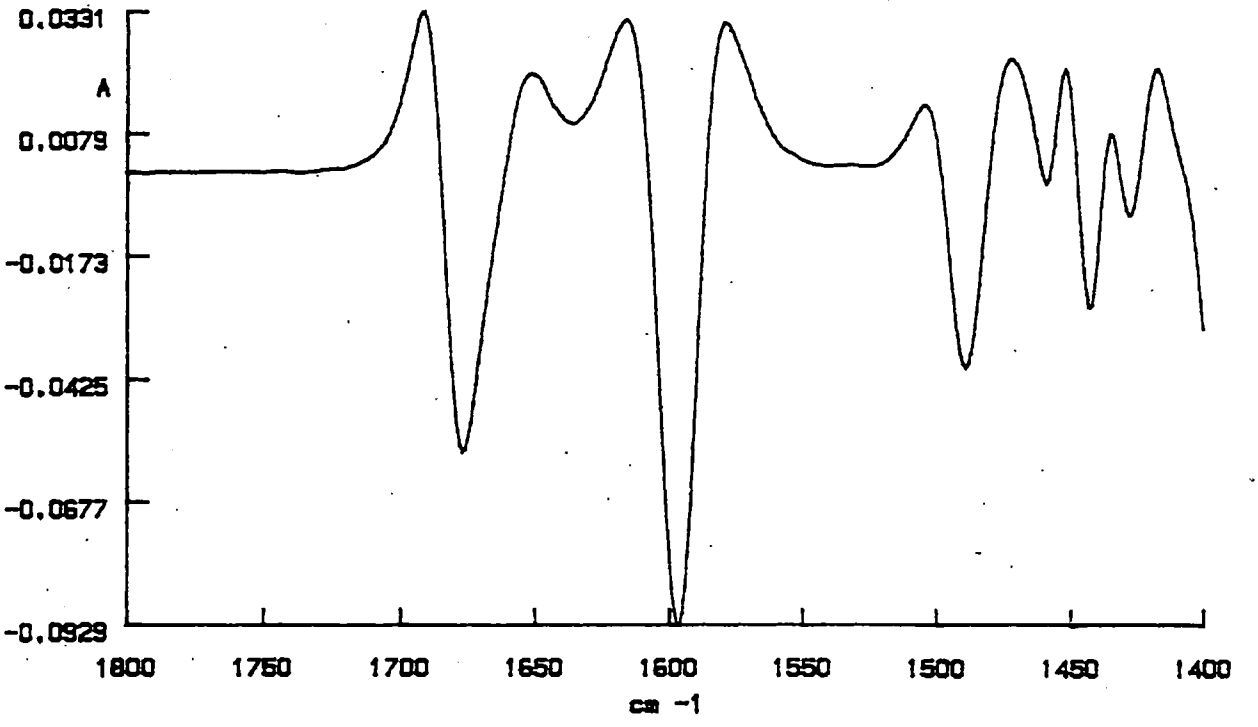

intensities during reactions and for this reason, second derivative spectra were used throughout the kinetic studies.

The assignment of the 1731cm^{-1} band in AcGlyGly was made by comparison with the spectrum of N-glycylglycine, GlyGly, which has a carboxylic acid carbonyl band at the same frequency in 1.0M DCl (Figure 2.16a). This is complemented in D_2O by the asymmetric stretch of the carboxylate anion at 1596cm^{-1} (Figure 2.16b), the symmetric stretch (not shown) occurring at 1395cm^{-1}. The 1731cm^{-1} band of AcGlyGly is therefore assigned to the acid carbonyl. Spectra of AcGlyGly in D_2O and M DCl are identical. To distinguish between the other two carbonyl bands, N-(N'-1-^{13}C-acetylglycyl) glycine was synthesised from acetyl -1- ^{13}C chloride and N-glycylglycine benzyl ester, GlyGlyOBz (Scheme 2.5).

Scheme 2.5

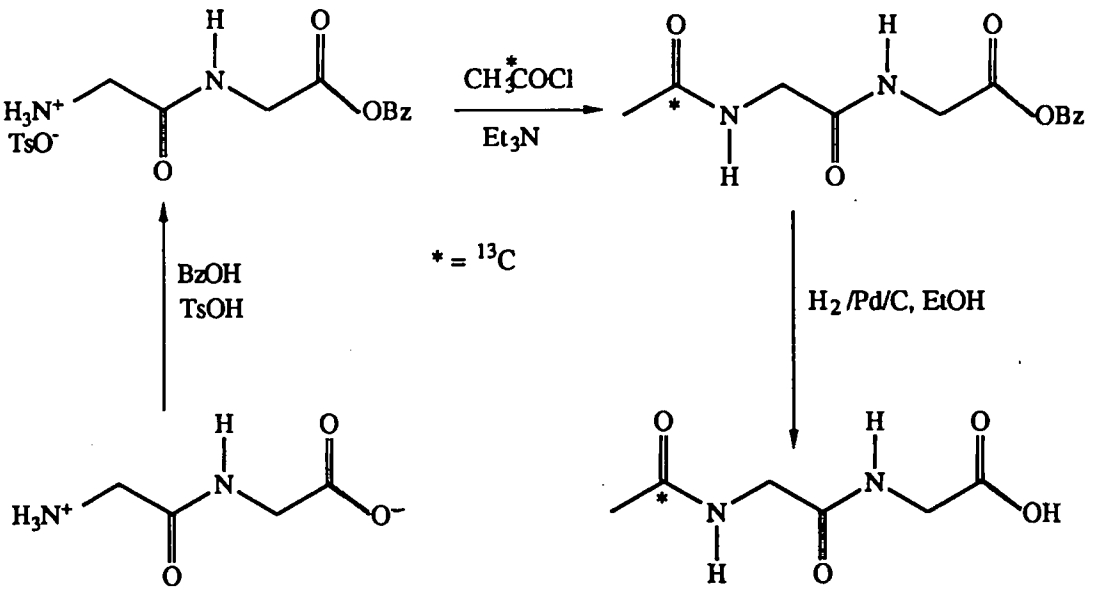

(Bz = benzyl, Ts = p-toluenesulphonate)

The spectrum of this compound in D_2O shows the acid carbonyl band at 1728cm^{-1}, a broader amide band at 1654cm^{-1} and a second amide carbonyl band, associated with the ^{13}C atom, which has moved down to 1596cm^{-1} (Figure 2.17a). This frequency is in good agreement with the formula (Equation 2.1) for a simple diatomic oscillator:

Figure 2.17a

^{13}C AcGlyGly in 1.0M DCl at 25°C, 2nd derivative

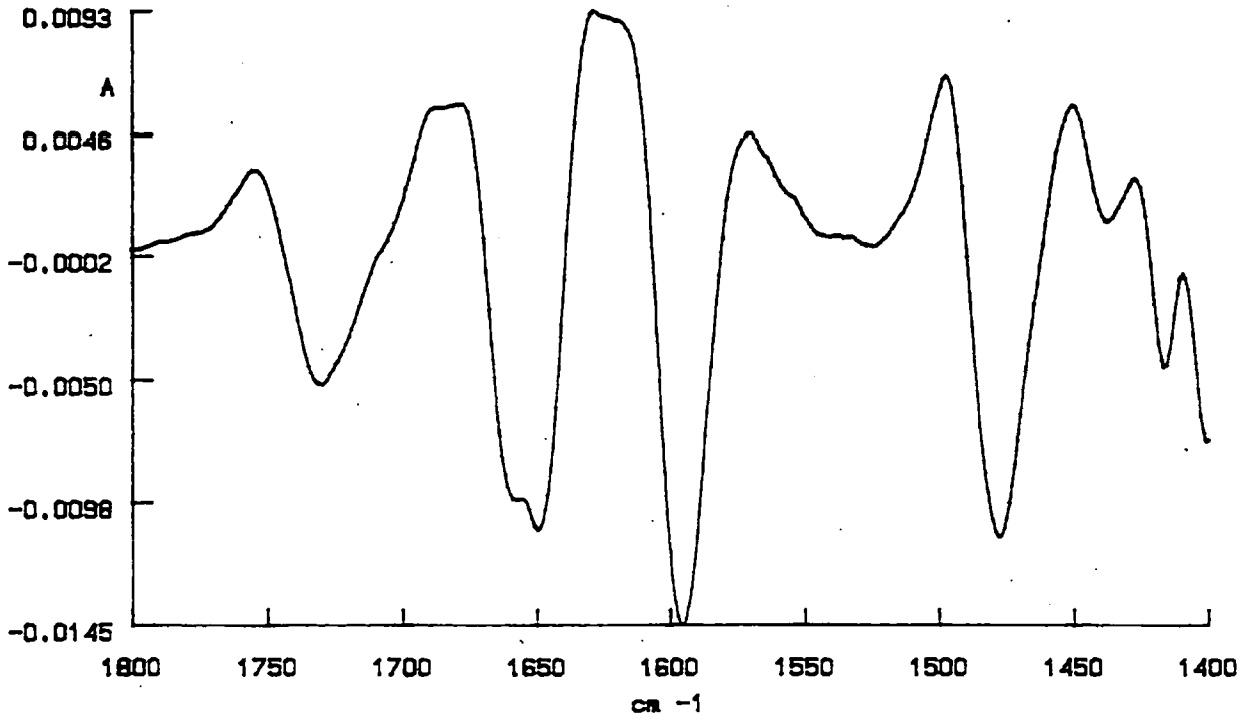

Figure 2.17b

AcGlyGly in 1.0M DCl at 25°C, 2nd derivative

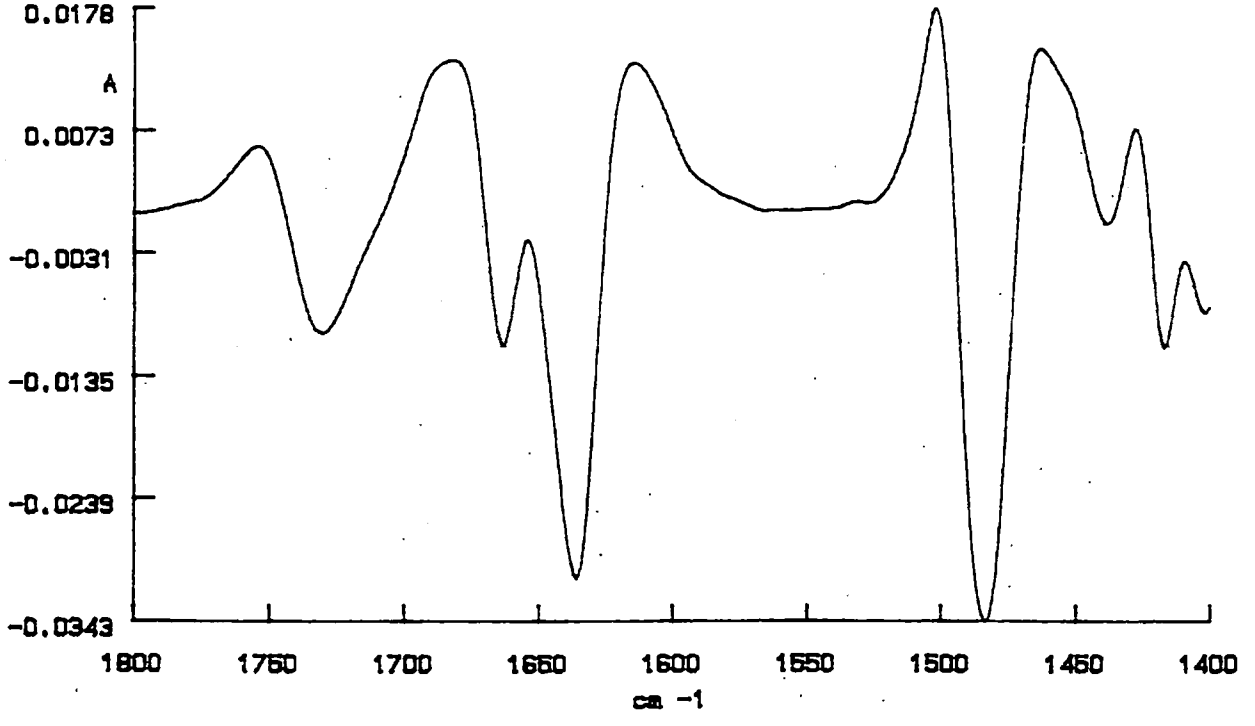

$$f = \frac{1}{2\pi}\sqrt{\frac{k(m_1+m_2)}{m_1 m_2}} \qquad \text{Equation 2.1}$$

which predicts a shift of frequency (f) from 1635cm^{-1} to 1599cm^{-1} on substituting ^{13}C for ^{12}C (m_1) while keeping m_2 (^{16}O) constant and assuming that the force constant (k) does not vary.
Thus, in the AcGlyGly spectrum, the assignments of the carbonyl bands are as follows:

Frequency/cm^{-1}	*Assignment*
1732	HOC=O
1664	HNC=O
1636	CH_3C=O
1482	amide II

The assignment of the 1482cm^{-1} band is not proven, but is probable because of its position and intensity.

2.15 The spectrum of N-acetyl-N-nitrosoglycylglycine

The spectrum of N-acetyl-N-nitrosoglycylglycine Ac(NO)GlyGly (Figure 2.18a), by comparison with the spectrum of AcGlyGly (Figure 2.18b), shows a loss of the acetyl carbonyl band at 1636cm^{-1} while the acid carbonyl band has become more intense, indicating the N-nitrosamide carbonyl band occurring at the same frequency. The peptide carbonyl absorption at 1662cm^{-1} remains. The amide II band at 1482cm^{-1} (in which the in-plane N-H deformation is coupled with the C-N stretch[59]) is less intense than for AcGlyGly with the loss of one N-H group, while the N=O stretching band appears at 1520cm^{-1}. Thus the assignments of the carbonyl bands of N-acetyl-N-nitrosoglycylglycine are as follows:

Frequency/cm^{-1}	*Assignment*
1731	HOC=O, ONNC=O
1662	HNC=O
1520	N=O
1478	amide II

Figure 2.18a

Ac(NO)GlyGly in D_2O at 25 °C, 2nd derivative (unstable in 1.0M DCl)

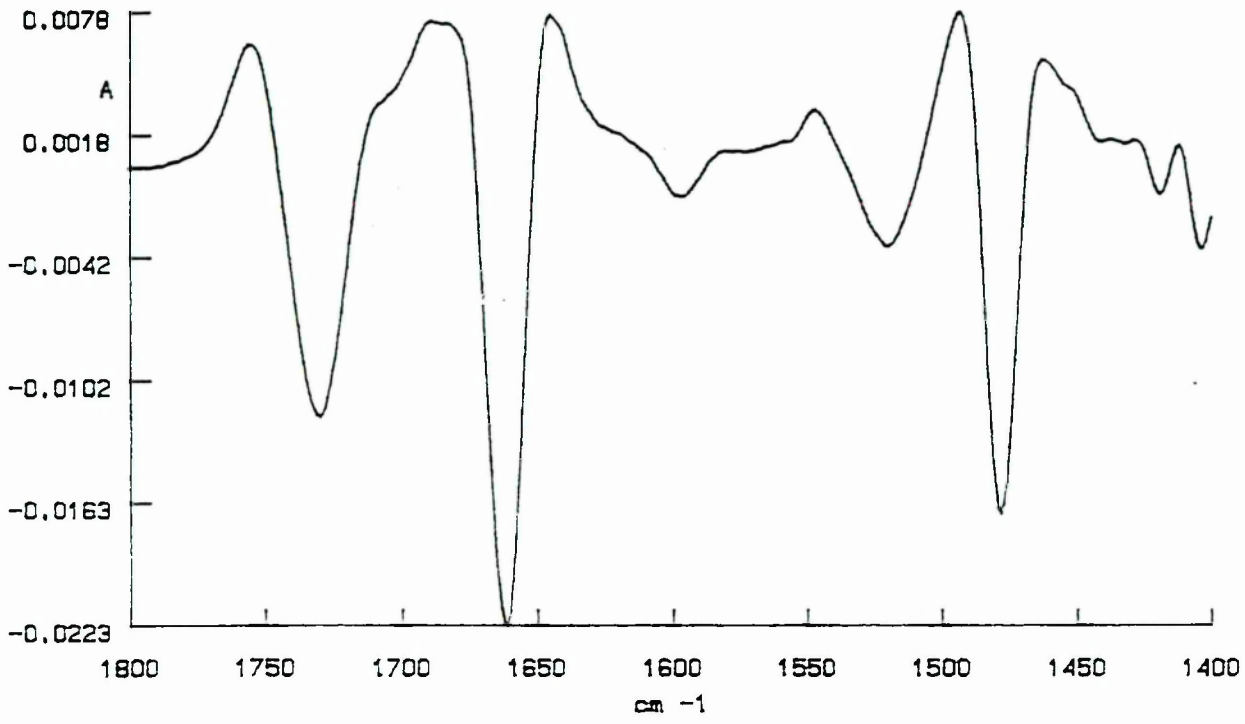

Figure 2.18b

AcGlyGly in 1.0M DCl at 25 °C, 2nd derivative

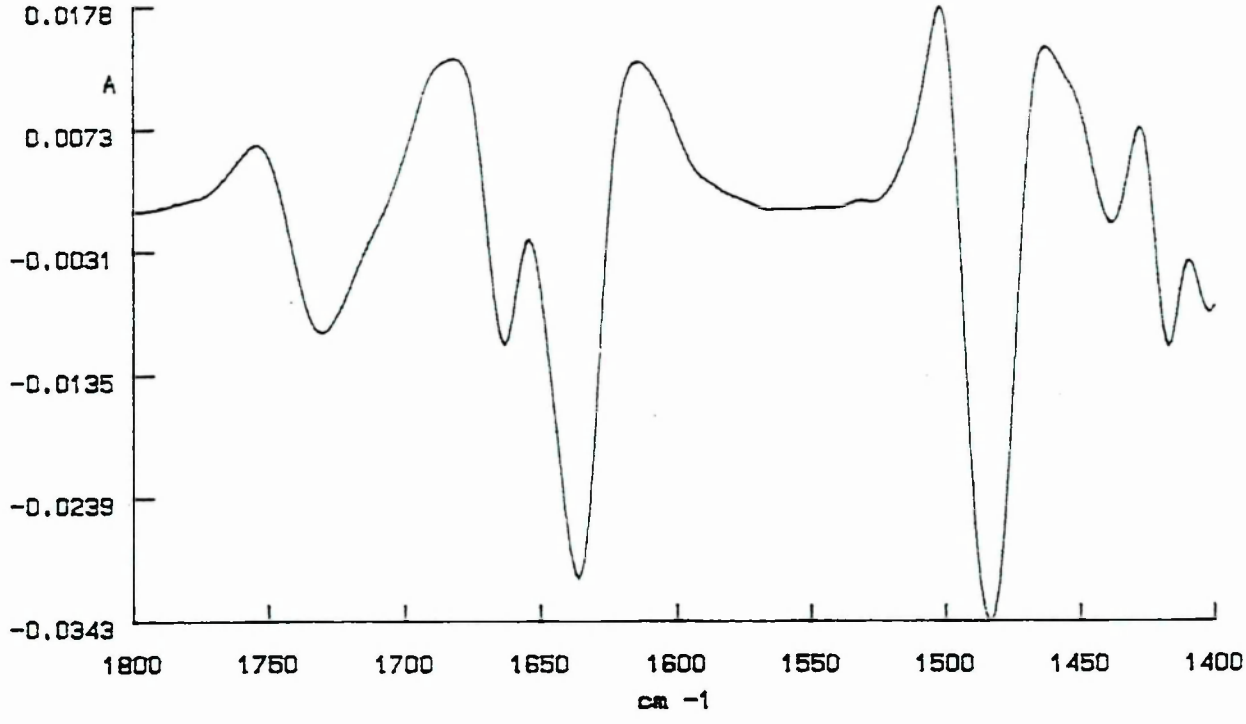

2.16 Choice of concentrations for the kinetics of nitrosation of N-acetylglycylglycine

To simplify the acquisition of the kinetic data, the aim was to follow the nitrosation of AcGlyGly using the carbonyl bands of the peptide under *pseudo* first order conditions. Hence the peptide had to be present in the lowest concentration, with the DNO_2 about 10 times greater. The maximum concentration of the sulphamic acid quench was about 1.4M, as its solubility at room temperature is 1.5M. The use of $0.3cm^3$ sulphamic acid solution to quench $0.75cm^3$ reaction mixture meant that there was enough sulphamic acid to react with $0.75cm^3$ of 0.6M nitrite, but diluted the peptide to 71% of its original concentration.

The usual noise level in AcGlyGly spectra corresponded to a peptide concentration of ca 0.001M. To obtain reliable kinetic data, unreacted peptide at three half-lives should be greater than 0.003M (ie signal:noise ratio = 3). It follows that the initial AcGlyGly concentration should be about 0.024M. Allowing for dilution by the sulphamic acid, 0.03M is a reasonable minimum. Thus the DNO_2 concentration should then be $\geq$ 0.3M.

A 1.0M concentration of DCl gave a minimum of 5% transmittance in the FTIR carbonyl region. Increasing the DCl concentration reduced transmittance, causing a lower signal to noise ratio and larger errors for the peptide absorbance measurements. It also increased corrosion of the stainless steel cell and fittings, and of the calcium fluoride windows. Thus, 1.0M DCl represented a reasonable maximum acidity.

To maintain a 50% excess of sulphamic acid over DNO_2 during quenching, DNO_2 concentrations > 0.4M would necessitate a greater volume of quench than in the example above, and therefore a higher initial concentration of peptide. Nitrite concentrations above 0.4M, reacting with M DCl, also produced an uncontrollable decomposition of nitrous acid on first mixing the reagents, even at temperatures where the solutions were beginning to freeze. Hence, 0.4M nitrite was chosen as the maximum practical value.

Thus, concentrations of 0.03M peptide,1.0M DCl and 0.4M $NaNO_2$ were selected to provide *pseudo* first order conditions for the peptide nitrosation kinetics. At 25°C, the half-life for the nitrosation of AcGlyGly was about 5h, which was slower than ideal but measurable.

Chapter 3

Results and discussion 2

Peptide Nitrosation

Figure 3.1
Second derivative FTIR spectra with respect to time for the reaction of 0.03M AcGlyGly and 0.4M $NaNO_2$ in 1.0M excess DCl at 25°C

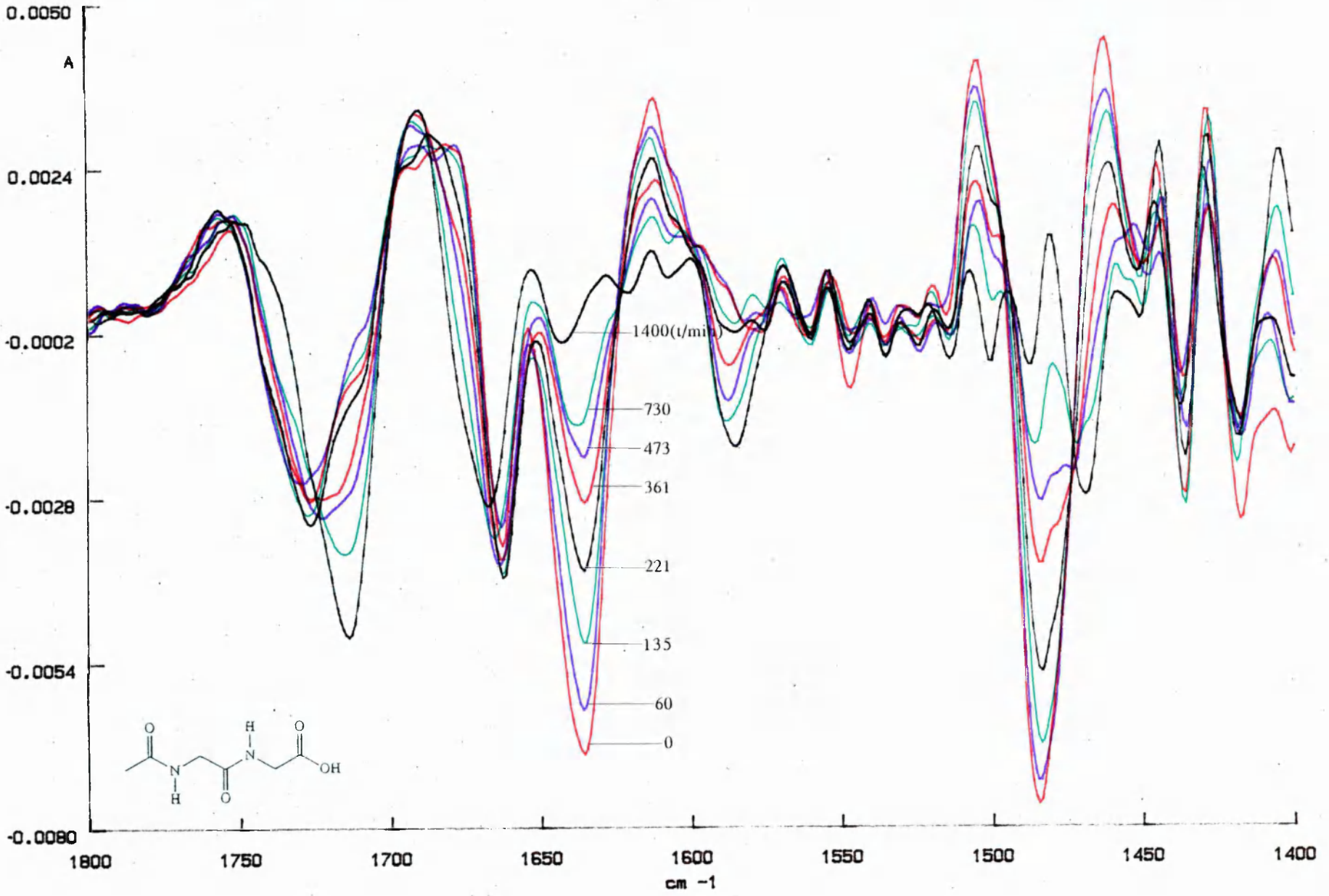

3.1 The nitrosation of AcGlyGly by HNO_2 in DCl

Because of its uncomplicated structure and ready availability, AcGlyGly was investigated in detail to examine the kinetics and mechanism of nitrosation.

Figure 3.1 shows the variation in the FTIR spectra with time for reaction of 0.03M AcGlyGly with 0.4M $NaNO_2$ in 1.0M DCl at 25°C. The series of spectra is typical of those obtained for all of the reactions. Examination of the spectra shows that the acetyl carbonyl band at 1636cm^{-1} diminishes steadily, indicating that the nitrosation occurs at the N-D adjacent to the acetyl group. The amide II band at 1490cm^{-1} also diminishes as expected if one N-D bond becomes N-NO. The acid carbonyl band at 1732cm^{-1} varies in a more complicated way. Initially, it increases in intensity due to the formation of the N-nitrosopeptide, which absorbs at the same frequency, to reach a maximum at t=221min. It then decreases because hydrolysis of the N-nitroso peptide proceeds concurrently with its formation. As well as decreasing in intensity, the 1732cm^{-1} band steadily shifts to 1713cm^{-1} at the end of the reaction due to the formation of acetic acid by hydrolysis of the N-nitrosopeptide (Scheme 3.1).

Scheme 3.1

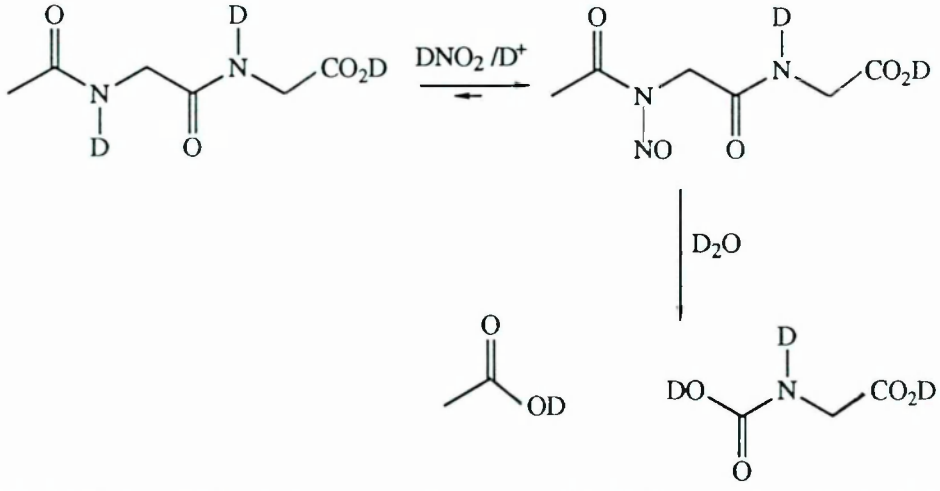

Confirmation of the above interpretation of the FTIR changes was obtained by parallel UV-visible and ^{1}H-NMR studies of the reaction mixture. The variation in the visible absorbance of the reaction mixture at λ_{max}= 410nm, which is characteristic of the N-nitrosopeptide, is shown in Figure 3.2. This increases to a maximum at 221 min, before decreasing. It agrees favourably with the FTIR results, confirming that the changes in the 1732cm^{-1} band are indeed due to the N-nitrosopeptide.

Figure 3.2

Variation of UV absorbance with time for reaction of AcGlyGly at three concentrations with 0.03M $NaNO_2$ in 1.0M DCl at 25 ℃

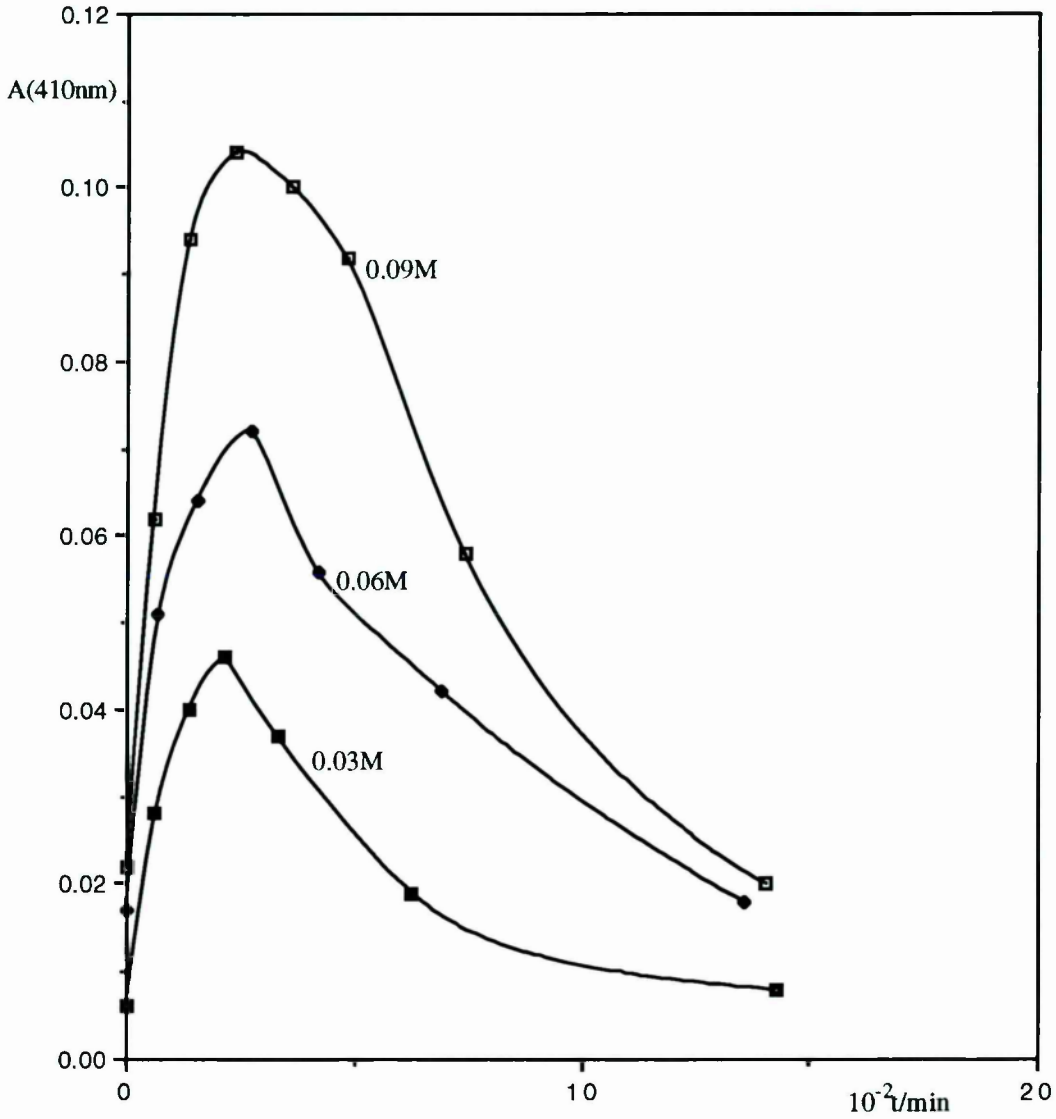

Figure 3.3

^1H NMR spectra with respect to time for the reaction of 0.03M AcGlyGly and 0.4M $NaNO_2$ in 1.0M excess DCl at 25°C

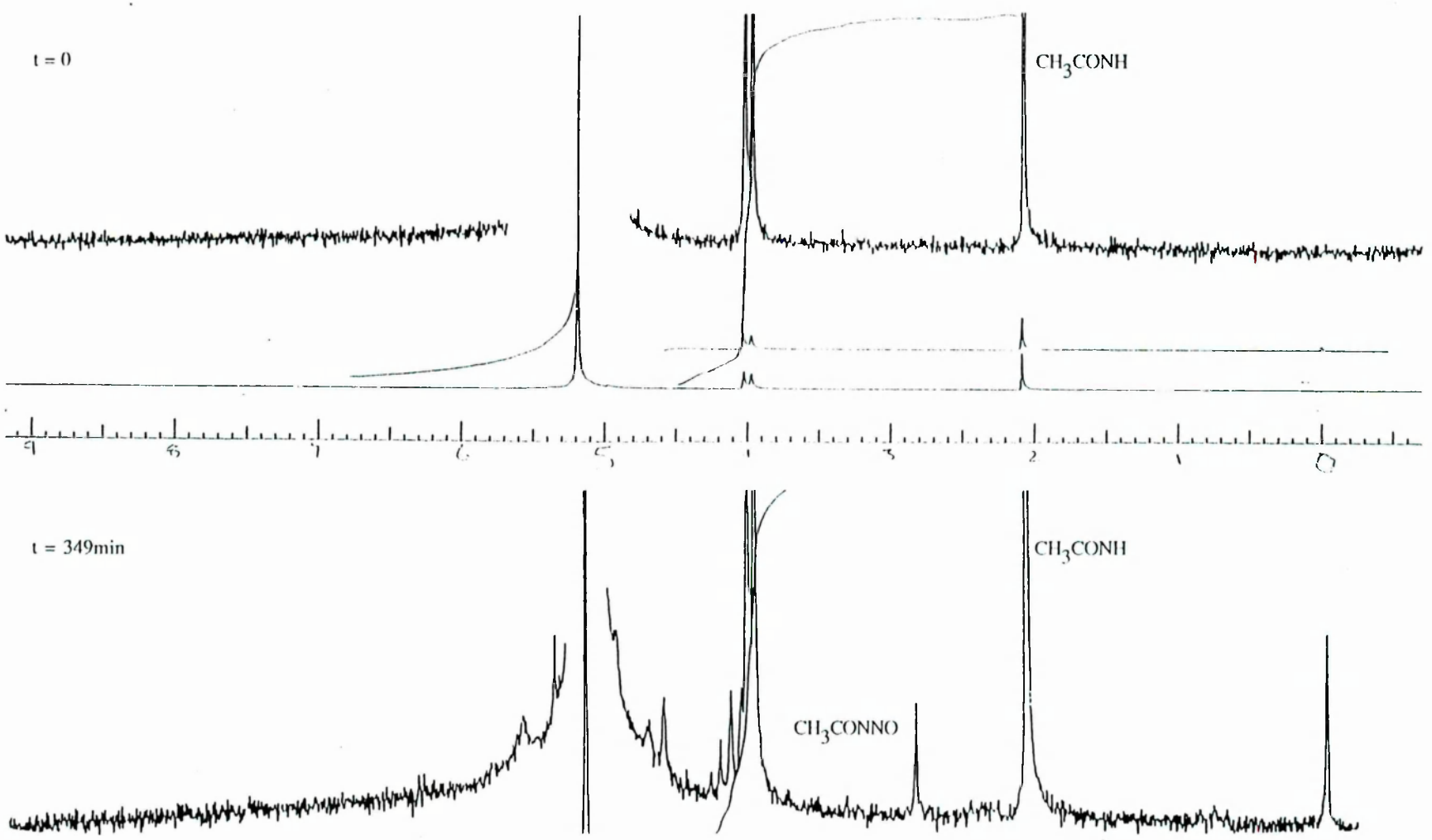

The ^1H NMR spectrum of the reaction mixture (Figure 3.3) shows a new peak at 2.87ppm, due to the CH_3CONNO moiety, after 349 min which is not present at t=0.

Figure 3.1 shows that four IR bands (1732, 1636, 1585 and 1490cm^{-1}) undergo coherent changes of intensity in the course of nitrosation. The variation of these intensities at $\bar{\nu}$ = 1636, 1585 and 1490cm^{-1} are reported in Table 3.1. In principle, changes in any one of these bands with time can be used to compute the reaction rates, but those for $\bar{\nu}$ = 1636cm^{-1} are the only ones suitable. This band shows a large change during the course of the reaction and disappears on completion, so an infinity absorbance of zero can be assumed. It is unaffected by the subsequent decomposition of the N-nitrosopeptide which simplifies the data handling. Further, unlike the band at 1482cm^{-1}, it is unaffected by a neighbouring product band which appears as a shoulder in the early part of the reaction.

Table 3.1

Changes in intensity (peak height) of IR bands during the nitrosation of AcGlyGly at 25°C. Initial [AcGlyGly] = 0.03, [$NaNO_2$] = 0.4, DCl = 1.0M

	peak height,h/mm at $\bar{\nu}$/cm^{-1}		
10^{-3}t/s	*1636*	*1587*	*1482*
0	79.2	0	88.3
3.60	71.0	0	84.2
8.00	58.8	0.5	77.1
13.26	45.4	1.9	64.1
21.66	33.0	8.0	44.2
28.38	24.7	14.4	32.8
43.80	19.0	18.3	22.5
84.00	3.8	22.9	8.1

$$\text{Rate} = k_0[\text{AcGlyGly}] \qquad \text{Equation 3.1}$$

Pseudo first order rate coefficients were therefore calculated from the variance of the second derivative peak height (h) of the 1636cm^{-1} band with time, starting from the zero line and assuming zero height at time infinity. In practice, the peak height was measured in absorbance, A, ln A was plotted against time and k_0 calculated from the slope of the plot.

* because of band overlap and relative intensities,

Figure 3.4

First order rate plot for the nitrosation of AcGlyGly at 25 ℃

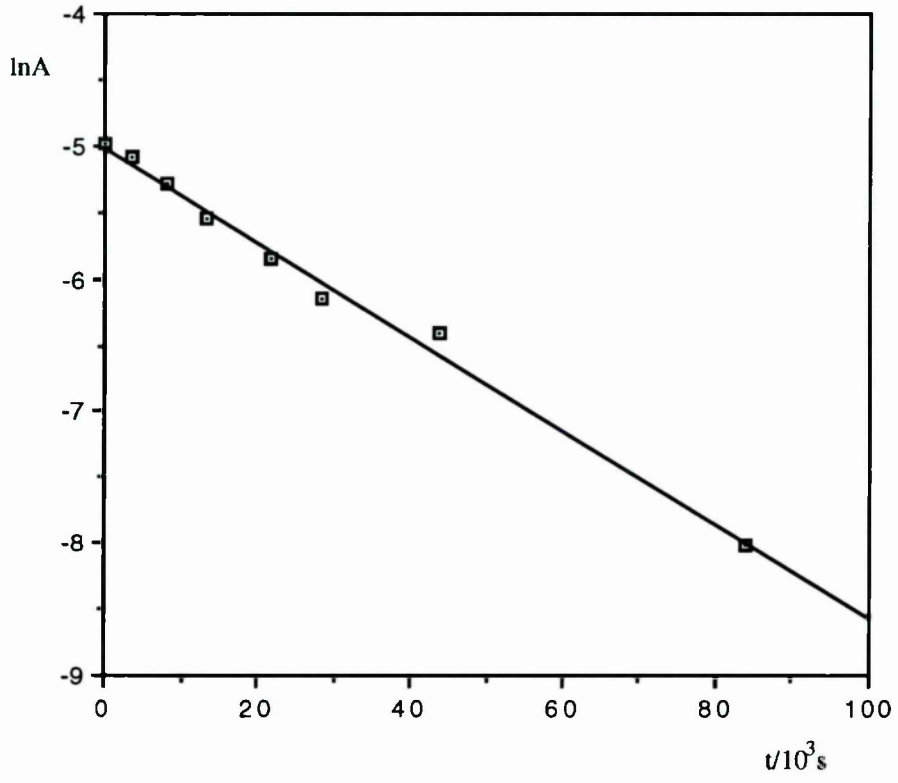

These data are summarised in Table 3.2, A_0 and A_t being the absorbances at times 0 and t respectively. The corresponding plot, which is shown in Figure 3.4, is linear, confirming the validity of Equation 3.1.

Table 3.2
FTIR data for nitrosation of AcGlyGly at 25°C

$10^3t/s$	*h/mm*	*lnA*	$10^5 ln(A_t/A_0)/t$
0	79.2	-4.9815	-
3.60	71.0	-5.0908	3.04
8.00	58.8	-5.2793	3.68
13.26	45.4	-5.5379	4.20
21.66	33.0	-5.8569	4.04
28.38	24.7	-6.1466	4.11
43.80	19.0	-6.4090	3.26
84.00	3.8	-8.0184	3.62

3.2 Determination of reaction orders with respect to peptide, nitrite and acid

The peptide concentration at a given time is measured by the absorbance of the changing carbonyl band. Because these reactions are monitored by loss of the peptide starting material, all the data will give information about the first reaction of the series, the nitrosation step. The rates of successive reactions will make no difference, provided that they are irreversible. The only reaction which will affect the result is the reverse of the first step, the denitrosation, if it occurs to any appreciable extent.

3.3 Dependence of the rate of AcGlyGly nitrosation on peptide concentration

Although the excellent linearity of the ln A versus time plots (Figure 3.4) implies a first order dependence on [AcGlyGly], this was confirmed by carrying out reactions with different initial [AcGlyGly] in 1.0M DCl at 25°C. Values of k_0 (see Table 3.3) are virtually independent of [AcGlyGly] which confirms the validity of Equation 3.1.

The reactions were also followed by changes in the UV absorbance at 410nm, due to the N-nitrosopeptide (Figure 3.2) Significantly, the maximum absorbance occurs approximately at the same time after the start

of each reaction and each maximum is approximately proportional to the initial concentration of peptide, as expected for Equation 3.1[60].

Table 3.3

Effect of peptide concentration on the nitrosation of AcGlyGly at 25 °C

[DCl]	*[$NaNO_2$]*	*[AcGlyGly]*	*$10^5 k_o$ /s^{-1}*
1.0	0.40	0.09	3.09
1.0	0.40	0.06	2.94
1.0	0.40	0.03	3.35

3.4 Dependence of the rate of AcGlyGly nitrosation on nitrite concentration

Nitrite ion is a weak base (pK_a = 3.37 at 12.5°C)[61] and therefore reacts with one equivalent of DCl to produce DNO_2. The amount of DCl added to the reaction solution must allow for this reaction in addition to producing the required concentration of DCl. Thus, in the reaction mixture where $[D^+]$ was 1.0M and $[DNO_2]$ was 0.4M, $[Cl^-]$ would be 1.4M. In experiments where the concentration of nitrite was varied, sodium chloride was therefore added to maintain a constant total chloride concentration of 1.4M.

Values of k_0 (Equation 3.1) for 0.3M AcGlyGly in 1.0M DCl ($[Cl^-]$ = 1.4M) at 25°C for a four-fold change in DNO_2 concentration are reported in Table 3.4. Values of k_2 refer to Equation 3.2.

Table 3.4

Effect of nitrite concentration on the nitrosation of AcGlyGly at 25 °C

[DCl] (added)	*[DCl] (excess)*	*[$NaNO_2$]*	*[AcGlyGly]*	*[NaCl]*	*$10^5 k_o/s^{-1}$*	*$10^5 k_2 M^{-1} s^{-1}$*
1.4	1.0	0.40	0.03	0.00	3.35	8.4
1.3	1.0	0.30	0.03	0.10	2.45	8.2
1.2	1.0	0.20	0.03	0.20	1.55	7.8
1.1	1.0	0.10	0.03	0.30	0.61	6.1

Figure 3.5

Effect of nitrite concentration on the nitrosation of AcGlyGly at 25°C

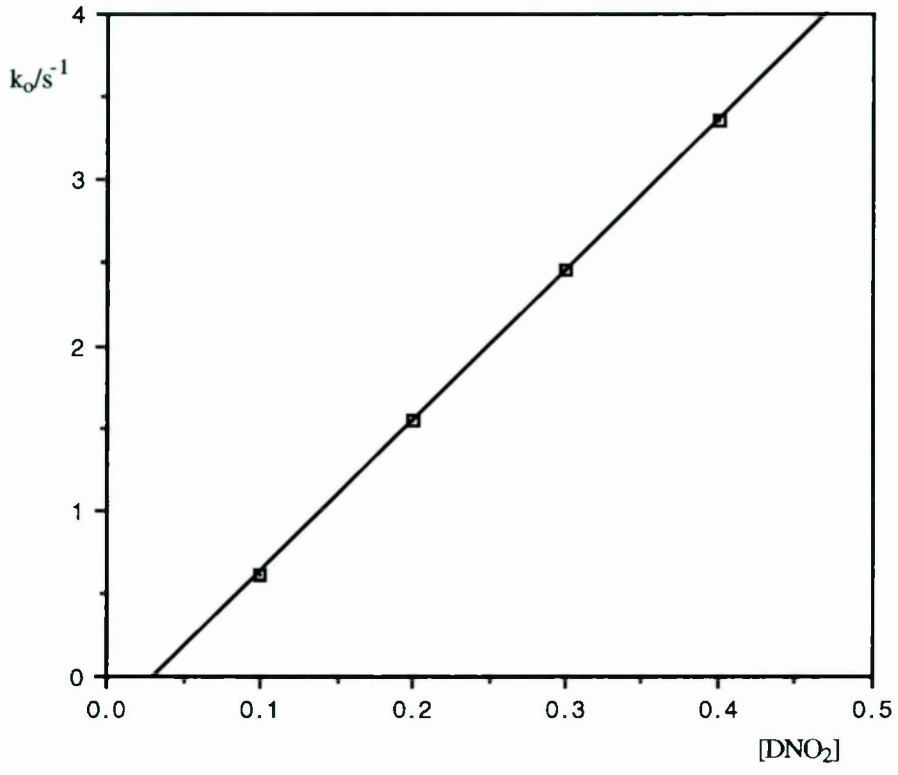

The graph of [DNO_2] against k_0 is linear (Figure 3.5) consistent with a first order rate dependence on nitrite concentration. The intercept on Figure 3.5 is negative, which probably relates to loss of nitrite on mixing the reactants, or insufficient excess nitrite to achieve *pseudo* first order conditions at the lower DNO_2 concentrations. This aside, the nitrosation of AcGlyGly is best described by Equation 3.2.

$$\text{Rate} = k_2[DNO_2]\{\text{AcGlyGly}] \qquad \text{Equation 3.2}$$

3.5 Dependence of the rate of AcGlyGly nitrosation on acid concentration

Most nitrosation reactions are strongly acid catalysed[62]. The effect of different DCl concentrations and of using D_2SO_4 were briefly examined using 0.03M AcGlyGly and 0.4M $NaNO_2$ at 25°C. The results are reported in Table 3.5 together with the relevant values of the amide acidity function (d_A). Use of a wider range of solvent acidities proved unfeasible; with [DCl] < 0.25M, reaction rates were extremely slow; with [DCl] > 1.0M, significant denitrosation of the N-nitrosopeptide occurred which vitiated the evaluation of k_0 (see below).

Table 3.5

Effect of acidity on the nitrosation of AcGlyGly at 25 °C

Initial [AcGlyGly] 0.03M and [$NaNO_2$] 0.4M

	[acid] (added)	*[acid] (excess)*	$^*d_A$	$10^6k_0/s^{-1}$	$10^6k_0/d_AM^{-1}s^{-1}$
DCl	1.40	1.00	1.58	33.5	21.2
DCl	0.90	0.50	0.63	12.7	20.1
DCl	0.65	0.25	0.28	6.0	21.4
D_2SO_4	1.05	0.85	1.57	38.1	24.1

*where $D_A = -\lg d_A$

The results in Table 3.5 confirm that peptide nitrosation is acid-catalysed, with a 5-fold increase in going from 0.25M DCl to 1.0M DCl. Molarity is known to be an ineffectual measure of acidity for concentrated acids (>0.5M)[63] and the use of acidity functions is preferred. The most appropriate acidity function for peptide reactions is that using amide indicators (H_A) because of the similarity in structure. H_A and H_0 (using

Figure 3.6

Second derivative FTIR spectra with respect to time for the reaction of 0.03M AcGlyGly and 0.4M $NaNO_2$ in 1.0M excess D_2SO_4 at 25°C

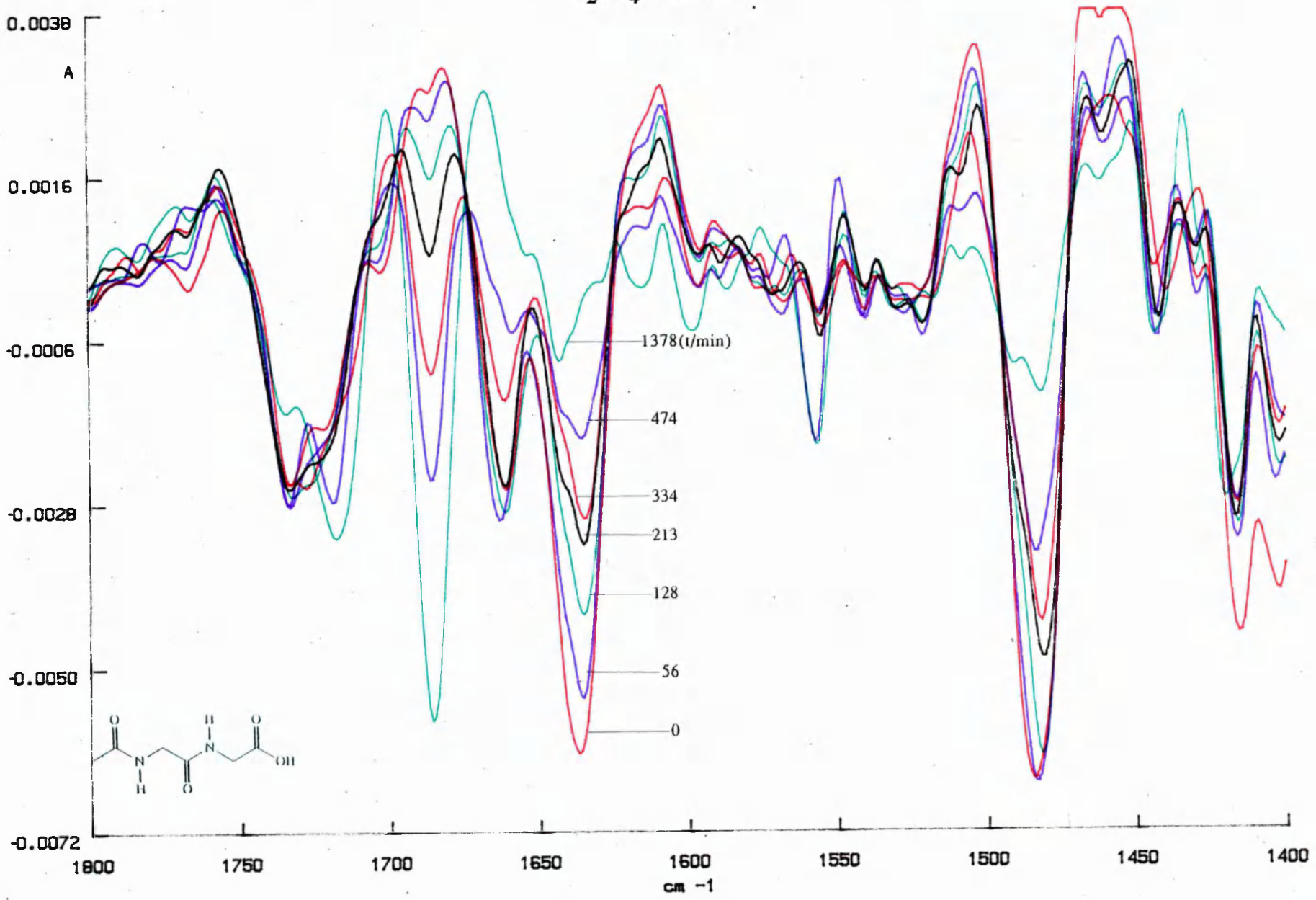

amine indicators) have been shown to be numerically similar for both HCl and H_2SO_4 in the range of concentrations studied [64 65]. The acids in the present experiments are DCl and D_2SO_4, so D_A values rather than H_A values are more appropriate. Acidity function values have been shown to be identical for HCl and DCl but different for H_2SO_4 and D_2SO_4[66 67]. The relevant values of D_A were used to calculate the ratio k_0/d_A reported in Table 3.5. The k_0/d_A ratios are constant within experimental error, which confirms the acid catalysis.

3.6 Possible catalysis of the nitrosation of AcGlyGly by chloride ion

Most nitrosation reactions are strongly catalysed by nucleophilic anions (eg Cl^-) because of the formation of powerful reactants such as NOCl[68]. Exceptionally, catalysis is not observed for amide substrates which has been attributed to rate-limiting H^+ loss from the N-nitrosonium ion intermediate[42]. The effect of added Cl^- on the nitrosation of AcGlyGly in 0.25M DCl at 25° was briefly examined and the results in Table 3.6 below obtained. Addition of 1.0M NaCl approximately doubles k_0 and 1.0M $NaClO_4$ has a similar effect. The increase by both salts reflects an ionic strength effect on the solvent molarity. Their similarity suggests that Cl^- exerts no catalysis. Thus, the nitrosation of peptides must be mechanistically similar to amides with H^+ loss as the rate limiting step.

Table 3.6

Effect of added NaCl on the nitrosation of AcGlyGly at 25 °C

Initial [DCl] = 0.25M; [AcGlyGly] = 0.03M; [$NaNO_2$] = 0.4M.

[NaCl]	*[$NaClO_4$]*	*$10^5 k_0/s^{-1}$*
0.00	0.00	0.60
0.00	1.00	1.28
1.00	0.00	1.43

3.7 The nitrosation of AcGlyGly in D_2SO_4

Although reaction rates for a given d_A value are very similar in D_2SO_4 and DCl, striking differences in the FTIR spectra of the reaction products are clearly evident from the comparison of Figure 3.1 and Figure 3.6. Both Figures show similar changes for DCl and D_2SO_4 in the N-acetyl and carboxylic acid bands at 1636 and 1732cm^{-1} respectively, but the following differences are also evident:

Figure 3.7
Second derivative FTIR spectra with respect to time for the reaction of 0.03M GlyGly and 0.4M $NaNO_2$ in 0.09M excess DCl at 25°C

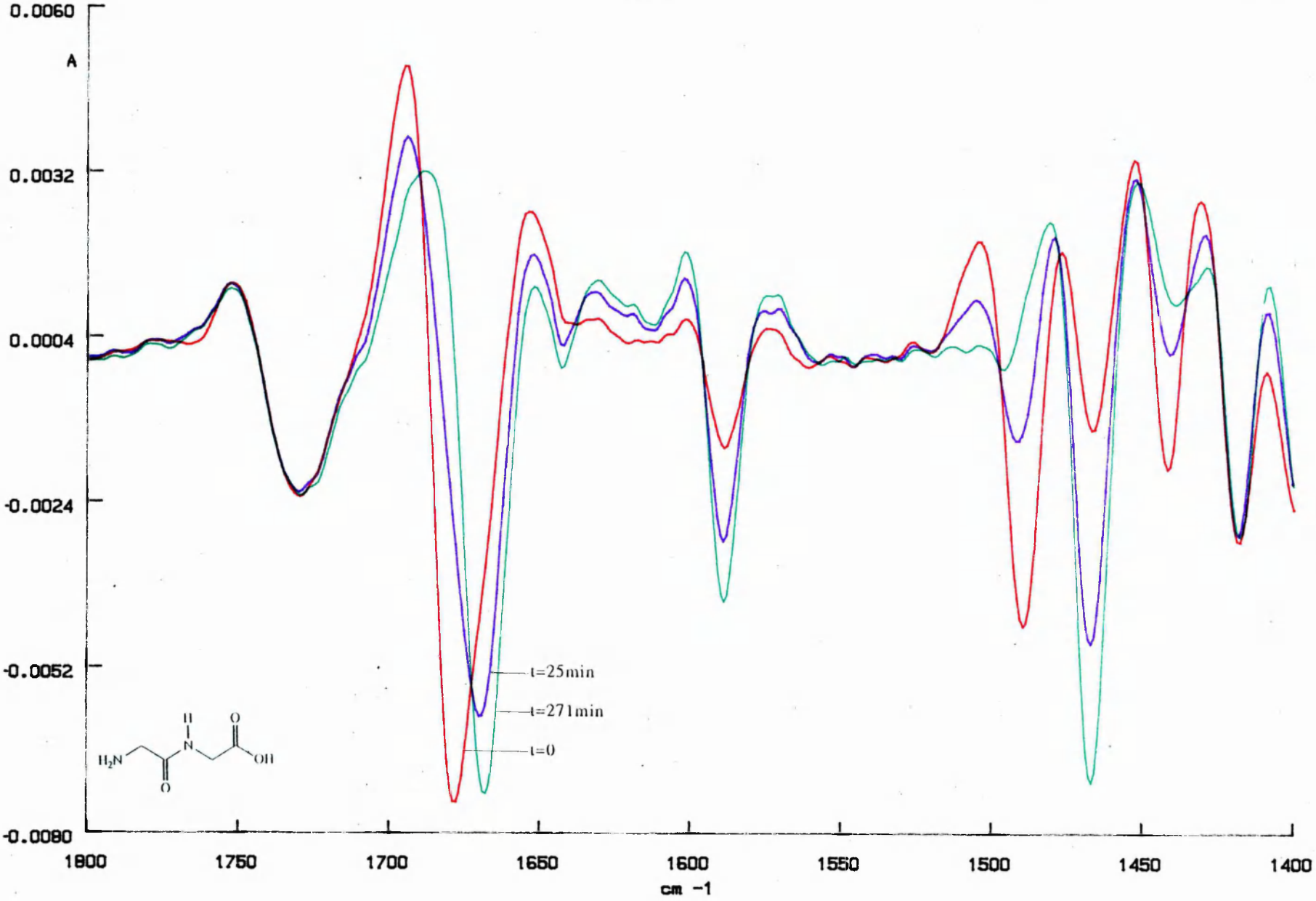

Figure 3.8

Second derivative FTIR spectra with respect to time for the reaction of 0.03M GlyGly and 0.4M $NaNO_2$ in 0.07M excess D_2SO_4 at 25°C

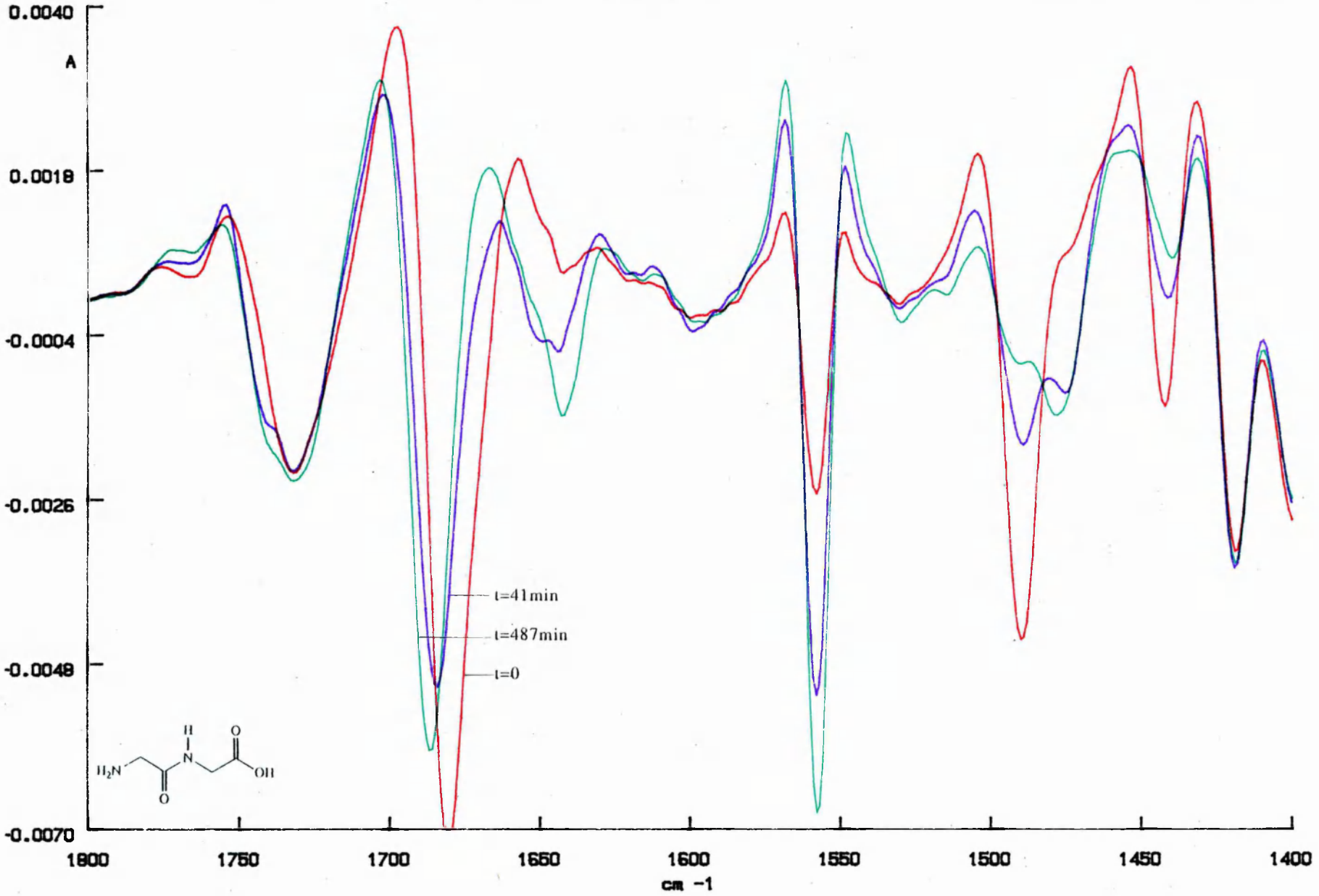

1. The amide II band finishes at 1480cm^{-1} for D_2SO_4 instead of at 1467cm^{-1} for DCl.
2. A product band appears at 1558cm^{-1} for D_2SO_4 instead of at 1587cm^{-1} for DCl.
3. The amide carbonyl band at 1660cm^{-1} in D_2SO_4 disappears and reappears at 1685cm^{-1}, with what appears to be an isosbestic point between the two.

The changes suggest that the initial reaction to give an N-nitrosopeptide in both acids is identical, but that subsequent steps are different.

To confirm that the N-nitrosopeptide in DCl and in D_2SO_4 decomposed via a common diazo intermediate (Scheme 2.1), the nitrosation of GlyGly was investigated in both acids and the FTIR spectra (Figures 3.7 and 3.8) compared with those for AcGlyGly (Figures 3.1 and 3.6). Since GlyGly has a terminal primary amino group, it is expected preferentially to form this diazo intermediate directly (Scheme 3.2)[69 70].

Scheme 3.2

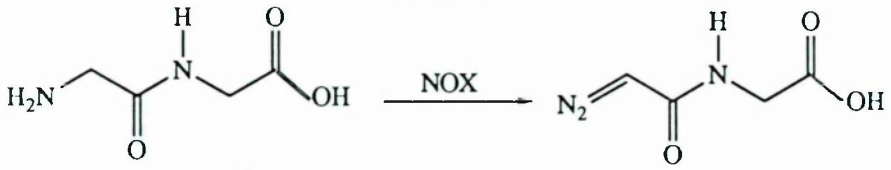

3.8 Products of the nitrosation of AcGlyGly and GlyGly in DCl and D_2SO_4

The FTIR bands evident at the conclusion of the four reactions, ie corresponding to the spectrum at the longest time in each of Figures 3.1, 3.6-3.8, are summarised in Table 3.7.

Table 3.7
Product FTIR bands for nitrosation by DNO_2/cm^{-1}

GlyGly/DCl	1732	1669	1642	1589	1467
AcGlyGly/DCl	1715	1668	1642	1587	1467
GlyGly/D_2SO_4	1732	1686	1642	1558	1477
AcGlyGly/D_2SO_4	1719	1686	1642	1557	1480

The differences noted above for AcGlyGly in DCl and D_2SO_4 also apply to reactions of GlyGly. Comparison of AcGlyGly and GlyGly, however,

Figure 3.9

Acetic acid in 1.0M DCl at 25°C, 2nd derivative

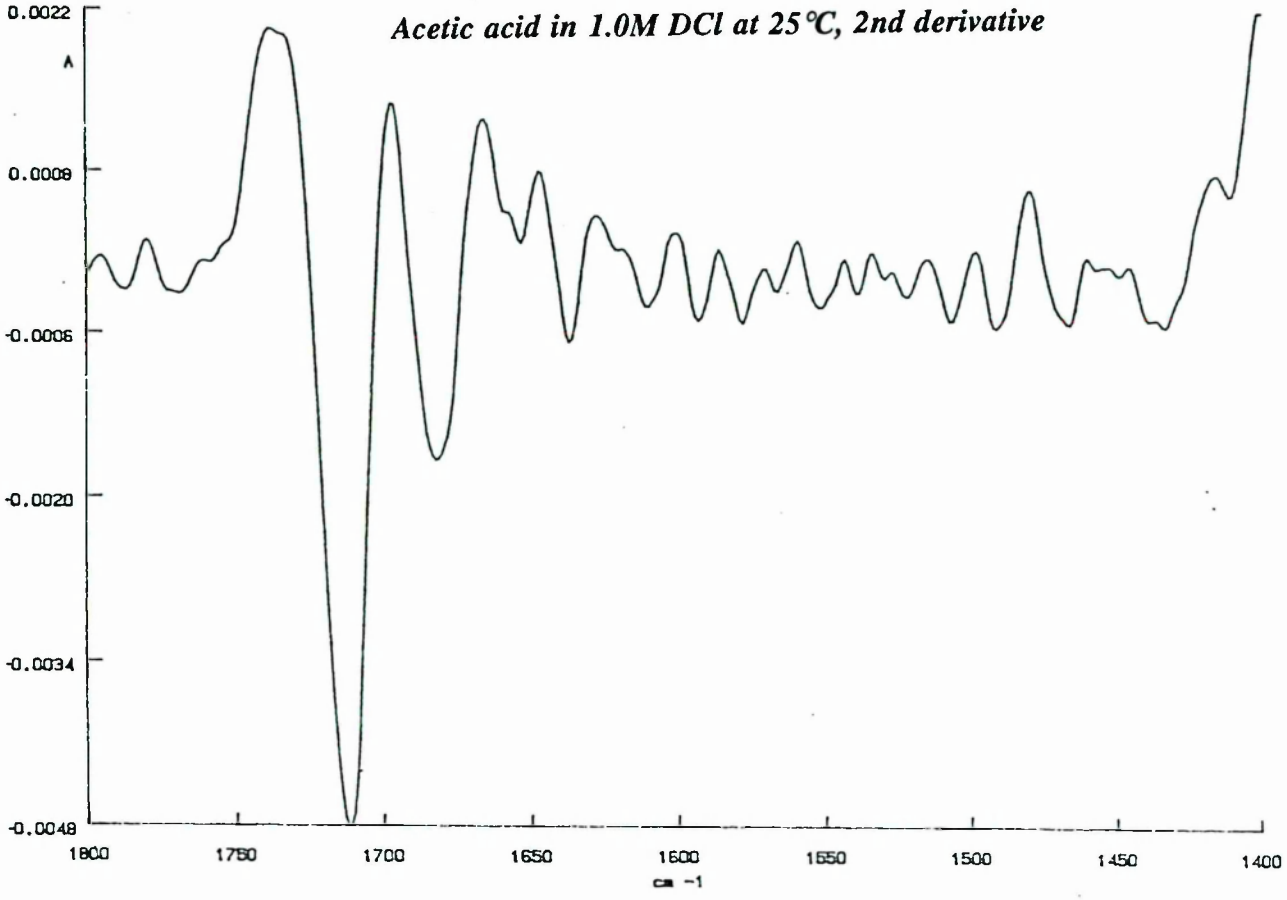

Figure 3.10

2-hydroxyacetylglycine in 1.0M DCl at 25°C, 2nd derivative

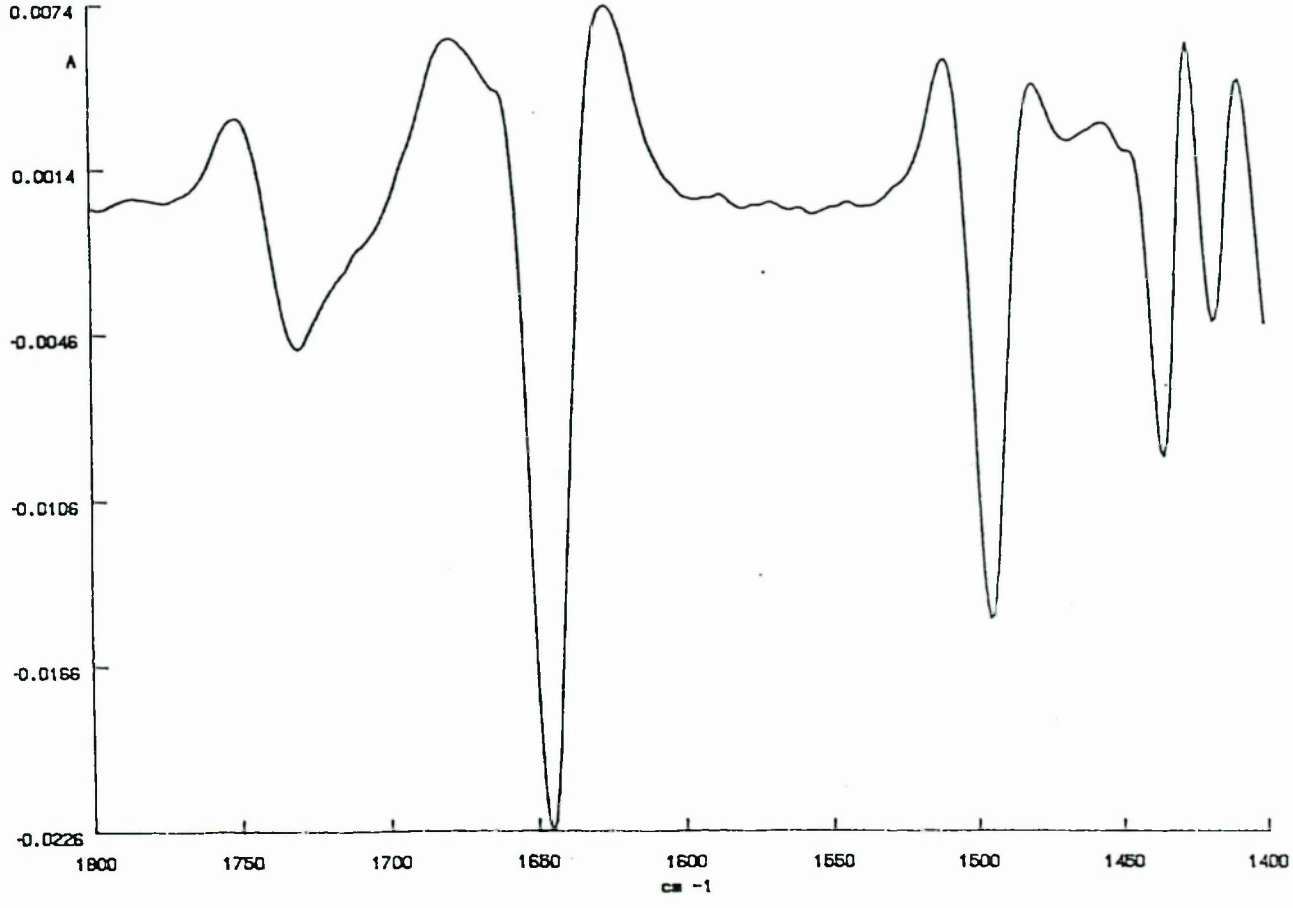

Figure 3.11

2-chloroacetylglycine in 1.0M DCl at 25℃, 2nd derivative

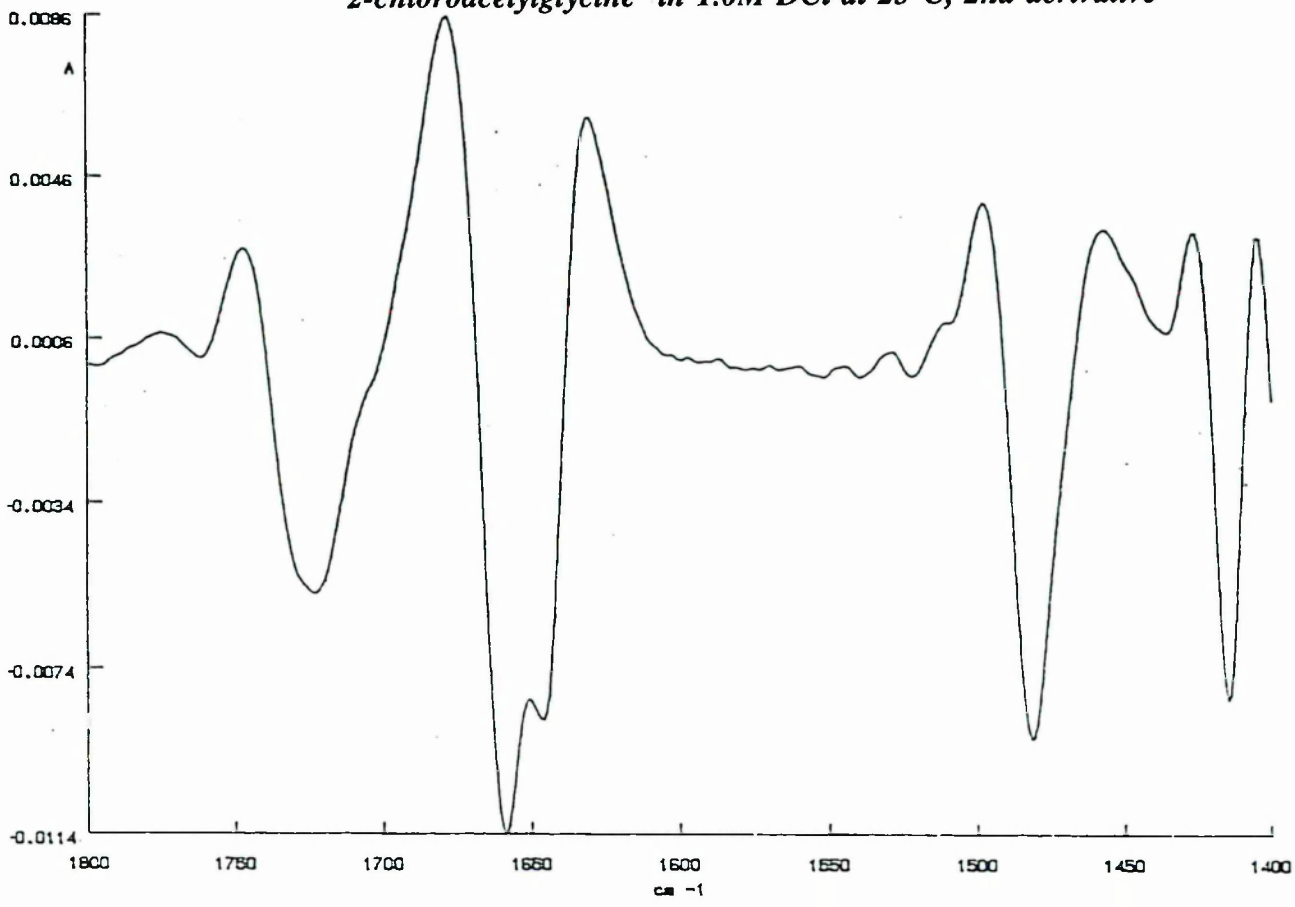

Figure 3.12

Iminodiacetic acid in 1.0M DCl at 25℃, 2nd derivative

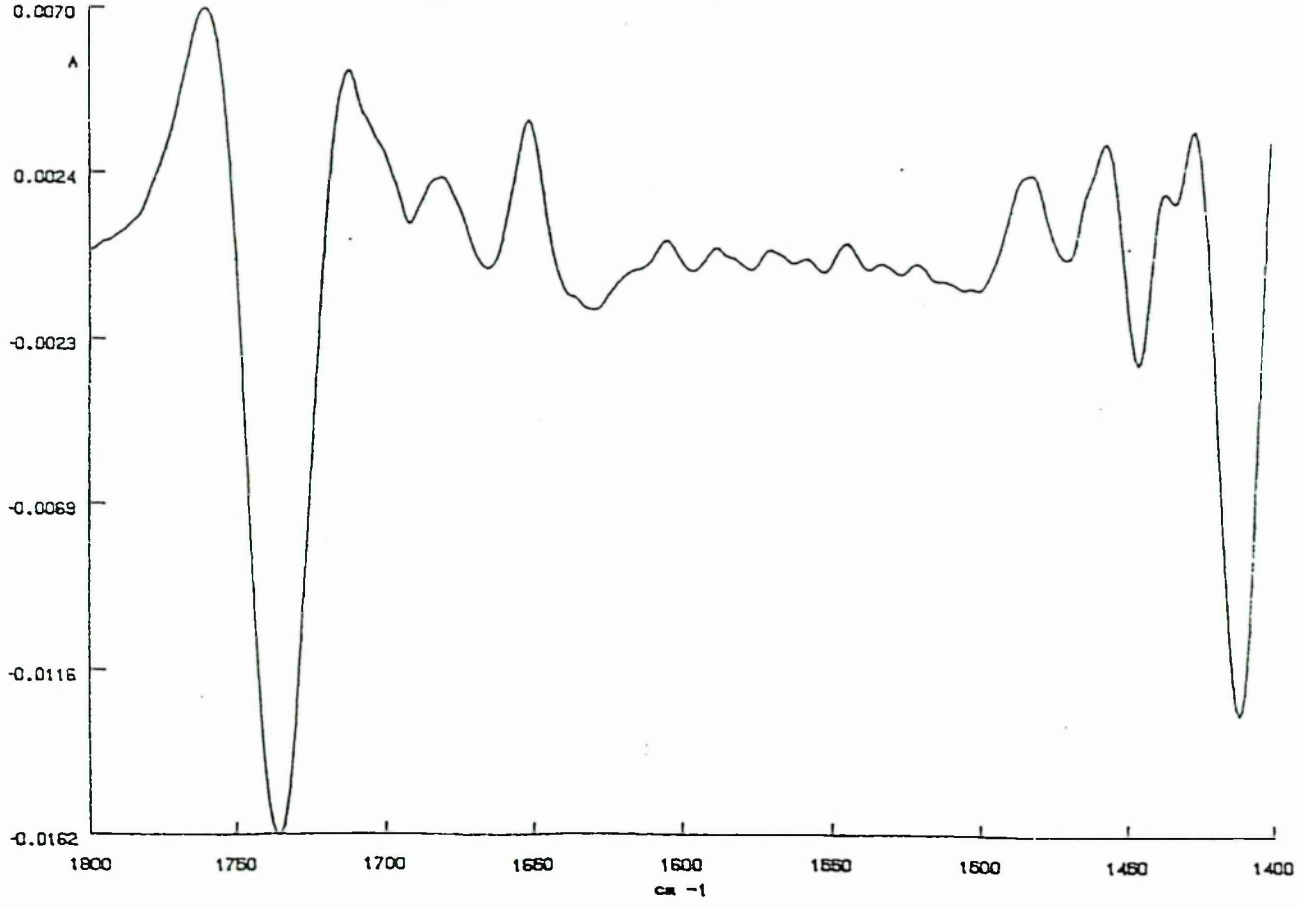

show very similar product bands for both reactions. It therefore seems very likely that they proceed by the same N-(2-diazoacetyl)glycine intermediate. The only significant difference, the peak at 1715 (or 1719) cm^{-1} for the AcGlyGly reactions as opposed to 1732cm^{-1} for the GlyGly reactions is consistent with the formation of acetic acid from decomposition of the N-nitrosoacetyl product (Scheme 3.1).

The IR spectra of the expected reaction products (Scheme 2.1) are shown (Figures 3.9 - 3.12) and the main band frequencies summarised in Table 3.8.

Table 3.8

Principal FTIR bands for the expected products from the nitrosation of AcGlyGly and GlyGly /cm^{-1}

Acetic acid	1712	1682	
N-(2-hydroxyacetyl)glycine	1731	1645	1495
N-(2-chloroacetyl)glycine	1724	1659	1482
Iminodiacetic acid	1736		

Iminodiacetic acid does not appear in Scheme 2.1, but is known to form by the Wolff rearrangement of the N-(2-diazoacetyl)glycine (Scheme 3.3)[71].

Scheme 3.3

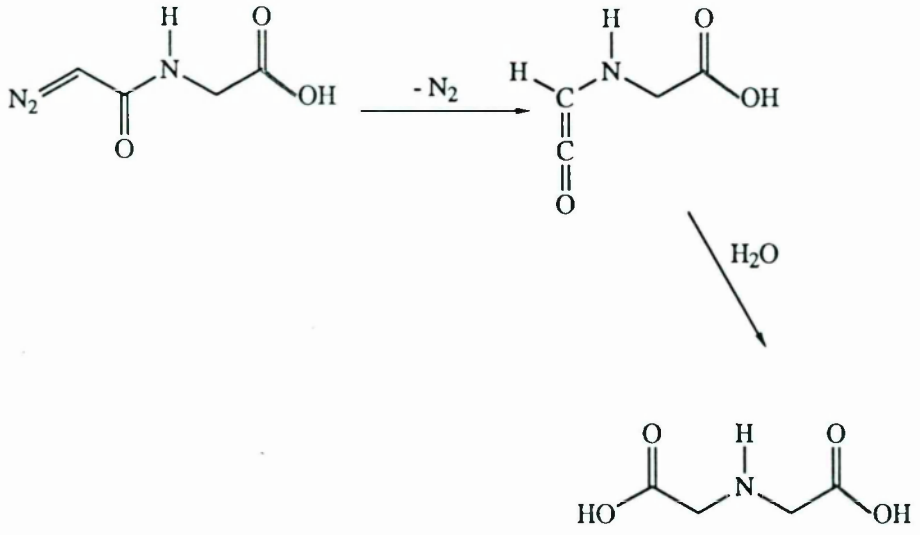

None of these expected products are evident in the FTIR spectra in Figures 3.1 and 3.6-3.8, except the recurring band at 1642cm^{-1} which could indicate that N-(2-hydroxyacetyl)glycine is a minor product, whose other

Figure 3.13

Mass spectrum of the products of the reaction of 0.03M GlyGly and 0.4M $NaNO_2$ in 1.0M excess DCl at 25°C

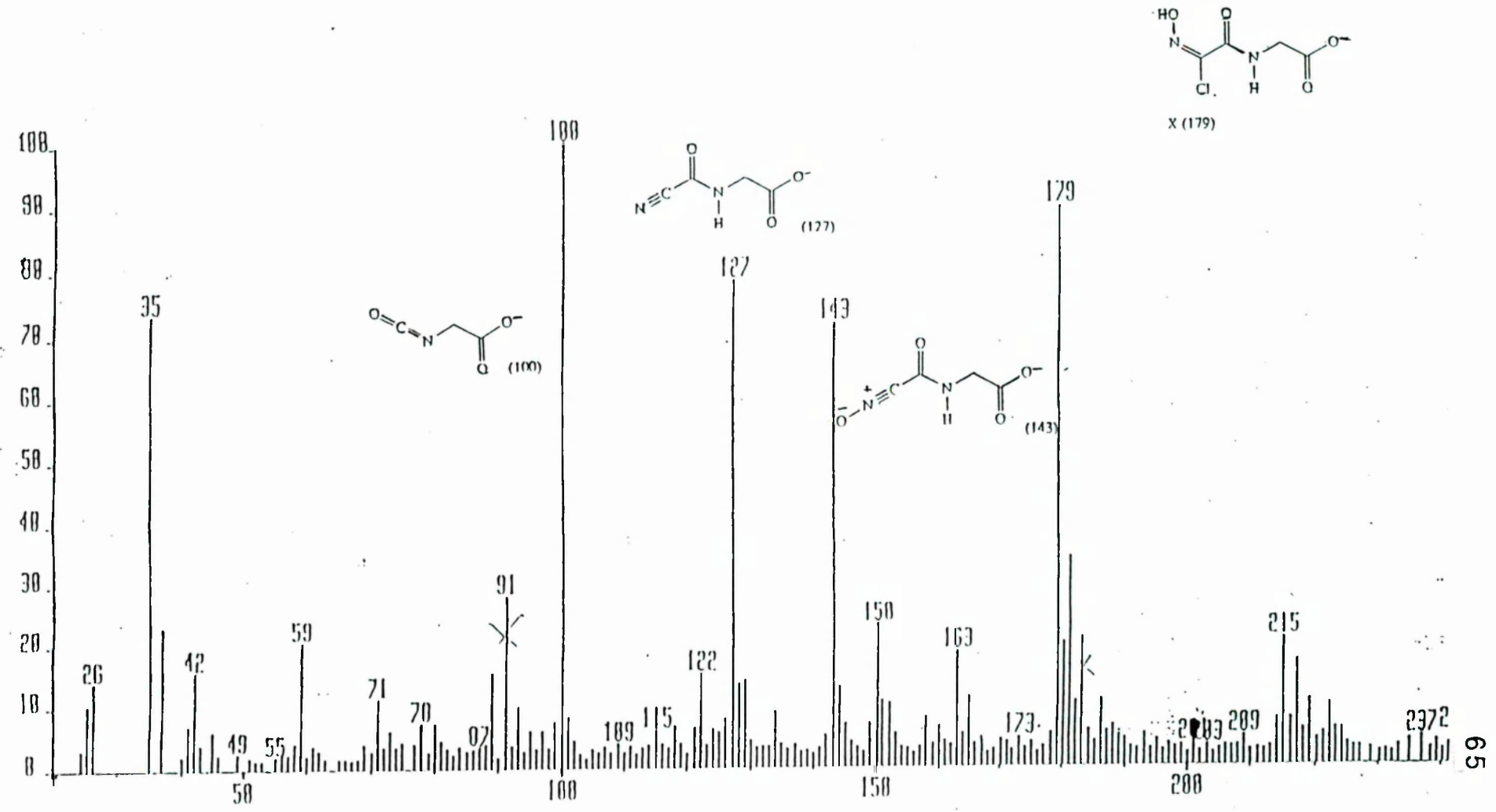

Figure 3.14

Mass spectrum of the products of the reaction of 0.03M AcGlyGly and 0.4M $NaNO_2$ in 1.0M excess DCl at 25°C

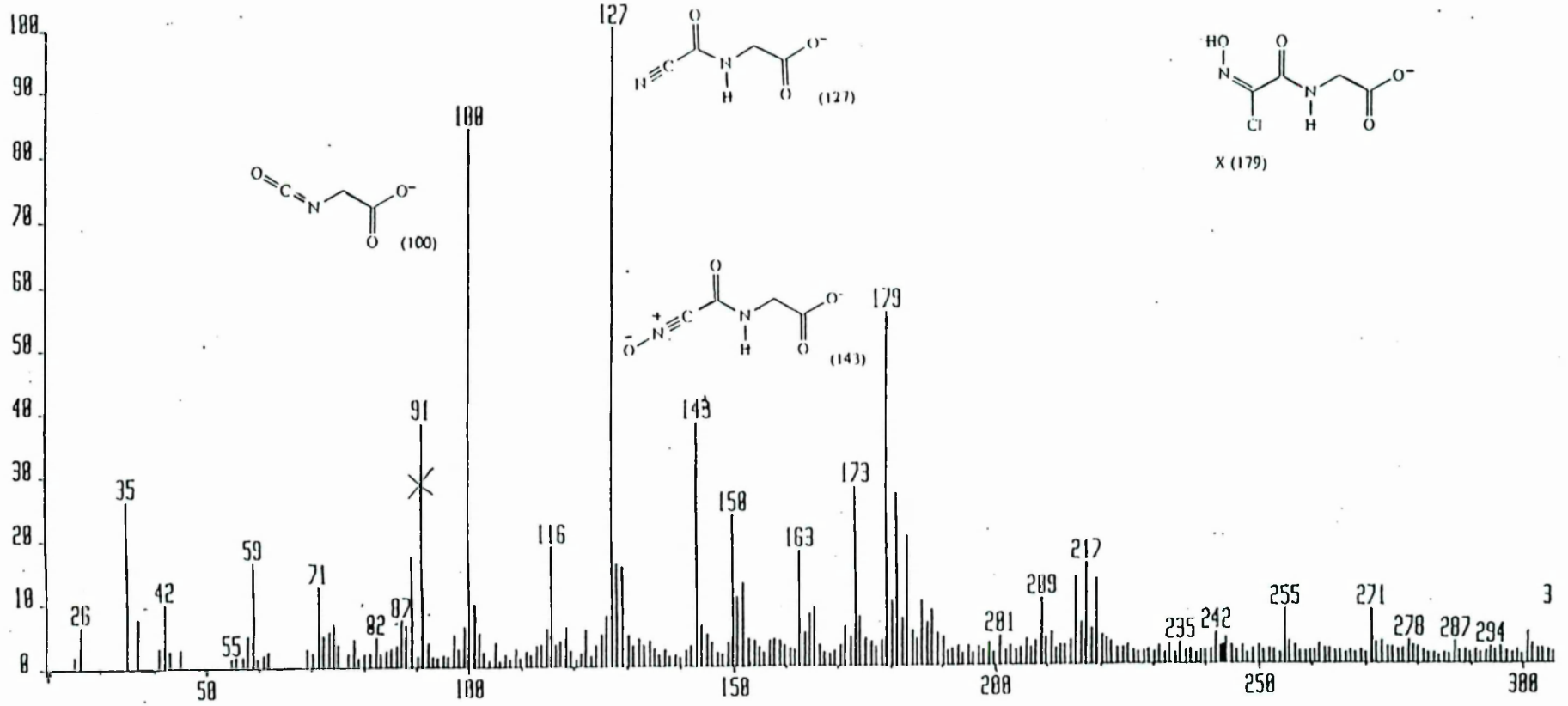

absorbances are masked by other components. It was therefore necessary to identify the reaction products by alternative methods.

3.9 Use of Mass Spectroscopy to identify products of AcGlyGly and GlyGly nitrosation reactions

$5cm^3$ of each reaction mixture (containing 0.03M peptide, 0.4M $NaNO_2$ and either 1.0M excess DCl or 0.85M excess D_2SO_4) was made up as before, sealed in vials and left in a 25° bath for 24h. The ethyl acetate extract of each reaction solution was dried ($MgSO_4$) and after vacuum evaporation of the solvent, the solid residue was analysed by FAB mass spectroscopy.

The reactions of GlyGly and AcGlyGly in DCl gave the FAB (negative ion) mass spectra shown in Figures 3.13 and 3.14 respectively. Both spectra show a significant peak at m/z = 179 and 181, and other fragmentation peaks, which are characteristic of N-(2-chlorohydroxyiminoacetyl)glycine (X). The fragmentation of X to give the FAB negative ion spectra in Figure 3.13 and Figure 3.14 are outlined in Scheme 3.4.

Scheme 3.4

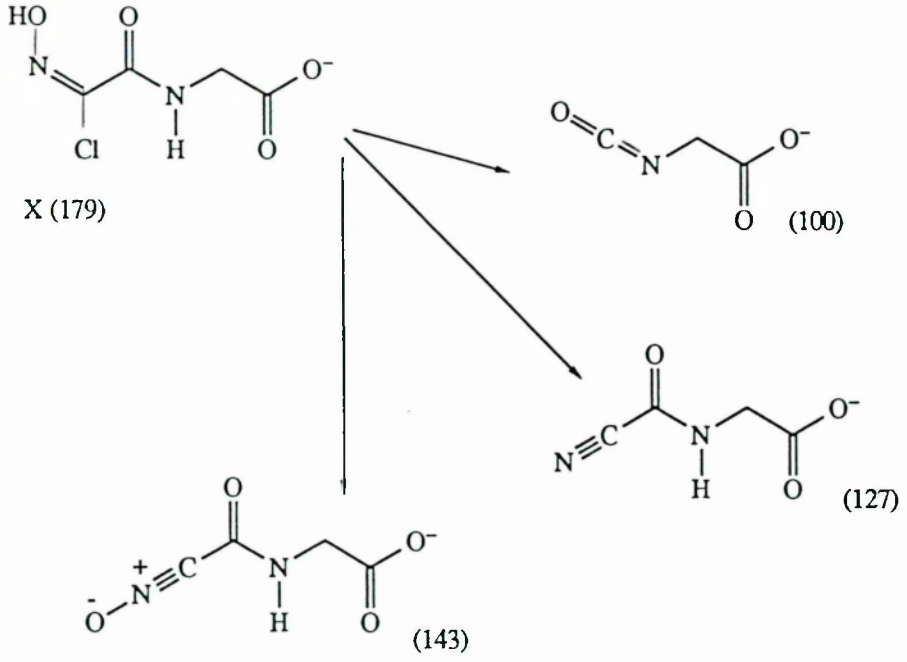

The product (X) was detected in reactions of glycyl peptides in the presence of excess nitrite, by Glover[72] who rationalised its formation by NOCl nitrosation of the diazo intermediate as outlined in Scheme 3.5.

Scheme 3.5

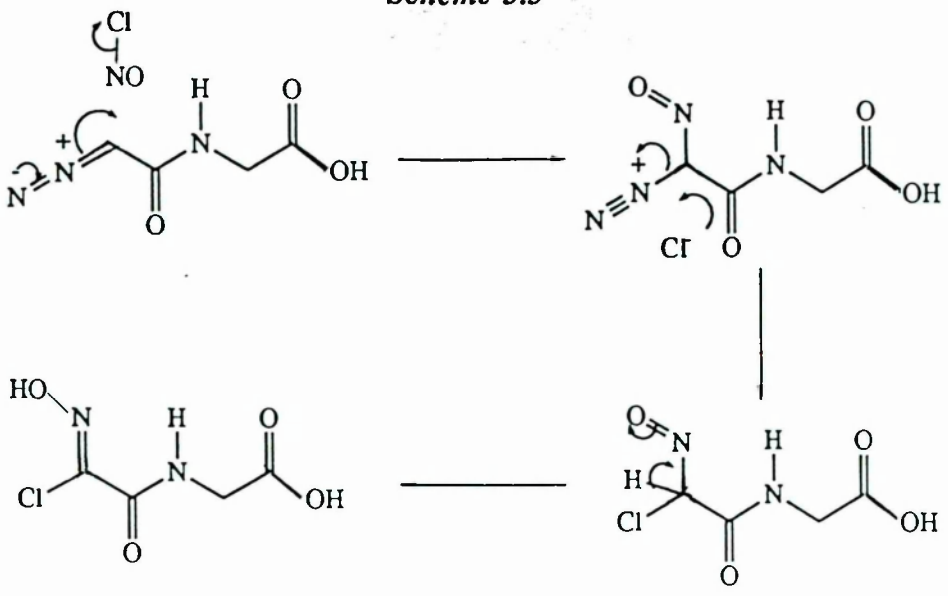

Scheme 3.6

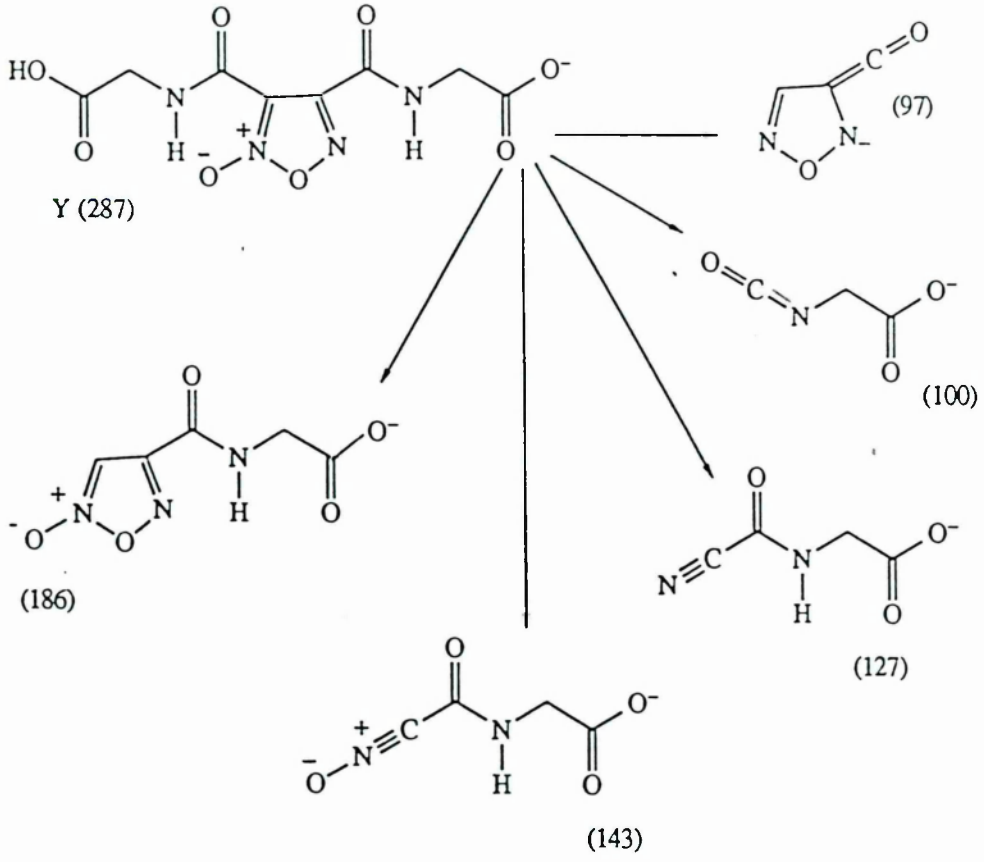

In confirmation, both the FAB negative ion mass spectrum and the FTIR spectrum (Figure 3.15) of authentic N-(2-chlorohydroxyiminoacetyl) glycine, synthesised independently (see Experimental), are very similar to

Figure 3.15

Comparison of FTIR spectra of reaction products with authentic compound

(a) products of AcGlyGly, $NaNO_2$, DCl

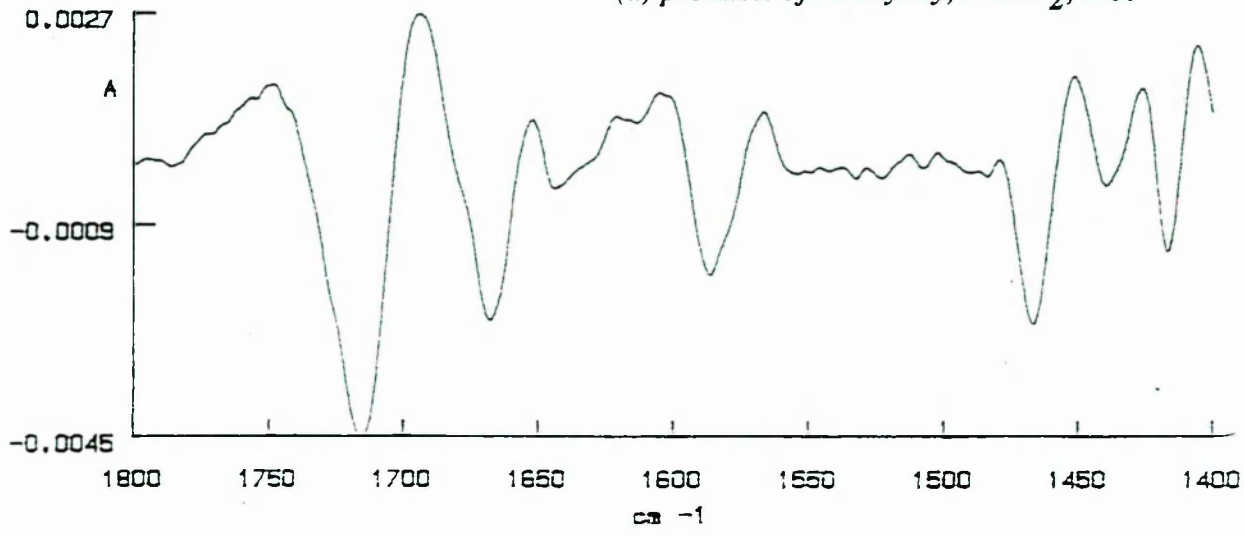

(b) products of GlyGly, $NaNO_2$, DCl

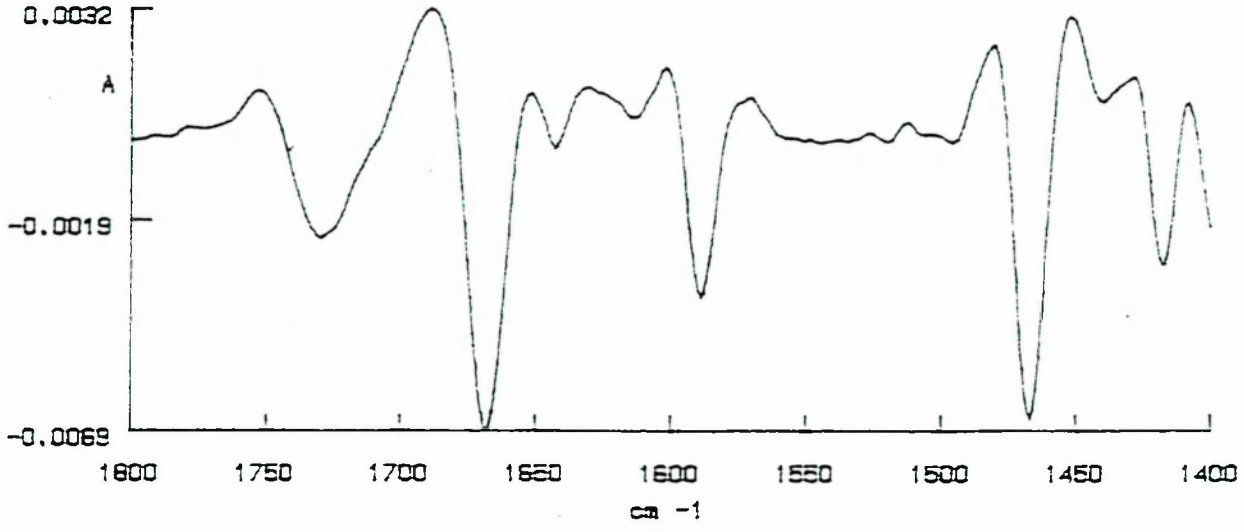

c) N-(2-chloro-hydroxyiminoacetyl)glycine

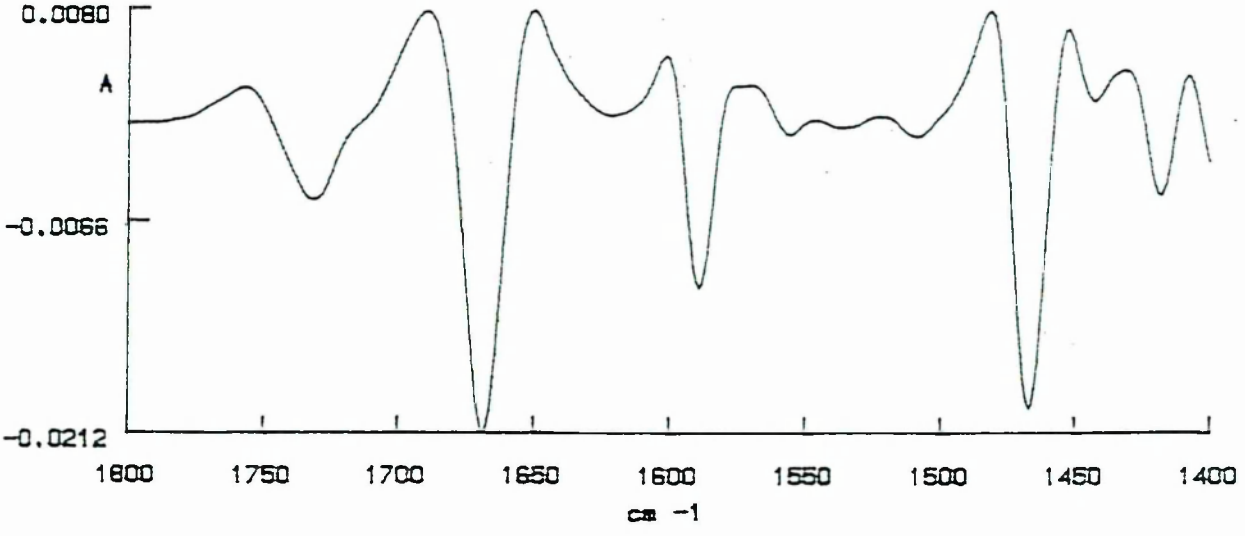

Figure 3.16

Mass spectrum of the products of the reaction of 0.03M GlyGly and 0.4M $NaNO_2$ in 0.85M excess D_2SO_4 at 25°C

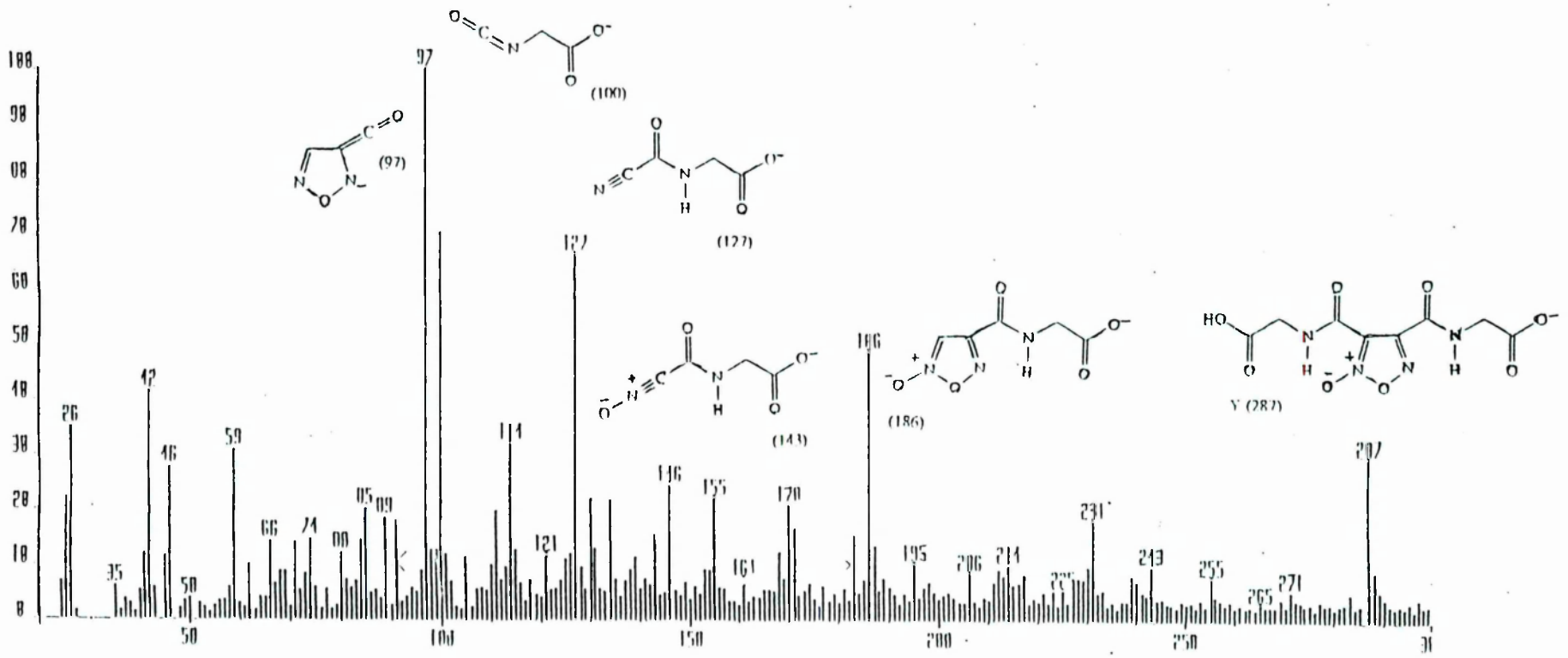

Figure 3.17

Mass spectrum of the products of the reaction of 0.03M AcGlyGly and 0.4M $NaNO_2$ in 0.85M excess D_2SO_4 at 25°C

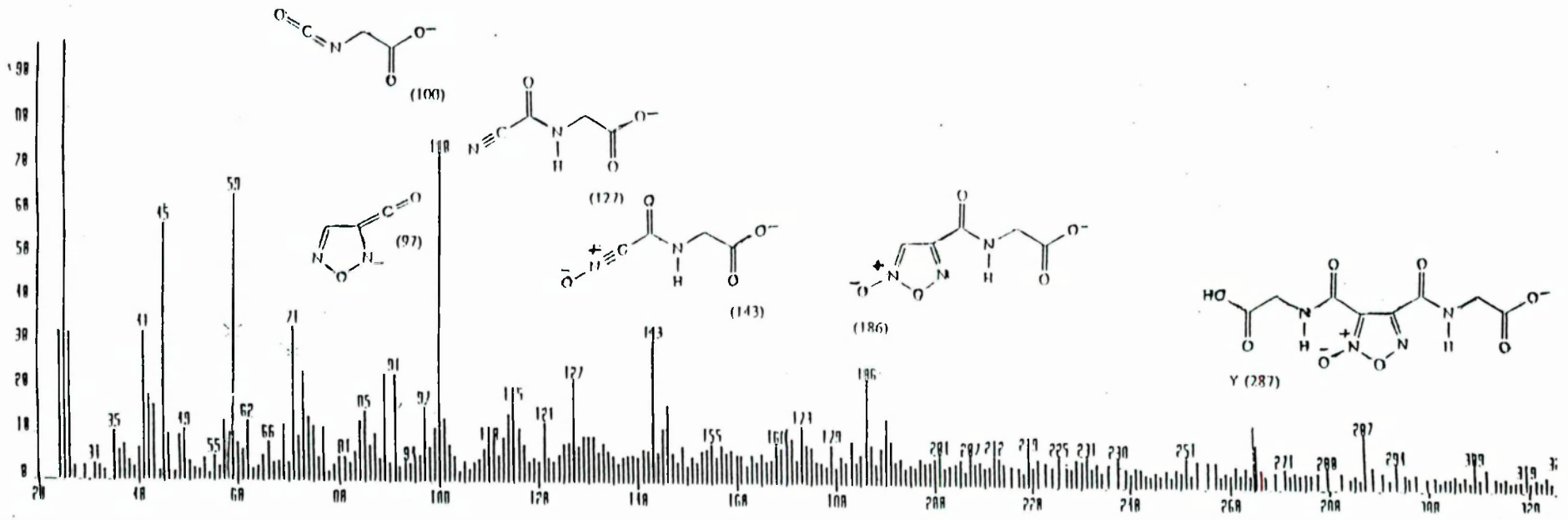

those of the major product of the reactions of GlyGly and AcGlyGly with $NaNO_2$/DCl.

The FAB (negative ion) mass spectra of the principal product of the nitrosation of GlyGly and AcGlyGly in D_2SO_4 are shown in Figures 3.16 and 3.17. These show a M - H^+ ion at m/z = 287, which can be ascribed to the presence of the nitrile oxide dimer (Y). The fragmentation of (Y) to give the ions shown in Scheme 3.6 strongly supports this identification.

Thus, nitrosation of the diazopeptide intermediate, Z, could produce the nitrile oxide (Scheme 3.7) and these compounds are well known to dimerise[73]. Attempts to synthesise the authentic nitrile oxide dimer, in order to compare its FTIR spectrum with that of the products from the nitrosation of AcGlyGly and GlyGly in D_2SO_4, were unsuccessful.

Scheme 3.7

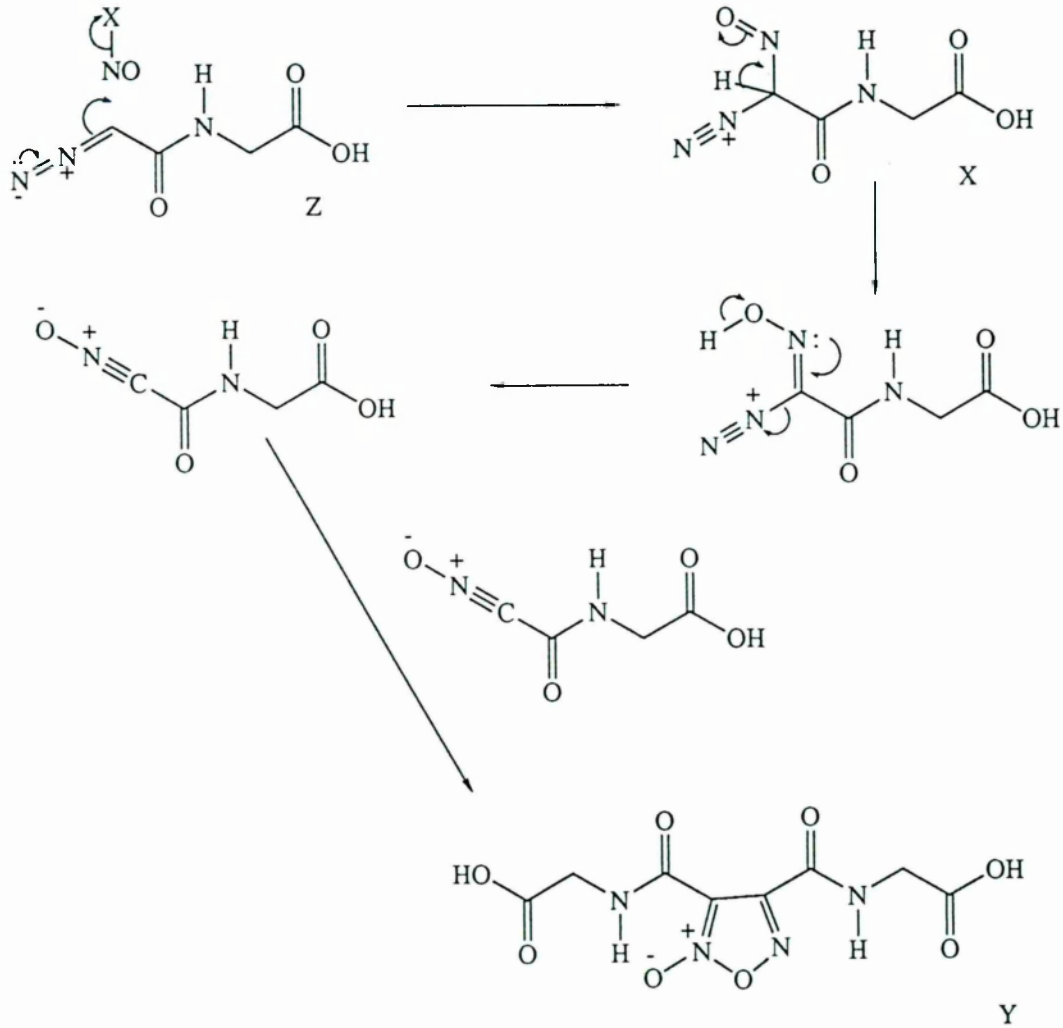

Figure 3.18
Peptide structures

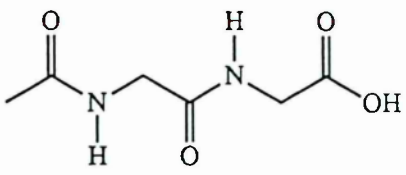

AcGlyGly

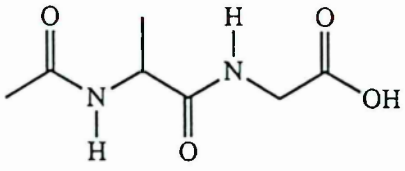

AcAlaGly

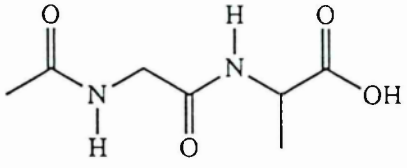

AcGlyAla

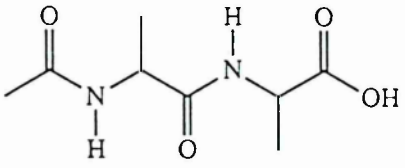

AcAlaAla

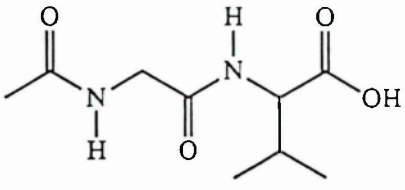

AcGlyVal

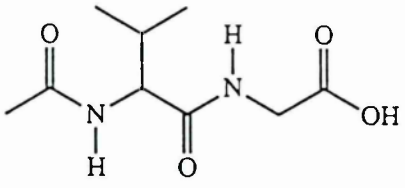

AcValGly

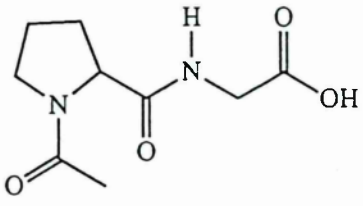

AcProGly

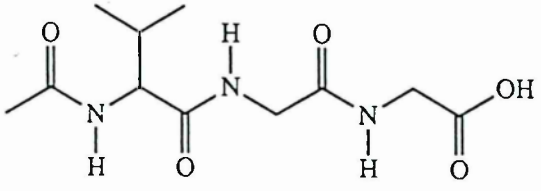

AcValGlyGly

3.10 Nitrosation of other peptides in 1.0M DCl at 25°C

N-Acetylglycine, six N-acetyl dipeptides and N-((N"-acetylvalyl)-N'-glycyl)glycine were prepared and their nitrosation reactions compared with that of AcGlyGly using a similar FTIR procedure. The aim was to obtain information about both the rate of nitrosation and the relative reactivities of the different compounds under standard conditions of 1.0M excess DCl and 25°C. The reactant concentrations were 0.4M $NaNO_2$ and 0.03M peptide throughout, so the reactions should follow Equation 3.1 and comparison of the *pseudo* first order rate coefficient k_0 should reflect relative reactivities. The structures of those substrates are shown in Figure 3.18. The assignment of their IR bands was made on the assumption that the acid, amide I and N-acetyl carbonyl absorptions follow in the same order, from high to low frequency, as those of AcGlyGly. This assumption is supported by the close proximity of corresponding band frequencies in compounds of similar structure evident in Table 3.9, and by the fact that the site of N-nitrosation in different peptides followed a consistent pattern as reported below. For each compound, the changes in the FTIR spectra in the carbonyl region with time are shown and the value of k_0 (Equation 3.1), calculated from the changes in the overlapping spectra with time, is reported.

Table 3.9

Wavenumbers (cm^{-1}) of the peptide absorptions in the carbonyl region for dilute solutions in 1.0M DCl at 25°C

	Acid	*Amide I*	*Acetyl*	*Amide II*
AcGly	1729		1633	1490
AcGlyGly	1732	1662	1636	1482
AcGlyAla	1718	1659	1633	1478
AcGlyVal	1717	1658	1631	1471
AcAlaGly	1732	1650	1633	1480
AcAlaAla	1719	1649	1629	1477
AcValGly	1730	1649	1629	1478
AcValGlyGly	1731	1649	1625	1477
AcProGly	1731	1653	1608	1476

Figure 3.19

Second derivative FTIR spectra with respect to time for the reaction of 0.03M AcGly and 0.4M $NaNO_2$ in 1.0M excess DCl at 25°C

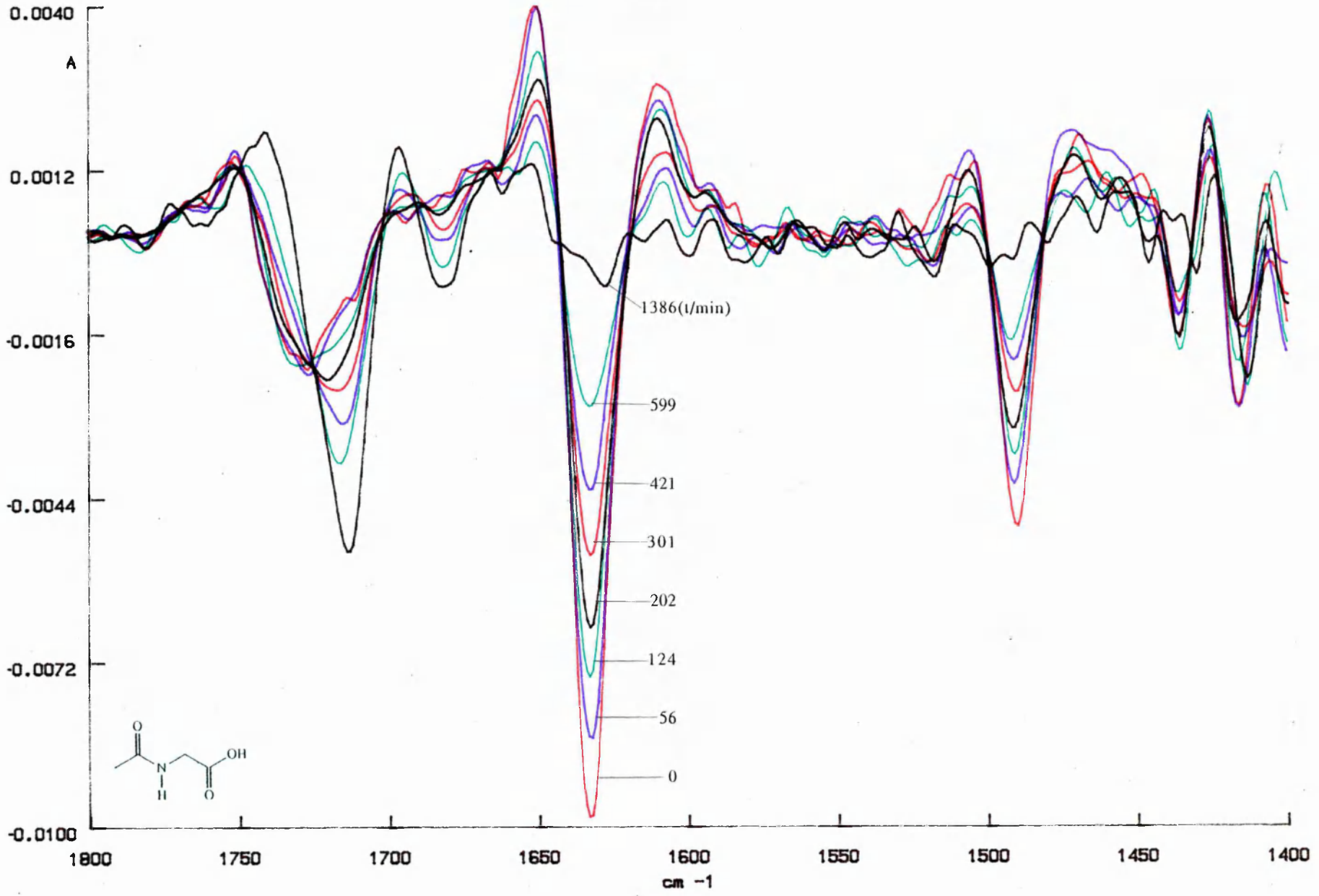

Figure 3.20

Second derivative FTIR spectra with respect to time for the reaction of 0.03M AcProGly and 0.4M $NaNO_2$ in 1.0M excess DCl at 25°C

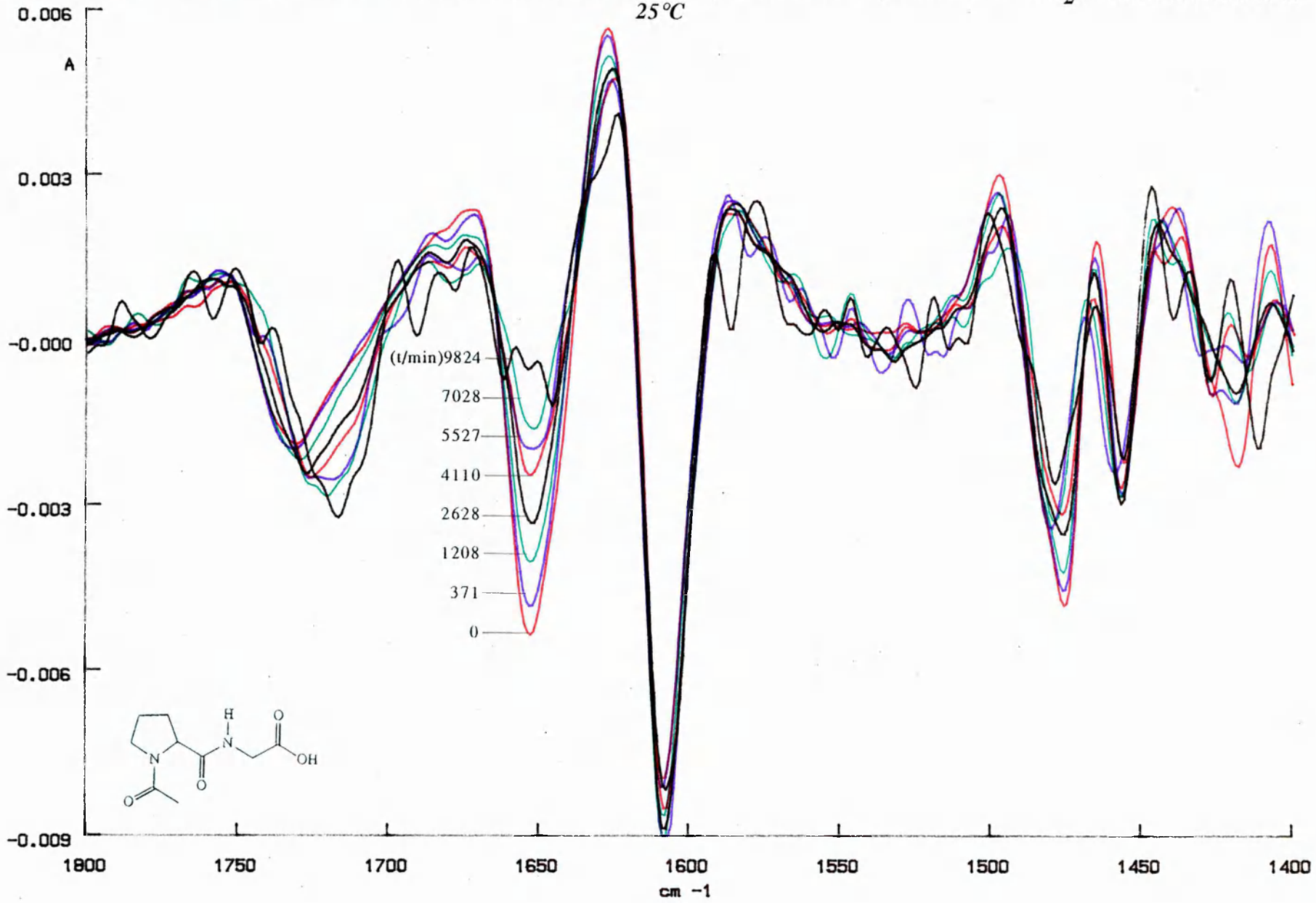

3.10.1 AcGly

This was the simplest compound examined and obviously, has only one reactive site. The ultimate products of N-nitrosation are expected to be chloroacetic acid or glycollic acid and acetic acid. The reaction spectra (Figure 3.19) show the carbonyl absorbance at 1633cm^{-1} and the amide II band at 1490cm^{-1} both diminishing to zero. In the absence of other peaks, both absorbances of the product acetic acid can be seen at 1712cm^{-1} and 1682cm^{-1}. The bands of the other expected products: glycollic acid (1728 and 1667cm^{-1}) and chloroacetic acid (1720 and 1664cm^{-1}) may be present under the acetic acid bands.

The rate of this reaction calculated from the decrease in the absorption at 1633cm^{-1} in Figure 3.19 gives k_0 = 33.0 x 10^{-6}s^{-1} (Table 3.11). It is the same as that of AcGlyGly. An initial increase in intensity of the 1729cm^{-1} band with N-nitrosation is not observed, unlike the reaction with AcGlyGly.

3.10.2 AcProGly

This compound is of particular interest because it also contains only one N-H group, so that nitrosation is only possible at the peptide N-atom. The reaction spectra (Figure 3.20) show the peptide (amide) carbonyl band at 1653cm^{-1} diminishing with time as expected. Whilst changes in the acid carbonyl band consistent with peptide N-nitrosation are apparent, it is difficult to distinguish between these and the carbonyl band of the N-nitroso product. Changes in intensity of the acetyl carbonyl band at 1608cm^{-1} during the reaction cannot arise from nitrosation of the prolyl N-atom but probably result from changes in electron density transmitted through the molecule from the reaction site.

The rate of N-nitrosopeptide formation calculated from changes of the 1653cm^{-1} band of Figure 3.20 with time give k_0 = 3.83 x 10^{-6}s^{-1} (Table 3.11). Thus the nitrosation of AcProGly is about 10-fold slower than AcGlyGly.

Figure 3.21

Second derivative FTIR spectra with respect to time for the reaction of 0.03M AcGlyAla and 0.4M $NaNO_2$ in 1.0M excess DCl at 25°C

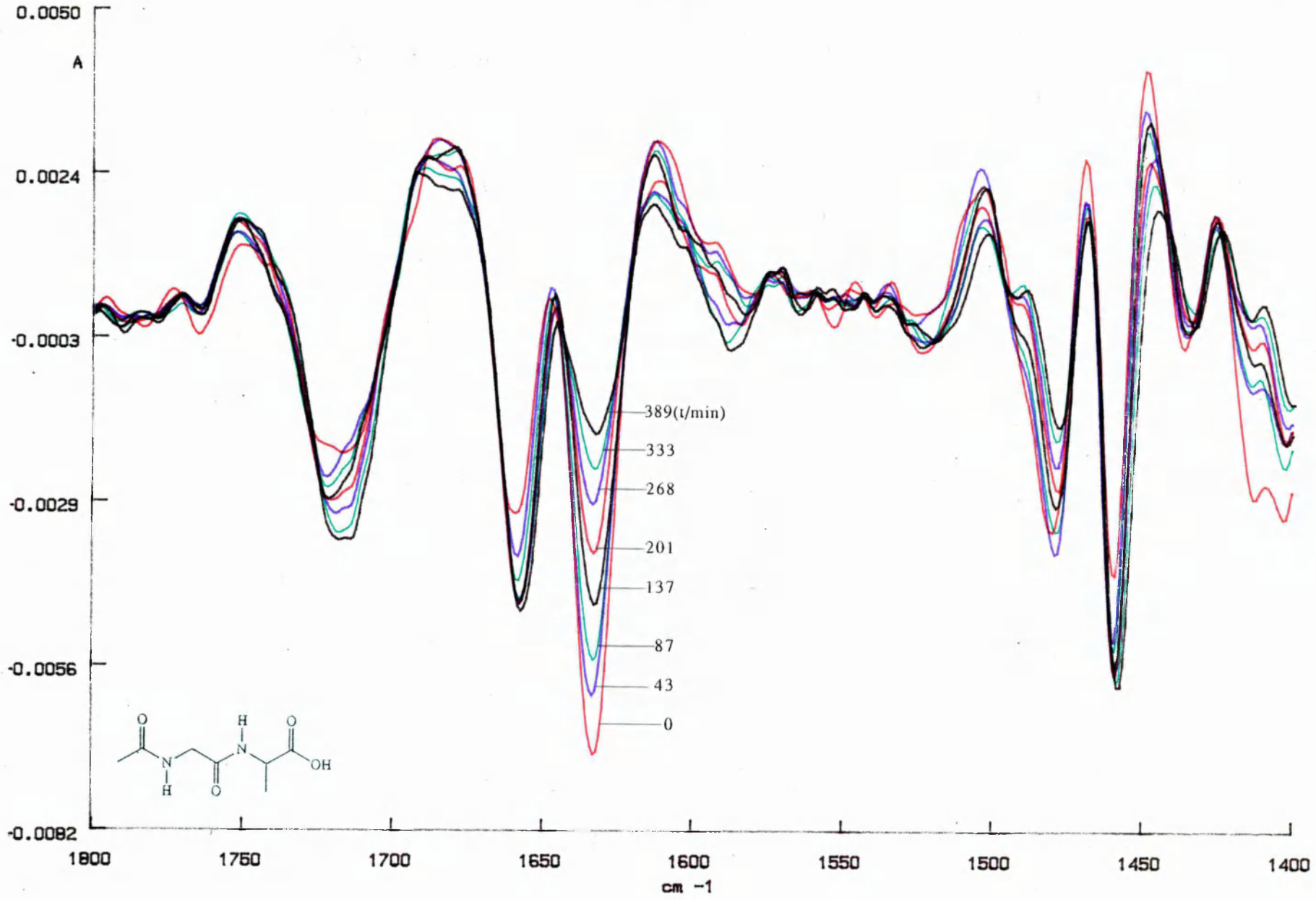

Figure 3.22

Second derivative FTIR spectra with respect to time for the reaction of 0.03M AcGlyVal and 0.4M $NaNO_2$ in 1.0M excess DCl at 25°C

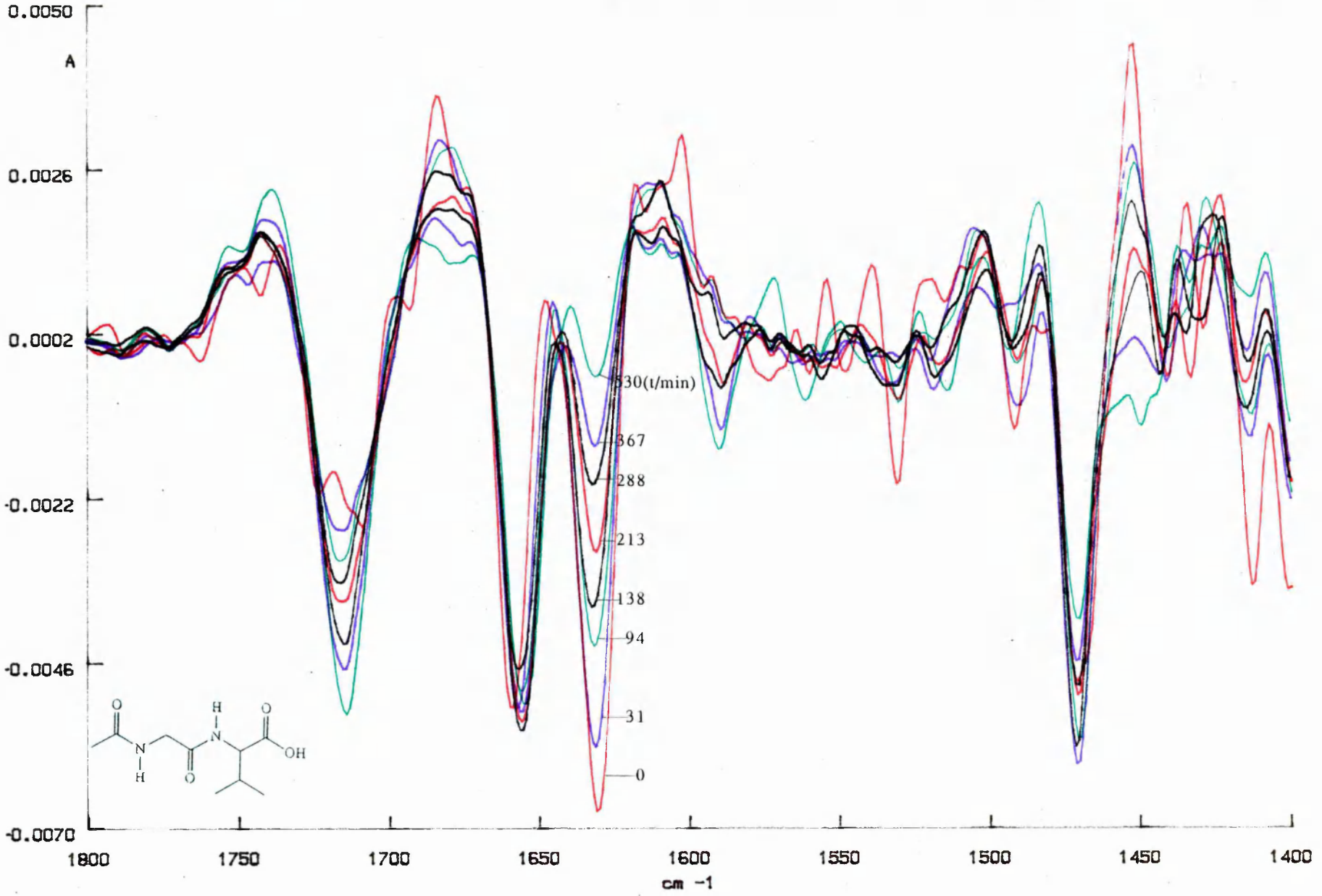

3.10.3 AcGlyAla and AcGlyVal

For both of these peptides, the reaction spectra (Figures 3.21 and 3.22) show a decrease with time of the N-acetyl absorptions at 1633 and 1631cm^{-1} respectively. Thus, N-nitrosation occurs adjacent to the acetyl carbonyl group and the reaction spectra are very similar to those of AcGlyGly. The N-nitrosopeptide band cannot be distinguished under the product acid band. although changes in intensity are apparent. The rates of N-nitroso-N-acetyl peptide formation calculated from the decrease in the 1633 and 1631cm^{-1} bands respectively of Figures 3.21 and 3.22 give values of k_0 = 55.1 x $10^{-6}s^{-1}$ and 73.0 x $10^{-6}s^{-1}$ (Table 3.11). Thus, both reactions are faster than AcGlyGly.

Figure 3.23

Second derivative FTIR spectra with respect to time for the reaction of 0.03M AcValGly and 0.4M $NaNO_2$ in 1.0M excess DCl at 25°C

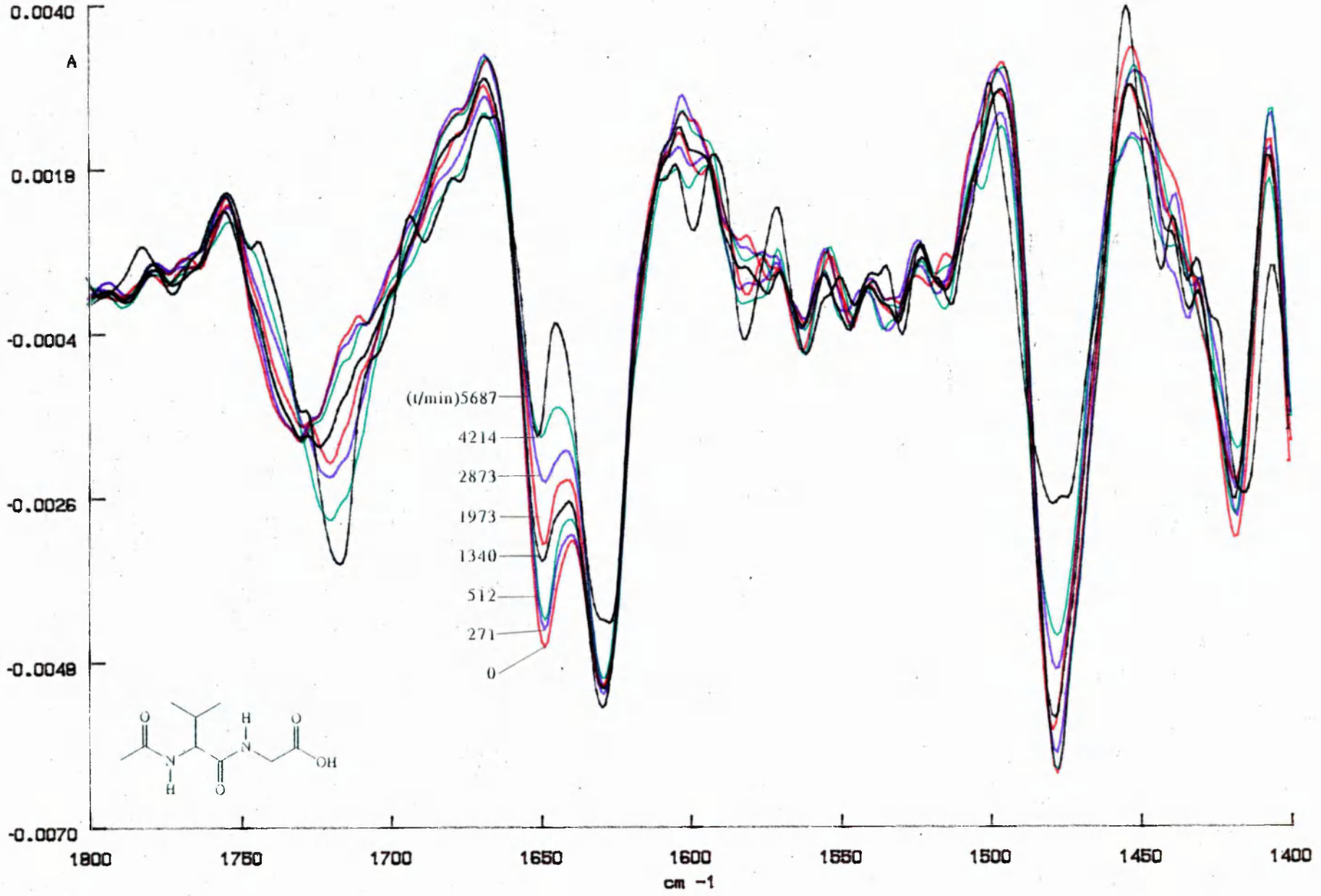

Figure 3.24

Second derivative FTIR spectra with respect to time for the reaction of 0.03M AcValGlyGly and 0.4M $NaNO_2$ in 1.0M excess DCl at 25°C

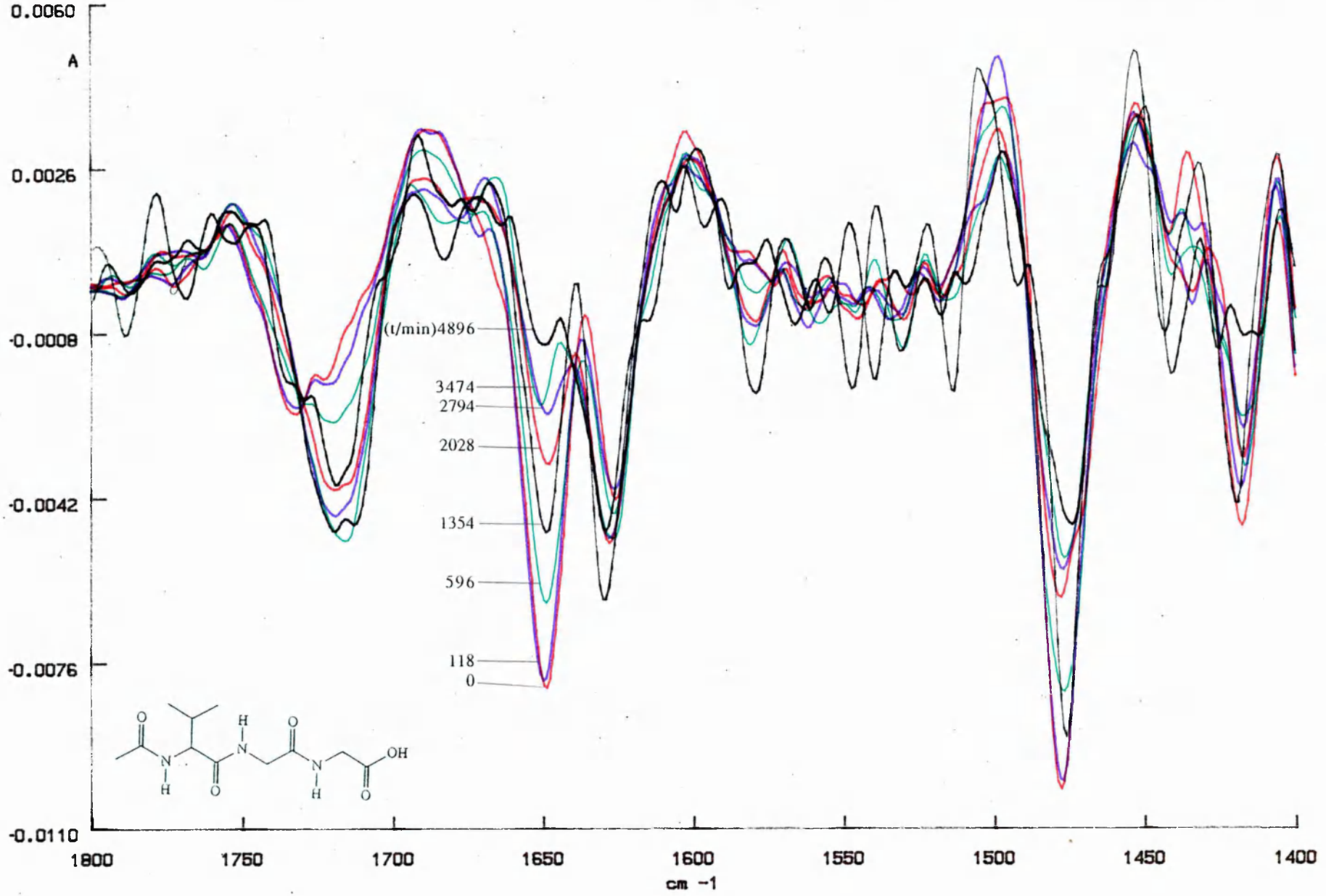

3.10.4 AcValGly and AcValGlyGly

In contrast to the above, the time dependent IR spectra (Figures 3.23 and 3.24) for these compounds show both the amide I (at 1649cm^{-1}) and the amide II (at 1478 and 1477cm^{-1}) decreasing, whereas the acetyl band intensity (at 1629 and 1625cm^{-1}) remains about the same and the acid band (at 1730 and 1731cm^{-1}) does not increase but moves to a lower wave number. All of these changes are consistent with nitrosation at the peptide N atom. The N-nitrosopeptide product is not visible as an increased band intensity at about 1730cm^{-1}, presumably because it decomposes as fast as it forms. The rates of N-nitrosopeptide formation calculated from changes of the 1649cm^{-1} bands of Figures 3.23 and 3.24 with time give k_0 = 3.83 x $10^{-6}s^{-1}$ for AcValGly and k_0 = 6.88 x $10^{-6}s^{-1}$ for AcValGlyGly. Thus, whilst otherwise similar, the reaction of AcValGlyGly is about 2-fold faster than that of AcValGly suggesting that nitrosation occurs at the glycyl residue in AcValGly and at both glycyl residues in AcValGlyGly. In the latter, both the amide absorbances occur at 1649cm^{-1} so that they cannot be distinguished.

Figure 3.25

Second derivative FTIR spectra with respect to time for the reaction of 0.03M AcAlaGly and 0.4M $NaNO_2$ in 1.0M excess DCl at 25°C

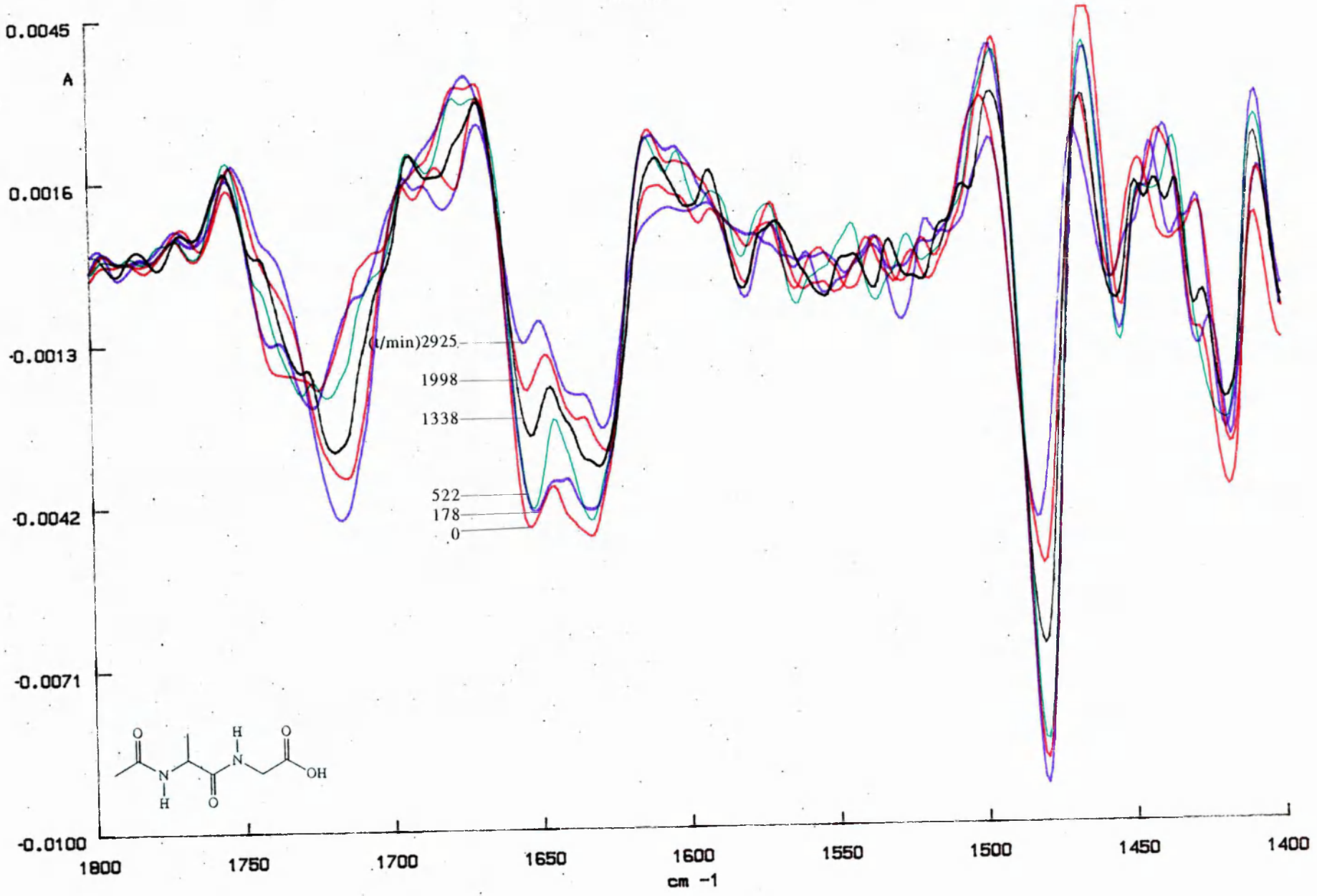

Figure 3.26

Second derivative FTIR spectra with respect to time for the reaction of 0.03M AcAlaAla and 0.4M $NaNO_2$ in 1.0M excess DCl at 25°C

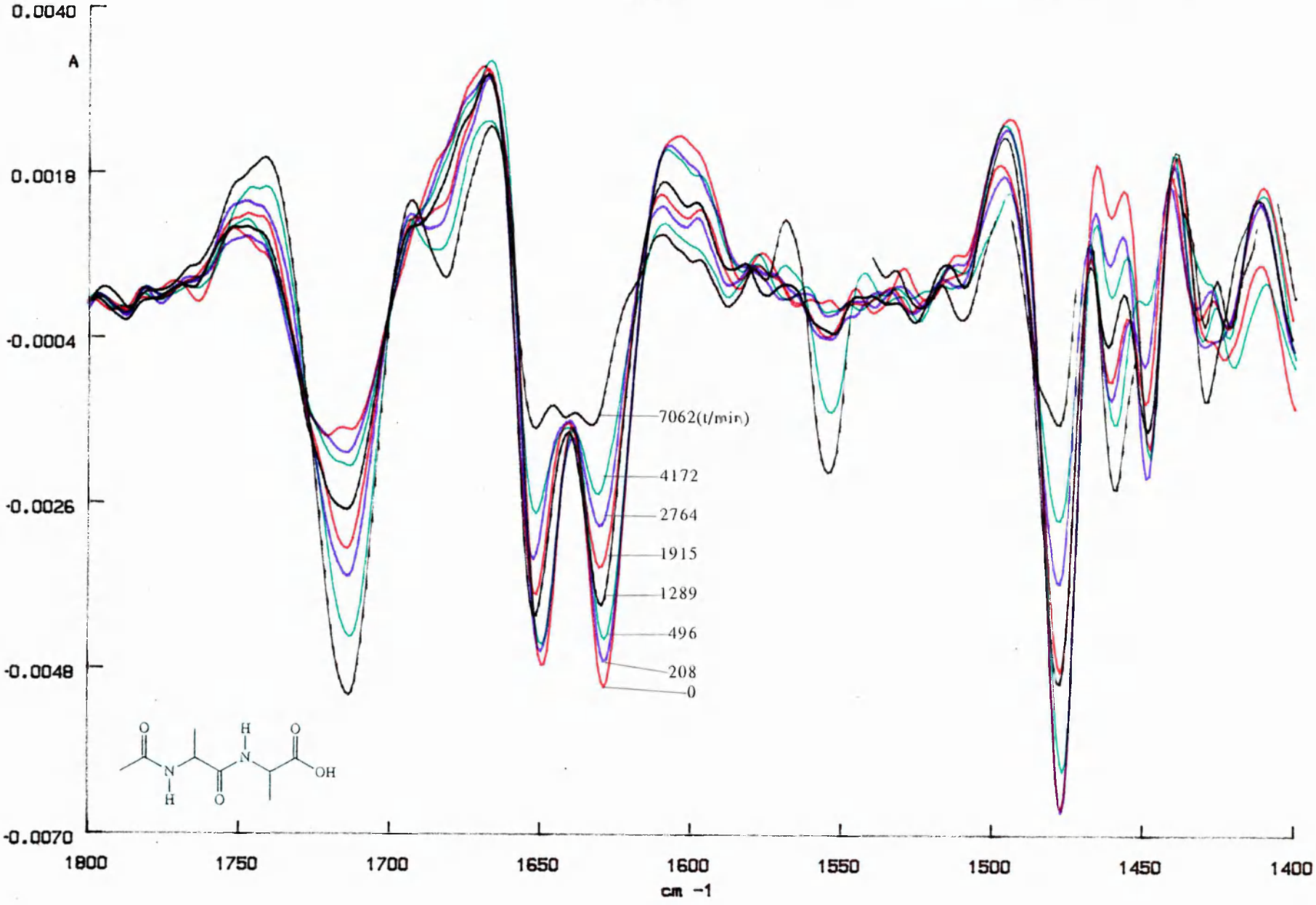

3.10.5 AcAlaGly and AcAlaAla

The time dependent changes in the IR spectra for both AcAlaGly and AcAlaAla (Figures 3.25 and 3.26) were more complex than for the other compounds. It was difficult to obtain reliable kinetic data for AcAlaGly (Figure 3.25) because the carbonyl bands at 1650 and 1633cm^{-1} are of relatively low intensity and overlap. Both decrease in intensity with time. While the main reaction appears to take place at the peptide N-atom (decreasing 1650cm^{-1} band), there is clear evidence of concurrent reaction at the N-acetyl position as well (decrease of the 1633cm^{-1} band). Further, the N-nitroso products are not visible as significantly increased band intensity at 1732cm^{-1}, presumably because they decompose as rapidly as they form.

Changes in the 1650cm^{-1} band with time (Figure 3.25) were used to calculate the rate of N-nitrosopeptide formation. This led to a value of k_0 = 7.30 x 10^{-6}s^{-1} (Table 3.11) which compares favourably with a similar reaction for AcValGly. It was not feasible (because the changes were too small) to calculate the corresponding rate of N-nitroso-N-acetyl peptide formation from the 1633cm^{-1} band. Comparison with AcAlaAla (below) suggests that this reaction will proceed with k_0 ca 2.65 x 10^{-6}s^{-1}, which explains the relative rates of change of the 1650 and 1633cm^{-1} bands.

The spectral changes for AcAlaAla (Figure 3.26) show clear evidence of concurrent nitrosation at both the acetyl-N and peptide-N atoms. Thus, both amide I band (at 1649cm^{-1}) and the N-acetyl band (at 1629cm^{-1}) decrease steadily with time. Concurrent changes of the amide II band at 1480cm^{-1} are also clearly apparent and lead to a k_0 value of 6.33 x 10^{-6} s^{-1}. A somewhat lower value would be expected from the amide II band which results from a combination of N-D bending and C-H stretching vibrations. Thus, whilst the N-D component would reach zero in this reaction, some C-N contribution would remain. As for AcValGly and AcAlaGly, there is no evidence of a significant build-up in N-nitroso products by an increased absorbance at ca 1730cm^{-1}. As before, it appears that both N-nitroso products decompose as rapidly as they form.

Evaluation of the rates from the spectral changes in Figure 3.26 lead to k_0 = 2.38 x10^{-6}s^{-1} for N-nitrosopeptide formation (from the 1649cm^{-1} band) and k_0 = 2.65 x 10^{-6}s^{-1} for N-nitroso-N-acetyl peptide formation (from the 1629cm^{-1} band). The sum of k_0 values compares favourably with that calculated from concurrent changes of the amide II band at 1477cm^{-1}, (k_0

Figure 3.27
Variation of UV absorbance with respect to time for peptide nitrosation

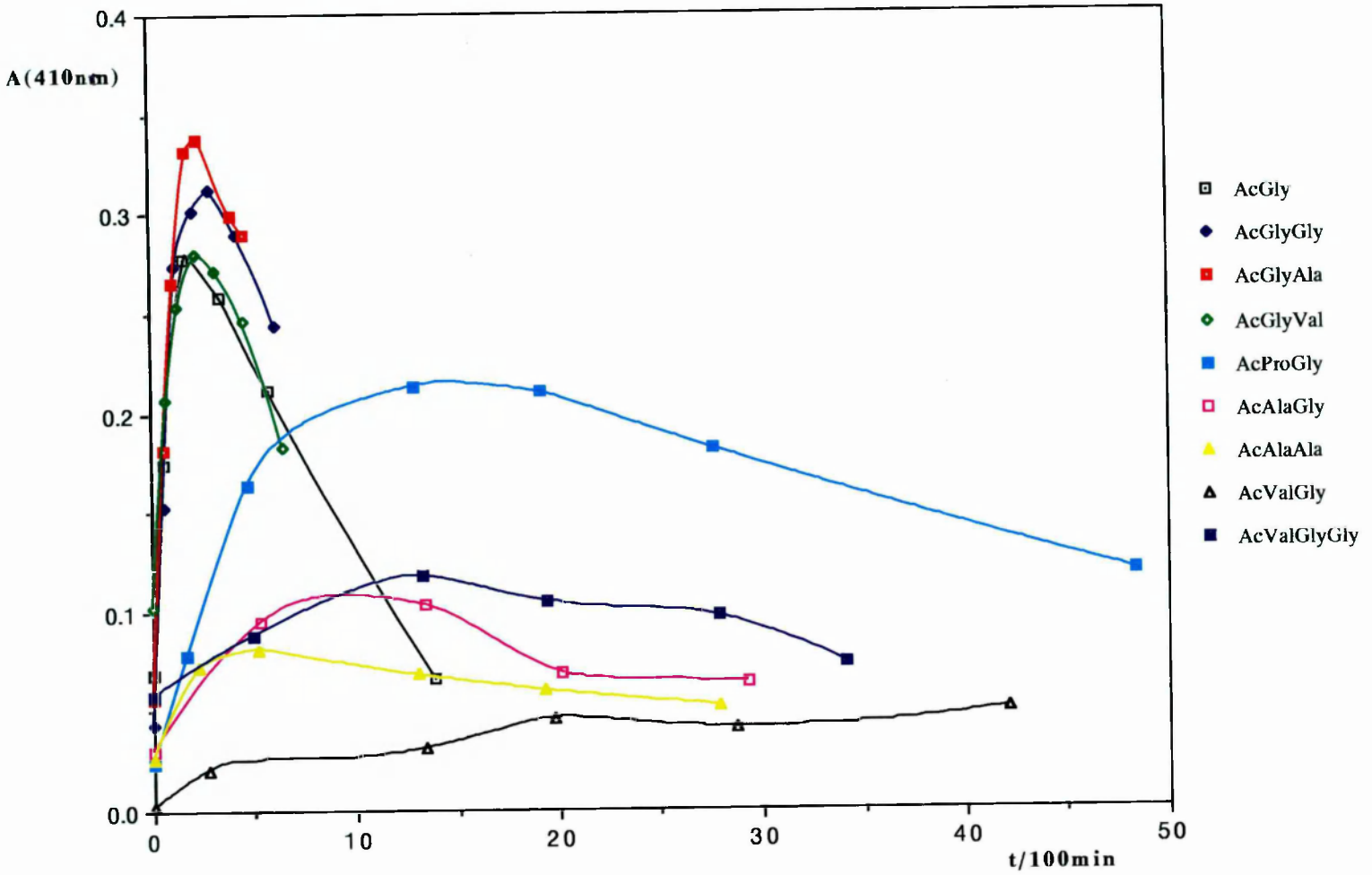

$= 3.54s^{-1}$). The rates are slower than other peptides, which is indicative of steric effects to nitrosation at both the acyl and peptide N-atoms.

3.11 The UV spectra for peptide nitrosation

The nitrosation reactions of the peptides were also examined by UV spectrophotometry under identical conditions (ie 0.03M peptide, 0.4M $NaNO_2$, 1.0M excess DCl, 25°C) as those used for the FTIR studies. Here, formation of the N-nitroso products was monitored by changes at 410nm which corresponds to an absorption maximum for both N-nitrosopeptides and N-nitrosamides. The results obtained are summarised in Figure 3.27 as plots of absorbance versus time for the various substrates. The reactions fall into two groups with respect to the rate of product formation, which correspond exactly with division into reaction at the N-acetyl or peptide-N positions as revealed by the FTIR studies. Compounds with a glycyl reside next to the acetyl group show more rapid reaction with a maximum absorbance after 200-300min, while others show a slower increase in absorbance, without a clear maximum. Of the four peptides which are nitrosated at the N-acetyl site, (AcGlyAla, AcGlyGly, AcGly, and AcGlyVal), the first two show higher maxima than the last two. This may relate to concurrent reaction at the peptide N-atom, or more likely, to the different stabilities of the corresponding N-nitroso products. AcProGly reacts less rapidly and the N-nitroso product appears to be relatively stable. Of the other four substrates, the three which could react at two sites (AcValGlyGly, AcAlaGly and AcAlaAla) show higher absorbances than AcValGly which presumably cannot. These absorbances, however, reflect both the rate of formation and rate of decomposition of the N-nitrosopeptide as well as the number of reactive sites and any specific conclusions must be tenuous. It is clear, however, that the steady state concentration of N-nitrosopeptide is much lower for AcValGly, AcValGlyGly, AcAlaGly and AcAlaAla than AcGlyGly, AcGly, AcGlyAla and AcGlyVal, whereas that for AcProGly is intermediate. This corresponds well with the observations of the N-nitroso products in the FTIR spectra. The low steady-state concentration reflects the slower rate of N-nitroso product formation evident in the FTIR k_0 values and probably a faster rate of decomposition.

Two methods were used to estimate rate coefficients from the UV data in order to compare them with those obtained by FTIR. In the first, tangents

Figure 3.28

First order rate plot for the nitrosation of AcGlyAla at 25 ℃

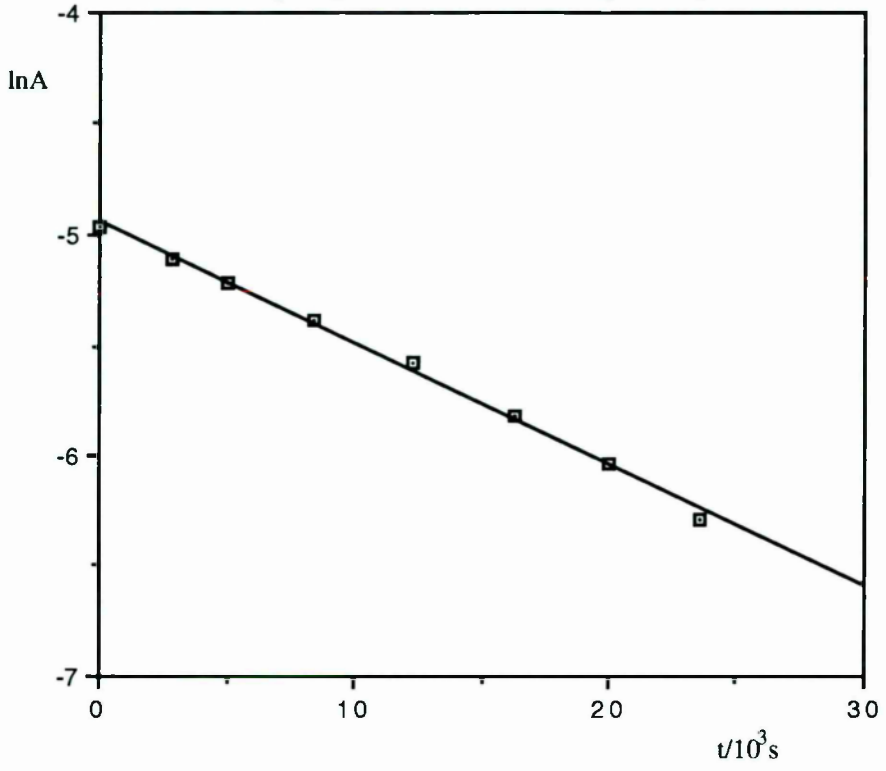

Figure 3.29

First order rate plot for the nitrosation of AcProGly at 25 ℃

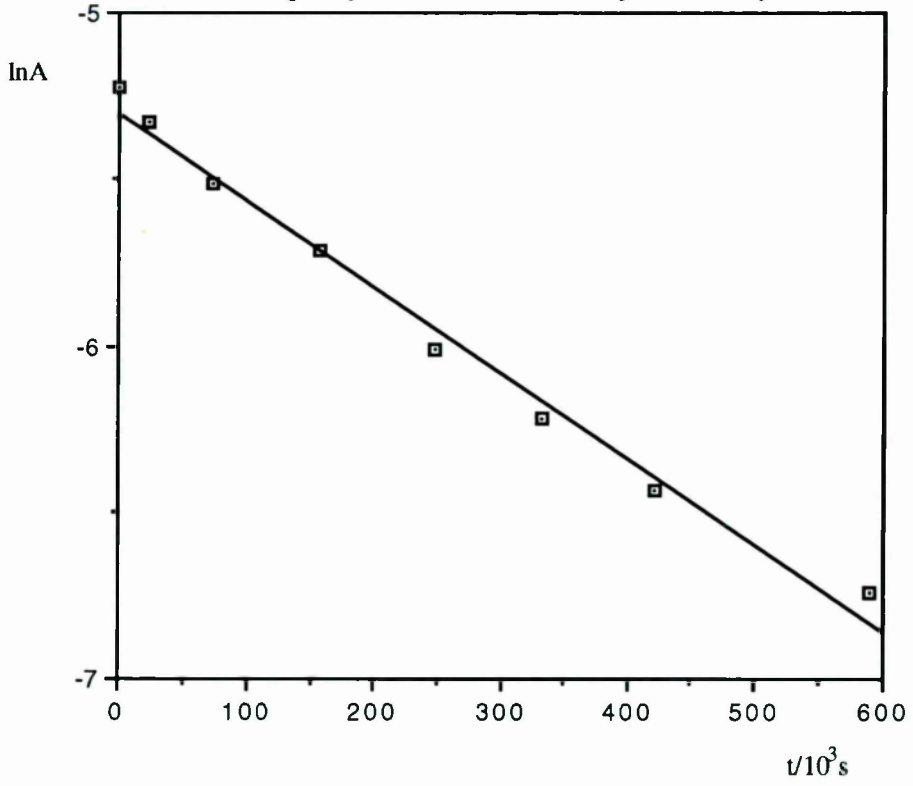

were drawn to the plots in Figure 3.27 at t=0 to obtain initial rates. In the second, the maximum point on each UV plot was taken as a $t = \infty$ value for each nitrosation reaction and the gradient of a plot of $\ln(A_\infty - A_t)$ against time was obtained. These plots were linear and gave gradients (k'_0) which were proportional to, but not equal to the rate coefficients, as expected for consecutive first order processes[74]. The values obtained by both methods compare favourably with those obtained by FTIR, as shown in Tables 3.10 and 3.11.

Table 3.10

Pseudo first order rate constants for peptide nitrosation in excess 1.0M DCl at 25°C by UV; Initial [substrate] = 0.03M, [$NaNO_2$] = 0.4M

Name	$10^6 k_0 s^{-1}$ *(from tangent)*	$10^6 k'_0 s^{-1}$ *(from log plot)*
AcGly	32	222
AcGlyGly	23	299
AcGlyAla	32	208
AcGlyVal	32	226
AcProGly	5.8	42
AcValGly	5.9	17
AcValGlyGly	1.2	26
AcAlaGly	1.4	67
AcAlaAla	5.7	140

In conclusion, the UV data confirm the deductions from the IR about both the rate of N-nitroso product formation and the reaction site.

3.12 Summary and discussion of peptide nitrosation reactions

All of the peptide nitrosation reactions were studied in quadruplicate to evaluate k_0 (Equation 3.1) from the FTIR absorbances. These were reproducible to ±10% and a mean value is reported for convenience in Table 3.11. Typical examples of the ln A versus time plots for reaction of AcGlyAla and AcProGly are shown in Figures 3.28 and 3.29 respectively. Both are nicely linear, which confirms the validity of Equation 3.1, as for reactions of AcGlyGly (Section 3.1).

Scheme 3.8

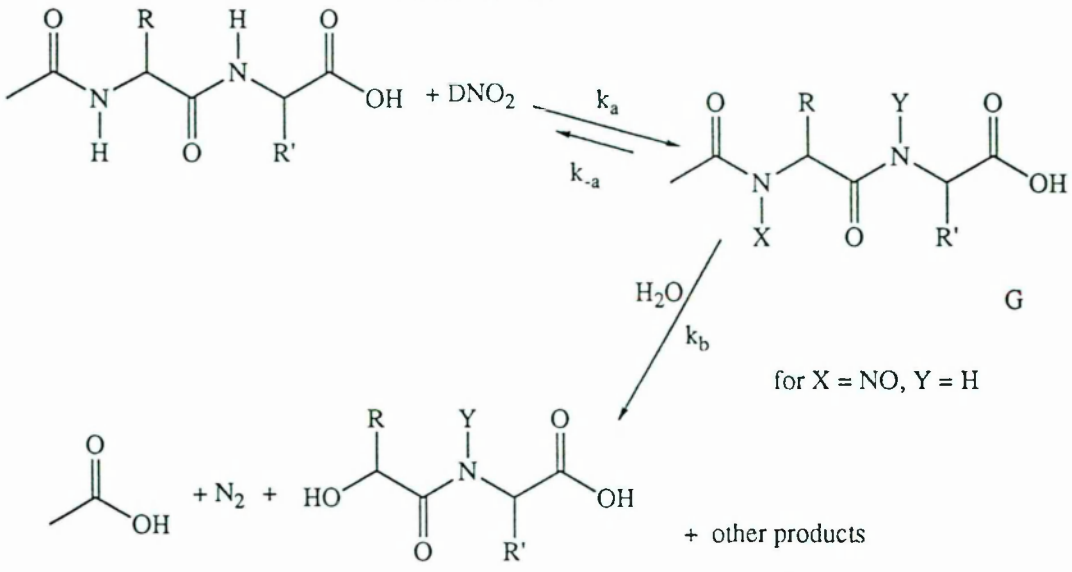

It seems reasonable to suppose that the nitrosation of all the peptide substrates follow the same rate expressions as for AcGlyGly. Thus, the full rate expression is Equation 3.3,

$$-\frac{d[\text{substrate}]}{dt} = k_3[\text{substrate}][DNO_2][D^+] \qquad \text{Equation 3.3}$$

and the reactions are not significantly catalysed by strong nucleophiles such as Cl^-. The significance of the k_0 and k_3 coefficients warrants further enquiry.

It is evident from this and previous investigations[38 41 75] that the formation and decomposition of N-nitrosopeptides and N-nitrosamides is described by Scheme 3.8. The N-nitroso product (G) is effectively a reactive intermediate which may decompose either to reactants (step k_{-a}) or to products (step k_b). In the present study, values of k_0 were obtained from the decrease in the peptide reactant concentration. The k_0 values relate to the individual steps of Scheme 3.8 in a complex manner (Equation 3.4).

$$-\frac{d[\text{substrate}]}{dt} = k_a[\text{substrate}] - k_a[G] \qquad \text{Equation 3.4}$$

This relationship, however, simplifies to Equation 3.5 where the initial nitrosation is not highly reversible (ie $k_{-a} \rightarrow 0$).

Under this circumstance,

Figure 3.30

Release of NO_2^- from Ac(NO)GlyGly in 1.0M DCl at 25 °C

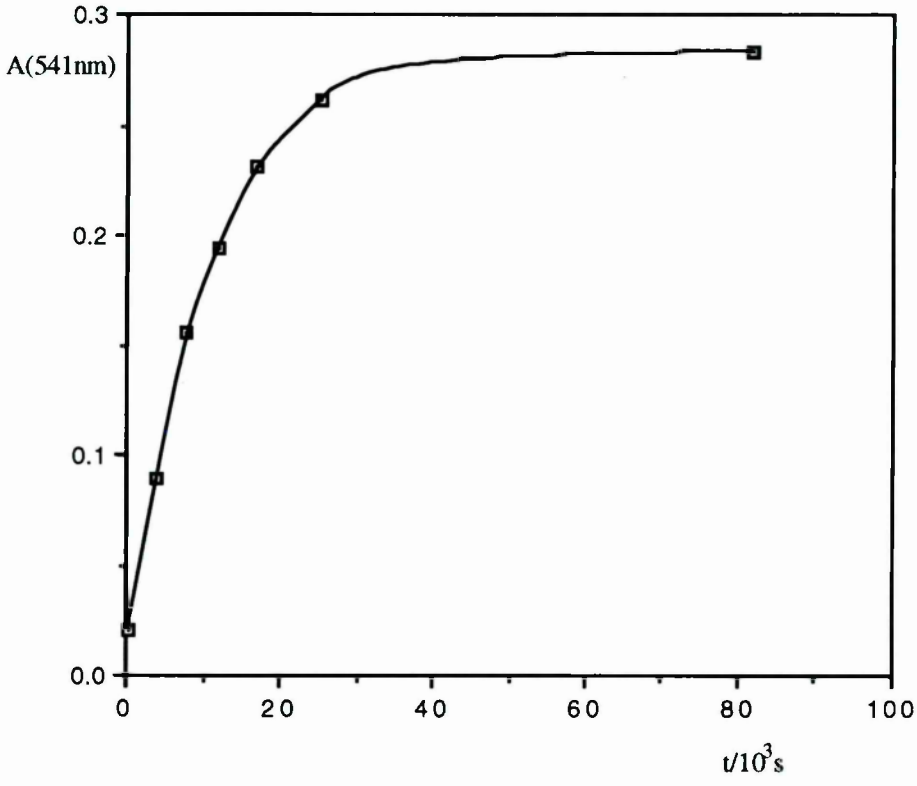

the observed rate of substrate loss equals the rate of substrate nitrosation (ie $k_o = k_a$).

$$-\frac{d[substrate]}{dt} = k_a[substrate] \qquad \text{Equation 3.5}$$

The validity of this simplification was tested for the nitrosation of AcGlyGly by determining the extent of denitrosation accompanying the decomposition of authentic N-nitroso-N-acetylglycylglycine in 1.0M DCl at 25°C. Thus a solution of Ac(NO)GlyGly (0.01M) and sulphanilamide (0.03M) in DCl (1.0M) was reacted at 25°C for 23h, the time taken for the complete nitrosation of AcGlyGly. By this time, the Ac(NO)GlyGly had completely decomposed and it was evident from independent UV spectrophotometry of the reaction solution that $t_{1/2}$(decomposition) is ca 156min which gives $k_b = 7.38 \times 10^{-5} s^{-1}$. Using the above procedure, nitrite arising from the decomposition of Ac(NO)GlyGly is trapped as soon as it is formed, by reaction with the sulphanilamide to form the diazo compound. Aliquots of the reaction solution were removed at timed intervals, reacted with N-(1-naphthyl)ethylene diamine dihydrochloride to form an azo dye, diluted 100 times and the absorbance at 541nm determined (Shinn's Method)[76]. A typical plot of azo dye absorbance versus time is shown (Figure 3.30). The intensity of the azo dye is proportional to the concentration of released nitrite ions. Separate experiments with authentic $NaNO_2$ solutions gave 1.0×10^{-6}M nitrite equivalent to 0.053A at 541nm. The highest absorbance found after 14h was 0.283A. This corresponds to an $[HNO_2] = 5.3 \times 10^{-4}$ M. This corresponds to 5.3% denitrosation of Ac(NO)GlyGly under the conditions of AcGlyGly nitrosation. This confirms the assumption that $k_a >> k_{-a}$ and that $k_{-a} \rightarrow 0$. It follows that Equation 3.5 applies under the conditions of AcGlyGly nitrosation and the observed k_o values measure the rate of the peptide nitrosation.

In view of the insignificant denitrosation of Ac(NO)GlyGly, it was assumed that denitrosation was unimportant for the N-nitroso derivatives of the other peptide substrates and that k_o values reflected the rate of nitrosation throughout.

Referring to Table 3.11, the k_o values allow the following conclusions.

1) The acyl N-atom is the preferred (most reactive) site of nitrosation of AcGly peptides. Usually, it is ca 10-fold more reactive than peptide N-atoms.

2) The structure of the second aminoacid residue of N-acetylglycyl peptides affects their reactivity (AcGlyVal > AcGlyAla > AcGlyGly) for reasons which are not understood. The differences may reflect assumptions about the irreversibility of the N-nitrosation (ie k_{-a} negligible for all compounds) rather than structural effects on the rate of nitrosation.

3) For compounds other than AcGly peptides, nitrosation of the peptide N-atom is preferred (most reactive). This probably relates to steric inhibition of nitrosation of the N-acetyl atom by the first amino acid residue.

4) Nitrosation of the peptide N-atom is not strongly influenced by the aminoacid constituents and, *inter alia*, steric effects in the compound examined.

Table 3.11

Pseudo first order rate constants for peptide nitrosation in excess 1.0M DCl at 25 °C; Initial[substrate] = 0.03M, [$NaNO_2$] = 0.4M

Name	*Site*	*Band to calc. k_o/cm^{-1}*	*$10^6 k_o/s^{-1}$*
AcGly	N-acetyl	1633	33.0
AcGlyGly	N-acetyl	1636	33.5
AcGlyAla	N-acetyl	1633	55.1
AcGlyVal	N-acetyl	1631	73.0
AcProGly	peptide-N	1653	3.07
AcValGly	peptide-N	1649	3.83
AcValGlyGly	peptide-N	1649	6.88
AcAlaGly	peptide-N	1650	7.30
AcAlaAla	N-acetyl	1629	2.65
	peptide-N	1649	2.38

k_o reproducible to ± 10%

The difference in the molecular shapes of AcGlyGly and AcValGly is illustrated by the 'Macromodel' diagrams in Figure 3.30.

A few comments about the probable mechanism of peptide nitrosation in dilute acid are relevant. The reaction rates follow Equation 3.6

Figure 3.30

Molecular shapes of AcGlyGly and AcValGly by 'Macromodel'

AcGlyGly

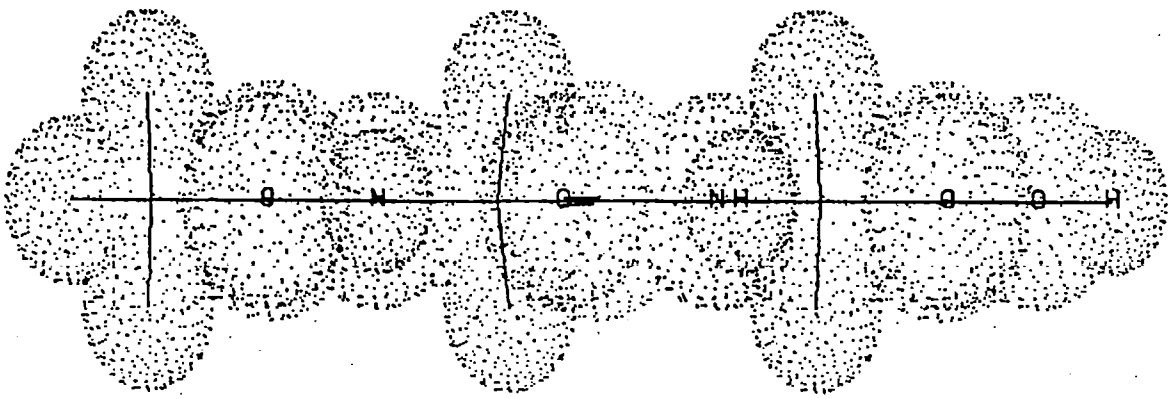

AcValGly

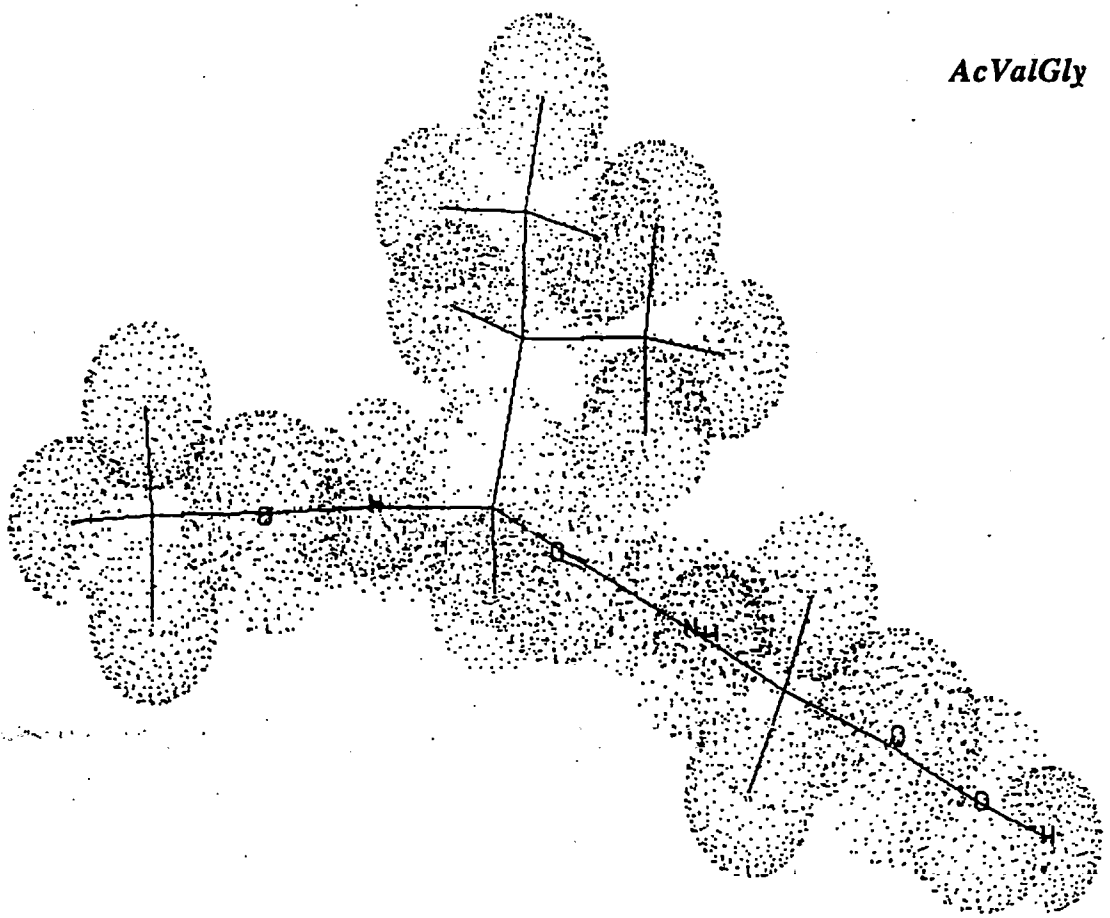

$$\text{Rate} = k_3[\text{peptide}][DNO_2][D^+] \qquad \text{Equation 3.6}$$

and are not strongly catalysed by Cl^-. This is consistent with the mechanism outlined in Scheme 3.9, where H^+ (D^+) loss from the N-nitrosonium ion intermediate (Z) is rate-limiting.

Scheme 3.9

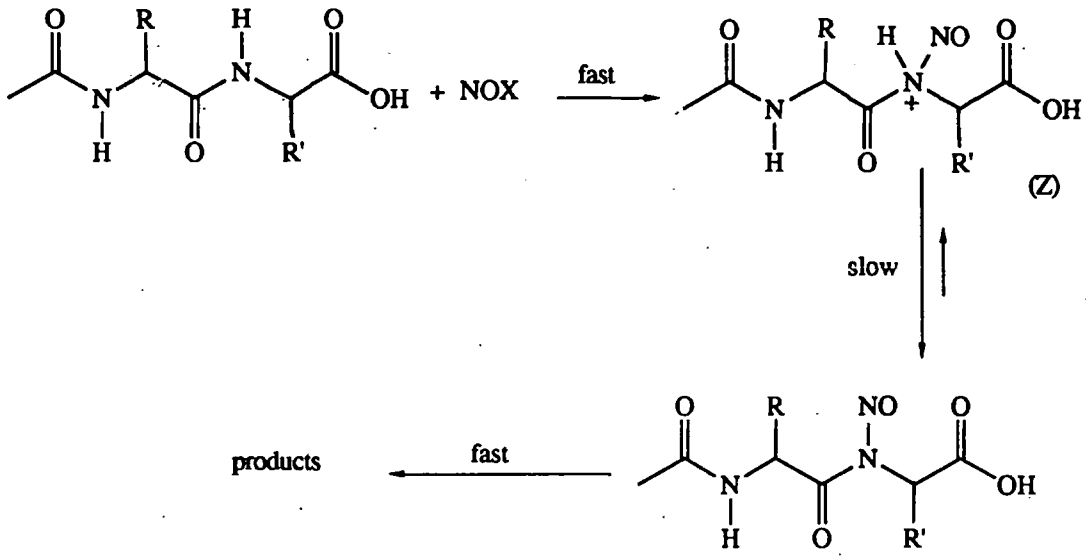

This mechanism is similar to that found for amide substrates in general[43].

Chapter 4

Results and discussion 3

Peptide Diazotisation

4.1 Introduction
4.2 The use of IR to study diazopeptides
4.3 The nitrosating agent
4.4 The rate of hydrolysis of 2-ethoxyethyl nitrite in water
4.5 FTIR measurements in aqueous media
4.6 Temperature choice and control
4.7 Choice of cell and scan conditions
4.8 Rate of hydrolysis of N-(2-diazoacetyl)glycine ethyl ester
4.9 Kinetics of the diazotisation of GlyGly
4.10 The diazotisation of other peptides by 2-ethoxyethyl nitrite in aqueous buffers at 25°C
4.11 The diazotisation of Glycine and 2,2-$[^2H_1]_2$-glycine
4.12 Summary
4.13 Discussion

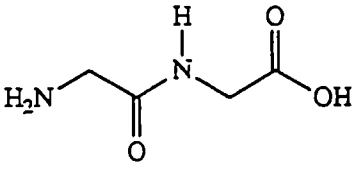

GlyGly

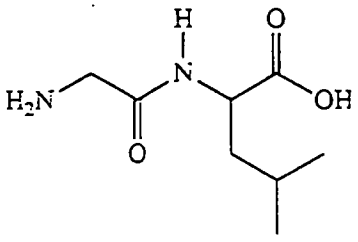

GlyLeu

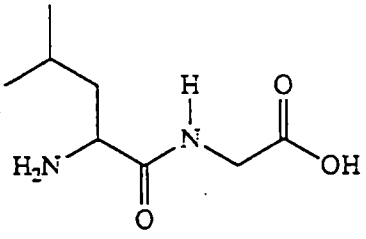

LeuGly

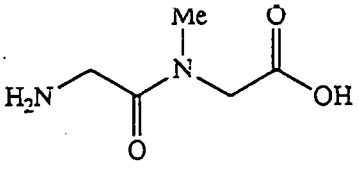

GlySar

4.1 Introduction

The two objectives of this part of the study were to develop an assay for 'total' diazopeptides and to obtain kinetic data on the formation of diazopeptides in water. None of this information is available at present and diazopeptides are known carcinogens. The primary N-terminus of peptides is attacked by nitrosating agents to produce diazopeptides, which is then decompose (hydrolyse) at a rate dependent on structure and the prevailing acidity. The example of N-glycylglycine (GlyGly), the simplest dipeptide, is given in Scheme 4.1.

Scheme 4.1

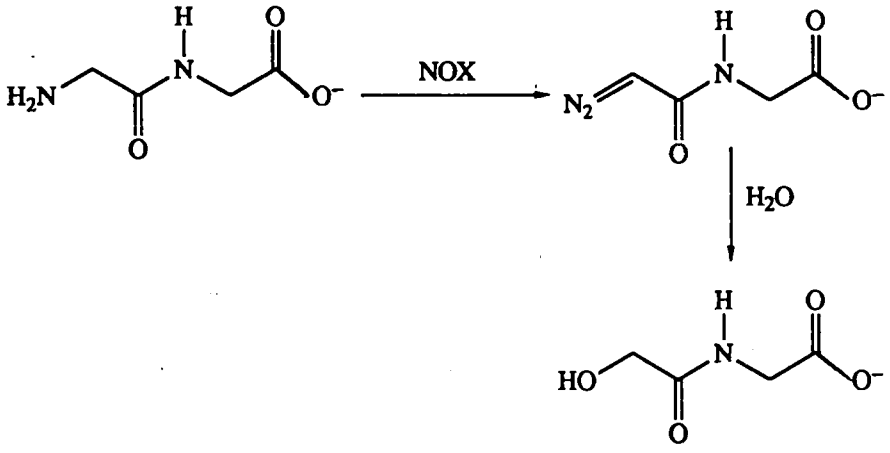

4.2 The use of IR to study diazopeptides

All diazopeptides have a characteristic IR band at about 2100cm^{-1} due to the $N^+{=}N^-$ stretch; the band is both sharp and intense, because of the polar nature of the group and there are few other bands in the region. It is therefore feasible to assay diazopeptides using the 2100cm^{-1} band.

4.3 The nitrosating agent

2-Ethoxyethyl nitrite was chosen as the nitrosating agent because it is reasonably soluble and stable in water between pH 8-11 (Section 4.4), yet much more reactive than simple alkyl nitrites, at these pH's. Its reaction product is ethanol whose IR spectrum does not interfere. As normally made and distilled, 2-ethoxyethyl nitrite was found to decompose faster than anticipated in water, probably because traces of nitrogen oxides present produced an acidic solution. It was more stable when added to an alkaline solution of excess peptide, which acted as a buffer. Consequently, 2-ethoxyethyl nitrite was added to a reaction mixture as the neat liquid rather than as an aqueous solution.

4.4 The rate of hydrolysis of 2-ethoxyethyl nitrite in water

The rate of hydrolysis of 2-ethoxyethyl nitrite (Scheme 4.2) was measured in aqueous borax buffers at 25°C by the decrease in the UV absorbance at 354nm. ($EtO(CH_2)_2ONO$, λ_{max} (H_2O)354nm, $\varepsilon = 86.5 dm^3 mol^{-1} cm^{-1}$). The nitrite product absorbed at the same wavelength (NO_2^-, λ_{max} (H_2O) 354nm, $\varepsilon = 22.8 dm^3 mol^{-1} cm^{-1}$) but 2-ethoxyethanol did not.

Table 4.1

Typical values for the hydrolysis of 2-ethoxyethyl nitrite in water at 25°C, pH 8/9. Initial [$EtOCH_2CH_2ONO$] ca 5×10^{-3}M

	pH 8		*pH 9*	
t/h	*A*	*ln* c_a^t	*A*	*ln* c_a^t
0	0.356	-5.863	0.333	-5.842
1	0.340	-5.956	0.323	-5.897
2	0.323	-6.065	0.313	-5.956
3	0.308	-6.172	0.302	-6.025
4	0.295	-6.274	0.291	-6.099
5	0.282	-6.389	0.280	-6.179
6	0.271	-6.498	0.270	-6.258
7	0.262	-6.596	0.260	-6.343
8	0.254	-6.692	0.252	-6.418
9	0.247	-6.785	0.243	-6.508
10	0.240	-6.888	0.236	-6.585
11	0.232	-7.019	0.229	-6.667
12	0.225	-7.150	0.223	-6.744
13	0.219	-7.278	0.217	-6.828
14	0.214	-7.398	0.212	-6.903
15	0.210	-7.507	0.208	-6.968
16	0.206	-7.628	0.203	-7.055
17	0.203	-7.730	0.201	-7.092
18	0.200	-7.843	0.195	-7.212
19	0.198	-7.926	0.194	-7.233
20	0.195	-8.066	0.188	-7.373
21	0.193	-8.172	0.187	-7.398
22	0.191	-8.289	0.185	-7.451
23	0.190	-8.354	0.183	-7.507
∞	0.175		0.148	

Figure 4.1

Hydrolysis of 2-ethoxyethyl nitrite in water at 25°C

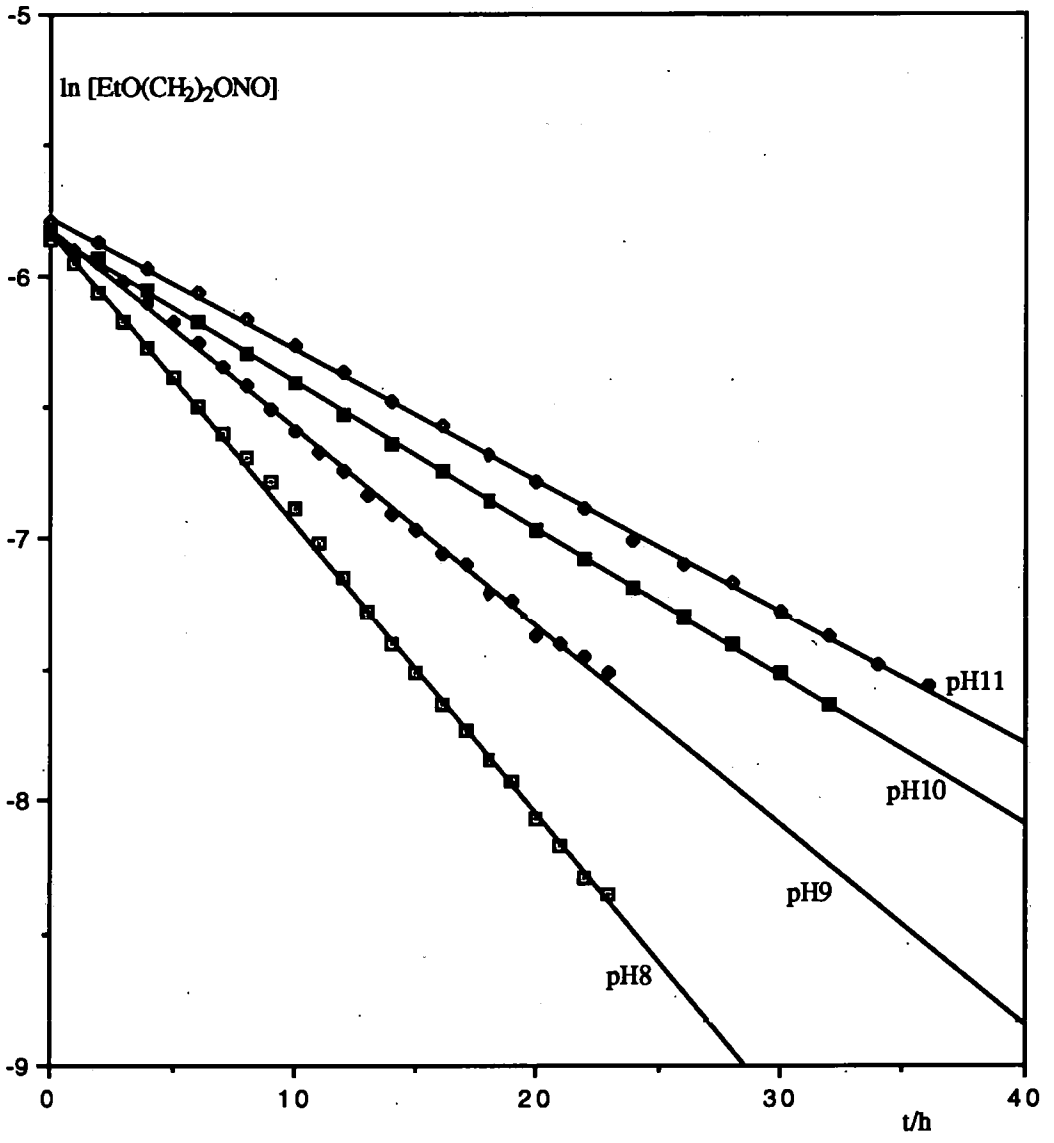

Scheme 4.2

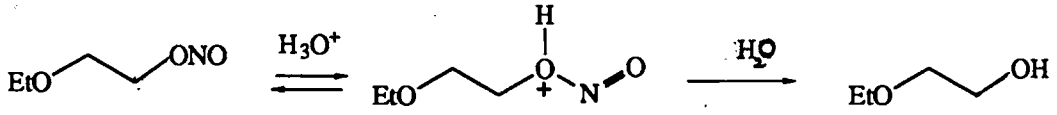

Hence, the expression for the concentration of 2-ethoxyethyl nitrite in terms of the measured total absorbance at 354nm is given by Equation 4.1,

$$c_a^t = \frac{A_{obs}^t - \varepsilon_n c_a^o}{\varepsilon_a - \varepsilon_n} \qquad \text{Equation 4.1}$$

where c_a^o and c_a^t are the concentrations of 2-ethoxyethyl nitrite at time 0 and t respectively, ε_a and ε_n are the extinction coefficients of 2-ethoxyethyl nitrite and of inorganic nitrite respectively, and A_{obs}^t is the total absorbance at time t (derivation in appendix). Results from typical experiments at pH 8 and 9 are given in Table 4.1. The absorbance changes are not large, but these data generate good, linear *pseudo* first order plots of ln c_a^t against time (Figure 4.1). Thus, the hydrolysis of 2-ethoxyethyl nitrite follows Equation 4.2 and average values of k_1 at pH 8 - 11 are summarised in Table 4.2.

$$\text{Rate} = k_1[EtO(CH_2)_2ONO] \qquad \text{Equation 4.2}$$

Table 4.2

Pseudo first order rate constants for the hydrolysis of 2-ethoxyethyl nitrite in aqueous buffers at 25°C. Initial $[EtO(CH_2)_2ONO]$ ca 5×10^{-3}M

pH	$10^4 k_1/s^{-1}$
11	0.13
10	0.17
9	0.20
8	0.30

The hydrolysis of 2-ethoxyethyl nitrite is significant and comparable to the rate of peptide diazotisation (Sections 4.9 - 4.11). It follows that the hydrolysis of 2-ethoxyethyl nitrite cannot be ignored in the presence of

Figure 4.2

FTIR spectra of H_2O at different temperatures (140μm)

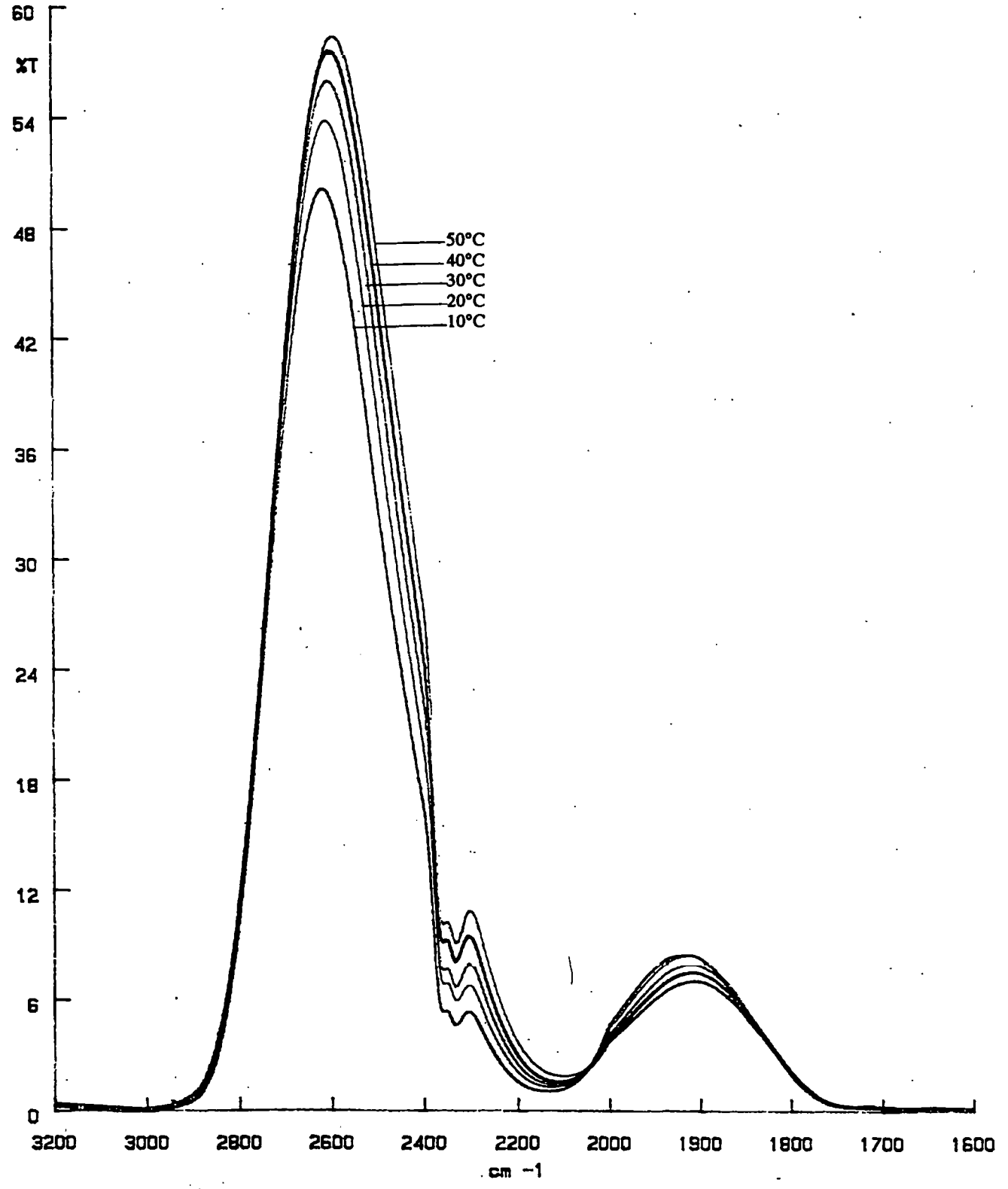

Figure 4.3

Absorbance of water at 2100cm^{-1} against temperature

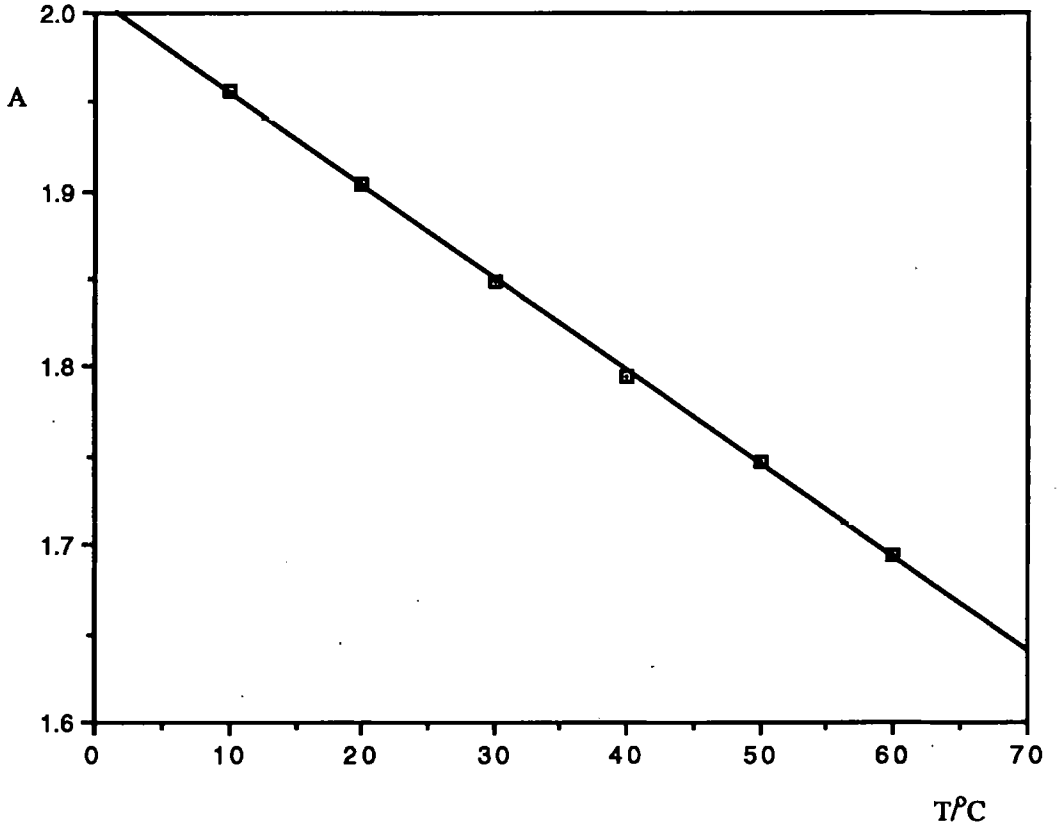

peptides. However, there is very little change in hydrolysis rate over pH 8 - 11, although base catalysed reactions where k_1 is proportional to [OH^-] become significant in 0.1M to 0.75M NaOH at 25°C[77]. The data in Table 4.2 are consistent with the hydrolysis mechanism outlined in Scheme 4.2.

4.5 FTIR measurements in aqueous media

The IR spectrum of water (Figure 4.2) shows a strong, broad absorption band between 2400 and 1900cm^{-1} and the 2100cm^{-1} region where the diazo band occurs is close to the point of lowest transmittance. Thus the scan conditions and cell pathlength need to be carefully chosen to make the best use of the remaining transmittance available. Further, the water band changes in intensity and position with temperature, so it is very necessary to control the temperature carefully during scans of reaction mixtures.

A graph of the absorbance of water at 2100cm^{-1} against temperature, measured under the conditions chosen for the scans of reaction mixtures (see Section 4.7), is shown in Figure 4.3. It indicates that, at 2100cm^{-1} and 25°C, the water absorbance will change by 5.4 x 10^{-3} A/°C. This is equivalent to a concentration change of ca 10^{-4}M N-(2-diazoacetyl)glycine ethyl ester for every 0.1°C (see Section 4.8).

4.6 Temperature choice and control

The peptide diazotisation reactions were to be carried out in the IR cell at 25°C. Thermostatting of the cell was achieved by attaching a hollow brass backplate, through which water circulated. The temperature of the cell was measured by a digital electronic thermometer to ± 0.1°C. It was kept at 25.0°C for at least 15 min before introducing the peptide solution, also at 25.0°C, to which the nitrosating agent had just been added. Using this procedure, the cell contents were kept at 25.0 ± 0.1°C throughout the reactions.

4.7 Choice of cell and scan conditions

The cell had a variable pathlength of 0-6mm. It was fitted with sapphire windows, which did not absorb in the region of interest and were extremely resistant to attack by the reaction mixture.

The scan conditions were chosen to measure the lowest possible concentration of a diazopeptide by means of its characteristic absorption band at about 2100cm^{-1}. Because there are no other bands in the vicinity, a

poor resolution could be tolerated but the signal to noise (S/N) ratio was as high as possible. Nine instrument variables were optimised to achieve this:

1. detector	2. OPD velocity	3. acquire mode
4. Jacquinot stop	5. attenuating filter	6. pathlength
7. resolution	8. apodisation	9. number of scans

Variables 1-3

The mercury cadmium telluride (MCT) detector was chosen because it was more sensitive than the deuterated triglycyl sulphate (TGS) detector. The MCT detector scans at high speed, so the highest available optical path difference (OPD) velocity (0.2) can be used. Exposure of the MCT detector to more than about 5% of the full beam energy causes saturation and consequently, distorted spectra. Hence, the detector could not be exposed to the full open beam for background measurements and the sample shuttle (the 'interleaved' acquire mode) was precluded. Therefore, the 'ratio' acquire mode was chosen, involving acquisition of the background spectrum first, followed by the sample spectrum.

Variables 4-6

The required maximum of about 5% of full beam energy can be obtained by a suitable combination of pathlength (0 - 6mm), filter (1, 4, 6, 14 or 32% transmittance) and Jacquinot stop (aperture size 1 or 2). The pathlength should be as long as possible, consistent with sufficient transmittance at 2100 cm^{-1} to detect the diazopeptide at the lowest possible concentrations. Measurements of beam energy and transmittance at 2100cm^{-1} were made while altering variables 4-6, and the results are shown in Tables 4.3 and 4.4.

Table 4.3

Beam Energies measured by TGS detector

1. Open beam: 38751 (1938 is 5%)
2. Cell containing water in beam:

Pathlength/μm	120	130	140	150
Jstop 2, no filter	3524	3241	2993	2789
Jstop 2, 32% filter	1111	1028	952	886
Jstop 1, no filter	2014	1860	1784	1650

Figure 4.4

Relation between % transmittance and beam energy for different Jstop, filter and pathlength

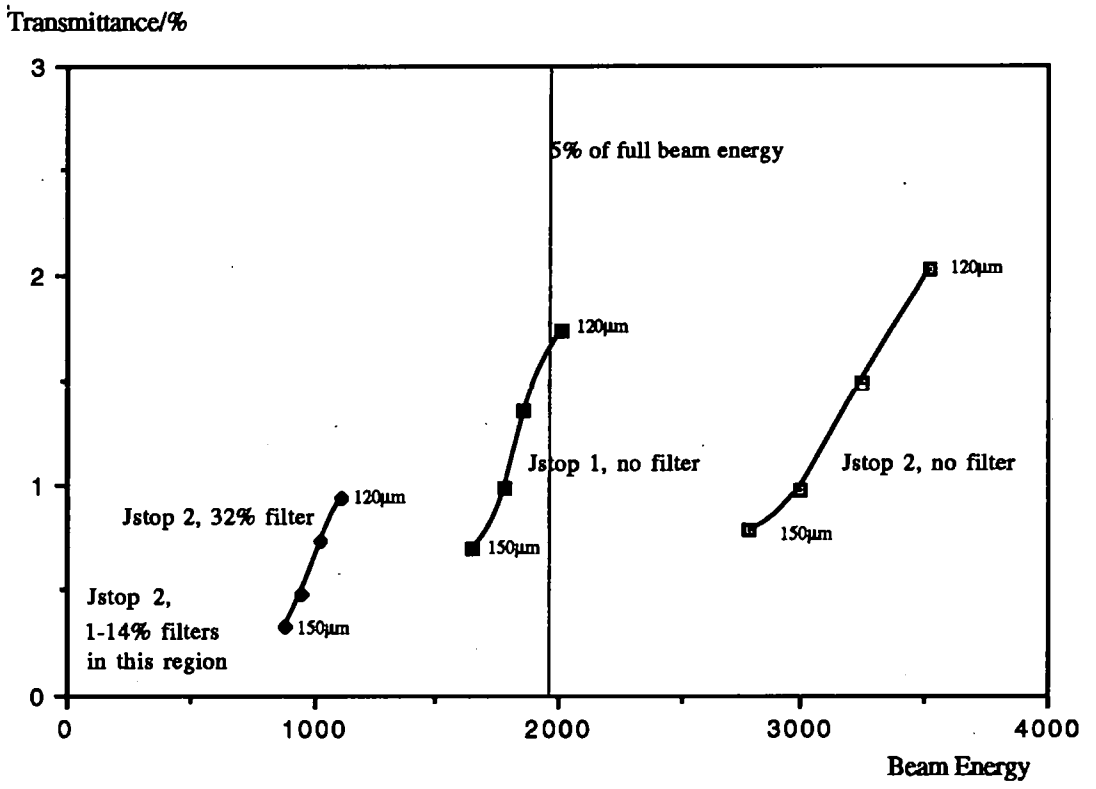

Transmittance measurements were made on the spectrum of water, run as 10 background scans, MCT detector, OPD velocity 0.2, Jstop 2, resolution $4cm^{-1}$, apodisation normal.

Table 4.4

Transmittance(%) at $2100cm^{-1}$ measured by MCT detector

Cell containing water in beam

Pathlength/μm	120	130	140	150
Jstop 2, no filter	2.02	1.48	0.97	0.78
Jstop 2, 32% filter	0.94	0.73	0.48	0.33
Jstop 1, no filter	1.73	1.36	0.99	0.69

Beam energy is plotted against transmittance in Figure 4.4, which shows that Jstop 1 with no filter gives the highest transmittance for the longest pathlength, with the beam energy near the required 5%. Jstop 1 and no filter were therefore chosen as the best conditions.

It remained to optimise the pathlength, but to do this it was necessary to run sample spectra, using aqueous N-(2-diazoacetyl)glycine ethyl ester (10^{-3}M and 10^{-4}M). For the background spectrum, the cell containing water was placed in the beam. The water spectrum was then automatically subtracted by the instrument during the scanning process, leaving the N-(2-diazoacetyl)glycine ethyl ester spectrum. In order to accumulate the spectra, variables 7-9 had to be given arbitrary values of 150 scans, resolution $4cm^{-1}$, apodisation normal. A pathlength of 140μ gave the maximum signal to noise ratios in the vicinity of the $2100cm^{-1}$ band.

Variables 7-9

The best S/N ratio is obtained at low resolution[78 79] The nominal resolution was decreased to find the lowest value for which the absorbance of the 10^{-4}M solution of N-(2-diazoacetyl)glycine ethyl ester could be seen. This proved to be $16cm^{-1}$, which was therefore chosen as the working value.

Strong apodisation gives the best S/N ratio[80 81]. Normal and all stronger types of apodisation were tried. Triangular apodisation was found to give the best results and was therefore chosen.

Finally, the number of scans was optimised at 300, taking 10min.

Thus, the optimum instrument settings for obtaining spectra of aqueous diazopeptides were:

Figure 4.5

FTIR spectra with respect to time for hydrolysis of 0.001M N-(2-diazoacetyl)glycine ethyl ester in 1.0M GlyGly at pH 9.00 and 25°C

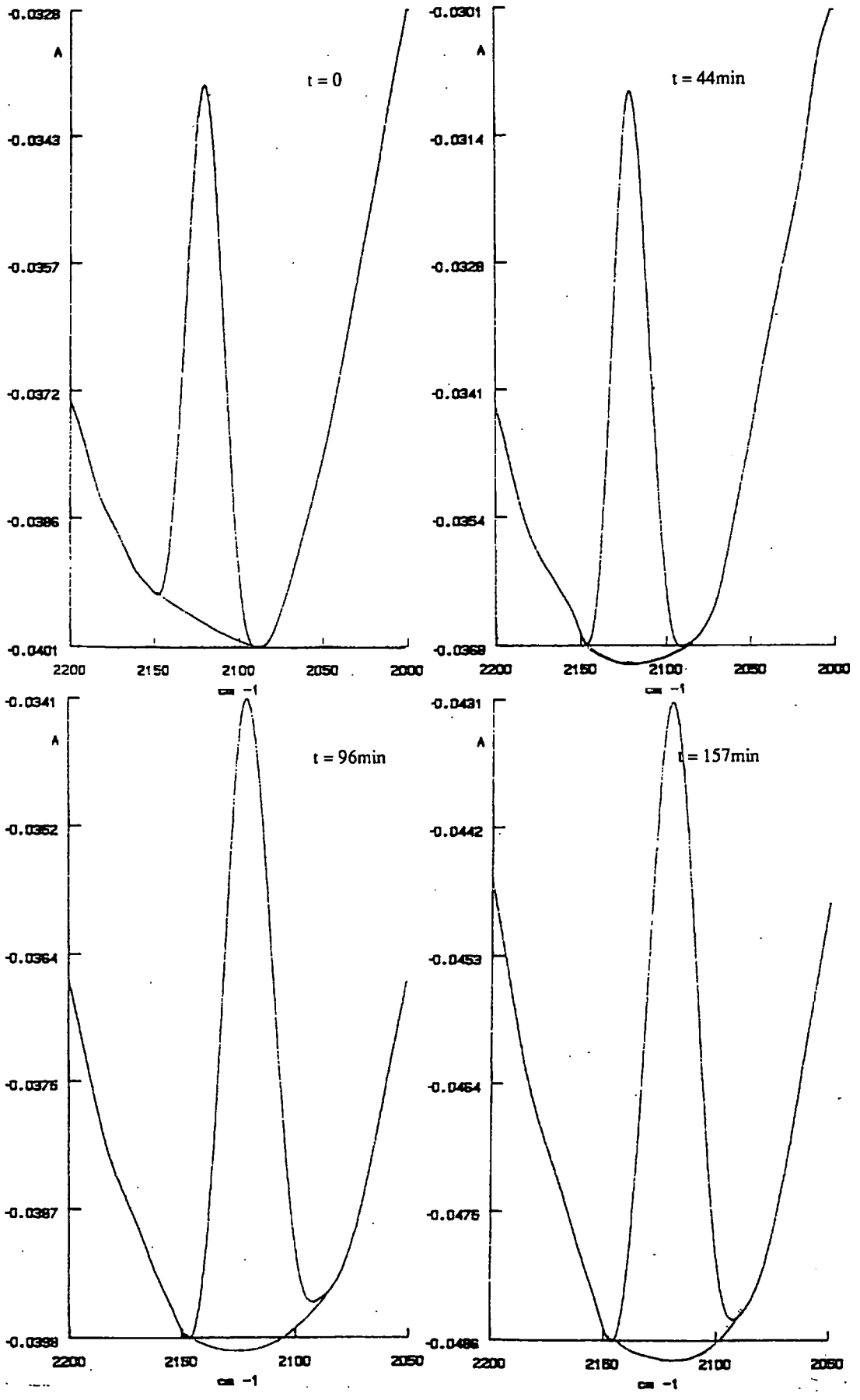

Cell			
Pathlength	*140μm*		
PE 1710 spectrometer			
Detector	*MCT*	*Attenuating filters*	*none*
OPD velocity	*0.2*	*Nominal resolution*	*16cm^{-1}*
Acquire mode	*ratio*	*Apodisation*	*triangular*
Jacquinot stop	*1*	*Number of scans*	*300*

Purging the instrument with nitrogen made little difference to the background spectrum (ie the spectrum of the air in the instrument cavity) near 2100cm^{-1} and a flow rate of 1dm^3/min of dry nitrogen kept the background sufficiently constant.

Preliminary experiments showed that the absorbance varied slightly with the level of liquid nitrogen around the MCT detector. Consequently, it was topped up just before running each spectrum.

4.8 Rate of hydrolysis of N-(2-diazoacetyl)glycine ethyl ester

From previous work[82], it is known that the diazopeptide product of the reaction in Scheme 4.1 will undergo hydrolysis concurrent with its formation. Since the rate of diazotisation is measured using the 2100cm^{-1} product band, it is necessary to establish that hydrolysis is much slower than the formation reaction.

The rate of the hydrolysis of N-(2-diazoacetyl)glycine ethyl ester in the presence of M GlyGly at pH 9 was measured by FTIR at 25°C, ie under identical conditions to the diazopeptide formation. The reactions were followed for 2.5h and the absorbance of the diazo band was determined at timed intervals. The spectra are shown in Figure 4.5; absorbances were found by peak height x the absorbance scale.

The spectra at each time point show that sharp diazo absorption bands with low noise levels are obtained, but that there is some doubt about the exact position of the baseline, which is often curved. There was no obvious solution to this problem, except to draw a baseline by hand, following the same curve. When several different reasonable positions of the baseline were compared, the difference in the measured absorbance was less than 5%.

Figure 4.6

FTIR spectra with respect to time for reaction of 1.0M GlyGly and 0.01M $EtO(CH_2)_2ONO$ at pH 7.50 and 25°C

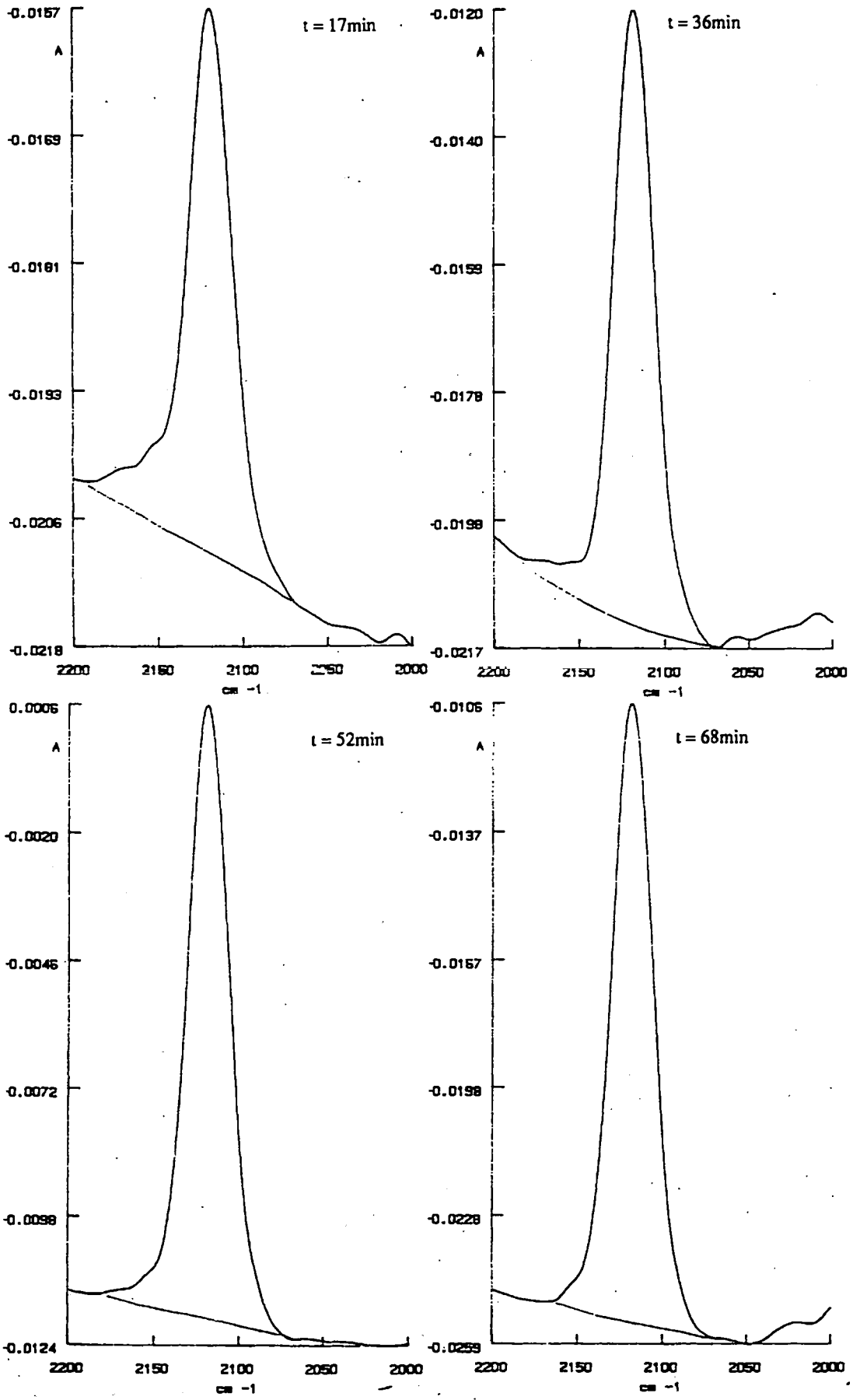

Figure 4.7

FTIR spectra with respect to time for reaction of 1.0M GlyGly and 0.01M $EtO(CH_2)_2ONO$ at pH 8.00 and 25°C

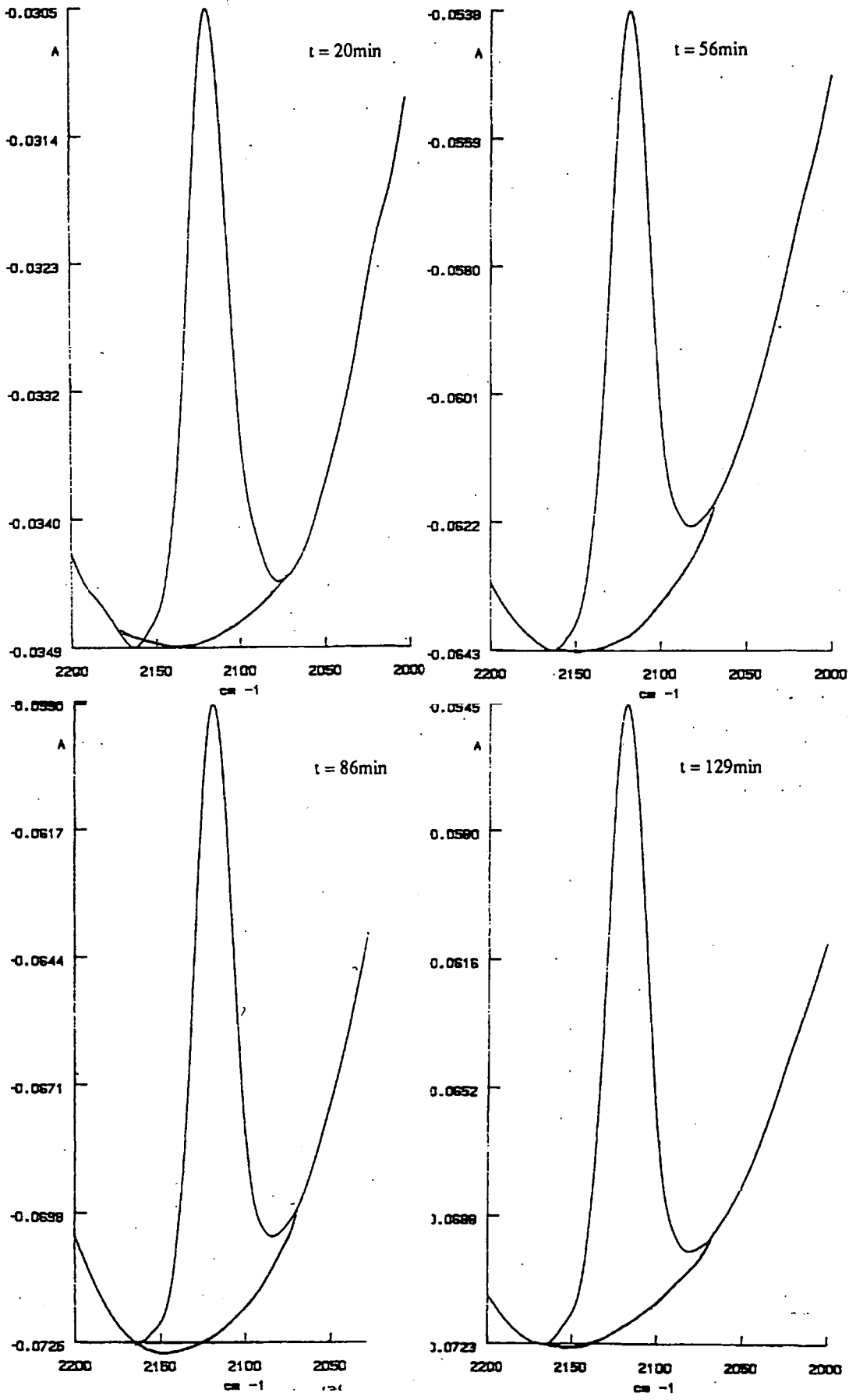

Figure 4.8

FTIR spectra with respect to time for reaction of 1.0M GlyGly and 0.01M $EtO(CH_2)_2ONO$ at pH 9.04 and 25°C

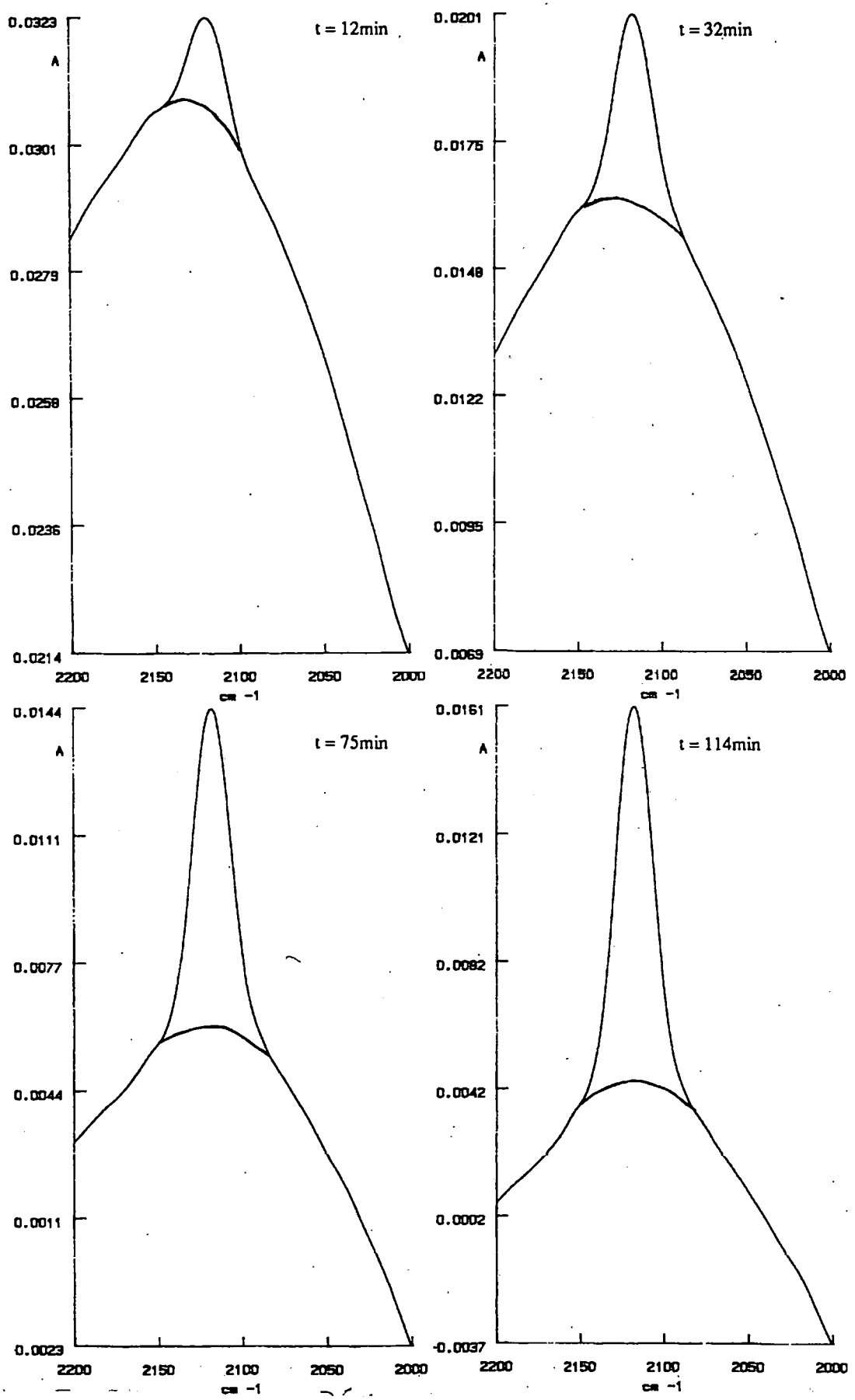

Figure 4.9

FTIR spectra with respect to time for reaction of 1.0M GlyGly and 0.01M $EtO(CH_2)_2ONO$ at pH 10.16 and 25°C

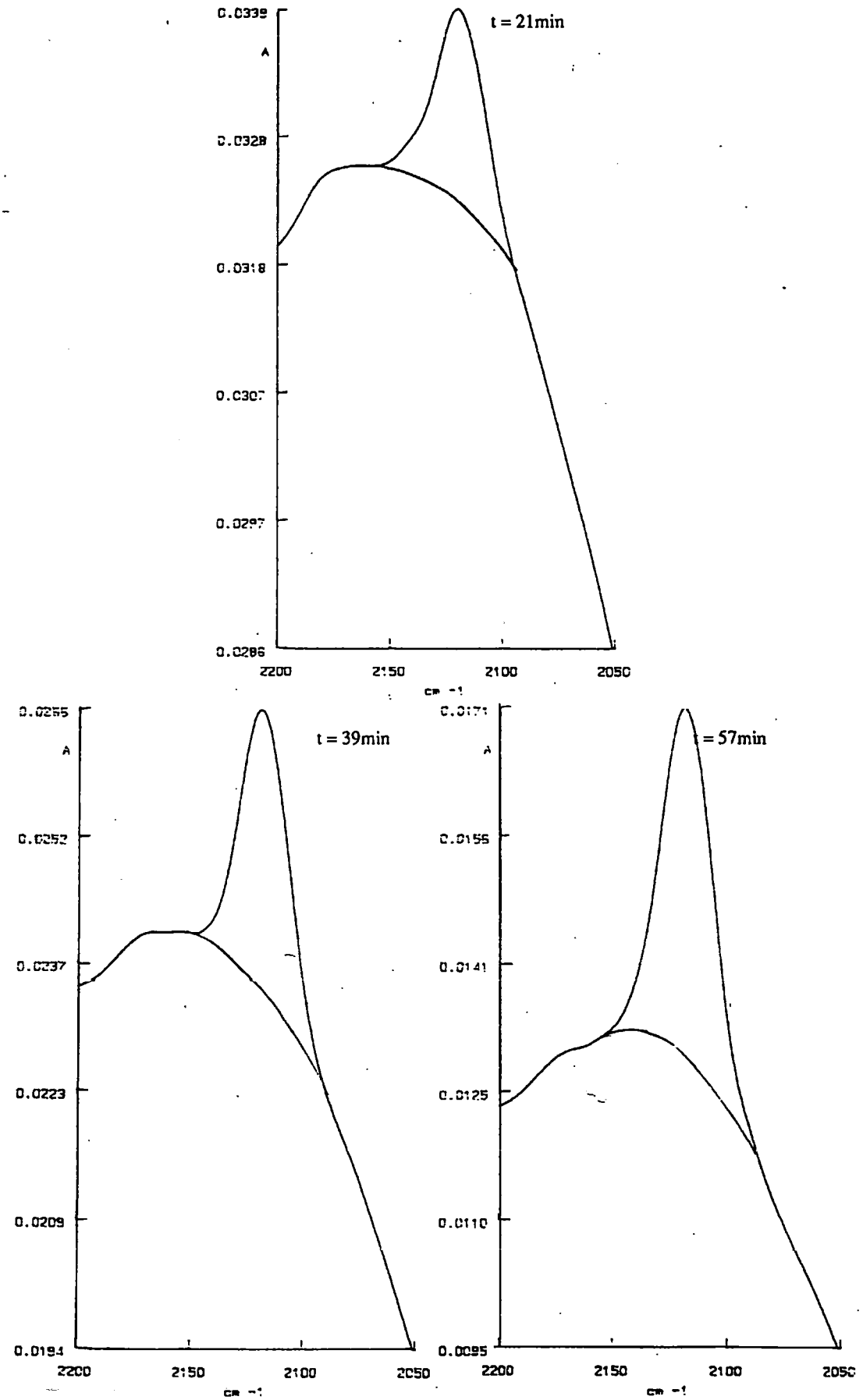

Figure 4.10

FTIR spectra with respect to time for reaction of 1.0M GlyGly and 0.01M $EtO(CH_2)_2ONO$ at pH 11.04 and 25°C

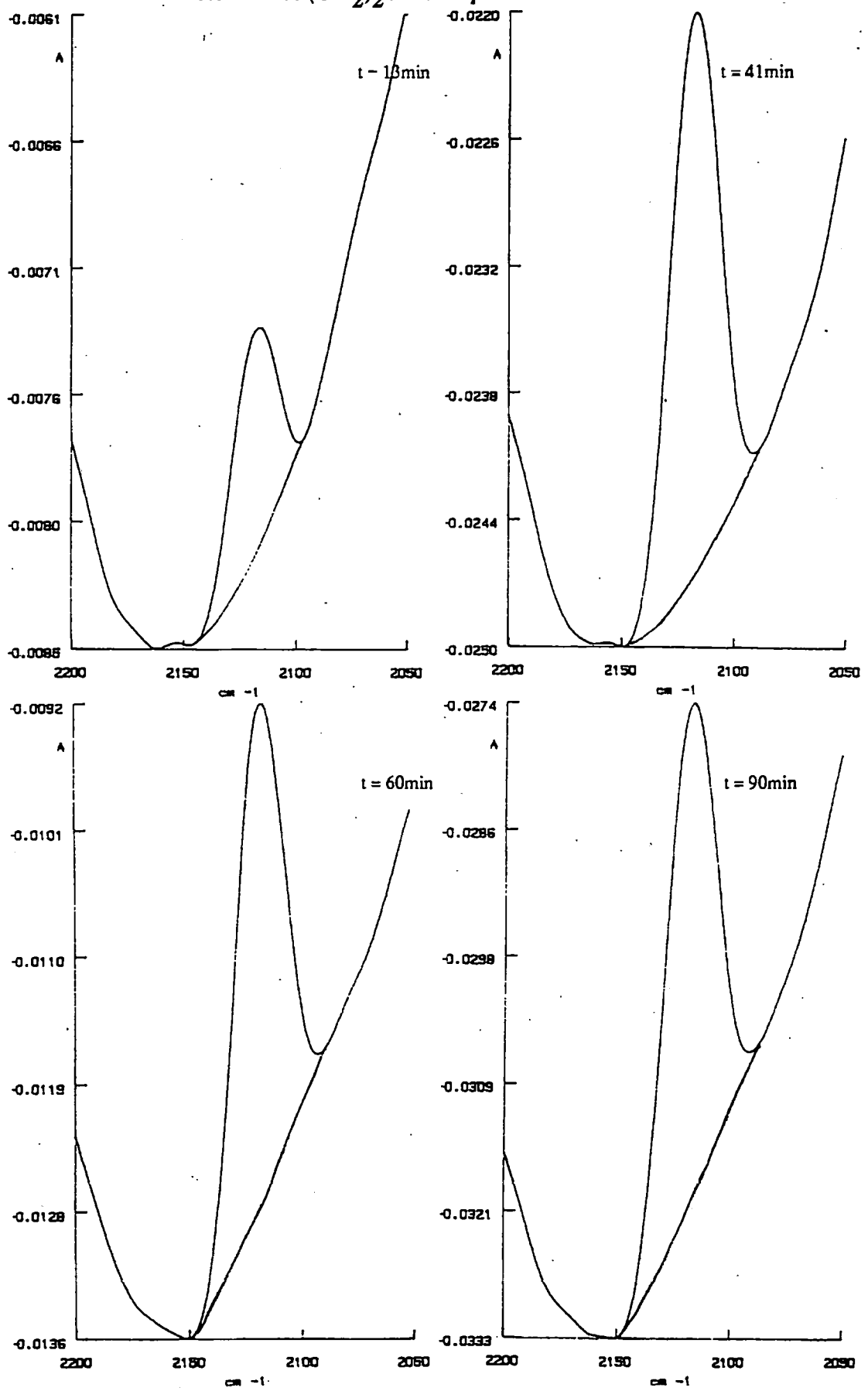

Figure 4.11

Absorbance of diazo product (ca 2100cm^{-1}) against time for reactions of GlyGly (1.0M) and EtO(CH$_2$)$_2$ONO (1.0 x 10^{-3}M) - typical plots

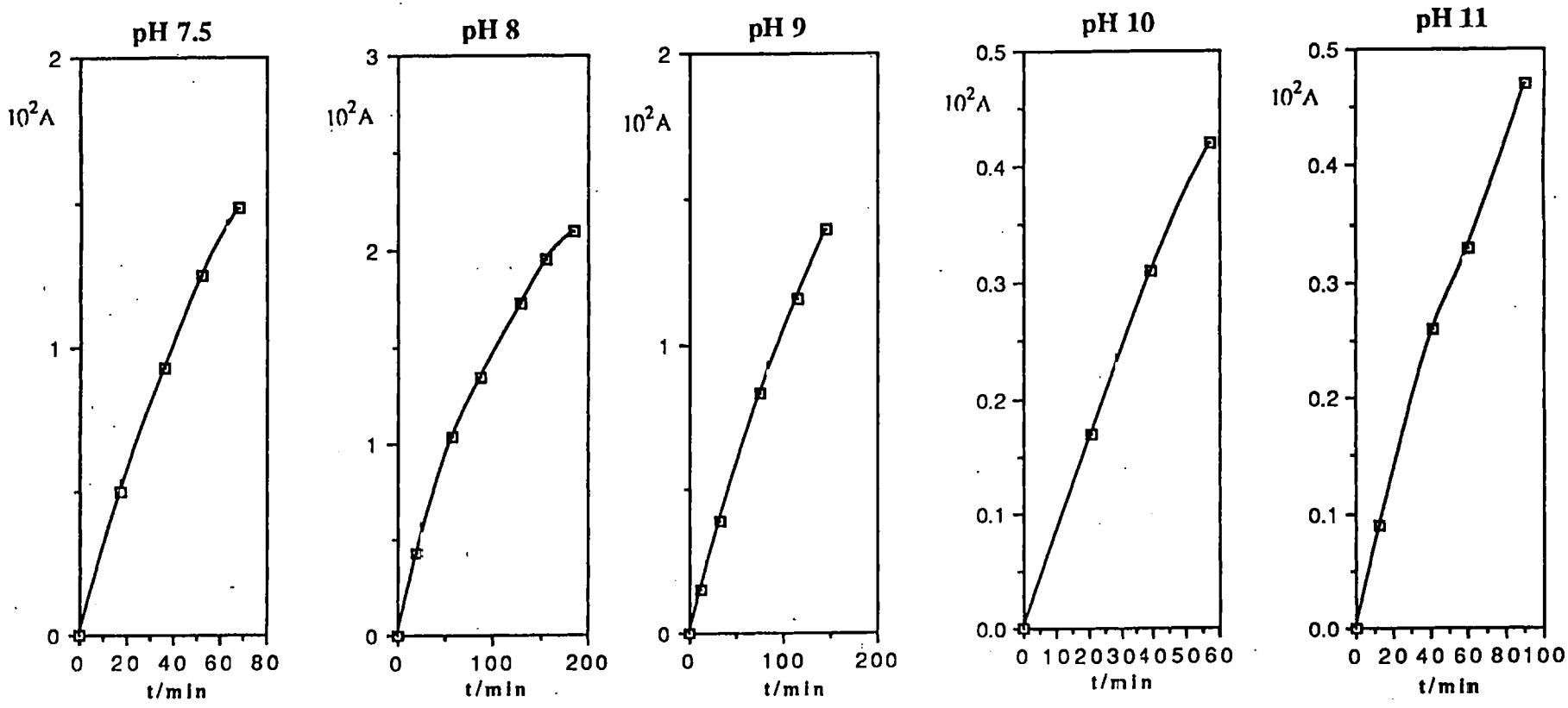

Because the spectrometer averages the spectra as they accumulate, the elapsed time was calculated from the moment of mixing the reagents to the mid-time of the scan sequence. The variation of absorbance at 2121cm^{-1} with time is listed in Table 4.5.

Table 4.5

Decomposition of N-(2-diazoacetyl)glycine ethyl ester in 1.0M GlyGly at pH 9 and 25°C. Initial [N-(2-diazoacetyl)glycine ethyl ester]=1.0 x 10^{-3}M

t/min	*10^3A(2121cm^{-1})*
0	6.15
44	5.83
96	5.81
157	5.64

Assuming that other diazodipeptides hydrolyse at a similar rate, at pH 9 and 25°C, the extent of product hydrolysis would be negligible (4.5% over the first 44min) and unlikely seriously to perturb rates of diazotisation calculated from the initial formation of diazopeptide product.

4.9 Kinetics of the diazotisation of GlyGly

Initial experiments were carried out with N-glycylglycine because of its simple structure and ready availability. The solutions of GlyGly were made up on the day of use by dissolving the peptide in distilled water and adding small amounts of 1.0M NaOH(aq) to adjust the pH to the required value. No anions which might have catalysed the reaction were added.

The reactions were started by adding a small amount of neat 2-ethoxyethanol nitrite ester (ca 17.3µl) via micropipette to 10cm^3 of aqueous peptide. After thorough mixing, the reaction solution was transferred to the IR cell and the IR absorbance was measured at timed intervals using the optimum scan conditions given in Section 4.7. Typical spectra at various time points for reactions at pH 7.5 - 11.04 are shown in Figures 4.6 - 4.10 and these illustrate the variation of the baseline. The absorbance data obtained from them are given in Table 4.6 and the absorbance versus time plots in Figure 4.11. The maximum absorbance of 0.021 reported in Table 4.6 corresponds to a N-(2-diazoacetyl)glycine concentration of 0.34 x 10^{-3} M and therefore 34% reaction, assuming that the extinction coefficients of N-(2-diazoacetyl)glycine and its ethyl ester are similar.

Table 4.6

Diazotisation of 1.0M GlyGly by 1.0x10^{-2} ethoxyethyl nitrite in aqueous buffers at 25°C Initial [GlyGly] = 1.0M, [EtO$(CH_2)_2$ONO] = 0.01M

pH	*t/min*	*10^2A*	*pH*	*t/min*	*10^2A*	*pH*	*t/min*	*10^2A*
7.50	17	0.50	9.04	12	0.15	11.04	13	0.09
	36	0.93		32	0.39		41	0.26
	52	1.25		75	0.83		60	0.33
	68	1.48		114	1.16		90	0.47
				145	1.40			
8.00	20	0.43	10.16	21	0.17			
	56	1.03		39	0.31			
	86	1.34		57	0.42			
	129	1.73						
	155	1.95						
	184	2.10						

Values of the *pseudo* first order rate coefficient (Equation 4.2) calculated from the initial slopes of the plots in Figure 4.11, assuming ε(N-2-diazoacetyl)glycine at 2115cm^{-1} = 439dm^{3}mol^{-1}cm^{-1}, are summarised in Table 4.7.

$$\text{Rate} = k_1[\text{EtO}(CH_2)_2\text{ONO}] \qquad \text{Equation 4.2}$$

Table 4.7

Diazotisation of GlyGly by ethoxyethyl nitrite in aqueous buffers at 25°C. Initial [GlyGly] = 1.0M; [EtO$(CH_2)_2$ONO] = 0.01M.

pH	*$10^7\frac{dC}{dt}M^{-1}s^{-1}$*	*$10^5k_1/s^{-1}$*
7.50	8.03	8.03
8.00	6.59	6.59
9.04	3.24	3.24
10.16	2.15	2.15
11.04	2.15	2.15

Figure 4.12

FTIR spectra with respect to time for reaction of 0.5M GlyGly and 0.01M $EtO(CH_2)_2ONO$ at pH 9.00 and 25°C

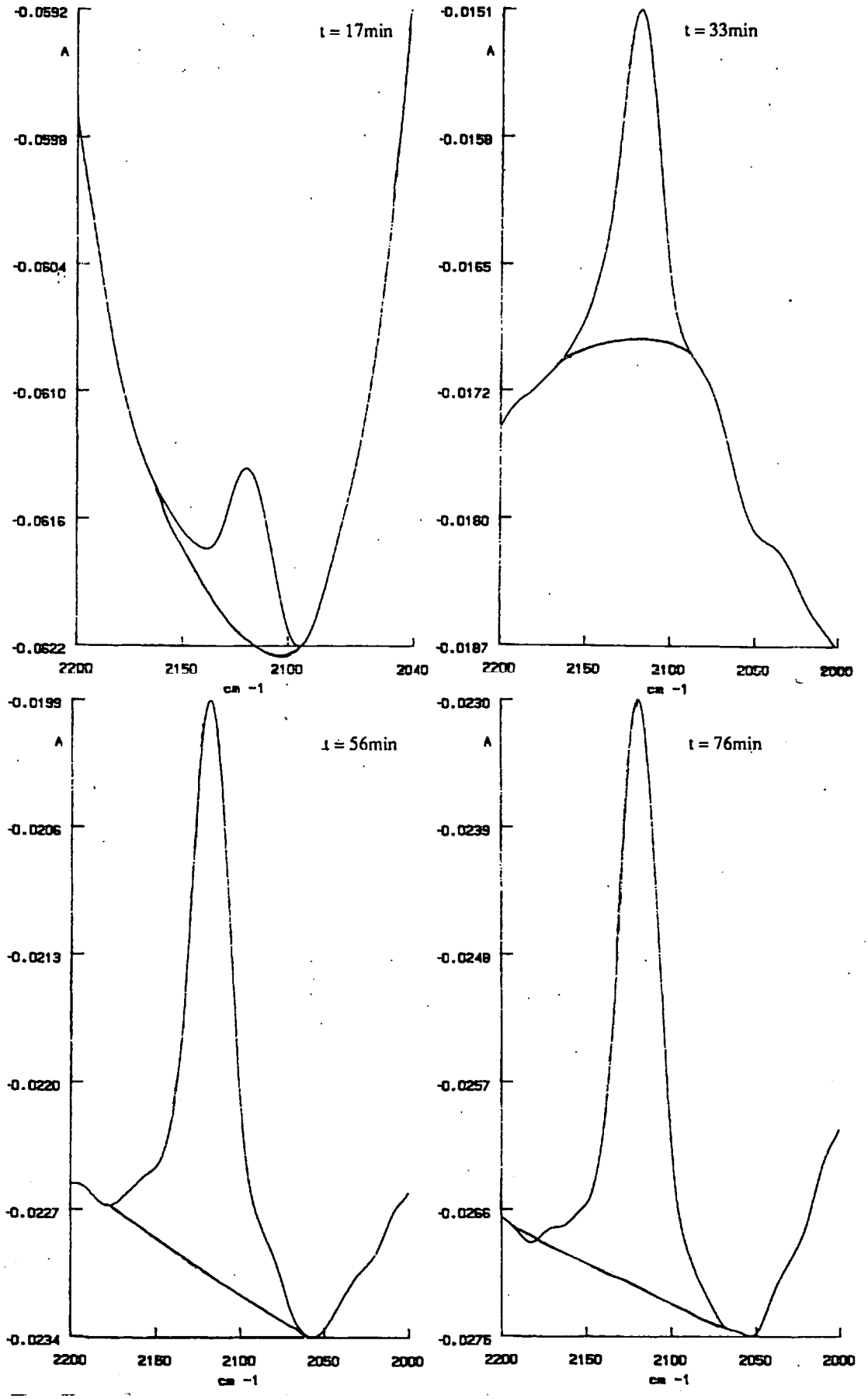

Figure 4.13

FTIR spectra with respect to time for reaction of 1.0M GlyGly and 0.005M $EtO(CH_2)_2ONO$ at pH 9.00 and 25°C

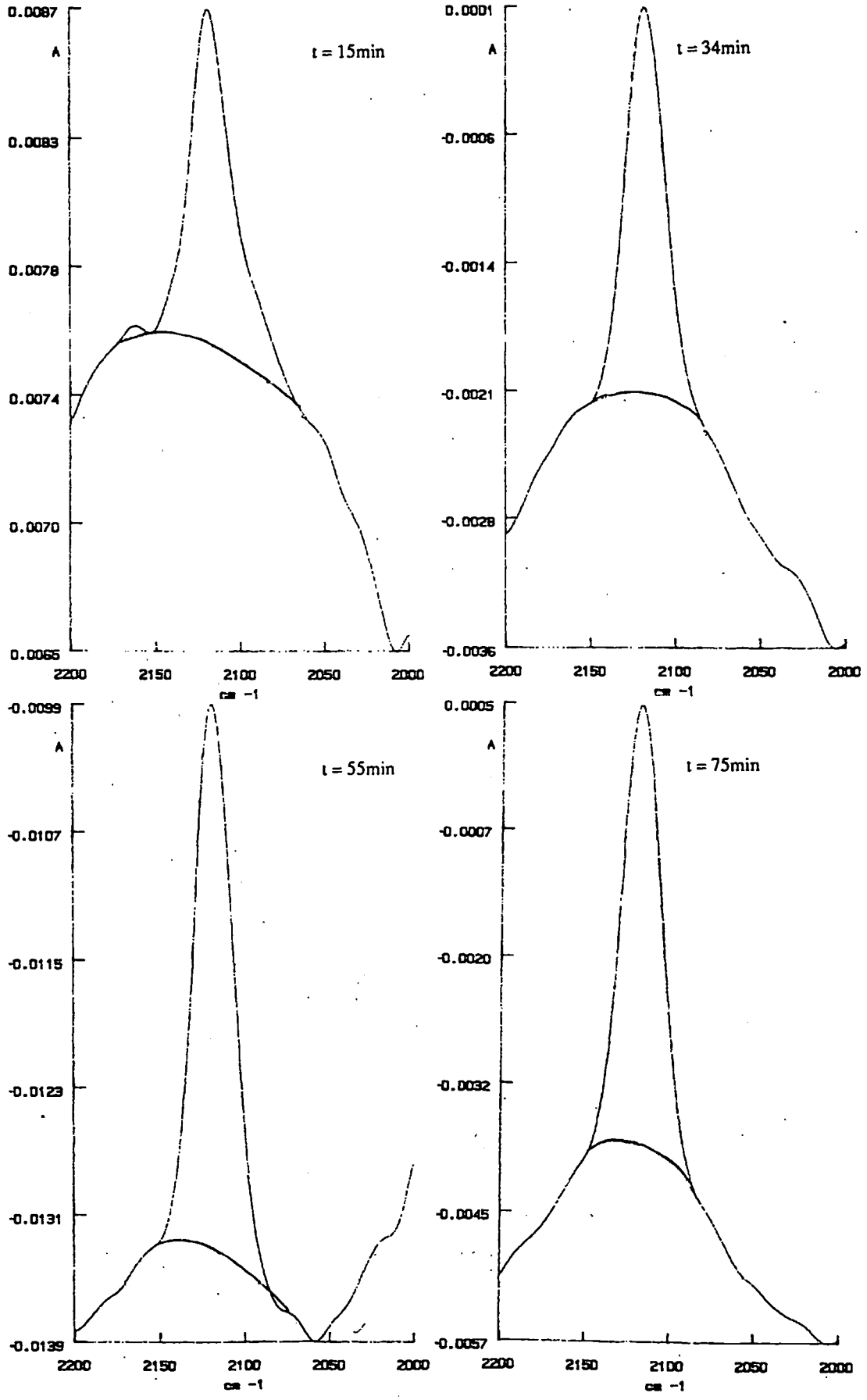

Figure 4.14
Variation in FTIR absorbance at 2118cm^{-1} with time for reaction of
a) 0.5M GlyGly with 0.01M EtO$(CH_2)_2$ONO and
b) 1.0M GlyGly with 0.005M EtO$(CH_2)_2$ONO

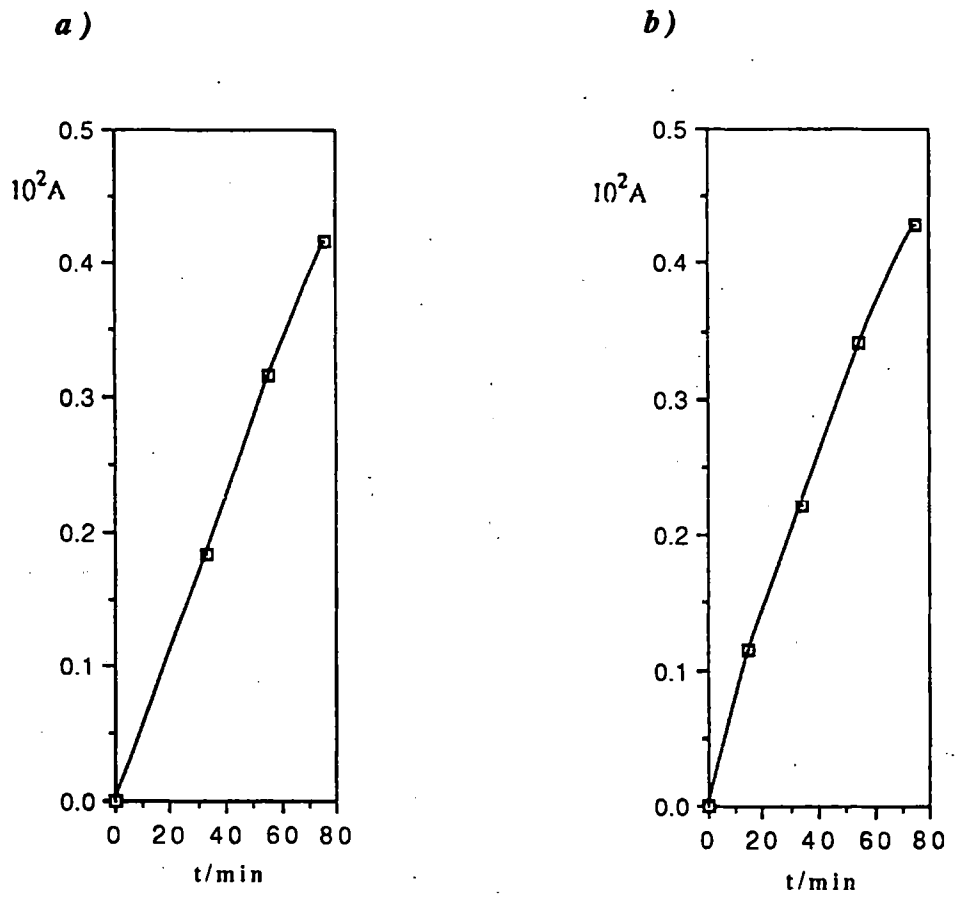

Interestingly, the values of k_1 are not strongly dependent on pH and the diazotisation of GlyGly by 2-ethoxyethyl nitrite does not seem to be strongly acid-catalysed.

The kinetic dependence of the diazotisation of GlyGly was briefly examined at pH 9 and 25°C by carrying out the reaction with 0.5 M GlyGly and 10^{-2} M 2-ethoxyethyl nitrite and with 1.0M GlyGly and 5 x 10^{-1}M 2-ethoxyethyl nitrite. The IR spectra obtained are shown in Figures 4.12 and 4.13 and the variation in the absorbance with time is summarised both in Table 4.8 and Figure 4.14.

Table 4.8

Diazotisation of GlyGly by 2-ethoxyethyl nitrite in aqueous buffers at 25 °C. Initial [GlyGly] = 0.5M (a) and 1.0M (b) Initial [$EtO(CH_2)_2ONO$] = 0.01M (a) and 0.005M (b).

(a) *pH*	*t/min*	10^2A	*(b)* *pH*	*t/min*	10^2A
9.00	17	0.067	9.00	15	0.115
	33	0.184		34	0.223
	56	0.316		55	0.341
	76	0.416		75	0.429

Values of k_1 (Equation 4.2) and k_2 (Equation 4.3) calculated from these data are summarised in Table 4.9. The constant values of k_2 suggest that the reaction is first order with respect to both 2-ethoxyethyl nitrite and peptide.

$$\text{Rate} = k_2[\text{GlyGly}][EtO(CH_2)_2ONO] \qquad \text{Equation 4.3}$$

Table 4.9

Second order rate constants for the diazotisation of GlyGly at pH 9 and 25 °C.

[GlyGly]	*[$EtO(CH_2)_2ONO$]*	$10^5k_1s^{-1}$	$10^5k_2/M^{-1}s^{-1}$
1.0	0.010	3.24	3.24
0.5	0.010	1.42	2.84
1.0	0.005	1.77	3.54

4.10 The diazotisation of other peptides by 2-ethoxyethyl nitrite in aqueous buffers at 25°C

The effect of peptide structure on the rate of diazotisation was very briefly examined at pH 9 and 25°C, using GlyLeu, GlySar and LeuGly. These reactions used 1.0M peptide and 0.01M 2-ethoxyethyl nitrite and were carried out in exactly the same way as for GlyGly. Variations of absorbance with time for the initial diazotisation of GlyLeu and GlySar are reported in Table 4.10, along with the k_1 values calculated from the initial rates.

Table 4.10

Diazotisation of 1.0M GlyLeu and GlySar by $1.0x10^{-2}M$ $EtO(CH_2)_2ONO$ at pH 9 and 25°C. Initial [peptide] = 1.0M, [$EtO(CH_2)_2ONO$] = 0.01M

	GlyLeu			*GlySar*	
pH	*t/min*	10^2A	*pH*	*t/min*	10^2A
9.03	18	0.33	9.00	10	0.24
	35	0.63		24	0.50
	51	0.84		38	0.68
	69	1.11		51	0.92
	$k_1 = 5.28 \times 10^{-5}s^{-1}$			$k_1 = 6.29 \times 10^{-5}s^{-1}$	

The diazotisation of 1.0M LeuGly with 10^{-2}M ethoxyethyl nitrite was very much slower than the other peptides and a product diazo peak was visible only after 11h. A maximum value of $k_1 = 5 \times 10^{-9}s^{-1}$ was estimated for LeuGly, 10^4 fold slower than the other peptides.

4.11 The diazotisation of glycine and 2,2-$[^2H_1]_2$-glycine

The formation of diazopeptides requires proton abstraction from the α-carbon to the terminal NH_2. To obtain some idea whether this is the slow step of the reaction, the diazotisation of the amino acid glycine and 2,2-$[^2H_1]_2$-glycine by ethoxyethyl nitrite was compared under identical conditions. These substrates rather than peptides were compared because of the availability of the deuterated glycine. The reactions could not be followed at pH 9 because the diazoacetic acid product band at $2100cm^{-1}$

Figure 4.15

FTIR spectra with respect to time for reaction of 1.0M glycine and 0.01M $EtO(CH_2)_2ONO$ at pH 11.00 and 25°C

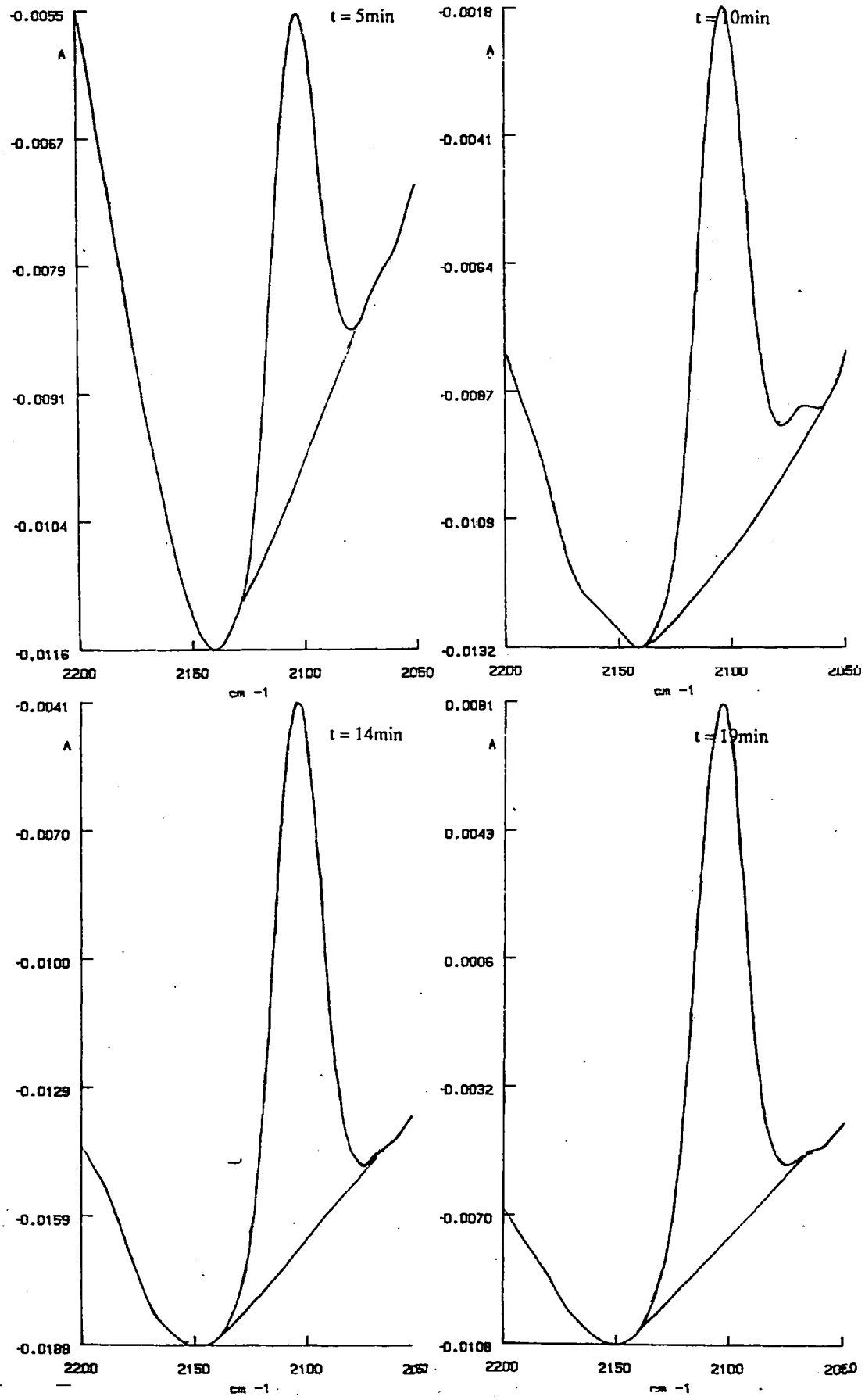

Figure 4.16

FTIR spectra with respect to time for reaction of 1.0M 2,2-[$^2H_1$]-glycine and 0.01M $EtO(CH_2)_2ONO$ at pH 11.00 and 25°C

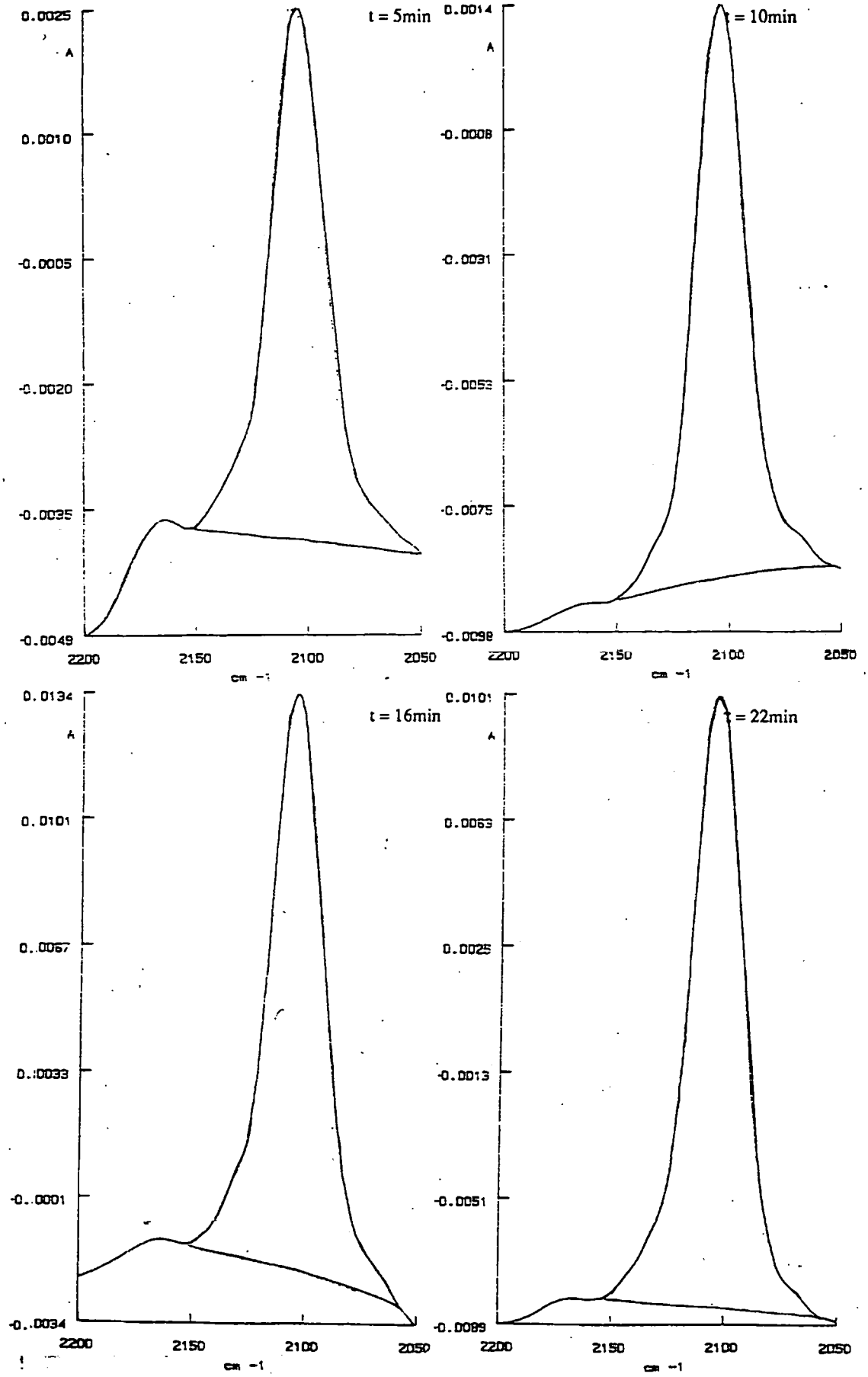

Figure 4.17

Variation of FTIR absorbance with time for reaction o 1.0M glycine with 0.01M $EtO(CH_2)_2ONO$ at pH 11 and 25°C

a) Glycine

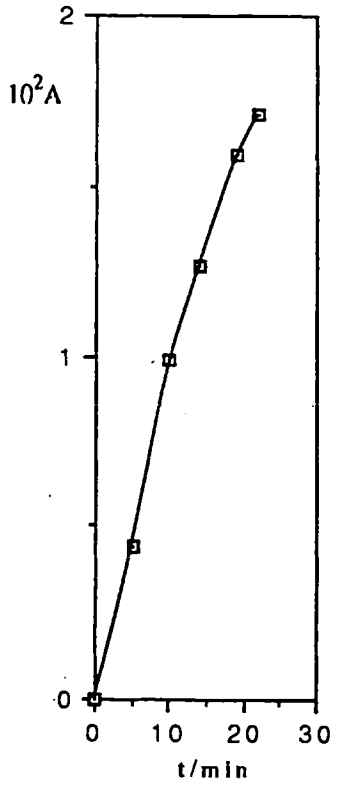

b) 2,2-[$^2H_1$]-Glycine

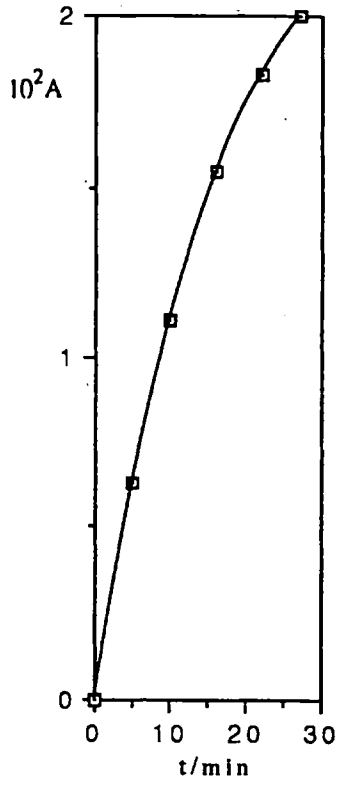

was not visible, presumably because it hydrolysed too quickly. At pH 11 and 25°C, diazoacetic acid was observed but the number of scans had to be cut to 50, resulting in a high noise level, because the evolution of gas in the cell contents caused errors in the absorbance measurements over longer times. Also, the rates of reaction were fast compared with the peptides and the spectra had to be obtained from shorter scan times.

Typical results for the diazotisation of the glycine substrates in the form of actual spectra are shown in Figures 4.15 and 4.16 and the variation of absorbance with time is reported in Table 4.11 and Figure 4.17. The k_1 values (Equation 4.2) are also given in Table 4.11.

Table 4.11

Diazotisation of Glycine by $EtO(CH_2)_2ONO$ at pH 11 and 25°C.

Initial [glycine] = 1.0M; [$EtO(CH_2)_2ONO$] = 0.01M

1.0M Glycine		*1.0M 2,2-[$^2H_1$]$_2$-Glycine*	
t/min	*10^2A*	*t/min*	*10^2A*
5	0.44	5	0.63
10	0.99	10	1.11
14	1.27	16	1.54
19	1.59	22	1.83
22	1.71	27	2.00
k_1 = 2.86 x $10^{-4}s^{-1}$		k_1 = 3.01 x $10^{-4}s^{-1}$	

It is apparent that no primary deuterium isotope effect applies to the diazotisation of glycine, and H^+-loss from the α–carbon atom cannot be rate limiting.

4.12 Summary

The diazo products of the various reactions had diazo absorption bands at the slightly different frequencies reported in Table 4.12. The *pseudo* first order rate constants (Equation 4.2) for all the substrates reported above are summarised in Table 4.13. The k_1 values suggest that a given pH, glycine reacts ca 10-fold faster than glycyl peptides, and that the reactivity of glycyl peptides is not strongly influenced by the structure of the second amino acid residue. Further, glycyl peptides react ca 60-fold faster than water with 2-ethoxyethyl nitrite which reflects their higher basicity and nucleophilicity.

Table 4.12

Frequencies of diazo bands in aqueous media at 25°C

Substrate	*pH*	*Wavenumber/cm^{-1}*
GlyGly	9	2118
GlyLeu	9	2117
GlySar	9	2121
LeuGly	9	2090
Glycine	11	2105
2,2-[$^{2}H_1$]$_2$-glycine	11	2104

Table 4.13

Pseudo first order rate constants for the diazotisation of dipeptides and glycine by ethoxyethyl nitrite in aqueous buffers at 25°C

		$10^5 k_1/s^{-1}$				
Substrate	*pH*	*11*	*10*	*9*	*8*	*7.5*
GlyGly		2.15	2.15	3.24	6.59	8.03
Glycine		28.6				
2,2-[$^{2}H_1$]$_2$-glycine		30.1				
GlyLeu				5.28		
LeuGly				0.0005		
GlySar				6.29		
H_2O*		0.023	0.031	0.036	0.054	

(*Assuming [H_2O] = 55.56M)

The one unexpected result is the low k_1 value for LeuGly; either diazotisation of peptides is strongly decreased by steric effects or, more likely, the diazoproduct from LeuGly decomposes much more rapidly than those from glycyl peptides.

4.13 Discussion

The reaction of GlyGly with 2-ethoxyethyl nitrite, at pH 7-11 and 25°C, might be expected to follow the pathway outlined by Scheme 4.3.

Scheme 4.3

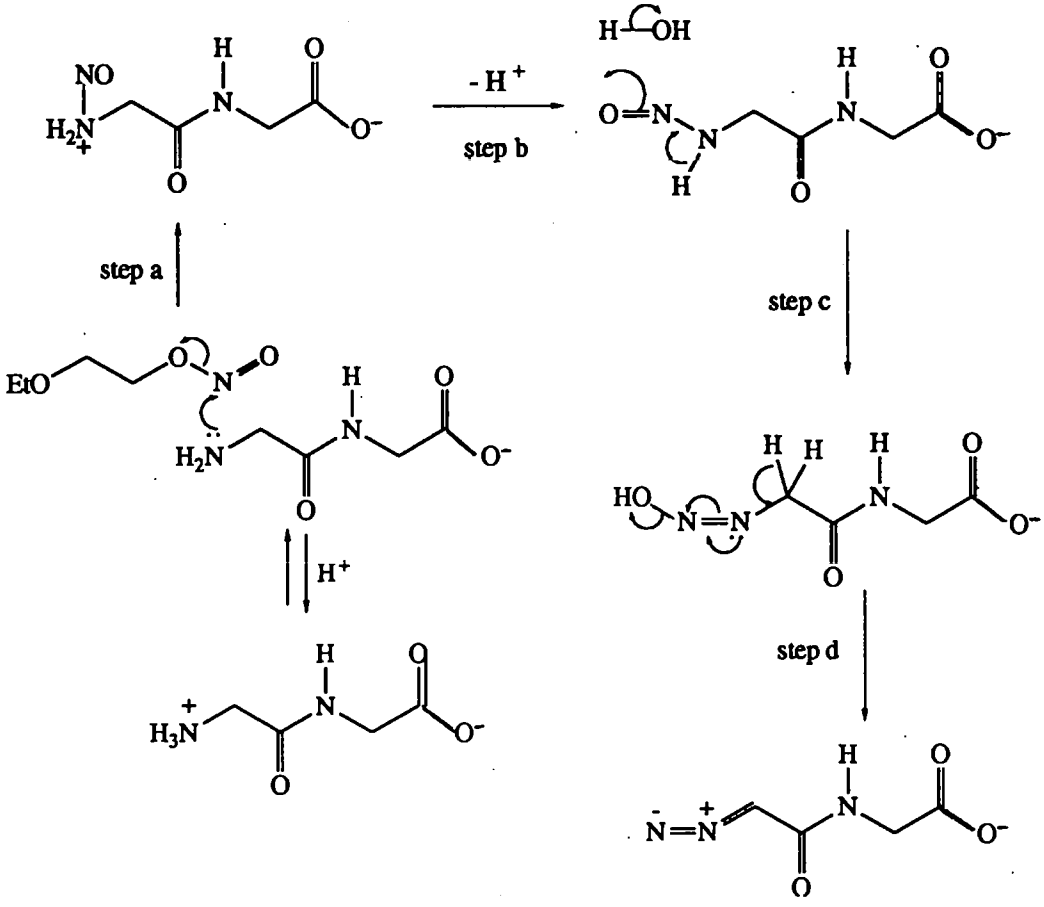

Unfortunately, insufficient time was available to carry through a kinetic study to prove this pathway unequivocally. The present results, however, do allow some mechanistic conclusions.

$$\text{Rate} = k_2[\text{GlyGly}][\text{EtO}(\text{CH}_2)_2\text{ONO}] \qquad \text{Equation 4.3}$$

Thus, the reaction rates for GlyGly follow Equation 4.3 which implies a bimolecular process involving both reactants, as shown in Scheme 4.3. Further, the results for glycine and 2,2-$[^2H_1]_2$-glycine suggest that H^+ loss from the α-carbon atom to the NH_2 group is rapid; the faster reactions for glycine relative to GlyGly suggest that slow rearrangement of an acyl nitroso intermediate (Scheme 4.4) is not involved; and the similar reaction rates for GlyGly and GlySar suggest that slow rearrangement of an N-nitroso intermediate (Scheme 4.5) is not involved.

Scheme 4.4

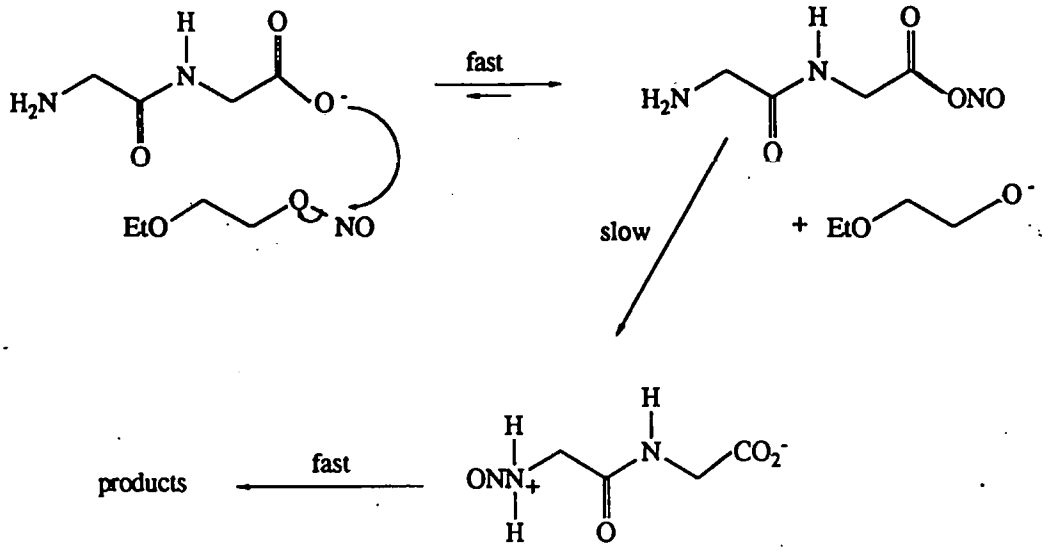

Scheme 4.5

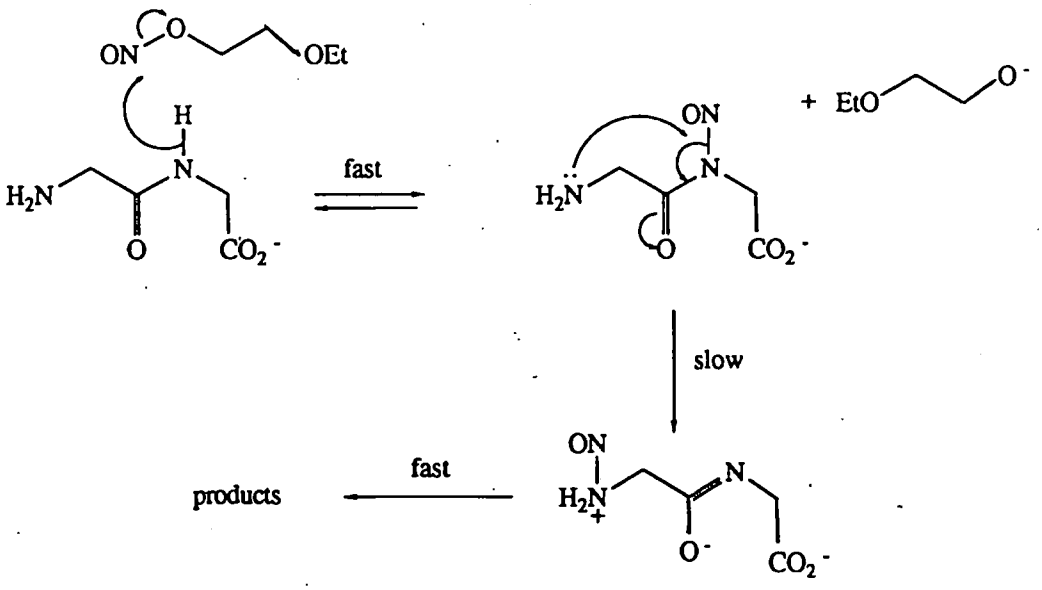

It therefore seems reasonable to conclude that the initial N-nitrosation of Scheme 4.3 (step k_a) is rate-limiting. This conclusion, however, is inconsistent with the pH independent rate observed for GlyGly (Table 4.13), because over the pH range 7-11, the concentration of neutral substrate (pK_a (GlyGly) = 8.13) must change by a factor of 10^4, whereas the k_1 values are virtually pH independent.

Thus Scheme 4.3, with step k_a rate limiting, fails to explain the lack of pH dependence observed for the nitrosation of GlyGly. Reactions involving the conjugate acid of 2-ethoxyethyl nitrite with the unprotonated peptide

seem to be excluded by the low pH dependence observed for the hydrolysis of 2-ethoxyethyl nitrite, unless this reaction also involves reaction of hydroxide ion with the conjugate acid of 2-ethoxyethyl nitrite. Clearly, further work is required to ascertain the detailed mechanism(s) of peptide diazotisation in aqueous buffers. These experiments should be feasible using FTIR to follow the reactions.

Appendix

Derivation of relation between concentration and absorbance for hydrolysis of ethoxyethyl nitrite in water

$A = \varepsilon c l$

where A = absorbance, c = concentration and l = cell path length

and $A_a^t + A_n^t = A_{obs}^t$

where a ≡ alkyl nitrite, n ≡ inorganic nitrite, t ≡ time t

so $\varepsilon_a c_a^t + \varepsilon_n c_n^t = A_{obs}^t$ since l = 1cm

$c_n^t = c_a^o - c_a^t$ where o ≡ time 0

so $\varepsilon_a c_a^t + \varepsilon_n [c_a^o - c_a^t] = A_{obs}^t$

ie $\varepsilon_a c_a^t + \varepsilon_n c_a^o - \varepsilon_n c_a^t = A_{obs}^t$

$[\varepsilon_a - \varepsilon_n] c_a^t + \varepsilon_n c_a^o = A_{obs}^t$

$$c_a^t = \frac{A_{obs}^t - \varepsilon_n c_a^o}{\varepsilon_a - \varepsilon_n}$$

Chapter 5

Experimental

5.1. General and Instrumentation

5.1.1 Physical Measurements

5.1.2 Reagents and reactants

5.2. Synthesis

5.2.1 Glycine benzyl ester

5.2.2 N-Glycylglycine benzyl ester

5.2.3 L-Alanine benzyl ester

5.2.4 L-Valine benzyl ester

5.2.5 N-(N'-Acetylglycyl)glycine benzyl ester

5.2.6 N-(N'-1-^{13}C-Acetylglycyl)glycine benzyl ester

5.2.7 N-(N'-Acetylglycyl)-L-alanine benzyl ester

5.2.8 N-(N'-Acetylglycyl)-L-valine benzyl ester

5.2.9 N-(N'-Acetyl-L-alanyl)glycine benzyl ester

5.2.10 N-(N'-Acetyl-L-alanyl)alanine benzyl ester

5.2.11 N-(N'-Acetyl-L-valyl)glycine benzyl ester

5.2.12 N-((N"-Acetyl-L-valyl)-N'-glycyl)glycine benzyl ester

5.2.13 N-(N'-Acetyl-L-prolyl)glycine benzyl ester

5.2.14 N-(N'-Acetylglycyl)glycine

5.2.15 N-(N'-1-^{13}C-Acetylglycyl)glycine

5.2.16 N-(N'-Acetylglycyl)-L-alanine

5.2.17 N-(N'-Acetylglycyl)-L-valine

5.2.18 N-(N'-Acetyl-L-alanyl)glycine

5.2.19 N-(N'-Acetyl-L-alanyl)alanine

5.2.20 N-(N'-Acetyl-L-valyl)glycine

5.2.21 N-((N"-Acetyl-L-valyl)-N'-glycyl)glycine

5.2.22 N-(N'-Acetyl-L-prolyl)glycine

5.2.23 N-(N'-Acetyl-N'-nitrosoglycyl)glycine benzyl ester

5.2.24 N-(N'-Acetyl-N'-nitrosoglycyl)-N-nitrosoglycine benzyl ester

5.2.25 N-(N' Acetyl-N'-nitrosoglycyl)glycine
5.2.26 N-(2-Diazoacetyl)glycine benzyl ester
5.2.27 N-(2-Hydroxyacetyl)glycine
5.2.28 N-(2-Chloroacetyl)glycine
5.2.29 N-(2-Chlorohydroxyiminoacetyl)glycine
5.2.30 2-Ethoxyethyl nitrite

5.3. Procedures

5.3.1 FTIR spectra of authentic compounds
5.3.2 Kinetics of peptide nitrosation
5.3.3 Kinetics of peptide diazotisation
5.3.4 Nitrite decomposition

5.1.1 Physical Measurements

Infra-red spectra of pure substances were recorded as thin films or as potassium bromide discs, using a Perkin-Elmer 1710 FTIR spectrometer, referenced to a helium-neon laser.

Ultra-violet/visible spectra were run in the solvents stated, on Cecil CE 5501, Kontron Uvikon 810P or LKB 4050 spectrophotometers, calibrated with a holmium filter.

Nuclear magnetic resonance spectra, in the solvents indicated, were recorded at 90 MHz on a Jeol FX90Q FTNMR spectrometer by Mr Gordon Howell. The internal standard was tetramethyl silane for organic solvents or the sodium salt of 3-(trimethylsilyl)-1-propane sulphonic acid for deuterium oxide.

Mass spectra were obtained by Mr Brandon Cook using a VG 20-250 instrument, with xenon as the ionising gas for fast atom bombardment of the sample in a glycerol matrix.

Microanalyses were supplied by Medac Ltd at Brunel University.

Melting points were measured on an Electrothermal digital melting point apparatus and are uncorrected.

pH measurements were made on a Radiometer PHM 82 pH meter, using Radiometer G2040C glass and K4040 calomel electrodes, calibrated with BDH standard buffers.

Refractive indices were measured on a Bellingham and Stanley refractometer at the temperature indicated.

5.1.2 Reagents and Reactants

$NaNO_2$, NaCl, $NaClO_4$ $Na_2B_4O_7$ and 1.0M NaOH for kinetic studies were AR grade, obtained from BDH. Glycylglycine, 98%, was obtained from Aldrich and other amino acids and peptides from Sigma, laboratory grade. Benzyl alcohol, toluene-4-sulphonic acid, acetic acid, sodium acetate, triethylamine, ethoxyethanol, 10% palladium charcoal and sodium nitrite for preparations were laboratory reagent grade from Aldrich or BDH. Nitrogen dioxide was obtained from Fisons. Chemicals were used as supplied, except triethylamine and solvents which were purified by standard methods[83]. Diazoacetylglycine ethyl ester was kindly provided by G. Okafo; acetylproline and N-nitroso-2-pyrrolidone by D.Trew.

Isotopically labelled compounds were supplied by MSD Isotopes as follows: deuterium oxide, 99.9 atom % D; deuterium chloride, 35% (w/w) in D_2O, 99.9 atom % D; deuterium sulphate, 96% (w/w) in D_2O, 99 atom % D; acetyl-1-^{13}C chloride, 99 atom % ^{13}C; glycine-2,2-d_2, 98.9 atom % D.

5.2. Synthesis

5.2.1 Glycine benzyl ester, GlyOBz

Glycine (5.7g, 76mmol), toluene-4-sulphonic acid (18g, 94.7mmol), benzyl alcohol (60cm^3) and toluene (60cm^3) were heated under reflux using a Dean-Stark head until no more water was produced (2-3h). After cooling, diethyl ether (200cm^3) was added and the mixture was left in an ice bath for 2 h. The white crystals of glycine benzyl ester toluene-4-sulphonate were filtered off, washed with ether and left to dry in the air. The product (5.06g, 15mmol) was dispersed in dichloromethane (200cm^3) and triethylamine (3.03g, 30mmol) was added. After leaving to stand for 10 min, the solution was washed with water (15cm^3), dried ($MgSO_4$) and the solvent removed under vacuum to give a semi-solid oil of glycine benzyl ester, 1.6g, 65%. This was used immediately in the peptide coupling reaction.

5.2.2 N-glycylglycine benzyl ester, GlyGlyOBz

This was prepared from glycylglycine (10g, 76mmol) using the method for glycine benzyl ester, yield 2.2g, 66%.

5.2.3 L-alanine benzyl ester, AlaOBz

This was prepared from L-alanine (6.76g, 76mmol) using the method for glycine benzyl ester, yield 1.4g, 52%.

5.2.4 L-valine benzyl ester, ValOBz

This was prepared from L-valine (8.9g, 76mmol) using the method for glycine benzyl ester, yield 2.0g, 64%.

5.2.5 N-(N'-acetylglycyl)glycine benzyl ester (AcGlyGlyOBz)

The toluene-4-sulphonic acid salt of glycylglycine benzyl ester (29.9g, 76mmol) was dissolved in dichloromethane (160cm^3). Triethylamine (16.16g, 160mmol) was added, followed by dropwise addition of acetyl

chloride (6.59g, 84mmol) dissolved in dichloromethane (10cm^3). The solution was stirred at room temperature for 2 h and then washed successively with 0.1M HCl (50cm^3), satd. aq. $NaHCO_3$ (50cm^3), and water (50cm^3). The solution was dried ($MgSO_4$), the solvent evaporated and the product recrystallised twice from ethyl acetate to give AcGlyGlyOBz (7.9g, 39%), mp128-129°C (lit. mp 104-107°C)[84]; ν_{max}(KBr disc) 3268(N-H), 1744(ester C=0), 1641(amide I, acetyl C=O), 1557cm^{-1}(amide II); $\delta_H(CDCl_3)$ 2.01(3H, s, C*H*$_3$), 3.98(2H, d, C*H*$_2$NHCOCH$_3$), 4.10(2H, d, C*H*$_2$COOH), 5.17(2H, s, C*H*$_2$Ph), 6.61(1H, br, N*H*), 6.98(1H, br, N*H*), 7.34(5H, s, *Ph*); m/z(FAB$^+$) (CH_2Cl_2/glycerol) 265(32%, MH$^+$), 223(3, MH$^+$-CH_2CO), 166(15, $^+H_3NCH_2COOBz$), 157(2, MH$^+$-BzOH), 100(10, $CH_3CONHCH_2CO^+$), 91(52 Bz$^+$); (FAB$^-$) 263(40, M-H$^+$), 173(48, M-Bz$^+$).

5.2.6 N-(N'-1-^{13}C-acetylglycyl)glycine benzyl ester (^{13}C-AcGlyGlyOBz)

The toluene-4-sulphonic acid salt of glycylglycine benzyl ester, made as described above was recrystallised from ethanol, mp. It was then treated with acetyl-1-^{13}C-chloride using the method above, but on a 3.18mmol scale, (0.19g, 34%), mp 130-131°C; ν_{max}(KBr disc) 3259(N-H), 1745(ester C=O), 1651(amide I), 1622(acetyl C=O), 1530cm^{-1}(amide II); $\delta_H(CDCl_3)$ 2.06(3H, d, C*H*$_3$), 3.97(2H, q, C*H*$_2$NHCOCH$_3$), 4.10(2H, d, C*H*$_2$COOBz), 5.19(2H, s, C*H*$_2$Ph), 6.33(1H, br, N*H*), 6.64(1H, br, N*H*), 7.35(5H, s, *Ph*); m/z(FAB$^+$)(CH_2Cl_2/glycerol) 266(37%, MH$^+$), 223(3, MH$^+$-CH_2CO), 166(16, $^+H_3NCH_2COOBz$), 158(2, MH$^+$-BzOH), 101(8, $CH_3CONHCH_2CO^+$), 91(56, Bz$^+$); (FAB$^-$) 264(45%, M-H$^+$), 174(53, M-Bz$^+$).

5.2.7 N-(N'-acetylglycyl)-L-alanine benzyl ester, AcGlyAlaOBz

N-acetylglycine (1.17g, 10mmol) and triethylamine (1.01g, 10mmol) were dissolved in dry tetrahydrofuran (60cm^3). Dry nitrogen was passed continuously through the mixture which was cooled to -10°C. Ethyl chloroformate (0.98g, 9mmol) in dry tetrahydrofuran (5cm^3) was introduced slowly and stirred for 30 min. L-alanine benzyl ester (1.65g, 10mmol) in tetrahydrofuran (5cm^3) was added. The mixture was allowed to warm to room temperature (about 30min). The solvent was evaporated and the white solid dissolved in dichloromethane (80cm^3) before washing successively with 0.1M HCl (20cm^3), satd. aq. $NaHCO_3$ (20cm^3) and

water ($20cm^3$). It was dried ($MgSO_4$) and the solvent removed under vacuum. Recrystallisation from ethyl acetate gave AcGlyAlaOBz (1.10g 44%), mp 109-111°C, ν_{max}(KBr disc) 3270(N-H), 1751(ester C=O), 1669(amide I), 1650(acetyl C=O), 1563cm^{-1} (amide II); $\delta_H(CDCl_3)$ 1.40(3H, d, CH_3CH), 2.01(3H, s, CH_3CO), 3.95(2H, d, CH_2NH), 4.60(1H, m, $CHCH_3$), 5.15(2H, s, $PhCH_2$), 6.50(1H, br, t, ($NHCH_2$), 6.95(1H, br, d, NHCH), 7.38(5H, s, *Ph*); m/z(FAB^+)(CH_2Cl_2/glycerol) 557(1%, M_2H^+), 279(29, MH^+), 237(2, MH^+-CH_2CO), 180(15, $^+H_3NCHCH_3COOBz$), 171(4, MH^+- HOBz), 100(5, $CH_3CONHCH_2CO^+$), 91(100, Bz^+); (FAB^-) 277(24%, $M\text{-}H^+$), 187(71, $M\text{-}Bz^+$).

5.2.8 N-(N'-acetylglycyl)-L-valine benzyl ester, AcGlyValOBz

This was made from N-acetyl glycine (1.17g, 10mmol) and L-valine benzyl ester by the method for AcGlyAlaOBz, giving AcGlyValOBz (0.74g, 30%), mp 73-74 °C; ν_{max}(KBr disc) 3273(N-H), 1744(ester C=O), 1679(amide I), 1642(acetyl (C=O), 1556cm^{-1}(amide II); $\delta_H(CDCl_3)$ 0.89(6H, dd, $(CH_3)_2CH$), 2.02(3H, s, CH_3CO), 2.20(1H, m, $CHCH(CH_3)_2$), 3.98(2H, d, NCH_2CO), 4.57(1H, m, $CH(CH_3)_2$), 5.17(2H, s, $PhCH_2$), 6.55(1H, br, t, $NHCH_2$), 6.91(1H, br, d, $NHCHCH(CH_3)_2$), 7.36(5H, s, *Ph*); m/z(FAB^+)(CH_2Cl_2/glycerol) 307(30%, MH^+), 265(3, MH^+-CH_2CO), 208(24, $^+H_3NCHCH(CH_3)_2COOBz$), 199(7, MH^+-HOBz), 100(8, $CH_3CONHCH_2CO^+$), 91(100, Bz^+), 72(53, $CH_3CONHCH_2^+$); (FAB^-) 612(6%, M_2-H^+), 305(27, $M\text{-}H^+$), 215(100, $M\text{-}Bz^+$).

5.2.9 N-(N'-acetyl-L-alanyl)glycine benzyl ester, AcAlaGlyOBz

This was made from N-acetyl-L-alanine (1.31g, 10mmol) and glycine benzyl ester (1.65g, 10mmol) by the method for AcGlyAlaOBz. Recrystallisation from ethyl acetate gave AcAlaGlyOBz (1.20g, 47%), mp 115-117°C; ν_{max}(KBr disc) 3298 (N-H), 1753,1739(ester C=O), 1669,1651(amide I), 1632(acetyl C=O), 1562cm^{-1}(amide II); $\delta_H(CDCl_3)$ 1.35(3H, d, CH_3CH), 1.98(3H, s, CH_3CO), 4.05(2H, d, CH_2NH), 4.60(1H, q, $CHCH_3$), 5.16(2H, s, $PhCH_2$), 6.33(1H, br, d, NHCH), 6.98(1H, br, t, $NHCH_2$), 7.35(5H, s, *Ph*); m/z(FAB^+)(CH_2Cl_2/glycerol) 557(2%, M_2H^+), 279(49, MH^+), 237(4, MH^+-CH_2CO), 166(58, $^+H_3NCH_2COOBz$), 114(36, $CH_3CONHCHCH_3CO^+$), 91(100 Bz^+),

86(24, $CH_3CONHCHCH_3^+$); (FAB$^-$) 277 (25%, M-H$^+$), 187(44, M-Bz$^+$).

5.2.10 N-(N'-acetyl-L-alanyl)alanine benzyl ester, AcAlaAlaOBz

This was made from N-acetyl-L-alanine (1.31g, 10mmol) and L-alanine benzyl ester (1.65g, 10mmol) by the method for AcGlyAlaOBz. Recrystallisation from ethyl acetate gave AcAlaAlaOBz (2.12g, 40%), mp 173-174.5°C; ν_{max}(KBr disc) 3299(N-H), 1731(ester C=O), 1632(amide I, acetyl C=O), 1541cm^{-1}(amide II); δ_H($CDCl_3$) 1.36 (3H, d, CH_3CH), 1.41(3H, d, CH_3CH), 2.00 (3H, s, CH_3CO), 4.54 (2H, m, both CHCH$_3$), 5.17 (2H, s, PhCH_2), 6.20 (1H, br, d, NHCH), 6.67 (1H, br, d, NH CH), 7.35(5H, s, *Ph*) ; m/z(FAB$^+$)(CH_2Cl_2/glycerol) 293(15%, MH$^+$), 251(4, MH$^+$-CH_2CO), 180(19, $^+H_3NCHCH_3COOBz$), 114(8%, $CH_3CONHCHCH_3CO^+$), 91(54, Bz$^+$), 86(10, $CH_3CONHCHCH_3^+$); (FAB$^-$) 291(6%, M-H$^+$), 201(20, M-Bz$^+$).

5.2.11 N-(N'-acetyl-L-valyl)glycine benzyl ester, AcValGlyOBz

This was made from N-acetyl-L-valine (1.50g, 10mmol) and glycine benzyl ester (10mmol, 1.65g) by the method for AcGlyAlaOBz. Recrystallisation from ethyl acetate gave AcValGlyOBz (1.49g, 54%), mp 169-170°C (lit. mp 169-170°C)[85] ; ν_{max}(KBr disc) 3283(N-H), 1765(ester C=O), 1636(amide I, acetyl C=O), 1551cm^{-1}(amide II); δ_H($CDCl_3$) 0.94(6H, d, $(CH_3)_2$), 2.01(3H, s, CH_3CO), 2.05(1H, m, CH$(CH_3)_2$) 4.05(2H, m, CH_2NH), 4.33(1H, m, CHCH$(CH_3)_2$), 5.18(2H, s, CH_2Ph), 6.26(1H, br, d, NHCH), 6.76(1H, br, t, NHCH_2), 7.36(5H, s, *Ph*); m/z(FAB$^+$)(CH_2Cl_2/glycerol) 307(17%, MH$^+$), 166(31, $^+H_3NCH_2COOBz$), 142(58, $CH_3CONHCHCH(CH_3)_2CO^+$), 114(47, $CH_3CONHCHCH(CH_3)_2^+$), 91(100, Bz$^+$), 72(64, $^+H_2NCHCH(CH_3)_2$); (FAB$^-$) 305(12%, M-H$^+$), 215(100, M-Bz$^+$).

5.2.12 N-((N''-acetyl-L-valyl)-N'-glycyl)glycine benzyl ester, AcValGlyGlyOBz

This was made from N-Acetyl-L-valine (1.50g, 10mmol) and N-glycylglycine benzyl ester (2.22g, 10mmol) by the method for AcGlyAlaOBz. Recrystallisation from ethanol gave AcValGlyGlyOBz (0.74g,15%), mp186-188°C. ν_{max}(KBr disc) 3290(N-H), 1740(ester C=O), 1667(amide I), 1633(acetyl C=O), 1547cm^{-1}(amide II). δ_H($CDCl_3$)

0.95(6H, d, $(CH_3)_2CH$), 2.00(3H, s, CH_3CO), 2.18(1H, m, $CHMe_2$), 4.07(4H, m, both CH_2), 4.27(1H, m, CHCO), 5.18(2H, s, CH_2Ph), 6.27(1H, m, NH), 6.64(1H, m, NH), 7.04(1H, m, NH), 7.35(5H, s, *Ph*); m/z(FAB$^+$)(CH_2Cl_2/glycerol) 364(17%,MH$^+$), 223(35, $^+H_3NCH_2CONHCH_2COOBz$), 199(8, $CH_3CONHCHCH(CH_3)_2CONHCH_2CO^+$), 166(21, $^+H_3NCH_2COOBz$), 142(48, $CH_3CONHCHCH(CH_3)_2CO^+$), 114(54, $CH_3CONHCHCH(CH_3)_2^+$), 91(95, Bz$^+$); (FAB$^-$) 362(25%, M-H$^+$), 272(51, M-Bz$^+$).

5.2.13 N-(N'-acetyl-L-prolyl)glycine benzyl ester, AcProGlyOBz

This was made from N-acetyl-L-proline (1.57g, 10mmol) and glycine benzyl ester (1.65g 10mmol) by the method for AcGlyAlaOBz and gave AcProGlyOBz as a colourless oil, (2.3g, 76%); ν_{max}(liquid film) 3297(N-H), 1749(ester C=O), 1633(amide I, acetyl C=O), 1537cm^{-1}(amide II); $\delta_H(CDCl_3)$ 2.04(3H, s, CH_3CO), 1.6-2.5(4H, m, 3-H_2 and 4-H_2), 3.2-3.8(2H, m, 5H_2), 4.01(2H, d, CH_2NH), 5.14(2H, s, CH_2Ph), 7.34(5H, s, *Ph*), 7.70(1H, br, t, NH). m/z(FAB$^+$)(CH_2Cl_2/glycerol) 305(19%, MH$^+$), 261(5, MH$^+$- CO_2), 140(53, MH$^+$- H_2NCH_2COOBz), 112(59, MH$^+$- $HCONHCH_2COOBz$), 91(100, Bz$^+$), 70(72, MH$^+$-$HCONHCH_2COOBz$ - CH_2CO); (FAB$^-$) 303(32%, M-H$^+$), 261(100, M-H$^+$-CH_2CO), 213(68 M-Bz$^+$), 195(76, M-H$^+$-BzOH).

5.2.14 N-(N'-acetylglycyl)glycine, AcGlyGly

AcGlyGlyOBz (1g, 3.8mmol) was dissolved in ethanol (40cm^3) and hydrogenated at room temperature and pressure in the presence of 10% palladium/charcoal (0.1g) until the theoretical volume of hydrogen had been taken up (2-3h). The mixture was heated to dissolve the product before removing the catalyst by filtration. The catalyst was washed several times with hot solvent and the combined filtrates evaporated. The white solid was recrystallised from methanol to give AcGlyGly (0.56g, 85%), mp 176-177°C (lit. mp 187-189°C)[86]; Found: C, 41.62; H, 5.84; N, 15.94. Calc. for $C_6H_{10}N_2O_4$: C, 41.38; H, 5.78; N, 16.09%. ν_{max}(KBr disc) 3340,3308(N-H), 3200-2200(COOH), 1712(acid C=O), 1663(amide I), 1618(acetyl C=O), 1557cm^{-1}(amide II); $\delta_H(D_2O)$ 2.05(3H, s, CH_3CO), 3.95(2H, s, $CH_2NHCOCH_3$, 3.99 (2H, s, CH_2COOH); m/z(FAB$^+$)(H_2O/glycerol) 349(6%,M_2H^+), 175(74, MH$^+$), 133(14, MH$^+$

- CH_2CO), 100(48, $CH_3CONHCH_2CO^+$), 76(29, $^+H_3NCH_2COOH$); (FAB$^-$) 347(11%, M_2-H^+), 173(100%, M-H^+).

5.2.15 N-(N'-1-^{13}C-acetylglycyl)glycine, ^{13}C-AcGlyGly

This was made by the hydrogenation of the benzyl ester (0.15g, $9.43x10^{-4}$ mol) as above, yield 0.08g, 81%, mp 175-175.5°C; Found: C, 41.35; H, 5.88; N, 15.68. Calc for $C_6H_{10}N_2O_4$: C, 41.71; H, 5.76; N, 15.99%. ν_{max}(KBr disc) 3339, 3307(N-H), 3200-2200(COOH), 1710(acid C=O), 1663(amide I), 1579(acetyl C=O), 1550cm^{-1}(amide II); $\delta_H(D_2O)$ 2.04(3H, d, CH_3CO), 3.94(2H, d, $CH_2NHCOCH_3$), 3.98(2H, s, CH_2COOH); m/z(FAB$^+$)(CH_3OH/glycerol) 351(1%, M_2H^+), 176(30, MH^+), 133(5, MH^+-CH_2CO), 101(16, $CH_3CONHCH_2CO^+$) 76(12%, $^+H_3NCH_2COOH$); (FAB$^-$) 349(5%, M_2-H^+), 174(94, M-H^+).

5.2.16 N-(N'-acetylglycyl)-L-alanine, AcGlyAla

N-acetyl-L-alanylbenzyl ester (1.0g, 3.60mmol) was hydrogenated as for AcGlyGly. Recrystallisation from methanol gave AcGlyAla (0.27g, 39%), mp183-184°C. ν_{max}(KBr disc) 3343,3313(N-H), 3200-2200(COOH), 1714(acid C=O), 1661(amide I), 1615(acetyl C=O), 1566,1542cm^{-1}(amide II). $\delta_H(D_2O)$ 1.41(3H, d, CH_3CH), 2.04(3H, s, CH_3CO), 3.92(2H, s, CH_2CONH), 4.38(1H, q, $CHCH_3$); m/z(FAB$^+$)(H_2O/glycerol) 377(11%, M_2H^+), 189(100, MH^+), 171(11, MH^+-H_2O), 147(25, MH^+-CH_2CO), 100(54, $CH_3CONHCH_2CO^+$), 90(97, $^+H_3NCHCH_3COOH$), 72(27, $CH_3CONHCH_2^+$); (FAB$^-$) 375(14%, M_2-H^+), 187(100%, M-H^+). Accurate FAB MH^+, Found 189.0875, $C_7H_{13}N_2O_4^+$ requires 189.0874.

5.2.17 N-(N'-acetylglycyl)-L-valine, AcGlyVal

N-acetylglycyl-L-valine benzyl ester (1g, 3.26mmol) was hydrogenated using the method for AcGlyGly, to give AcGlyVal, (0.76g, 100%), mp 134-136°C. ν_{max}(KBr disc) 3326(N-H), 3200-2200(COOH), 1728(acid C=O), 1657(amide I, acetyl C=O), 1546cm^{-1}(amide II); $\delta_H(D_2O)$ 0.93(6H, dd, $(CH_3)_2CH$), 2.06(3H, s, CH_3CO), 2.18(1H, m, $CH(CH_3)_2$), 3.95 (2H, s, CH_2NH), 4.26(1H, d, $CHCHCH(CH_3)_2$); m/z(FAB$^+$)(H_2O/glycerol) 434(10%, M_2H^+), 217(100, MH^+), 199(10, MH^+-H_2O), 175(16, MH^+-CH_2CO), 118(77, $^+H_3NCHCH(CH_3)_2COOH$), 100(20, $CH_3CONHCH_2CO^+$), 72(83, $CH_3CONHCH_2^+$); (FAB$^-$) 648(22%, M_3-H^+), 432(47, M_2-H^+),

215(100, M-H$^+$). Accurate FAB MH$^+$, Found 217.1188, $C_9H_{17}N_2O_4^+$ requires 217.1188.

5.2.18 N-(N'-acetyl-L-alanyl)glycine, AcAlaGly

This was made from N-acetyl-L-alanylglycine benzyl ester(1.0g, 3.60mmol) using the method for AcGlyGly to give AcAlaGly (0.36g, 52%), mp 183.5-185.5°C (d), Found: C, 44.67; H, 6.52; N, 14.80. Calc. for $C_7H_{12}N_2O_4$: C, 44.68; H, 6.43; N, 14.89%; ν_{max}(KBr disc) 3320,3271(N-H), 3200-2300(COOH) 1737(acid C=O), 1681(amide I), 1601(acetyl C=O), 1576cm^{-1}(amide II). δ_H (D_2O) 1.37(3H, d, C*H*$_3$CH), 2.02(3H, s, C*H*$_3$CO), 3.98(2H, s, C*H*$_2$COOH), 4.31(1H, q, C*H*CH$_3$); m/z(FAB$^+$) (H_2O/glycerol) 377(3%, M_2H^+), 189(55, MH$^+$), 147(10, MH$^+$-CH_2CO), 114(91, $CH_3CONHCHCH_3CO^+$), 102(22, $^+$OCNHCH$_2$COOH), 86(45, $CH_3CONHCHCH_3^+$); (FAB$^-$) 375(8%, M_2-H$^+$), 187(100, M-H$^+$).

5.2.19 N-(N'-acetyl-L-alanyl)alanine, AcAlaAla

N-(N'-acetyl-L-alanyl)alanine benzyl ester (2.0g, 6.85mmol) was hydrogenated as for AcGlyGly to give AcAlaAla (0.59g, 43%); mp 164-165°C. ν_{max}(KBr disc) 3349,3306(N-H), 1705(acid C=O), 1652(amide I), 1616(acetyl C=O), 1536cm^{-1}(amide II); δ_H (D_2O) 1.37(3H, d, C*H*$_3$CHCO), 1.42(3H, d, C*H*$_3$CHCO), 2.00(3H, s, C*H*$_3$CO), 4.35(2H, m, both C*H*CH$_3$); m/z(FAB$^+$)(H_2O/glycerol) 405(2%, M_2H^+), 203(43, MH$^+$), 161(9, MH$^+$-CH_2CO), 114(68, $CH_3CONHCHCH_3CO^+$), 90(45, $^+H_3NCHCH_3COOH$) , 86(44, $CH_3CONHCHCH_3^+$); (FAB$^-$) 403(12%, M_2-H$^+$), 201(100, M-H$^+$). Accurate FAB MH$^+$, Found 203.1032, $C_8H_{15}N_2O_4^+$ requires 203.1032.

5.2.20 N-N'-acetyl-L-valyl)glycine, AcValGly

N-acetyl-L-valyl glycine benzyl ester (0.5g, 1.63mmol) was hydrogenated as for AcGlyGly to give AcValGly (0.14g, 40%), mp 177-178°C (lit. mp 174-175°C)[85]; Found: C, 49.99; H,7.52; N, 12.94. Calc. for $C_9H_{16}N_2O_4$: C, 49.99, H, 7.46; N, 12.95%; ν_{max}(KBr disc) 3280(N-H), 3150-2400(COOH), 1745(acid C=O), 1637(amide I), 1549cm^{-1}(amide II); δ_H(D_2O)0.94(6H, m, (C*H*$_3$)$_2$), 2.07(3H, s, C*H*$_3$CO), 2.25(1H, m, C*H*(CH$_3$)$_2$), 3.85(2H, s, C*H*$_2$NH), 4.15(1H, d, C*H*CH(CH$_3$)$_2$). m/z(FAB$^+$)(H_2O/glycerol) 434(6%, M_2H^+), 217(86, MH$^+$), 201(4, MH$^+$-H_2O), 175(9, MH$^+$-CH_2CO), 142(100,

$CH_3CONHCHCH(CH_3)_2CO^+$), 114(95, $CH_3CONHCHCH(CH_3)_2^+$), 102(19, $^+CONHCH_2COOH$), 72(100, $^+H_2NCHCH(CH_3)_2$); (FAB$^-$) 432(17%, M_2-H^+), 215(100, M-H^+), 171(11, M-H^+-CO_2).

5.2.21 N-((N''-acetyl-L-valyl)-N'-glycyl)glycine, AcValGlyGly

N-((N''-Acetyl-L-valyl)-N'-glycyl)glycine benzyl ester (0.5g, 1.38mmol) was dissolved in ethanol (20cm^3) and hydrogenated at room temperature and pressure in the presence of 10% palladium/charcoal (0.05g) until the theoretical volume of hydrogen had been taken up (30min). The catalyst was removed by filtration and the solvent by evaporation to give AcValGlyGly (0.40g, 100%), mp 138-141°C; ν_{max}(KBr disc) 3293(N-H), 3150-2400(COOH), 1738(acid C=O), 1646(amide I, acetyl CO), 1543cm^{-1}(amide II); $\delta_H(D_2O)$ 0.96(6H, d, CH(CH_3)$_2$), 2.05(3H, s, CH_3CO), 2.22(1H, m, C*H*(CH_3)$_2$, 3.98(4H, d, both CH_2), 4.10(1H, m, C*H*CO); m/z(FAB$^+$)(H_2O/glycerol) 547(3%, M_2H^+), 274(33, MH^+), 256(3, MH^+- CH_2CO), 199(10, MH^+-H_2NCH_2COOH), 142(57, $CH_3CONHCHCH(CH_3)_2CO^+$), 133(51, $^+H_3NCH_2CONHCH_2COOH$), 114(69, $CH_3CONHCHCH(CH_3)_2^+$), 102(47, $^+OCNHCH_2COOH$), 72(100,$^+H_2NCHCH(CH_3)_2$); (FAB$^-$) 545(6%, M_2-H^+), 272(100, M-H^+). Accurate FAB MH^+, Found 274.1403, $C_{11}H_{20}N_3O_5^+$ requires 274.1402.

5.2.22 N-(N'-acetyl-L-prolyl)glycine, AcProGly

N-(N'-acetyl-L-prolyl)glycine benzyl ester (1.0g, 3.29mmol) was hydrogenated as for AcGlyGly to give AcProGly (0.35g, 50%), mp 209°C (d) (lit. mp 206-207°C)[85]; Found: C, 50.53; H, 6.65; N, 13.00. Calc. for $C_9H_{14}N_2O_4$: C, 50.46; H, 6.59; N, 13.08%; ν_{max}(KBr disc) 3329(N-H), 3200-2200(COOH), 1737(acid C=O), 1652(amide I), 1602(acetyl C=O), 1533cm^{-1}(amide II); $\delta_H(D_2O)$ 2.03(3H, d, CH_3CO), 1.70-2.50(4H, m, 3-H_2 and 4-H_2), 3.30-3.80(2H, m, 5-H_2), 3.99(2H, d, CH_2COOH), 4.30-4.70(1H, m, 2-*H*). m/z(FAB$^+$)(H_2O/glycerol) 429(7%, M_2H^+), 215(100, MH^+), 171(9, MH^+-CH_2CO), 140(88, MH^+-H_2NCH_2COOH), 112(84, MH^+- $HCONHCH_2COOH$), 102(24, $^+OCNHCH_2COOH$), 70(85, MH^+- $HCONHCH_2COOH$ - CH_2CO); (FAB$^-$) 427(7%, M_2-H^+), 213(100, M-H^+).

5.2.23 N-(N'-acetyl-N'-nitroso)glycylglycine benzyl ester, Ac(NO)GlyGlyOBz

AcGlyGlyOBz (0.73g, 2.8mmol) was dissolved in dichloromethane ($15cm^3$) containing anhydrous sodium acetate (1.14g, 15.9mmol). The mixture was cooled to 0°C. Liquid N_2O_4 ($0.183cm^3$, 2.9mmol) dissolved in dichloromethane ($5cm^3$) was added and the stirring continued for 45 min at 0°C. After filtration, the yellow solution was washed with satd. aq. $NaHCO_3$ ($10cm^3$), dried (Na_2SO_4) and the solvent removed under vacuum. The product was purified using a flash column of 15g silica 60 and $15cm^3$ portions of eluent varying from hexane:ether 5:10(v/v) to ether:methanol 10:5(v/v). The second compound eluting from the column, after evaporation of the solvent under vacuum, was a pale yellow solid, N-acetyl-N-nitrosoglycylglycine benzyl ester, (0.40g, 49%), mp 90-91°C. Found: C, 53.38; H, 5.16; N, 14.23. $C_{13}H_{15}N_3O_5$ requires: C, 53.24; H, 5.16; N, 14.33%. ν_{max}(KBr disc) 3240,3300(N-H), 1752(ester C=O), 1730(ONNC=O), 1684,1660(amide I), 1563cm^{-1}(amide II). δ_H($CDCl_3$) 2.84(3H, s, CH_3CO), 4.04(2H, d, CH_2COOBz), 4.48(2H, s, CH_2NNO), 5.18(2H, s, $PhCH_2$), 6.17(1H, br, *NH*), 7.35(5H, s, *Ph*). m/z(FAB^+)(CH_3OH/glycerol) 294(5%, MH^+), 265(30, MH^+-NO), 166(21, $^+H_3NCH_2COOBz$), 100(27, $CH_3CONHCH_2CO^+$), 91(100, Bz^+).

5.2.24 N-(N'-acetyl-N'-nitrosoglycyl)-N-nitroso-glycine benzyl ester, Ac(NO)Gly(NO)GlyOBz

From AcGlyGlyOBz (0.73g, 2.8mmol) using the above procedure with a larger quantity of liquid N_2O_4 ($0.366cm^3$, 5.8mmol). After vacuum evaporation of the solvent, purification by column chromatography on silica 60 as above gave, as the first compound eluting from the column, a deep yellow solid, N-acetyl-N,N'-dinitrosoglycylglycine benzyl ester (0.45g, 50%), mp 32-34°C. Found: C, 48.68; H, 4.35; N, 17.21. $C_{13}H_{14}N_4O_6$ requires: C, 48.45; H, 4.38; N, 17.39%. ν_{max}(KBr disc) 1736cm^{-1}(ester C=O, both ONNC=O). δ_H($CDCl_3$) 2.93(3H, s, CH_3CO), 4.49(2H, s, $ONNCH_2COO$), 5.12(2H, s, OCH_2Ph), 5.40(2H, s, $ONNCH_2NNO$), 7.36(5H, s, *Ph*). m/z(FAB^+)(CH_3OH/glycerol) 323(1%, MH^+), 294(4, MH^+- NO), 265(3, MH^+- 2NO), 100(25, $CH_3CONHCH_2CO^+$), 91(100, Bz^+).

5.2.25 N-(N'-acetyl-N'-nitrosoglycyl)glycine, Ac(NO)GlyGly

N-acetyl-N-nitrosoglycylglycine benzyl ester (0.1g, 0.34mmol) was dissolved in purified ethyl acetate (2cm^3) and ethanol (0.2cm^3) with 10% Pd/C catalyst (0.02g) added. It was treated with hydrogen at room temperature and pressure until one equivalent had been absorbed. After removing the catalyst by filtration and the solvent by evaporation under vacuum, the resulting deep yellow oil was recrystallised from warm ethyl acetate to give pale yellow crystals of Ac(NO)GlyGly (0.025g, 36%), mp62-64°C. ν_{max}(KBr disc) 3310(N-H), 1754(acid C=O), 1733(ONNC=O), 1686,1660 (amide I), 1565cm^{-1}(amide II). δ_H(D_2O) 2.83(3H, s, CH_3CO), 3.95(2H, s, CH_2COOH), 4.58(2H, s, CH_2NNO); m/z(FAB$^+$)(CH_2Cl_2/glycerol) 204(2%, MH$^+$), 186(19, MH$^+$-H_2O), 175(6, MH$^+$-NO), 100(11, $CH_3CONHCH_2CO^+$).

5.2.26 N-(2-diazoacetyl)glycine benzyl ester

To a stirred solution of glycylglycine benzyl ester tosylate salt (9.85g, 25mmol) in 2M aq. NaOAc (20cm^3) at 0°C, solid $NaNO_2$ (2.5g, 36mmol) was added, followed by glacial HOAc (1cm^3). After 5h at 0°C, yellow crystals were filtered off, washed with satd. aq. $NaHCO_3$ (10cm^3) followed by ice water (10cm^3) to give N-(2-diazoacetyl)glycine benzyl ester (2.23g, 40%), mp (from ethyl acetate) 86-88°C (lit. mp 98-99°C)[87]; ν_{max}(KBr disc) 3307(N-H), 2112(N=N), 1739(ester C=O), 1651,1611(amide I), 1555cm^{-1}(amide II). δ_H($CDCl_3$) 4.12(2H, d, CH_2NH), 4.81(1H, s, CHN_2), 5.18(2H, s, CH_2Bz), 5.64(1H, br, N*H*), 7.33(5H, s, *Ph*); m/z(FAB$^+$)(CH_2Cl_2/glycerol) 234(9%, MH$^+$), 91(56, Bz$^+$).

5.2.27 N-(2-hydroxyacetyl)glycine

N-(2-diazoglycyl)glycine benzyl ester (2.23g, 10mmol), was stirred overnight with cold water (50cm^3). The aqueous layer was freeze-dried to give N-(2-hydroxyacetyl)glycine benzyl ester. This compound (1g, 4.7mmol) was dissolved in methanol (40cm^3) and hydrogenated at room temperature and pressure until the theoretical volume of hydrogen had been taken up. Evaporation of the solvent produced N-(2-hydroxyacetyl)glycine as a white solid (0.6g, 54%), mp 91-94°C. ν_{max}(KBr disc) 3452,3329(N-H), 1717(acid C=O), 3100-2200(COOH), 1609(amide I), 1551(amide II). δ_H(CD_3COCD_3) 4.00(2H, s, CH_2OH), 4.03(2H, d, CH_2NH), 7.65(1H, br, N*H*); m/z(FAB$^+$)(H_2O/glycerol) 267(6%,

M_2H^+), 134(100, MH^+), 76(33, $^+H_3NCH_2COOH$); (FAB$^-$) 265(16%, M_2-H^+), 132(100, M-H^+).

5.2.28 N-(2-chloroacetyl)glycine

To a stirred solution of glycine (3.75g, 50mmol) in 1M aq. NaOH (50cm^3) at 0°C was added 2-chloroacetyl chloride (6.78g, 60mmol) and 1M NaOH (83cm^3) in portions. Stirring was continued at 0°C for 30 min. The acidity was adjusted to pH 2 using 5M HCl and the mixture evaporated to dryness. Extraction of the mixture into acetone (cm^3) followed by vacuum evaporation gave a colourless oil which changed to a white solid after triturating with petroleum ether 40-60°C, yield 2.04g, 27%, mp (from diethyl ether) 95-97°C (lit. mp 98-100°C)[88]; ν_{max}(KBr disc) 3318(N-H), 4100-2900(COOH), 1707(acid C=O), 1651(amide I), 1550(amide II), 771cm^{-1}(C-Cl). δ_H(CD_3COCD_3) 4.02(2H, d, C*H*$_2$NH), 4.17(2H, s, C*H*$_2$Cl), 7.77(1H, br, N*H*); m/z(FAB$^+$)(H_2O/glycerol) 154(52%, MH^+), 152(100, MH^+), 136(22, MH^+- H_2O), 134(44, MH^+-H_2O), 118(62, MH^+- HCl), 76(61, $^+H_3NCH_2COOH$). (FAB$^-$) 305(5%, M_2-H^+), 303(18, M_2-H^+), 301(26, M_2-H^+), 190(8, M+Cl^-), 188(37, M+Cl^-), 186(52% M+Cl^-), 152(41, M-H^+), 150(100, M-H^+).

5.2.29 N-(2-chlorohydroxyiminoacetyl)glycine

Glycylglycine (3.3g, 25mmol) was dissolved in 1.0M HCl and cooled to 0°C. A solution of sodium nitrite (6.9g, 100mmol) in water (5cm^3), also at 0°C was added slowly with stirring. The mixture was allowed to warm to room temperature after 4 h and was left stirring overnight. The white solid was filtered off. The remaining solution was evaporated to 1/5 of its volume and left for several hours at 0°Cto complete precipitation. The solid was washed in ice-cold water, dried and recrystallised from methanol (2.2g, 49%), mp 160°C(d), Found: C 26.42; H 2.84; N 15.22; Cl 19.78; Calc. for $C_4H_5N_2O_4Cl$: C, 26.61; H 2.79; N 15.52%; Cl 19.64; ν_{max}(KBr disc) 3382(amide N-H), 3300-2400(COOH), 3263(oxime O-H), 1720(acid C=O), 1644(amide I), 1610(C=N), 1539(amide II), 930cm^{-1}(N-O); δ_H(CD_3COCD_3) 4.06(2H, d, C*H*$_2CO_2H$), 8.25(1H, br, N*H*); m/z(FAB$^-$) (acetone/glycerol) 363(1%, M_2-H^+), 359(7, M_2-H^+), 219(11, M+Cl^-), 217(22, M+Cl^-), 215(31, M+Cl^-), 181(39, M-H^+), 179(100, M-H^+), 143(75, M-H^+-HCl), 127(97, M-H^+-HOCl), 100(94, O=C=N$CH_2CO_2^-$).

5.2.30 2-ethoxyethyl nitrite

To 2-ethoxyethanol (10g, 13.5mmol) in water ($25cm^3$) containing sodium nitrite (7g, 10.1mmol) at 0°Cwas added HCl (5M, $20cm^3$), also at 0°C. The reaction mixture was stirred at 0°C for 30 minutes. The upper, pale yellow organic layer was separated, washed (satd. aq. $NaHCO_3$, $3x10cm^3$) and dried ($MgSO_4$). It was distilled using a water pump to give a yellow liquid, (3.5g, 34%), bp 25-26°Cat 35mm (lit. bp 30-33°C at 15-20mm)[89]; n_D^{22} 1.3902; ν_{max}(liquid film) 1652(O-NO trans), 1615(O-NO cis), 1128cm^{-1}(C-O-C); δ_H(CD_3COCD_3) 1.07(3H, t, J=6.3Hz, CH_3CH_2O), 3.45(2H, q, J=6.3Hz, CH_3CH_2O), 3.67(2H, t, J=4.5Hz, OCH_2CH_2), 4.90(2H, t, J=4.5Hz, CH_2ONO). m/z (FAB$^-$) (acetone/glycerol) 269(27%, $(M+O)_2$-H^+), 134(100, M+O-H^+), 118(23, M-H^+), 89(15, M-NO^+), 46(22, NO_2^-).

5.3. Procedures

5.3.1 FTIR spectra of solutions of authentic compounds

Spectra were recorded on a Perkin-Elmer 1750 Fourier Transform Infra-Red spectrometer. Data were manipulated on a Perkin-Elmer 7500 data station using CDS-3 software. Solutions (0.03M to 0.3M) were made in D_2O or 1.0M DCl in D_2O. The solution was placed in a stainless steel thermostatted cell, fitted with a 50μ teflon spacer and calcium fluoride windows and maintained at 25.0 ± 0.2°C by circulating water. The spectrometer was purged with nitrogen at a flow rate of $9dm^3$/min for 15 min before, and during the acquisition of each spectrum, in order to reduce the intensity of the bands due to water vapour.

The scan conditions used were: deuterated triglycine sulphate (TGS) detector, 64 interleaved scans, resolution $4cm^{-1}$, Jacquinot stop 2, optical path difference (OPD) velocity 0.1, apodisation normal. Spectra of 1.0M DCl and of a solution of AcGlyGly in 1.0M DCl are shown in Figure 5.1. The spectrum of the solvent was run under identical conditions and subtracted from the solution spectrum using CDS-3 software to obtain the solute spectrum (Figure 5.2). A spectrum of HOD was obtained by subtracting a spectrum of D_2O from one of D_2O containing 1% H_2O. To remove the bands due to HOD, the HOD spectrum was subtracted interactively from the solute spectrum. The HOD spectrum is shown in

Figure 5.1

FTIR spectra of (a)1.0M DCl and (b)AcGlyGly in 1.0M DCl at 25°C

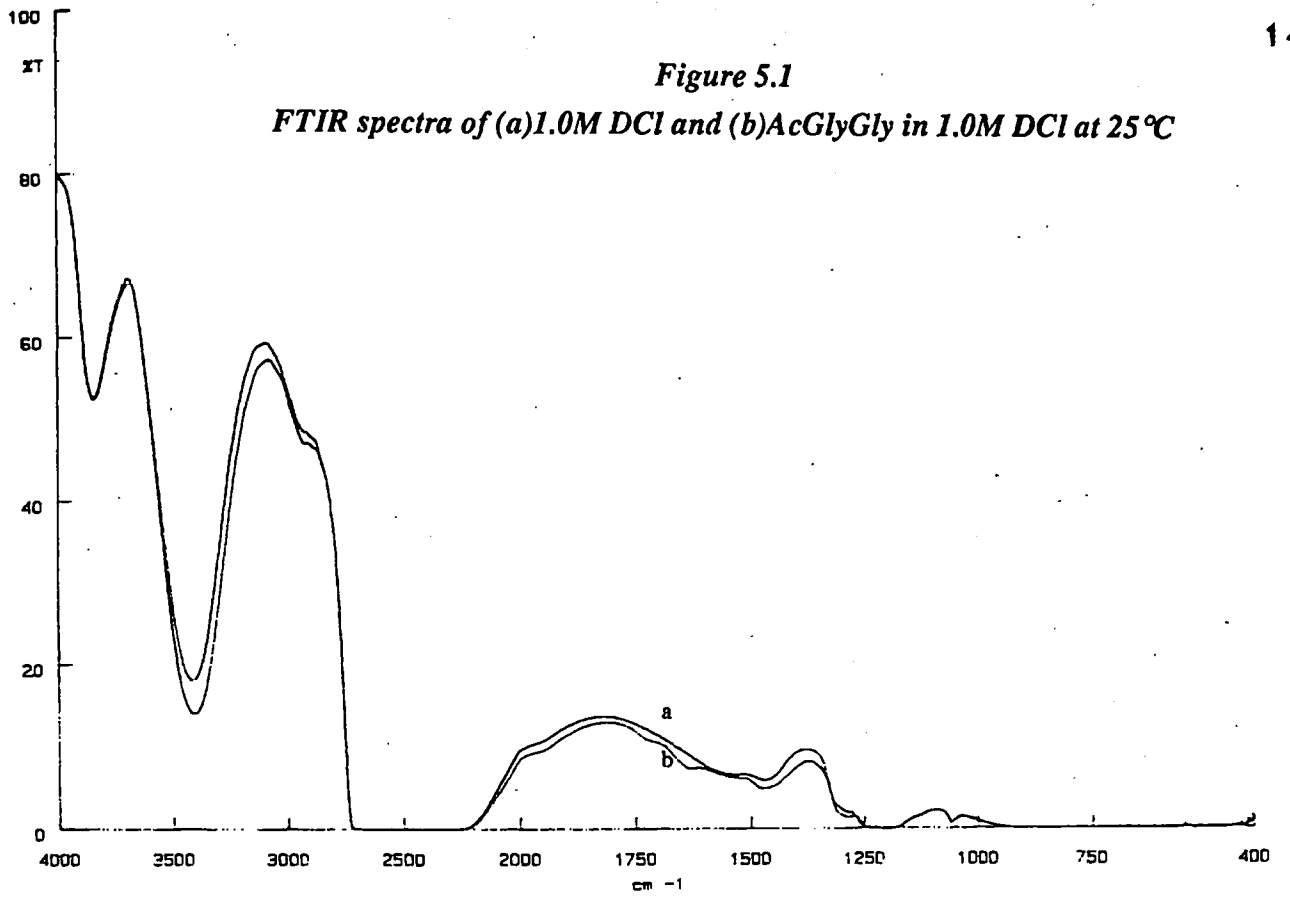

Figure 5.2

FTIR spectrum of AcGlyGly in 1.0M DCl at 25°C after subtraction of solvent

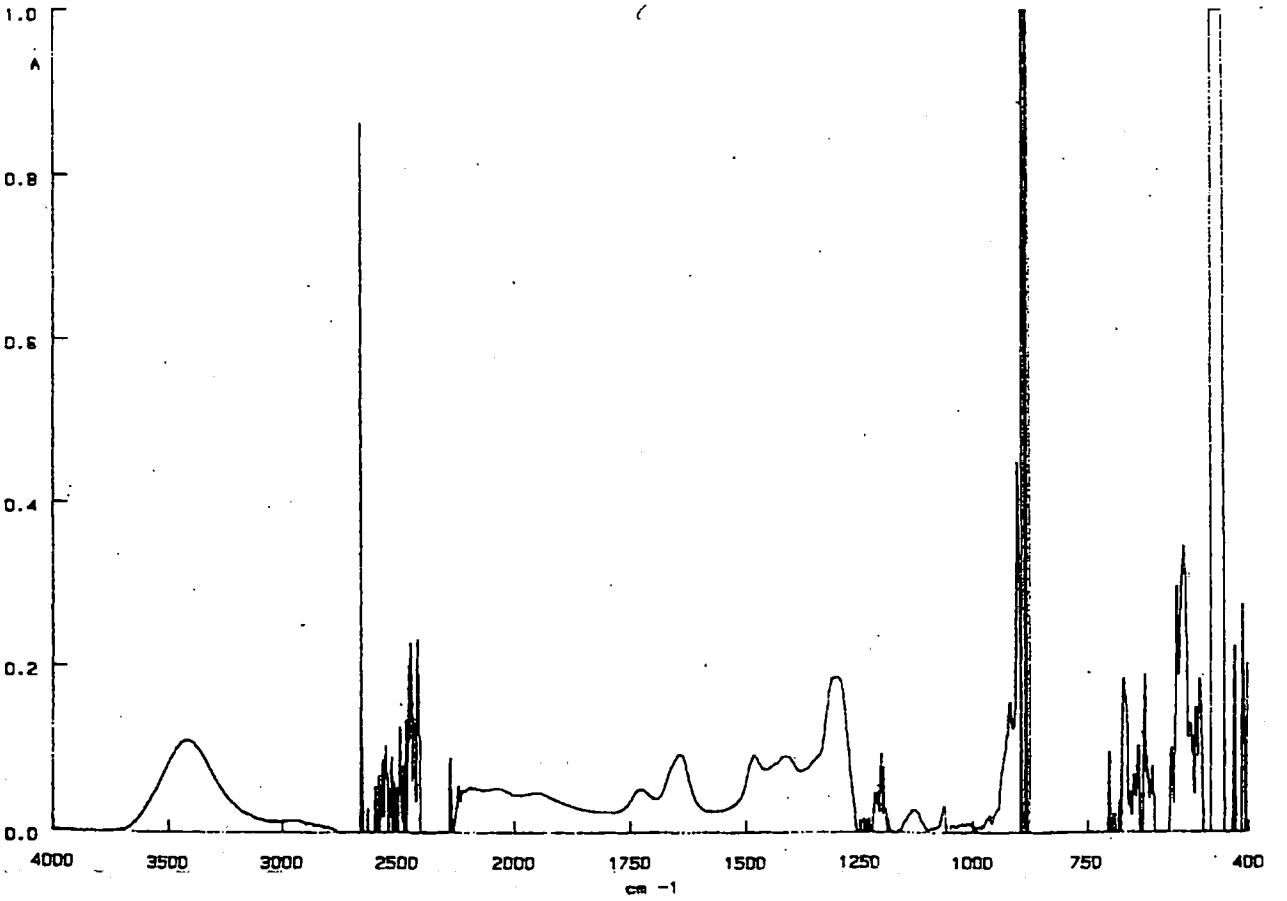

Figure 5.3

FTIR spectum of HOD at 25°C

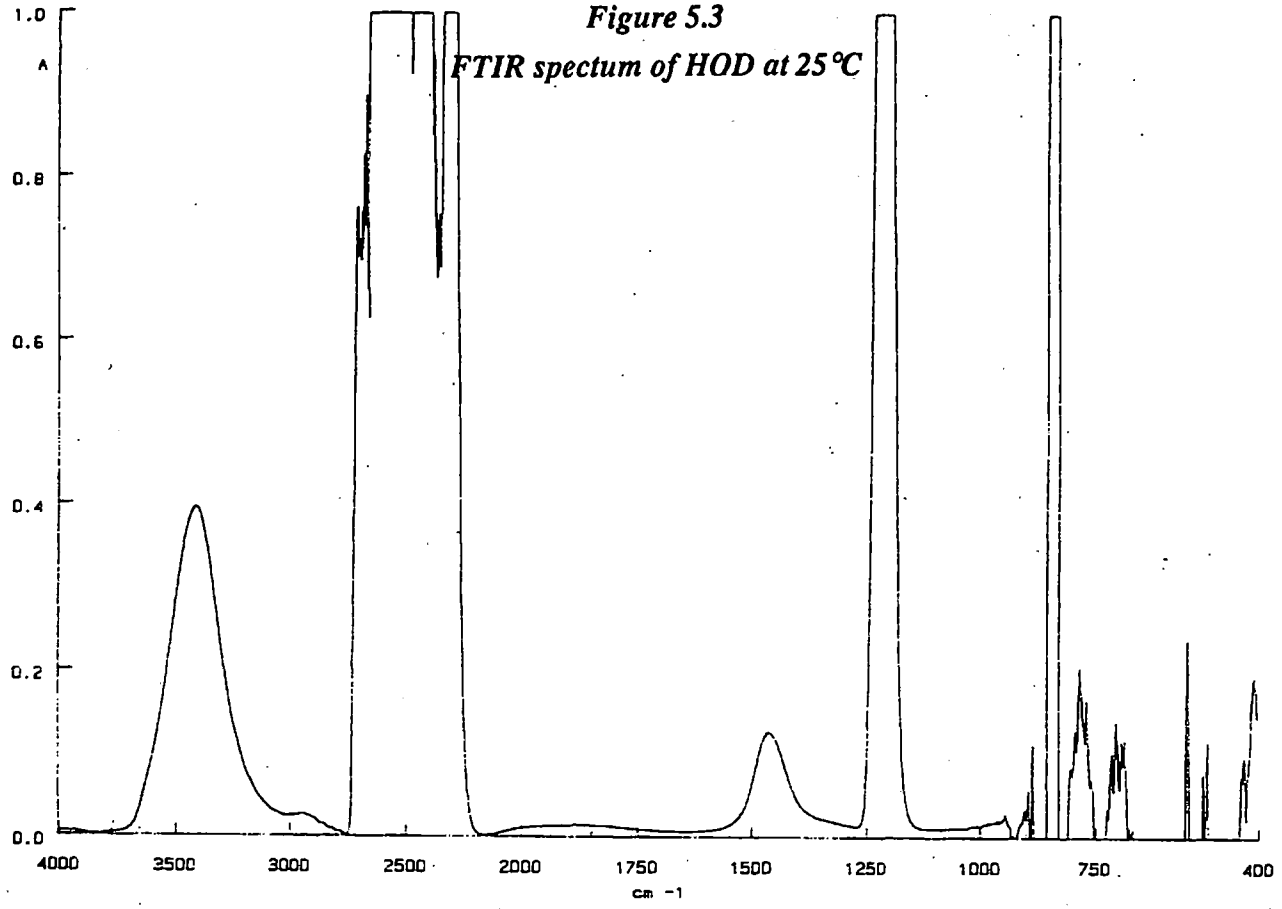

Figure 5.4

FTIR spectrum of AcGlyGly in 1.0M DCl at 25°C after subtraction of solvent and HOD

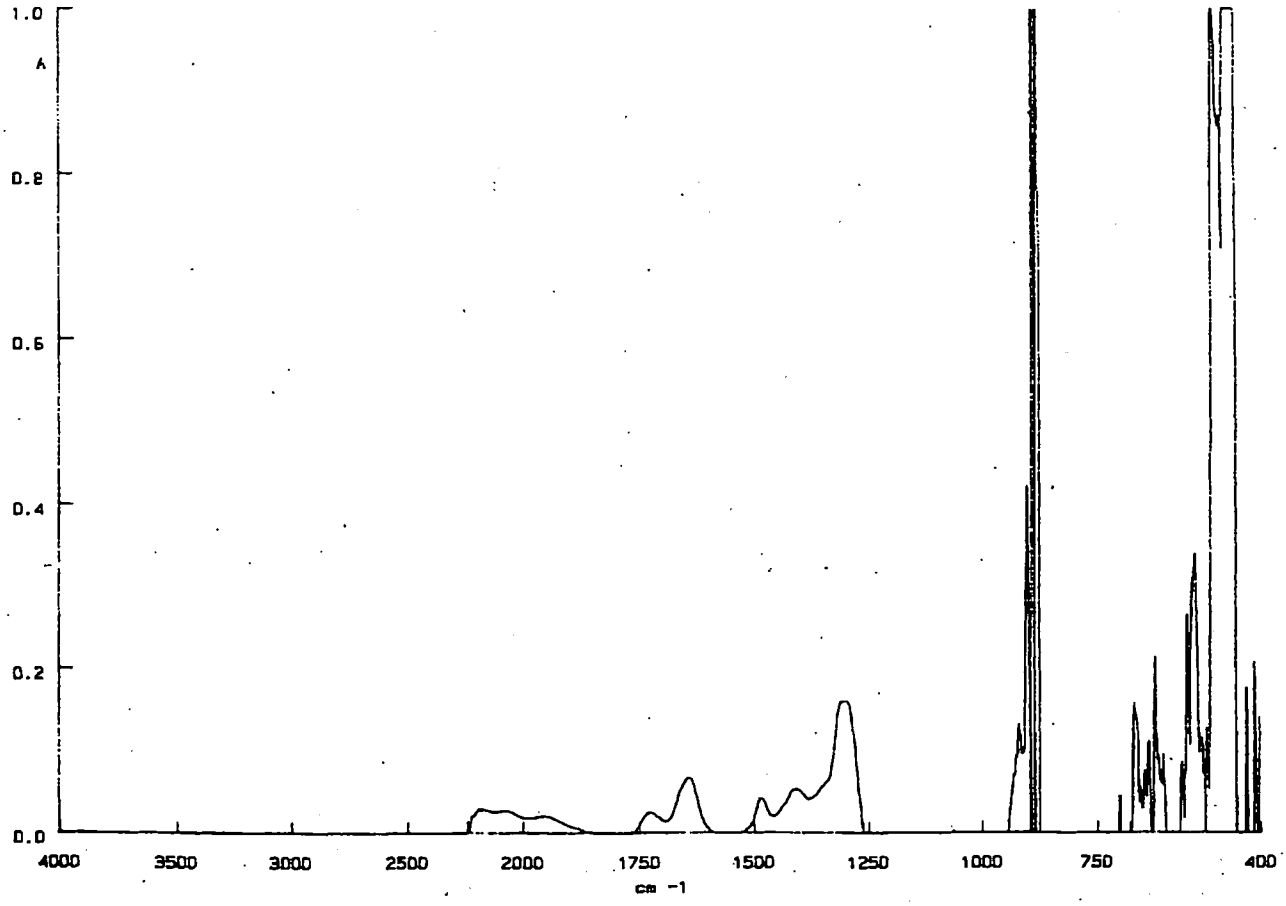

Figure 5.5

FTIR spectrum of water vapour at 25°C

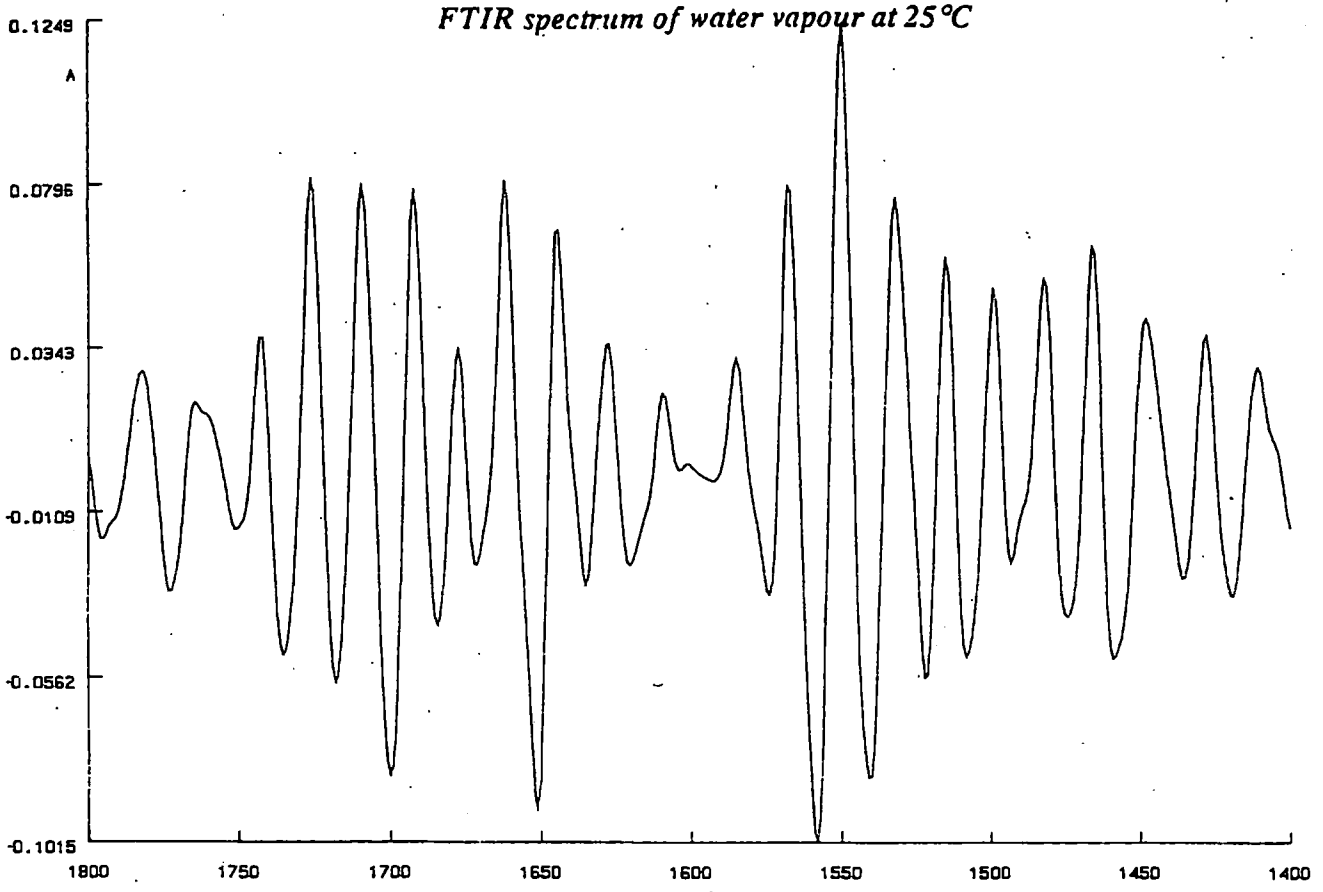

Figure 5.6

FTIR spectra of AcGlyGly in 1.0M DCl at 25°C (a) before and (b) after subtracting water vapour bands

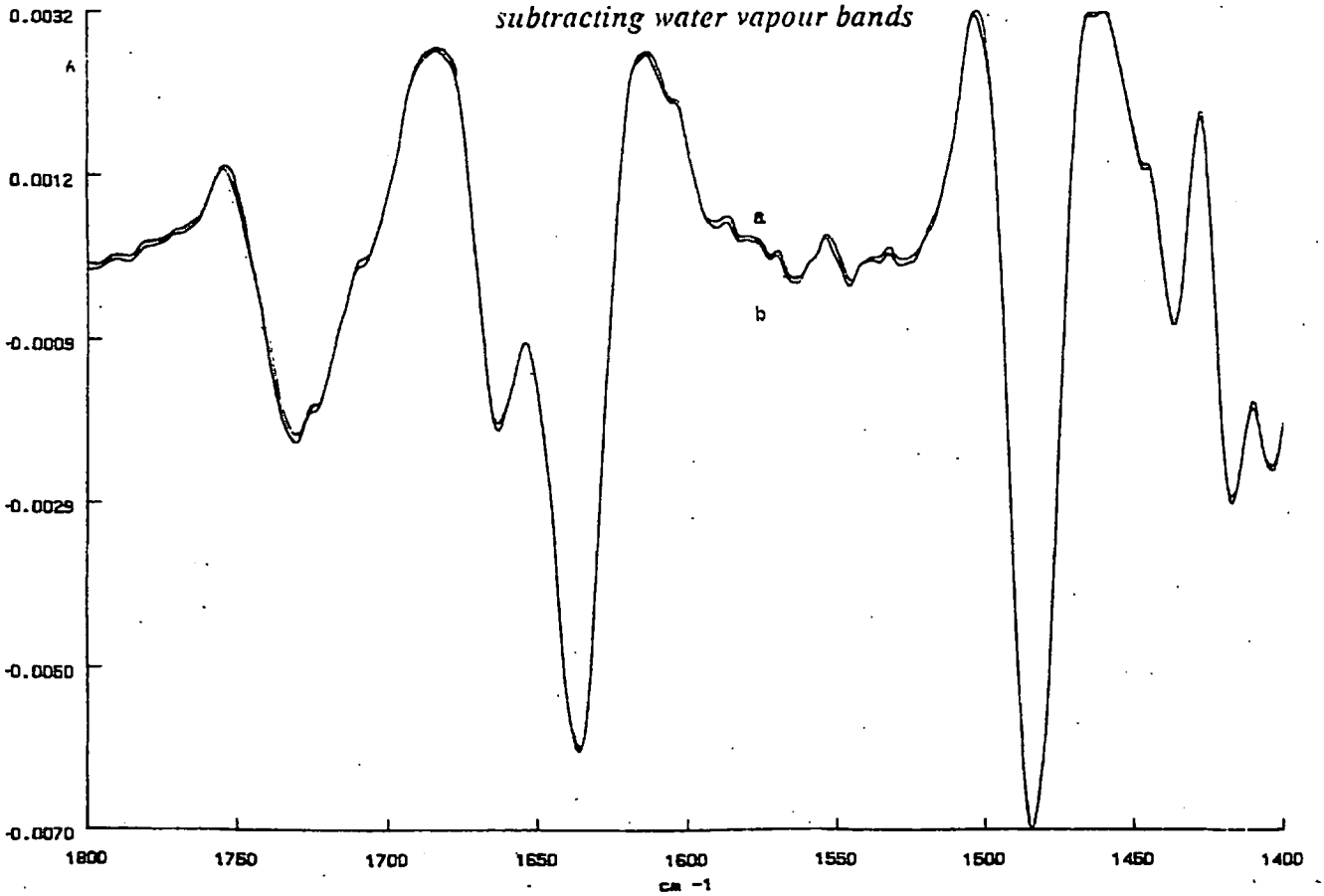

Figure 5.3 and the solute spectrum after subtraction of HOD in Figure 5.4. Successive subtractions of the same spectra gave errors of $<\pm 1\%$.
Second derivative spectra were then obtained with a width of 19 data points, using the CDS software. The remaining water vapour bands were removed by subtracting interactively a spectrum of water vapour (Figure 5.5). The second derivative spectrum of AcGlyGly, before and after subtraction of the water vapour bands, is shown in Figure 5.6. Here, as in most cases, the two are almost identical, showing that the use of the nitrogen purge and the interleaving of sample and background spectra had eliminated the water vapour bands already. The subtraction procedure remained as a safeguard.

5.3.2 Kinetics of peptide nitrosation

Solutions of the peptide (0.03-0.09M) in DCl (0.25-1.00M) and of $NaNO_2$ (8.0M) in D_2O were cooled in ice for 20 min and then mixed in a $10cm^3$ volumetric flask to give the required final concentrations of DCl (0.25 -1.0M), NO_2^-(0.10 - 0.40M)) and peptide (0.03 - 0.09M). The mixture was shaken gently and divided quickly between 8 small sample tubes ($1.2cm^3$), which were filled to the brim, closed with PTFE septa and screw rings and placed in the dark in a thermostatted water bath at 25°C. After allowing 10 min for temperature equilibration, sample tubes were withdrawn at timed intervals over two to three half-lives. An aliquot of the solution ($0.75cm^3$) was shaken with sulphamic acid in D_2O ($0.30cm^3$, 1.4M) which quenched the reaction by destroying excess nitrite. The mixture was left for 10 min in the dark to ensure 100% removal of nitrite before measuring the UV absorbance at 410nm. The IR spectrum (4000 - $450cm^{-1}$) was recorded as described for authentic compounds, except that the cell was filled from the exterior of the instrument using PTFE tubing.
The rate of the peptide nitrosation reaction was determined from variation of the absorbance (A) of the changing carbonyl band (at 1636 cm^{-1} for AcGlyGly) with time. The absorbance was measured as the height of the peak from the zero line in each second derivative spectrum x the ordinate scale. Absorbance of the carbonyl band in the second derivative spectrum was assumed to be proportional[58] to peptide concentration and the gradient of the graph of lnA against time was the *pseudo* first order rate constant under these conditions. Typical spectra are given in Figure 5.7, measurements in Table 5.1 and a rate plot in Figure 5.8. Each reaction

Figure 5.7

Second derivative FTIR spectra with respect to time for the reaction of 0.03M AcGlyGly and 0.4M $NaNO_2$ in 1.0M excess DCl at 25°C

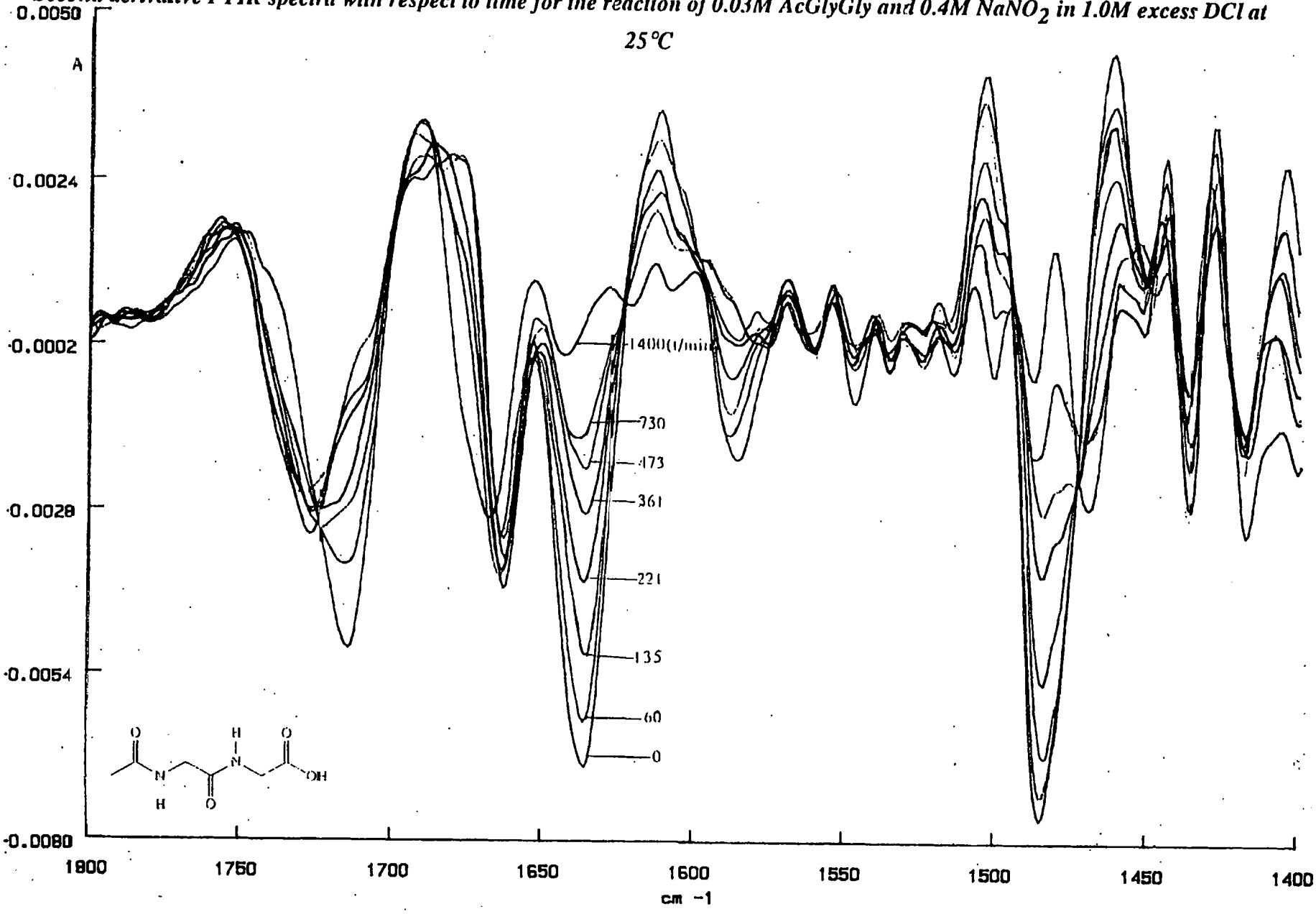

Table 5.1

Changes in intensity (peak height) of IR bands during the nitrosation of AcGlyGly at 25℃. Initial [AcGlyGly] = 0.03, [$NaNO_2$] = 0.4, DCl = 1.0M

	peak height/mm at $\tilde{\nu}$/cm^{-1}		
$10^{-3}t$/s	*1636*	*1587*	*1482*
0	79.2	0	88.3
3.60	71.0	0	84.2
8.00	58.8	0.5	77.1
13.26	45.4	1.9	64.1
21.66	33.0	8.0	44.2
28.38	24.7	14.4	32.8
43.80	19.0	18.3	22.5
84.00	3.8	22.9	8.1

Figure 5.8

First order rate plot for the nitrosation of AcGlyGly at 25℃

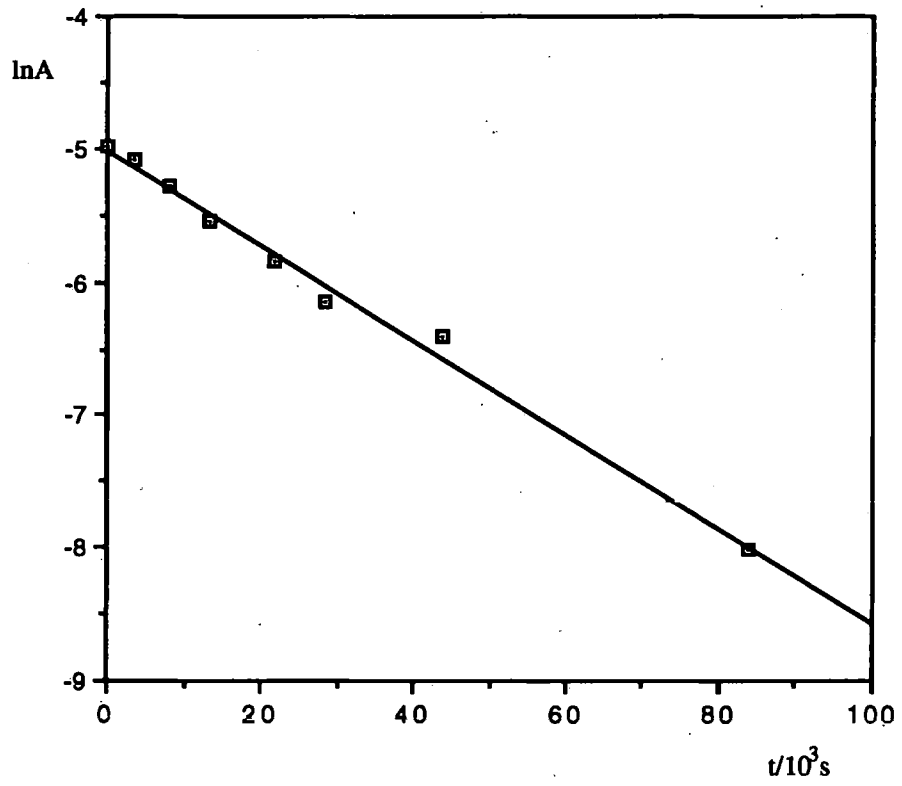

was carried out four times and the rate constants obtained were reproducible to ±10%.

5.3.3 Kinetics of peptide diazotization

Aqueous glycylglycine ($10cm^3$, 1.0M) at the required pH was thermostatted in a volumetric flask for 10 min in a 25°C bath. Ethoxyethyl nitrite (neat, 17.1µl, 1.0 $x10^{-4}$mol) was added and the mixture shaken for 2 min. An aliquot of the reaction mixture was placed in the IR cell (sapphire windows, 140µ pathlength) contained in the IR spectrometer and maintained at 25.0 ± 0.1°C, where it was left throughout the reaction. Spectra were recorded at timed intervals over about the first 10% of reaction, using a nitrogen purge at $1dm^3$/min and dispersing any bubbles five minutes before each scan.

The scan conditions were: mercury cadmium telluride (MCT) detector, 300 scans - ratioed against a background spectrum of the cell containing water, resolution $16cm^{-1}$, Jacquinot stop 1, optical path difference (OPD) velocity 0.2, apodisation triangular. A higher OPD velocity would have been preferable but was not available on the instrument.

The initial rates of reaction were determined from the change in absorbance of the diazo peak at $2120cm^{-1}$, measured from the zero order spectrum, with time, over the first 3% of the reaction, during which time decomposition of the diazopeptide would have been small. This was inferred from the fact that authentic diazoacetylglycine benzyl ester decomposed by only 4.5% over 44min at pH 9 (Section 4.8). A typical set of spectra is given in Figure 5.9. The corresponding absorbance plot together with the gradient used in the calculation is shown in Figure 5.10. Rate constants were reproducible to ±10%.

Figure 5.9

FTIR spectra with respect to time for reaction of 1.0M GlyGly and 0.01M $EtO(CH_2)_2ONO$ at pH 8.00 and 25°C

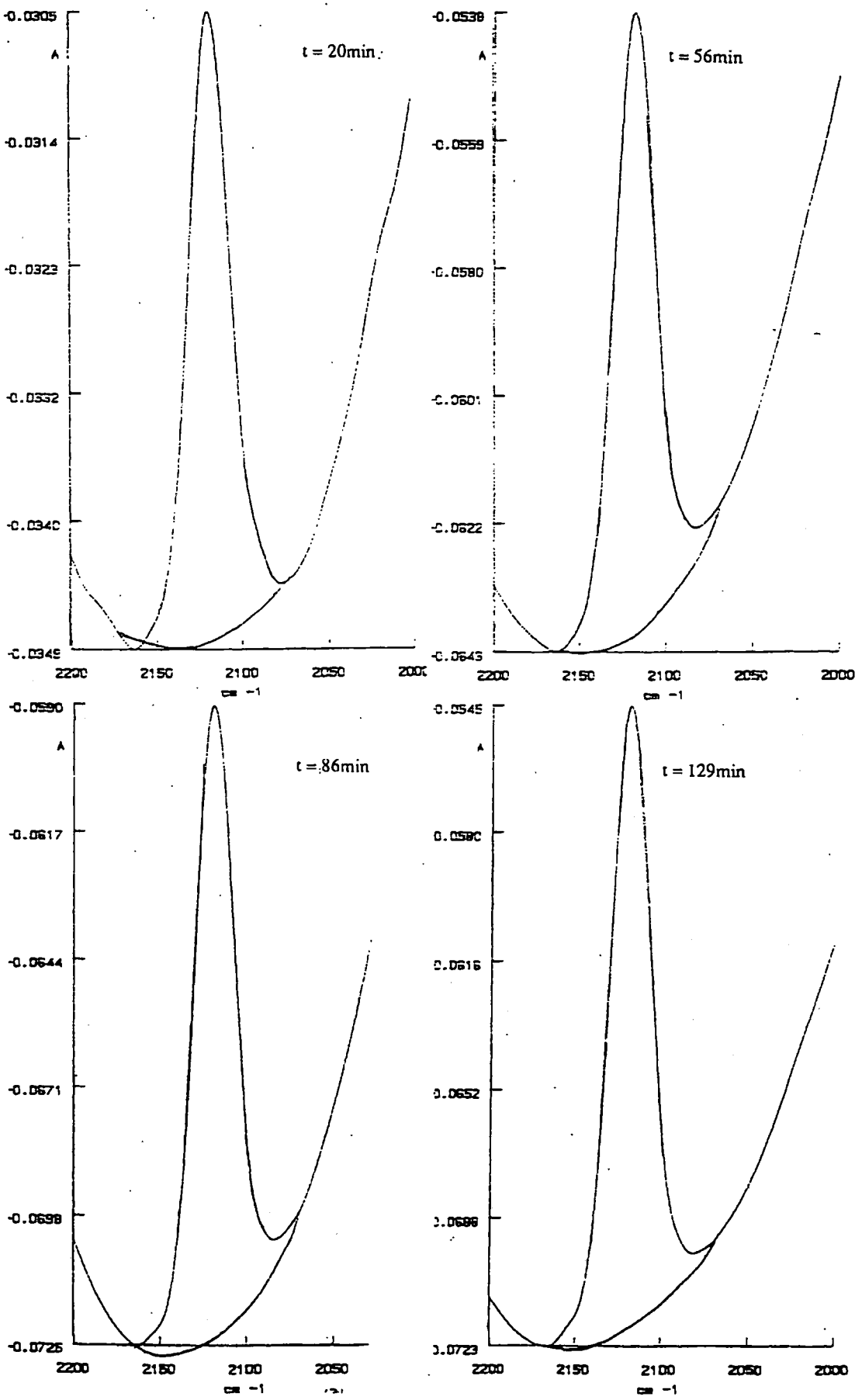

Figure 5.10

Variation of FTIR absorbance with time for reaction of 1.0M Glycylglycine with 0.01M $EtO(CH_2)_2ONO$ at pH 8 and 25°C

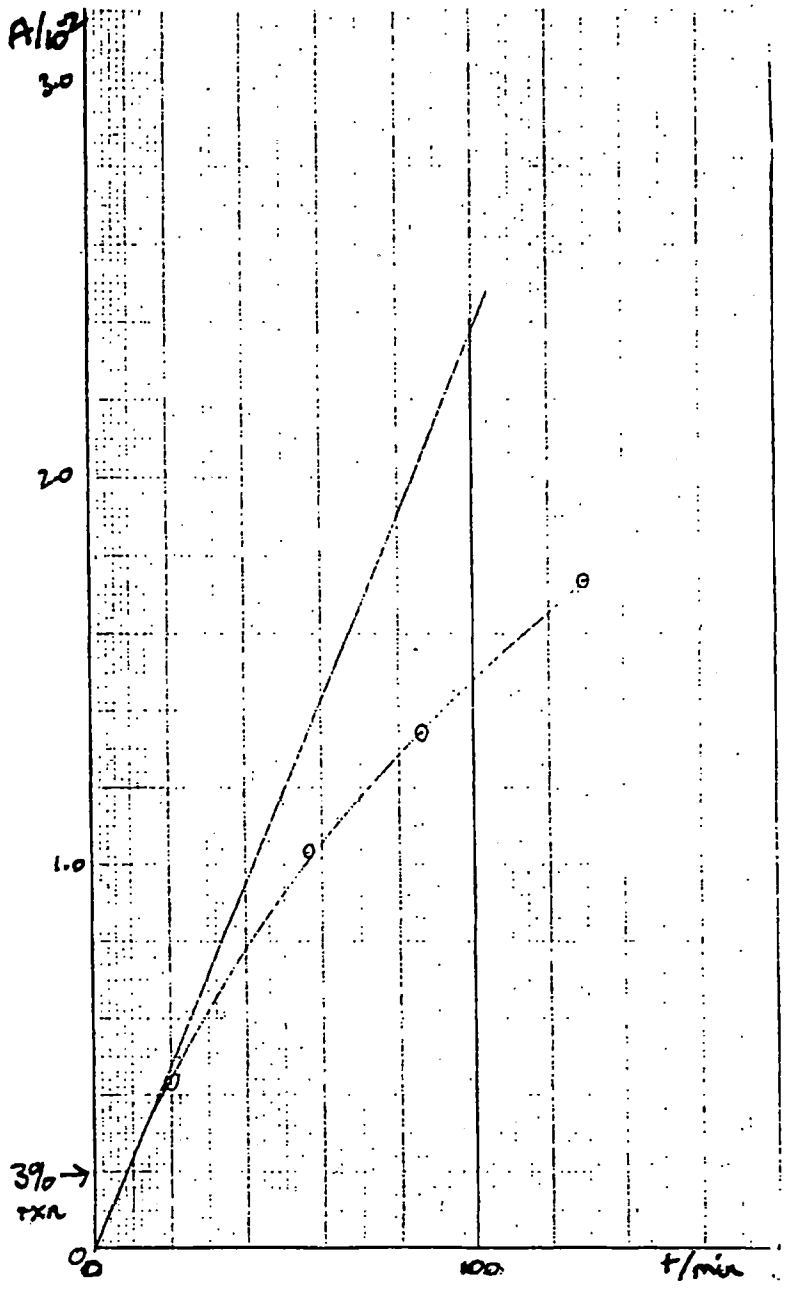

$k_1 = 6.39 \times 10^{-5}\ s^{-1}$

5.3.4 Nitrite decomposition

Reaction mixtures were made up as for FTIR runs (section 3.1.2) but without the peptide present. Aliquots ($1cm^3$) were placed in the reaction vials which in turn were placed in a thermostatted bath at 25°C. At timed intervals, the concentration of nitrite in the solution was measured by Shinn's Method[76]. A tube was opened and $0.05cm^3$ of the nitrite solution was added to a $50cm^3$ volumetric flask containing $2cm^3$ of 1% (w/w) sulphanilamide in 5M HCl. After 30 sec, $2cm^3$ of 0.1% (w/w) N-(1-naphthyl)ethylene diamine dihydrochloride was added. The mixture was made up to $50cm^3$ and left for 25 min before measuring the absorbance at 541nm in a UV/visible spectrophotometer.

Standard solutions of sodium nitrite were used to plot a calibration curve of absorbance versus [$NaNO_2$], which was linear over the range of concentrations 0 - 0.3M.

References

1 R Bonnett and P Nicolaidou, *Heterocycles,* 1977, **7**, 637.

2 T Curtius, *Chem. Ber.*, 1904, **37**, 1285.

3 T Curtius and A Darapsky, *Chem. Ber.*, 1906, **39**, 1373.

4 T Curtius and J Thompson, *Chem. Ber.*, 1906, **39**, 1379.

5 T Curtius and T Callan, *Chem. Ber.*, 1910, **43**, 2447.

6 JH Looker and JW Carpenter, *Canad.J. Chem.*, 1967, **45**, 1727.

7 BC Challis, in GG Gibson and C Ionnides (eds), *Safety Evaluation of Nitrosatable Drugs and Chemicals,* Taylor and Francis, London, 1981, p16.

8 A Kurosky and T Hofmann, *Can. J. Biochem.*, 1972, **50**, 1282.

9 BC Challis, BR Glover and JRA Pollock, in H Bartsch, IK O'Neill and R Schulte-Hermann (eds), *The Relevance of N-Nitroso Compounds to Human Cancer*, IARC Scientific Publications No 84, IARC, Lyon, 1987, p345.

10 PMG Bavin, DW Darkin and NJ Viney, in H Bartsch, IK O'Neill, M Castegnaro and M Okada (eds), *N-nitroso Compounds, Formation and Occurrence,* IARC Scientific Publications No 41, IARC, Lyon, 1982, p337.

11 BC Challis, MHR Fernandes, BR Glover and F Latif, in H Bartsch, IK O'Neill and R Schulte-Hermann (eds), *The Relevance of N-Nitroso Compounds to Human Cancer*, IARC Scientific Publications No 84, IARC, Lyon, 1987, p308.

12 E Goldstein, NF Peek, NJ Parkes, HH Hines, EP Steffey and B Tarkington, *Am. Rev. Resp. Dis.*, 1977, **115**, 403.

13 S Parodi, M Picca, C Bolognesi, M Cavanna, P Carlo, R Finolo,and G Brambilla, *Pharm. Res. Comm.*, 1977, **9**, 621.

14 JRA Pollock, *Fd. Chem. Toxicol.*, 1985, **23**, 701.

15 AR Tricker and R Preussmann, *Carcinogenesis*, 1986, **7**, 1523.

16 JR Outram and JRA Pollock, in IK O'Neill, RC Von Borstel, CT Miller, J Long and H Bartsch (eds), *N-Nitroso Compounds: Occurrence, Biological Effects and Relevance to Human Cancer*, IARC Scientific Publications No 57, IARC, Lyon, 1984, p71.

17 T Curtius and J Thompson, *Chem. Ber.*, 1906, **39**, 1379.

18 L Baldini and G Brambilla, *Cancer Res.*, 1966, **26**, 1754.

19 T Giraldi and C Nisi, *Pharm. Res. Comm.*, 1976, **8**, 279.

20 G Sava, T Giraldi and L Baldini, *Cancer Treatment Reports,* 1982, **66**, 179.

21 T Giraldi, AM Guarino, C Nisi and L Baldini, *Eur. J. Cancer,* 1979, **15**, 603.

22 G Brambilla, M Cavanna, S Parodi and L Baldini, *Eur. J Cancer,* 1972, **8**, 127.

23 C Monti-Bragadin, M Tamaro and E Banfi, *Antimicrobial Agents and Chemotherapy,* 1974, **6**, 655.

24 E Banfi, M Tamaro, B Pani and C Monti-Bragadin, *Bollettino dell Istituto Sieroterapico Milanese,* 1974, **531**, 632.

25 B Pani, N Babudri, F Bartoli-Klugmann, S Venturini and I de Fant, *Mutation Res.*, 1980, **78**, 375.

26 S Parodi, C Bolognesi, M Cavanna, RL Pollack, L Santi and G Brambilla, *Cancer Res.*, 1977, **37**, 4460.

27 G Brambilla, M Cavanna, P Carlo, R Finollo, L Sciaba, S Parodi and C Bolognesi, *J. Cancer Res. Clin. Oncol.*, 1979, **94**, 7.

28 S Parodi, M Picca, C Bolognesi, M Cavanna, P Carlo, R Finollo and G Brambilla, *Pharm. Res. Comm.*, 1977, **9**, 621.

29 G Brambilla, M Cavanna, A Maura, S Parodi, A Furlani, V Scarcia and R Della Loggia, *Arzneimittel-Forschung,* 1973, **23**, 690.

30 T Giraldi, C Monti-Bragadin and R Della Loggia, *Experientia,* 1974, **30**, 496.

31 R Della Loggia, A Furlani, F Savastano and V Scarcia, *Experientia,* 1976, **32**, 636.

32 CL Liu, K Ohtsuki and H Hatano, *J. Biochem.*, 1973, **73**, 671.

33 I Kregar, B Stanovnik, M Tisler, C Nisi, F Gubensek and V Turk, *Acta Biologica et Medica Germanica,* 1977, **36**, 1927.

34 F Ahmad and P McPhie, *Int. J. Peptide Protein Res.*, 1978, **12**, 155.

35 R Bonnett and P Nicolaidou, *Heterocycles,* 1977, **7**, 637.

36 R Bonnett and P Nicolaidou, *J. Chem. Soc., Perkin Trans. 1*, 1979, 1969

37 YL Chow and J Polo, *J. Chem. Soc., Chem. Comm.*, 1981, 297.

38 YL Chow SS Dhaliwal and J Polo, in IK O'Neill, RC Von Borstel, CT Miller, J Long and H Bartsch (eds) *N-Nitroso compounds: Occurrence, Biological Effects and Relevance to Human Cancer,* IARC Scientific Publications No 57, IARC, Lyon, 1984, p317.

39 J Garcia, J Gonzalez, R Segura and J Vilarrasa, *Tetrahedron*, 1984, **40**, 3121.

40 BC Challis, JR Milligan and RC Mitchell, *J. Chem. Soc., Chem. Comm.*, 1984, 1050.

41 BC Challis, AR Hopkins, JR Milligan RC Mitchell and RC Massey, in IK O'Neill, RC Von Borstel, CT Miller, J Long and H Bartsch (eds), *N-Nitroso Compounds: Occurrence, Biological Effects and Relevance to Human Cancer*, IARC Scientific Publications No 57, Lyon, 1984, p61.

42 BC Challis, JR Milligan and RC Mitchell, *J. Chem. Soc. Perkin Trans. 2*, 1991, 1595.

43 CN Berry and BC Challis, *J. Chem. Soc., Perkin Trans. 2*, 1974, 1638.

44 BC Challis, AR Hopkins, JR Milligan, RC Massey, D Anderson and SD Blowers, *Toxicol. Lett.*, 1985, **26**, 89.

45 D Anderson, BJ Phillips, BC Challis, AR Hopkins, JR Milligan and RC Massey, *Fd. Chem. Toxic.*, 1986, **24**, 289.

46 SD Blowers and D Anderson, *Fd. Chem. Toxic.*, 1988, **26**, 9.

47 SD Blowers, MH Brinkworth and D Anderson, *Fd. Chem. Toxic.*, 1988, **26**, 917.

48 PR Griffiths, *Chemical Infrared Fourier Transform Spectroscopy*, John Wiley and Sons, Chichester, 1975.

49 PR Griffiths (ed), *Transform Techniques in Chemistry*, Plenum Press, New York, 1978.

50 Perkin Elmer 1700 series *Infrared Fourier Transform Spectrometers, Operator's Manual*, Perkin Elmer, Beaconsfield, 1984.

51 BR Glover, PhD Thesis, London 1985, pp59 - 83.

52 EH White, *J. Am. Chem. Soc.*, 1955, **77**, 6008.

53 RJ Bruehlman and FH Verhoek, *J. Am. Chem. Soc.*, 1948, **70**, 1401.

54 NS Bayliss and DW Watts, *Aust. J. Chem.*, 1963, **16**, 927-32.

55 LJ Bellamy, *The Infrared Spectra of Complex Molecules*, Volume I, 3rd edition, Chapman and Hall, London, 1975, p238.

56 LJ Bellamy, *The Infrared Spectra of Complex Molecules*, Volume II, 2nd edition, Chapman and Hall, London, 1980, p181.

57 RB Homer and CD Johnson in *The Chemistry of Amides*, Ed. J Zabicky, John Wiley, Chichester, 1970, p188.

58 H Susi and DM Byler, *Biochem. and Biophys. Res. Comm.*, 1983, **115**, 391-397.

59 LJ Bellamy, *The Infrared Spectra of Complex Molecules*, Volume II, 2nd edition, Chapman and Hall, London, 1980, p280.

60 AA Frost and RG Pearson, *Kinetics and Mechanism*, 2nd Ed. John Wiley, Chichester, 1961, p166.

61 *CRC Handbook of Chemistry and Physics*, (eds) RC Weast and MJ Astle, 60th Edn., CRC Press, 1973.

62 BC Challis, BR Glover and JRA Pollock, in H Bartsch, IK O'Neill and R Schulte-Hermann (eds), *The Relevance of N-Nitroso Compounds to Human Cancer*, IARC Scientific Publications No 84, IARC, Lyon, pp308-314.

63 CH Rochester, *Acidity Functions*, Academic Press, New York, 1970.

64 K Yates and JC Riordan, *Canad. J. Chem.*, 1965, **43**, 2328.

65 K Yates, JB Stevens, AR Katritzky, *Canad. J. Chem.*, 1964, **42**, 1957.

66 MA Paul and FA Long, *Chem. Rev.*, 1957, **57**, 1.

67 E Hogfeldt and J Bigeleisen, *J. Amer. Chem. Soc.*, 1960, **82**, 15.

68 BC Challis and DEG Shuker, *J. Chem. Soc., Perkin Transactions 2*, 1979, 1020.

69 BR Glover, PhD Thesis, London 1985, p26.

70 MHR Fernandes, PhD Thesis, London 1986, pp23-24.

71 BR Glover, PhD Thesis, London 1985, p66.

72 BR Glover, PhD Thesis, London 1985, p77.

73 C. Grundmann, Nitrile Oxides, in *The Chemistry of the Carbon Nitrogen Triple Bond*, Ed. Patai, Wiley, Chichester, 1970, p816.

74 AA Frost and RG Pearson, *Kinetics and Mechanism*, John Wiley, Chichester, 1961, p176.

75 BC Challis and SP Jones, *J. Chem. Soc. Perkin Trans. 2.*, 1975, 153.

76 MB Shinn, *Ind. Eng. Chem. Anal.*, 1941,**13**,33.

77 DEG Shuker, PhD Thesis, London, 1979, p 85.

78 PR Griffiths, *Chemical Infrared Fourier Transform Spectroscopy*, John Wiley and Sons, Chichester, 1975, p 192.

79 Perkin Elmer 1700 series *Infrared Fourier Transform Spectrometers, Operators Manual*, Perkin Elmer, Beaconsfield, 1984, p9.

80 PR Griffiths, *Chemical Infrared Fourier Transform Spectroscopy*, John Wiley and Sons, Chichester, 1975, p 196.

81 Perkin Elmer 1700 series *Infrared Fourier Transform Spectrometers, Operators Manual*, Perkin Elmer, Beaconsfield, 1984, p7.

82 F. Latif, PhD Thesis, London 1986.

83 D D Perrin, W L F Armarego, D R Perrin, *Purification of Laboratory Chemicals*, 2nd Edition, Pergamon, Oxford, 1980.

84 DJ Annan, PhD Thesis, London 1987.

85 JR Milligan, PhD Thesis, London 1984.

86 JS Davies (ed), *Amino Acids and Peptides*, Chapman and Hall, London, 1985.

87 VK Antonov, Izv. Akad. Nauk. SSSR, Otd. Khim. Naut., 1963, 1129 quoted in BR Glover, PhD Thesis, London 1985.

88 PA Levene, HS Simms and MH Pfaltz, *J. Biol. Chem.*, 1934, **61**, 445 quoted in BR Glover, PhD Thesis, London 1985.

89 M Meadow and WM Whalley, *J.Chem. Soc.*, 1954, 1162.